PROCEEDINGS OF TWO SEMINARS OF TC207 ISSMGE in 2015

SOIL-STRUCTURE INTERACTION AND RETAINING WALLS

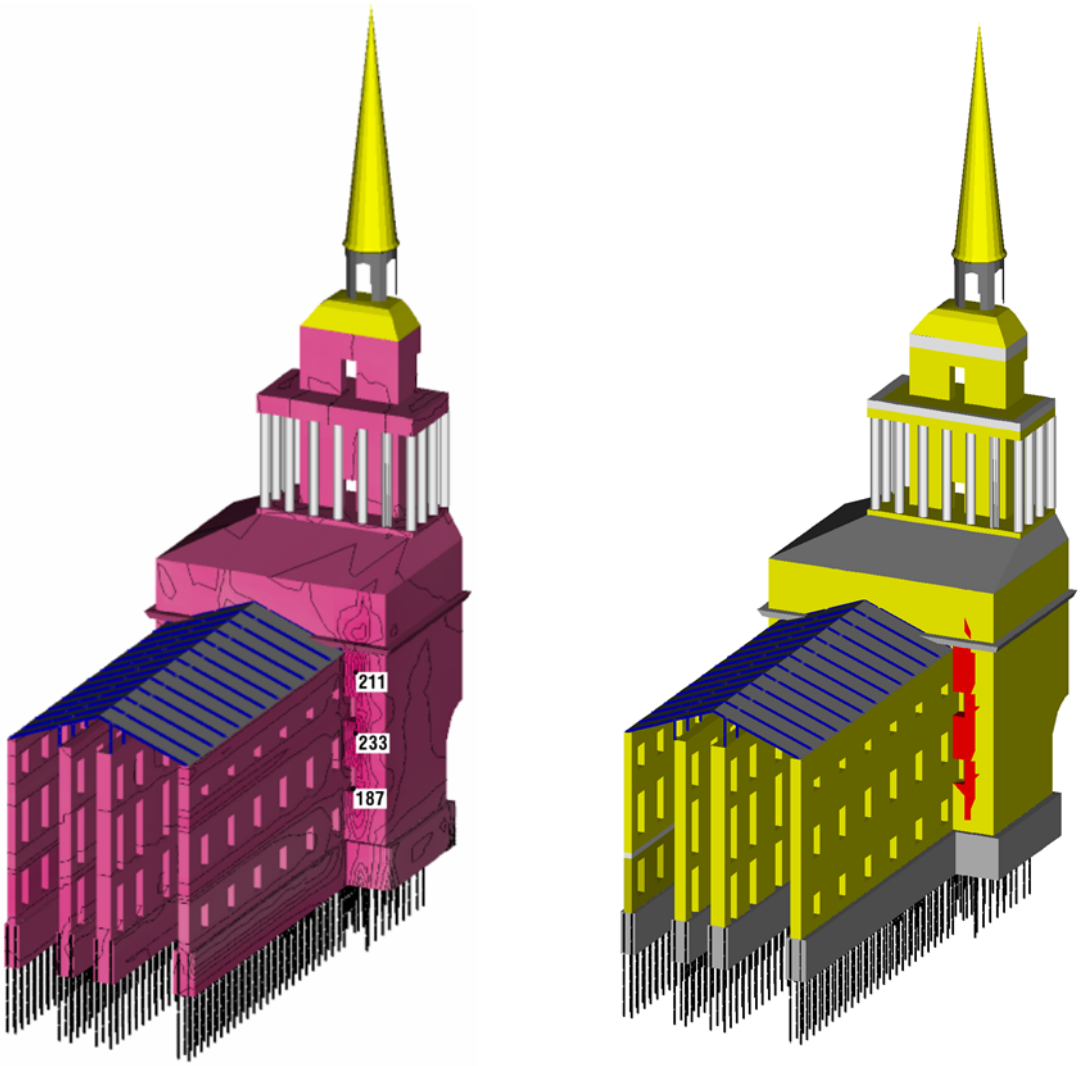

2016

SEMINARS ON SOIL-STRUCTURE INTERACTION AND RETAINING WALLS

13 September 2015, Edinburgh – Scotland

16 December 2015, Pune – India

Edited by:

Michael Lisyuk
Vladimir Ulitsky
Deepankar Choudhury

2016

Proceedings of two Seminars of TC207 ISSMGE in Edinburgh and Pune in 2015.

Published by: Georeconstruction Engineering Co.
190005 Russia, Izmaylovsky prospect 4
georeconstruction.com

ISBN 978-5-9906877-0-7

PREFACE

This proceeding volume contains technical papers submitted to two Workshops of ISSMGE Technical Committee TC 207 on Soil-Structure Interaction and Retaining Walls, which were held in 2015:

– Seminar on Soil-Structure Interaction and Retaining Walls at Edinburgh, Scotland, in collaboration with TC305 on Megacities, 13 September 2015, and

– Seminar on Soil-Structure Interaction and Retaining Walls at Pune, India, 16 December 2015, in collaboration with TC212 on Deep foundations.

Both Seminars dealt with the different aspects of interaction of structures with the ground.

Numerical calculations of buildings and structures in the framework of soil-structure interaction do not pertain only to the domain of design of unique and technically sophisticated or hazardous buildings and structures any more. They become actively involved in everyday design practice which, as a rule, includes geotechnical investigations. For example recently adopted Russian Federal Law No 384-93 regarding safety of buildings and structures has complicated the tasks associated with numerical modeling, as it requires account of "plastic and rheological properties of soils and construction materials".

The existing modern software complexes making numerical calculations do not always consider these particularities. Moreover, commercial software largely used in the global practice of construction design not always can confirm data obtained at real sites concerning actual strain-stress behaviour of buildings and structures. In a number of cases, software becomes a "black box", whereas a geotechnical engineer involved in calculations is not able to be an active participant of simulation. Application of soil models which are not tested and adapted to geotechnical conditions of a certain area is a factor of excessive risk for high-level responsibility of structures.

As regards new projects and preservation of the unique objects where there are actual data on differential settlements of their parts, good software for numerical simulation should at least predict these deformations. As for damaged buildings requiring reconstruction, such software should take into account actual strain-stress state at the moment of planned reconstruction.

In order to overcome these considerable shortcomings, authors from different countries have been developing and applying models of soil behavior which allows describing nonlinear soil deformation in time.

These models must be scrupulously verified in dozens of sites subjected to instrumented monitoring.

The proceedings of the two workshops include contributions of 36 authors from 11 countries. We hope that the proceedings will be useful for experts in the field soil-structure interaction and retaining structures.

Michael Lisyuk	Vladimir Ulitsky	Deepankar Choudhury
Chair of TC207	Past Chair of TC207	Secretary of TC207

St. Petersburg – Mumbai
27 April, 2016

MEMBERS OF TECHNICAL COMMITTEE 207
"SOIL-STRUCTURE INTERACTION AND RETAINING WALLS"
ISSMGE

Michael Lisyuk, Chairman, *Russia*
Vladimir Ulitsky, Past Chairman, *Russia*

Deepankar Choudhury, Secretary, *India*

William Van Impe, *Belgium*
Konstantin Shashkin, *Russia*
Chris Haberfield, *Australia*
Yasser El-Mossallamy, *Egypt*
Rolf Katzenbach, *Germany*
Hugh St. John, *UK*
Rich Finno, *USA*
Fang Liu, *China*
J. Kos, *Czech & Slovak Republics*
Kari Avellan, *Finland*
Catherine Jacquard, *France*
Olivier PAL, *France*
James Sze, *Hong Kong*
Venkataram Balakumar, *India*
G. Madhavi Latha, *India*
N.K. Samadhiya, *India*
Omar al-Farouk Salem al-Damluji, *Iraq*
H. Hazarika, *Japan*
Ohsumi Tsuneo, *Japan*
Mandy Korff, *Netherlands*
G. Horodecki, *Poland*
Florian Roman, *Romania*
Z.G. Ter-Martirosyan, *Russia*
Victor CW Ong, *Singapore*
A.R. Walker, *Singapore*
Paul Morrison, *UK*
Igor Sokolić, *Croatia*
Juan Manuel Fernández Vincent, *Argentina*
Omer Bilgin, *USA*
Jan Couck, *Belgium*
Claudio di Prisco, *Italy*
Guido Gottardi, *Italy*
Amir M. Kaynia, *Norway*
Balazs Moczar, *Hungary*
Javier Moreno, *Spain*
Pantelis Pantelidis, *Greece*
Lars Vollmert, *Germany*
Werner Bilfinger, *Brazil*
Arnoldas Norkus, *Lithuania*
Gökhan Baykal, *Turkey*
Talal Awwad, *Syria*

Askar Zhussupbekov, *Kazakhstan*
Doda Enver, *Albania*
Yuan Huina, *China*
Horatiu Popa, *Romania*
Castorina Silva Vieira, *Portugal*
Mehmet Berilgen, *Turkey*
Deniz Ulgen, *Turkey*
Alexandra Ene, *Romania*
Nuno Guerra, *Portugal*

CORRESPONDING Members

Lei Lou, *USA*
Kiyota Takashi, *Japan*
Atsuko Sato, *Japan*
Khoa Van Nguyen, *France*
Hamza Gullu, *Turkey*
Onder Akcakal, *Turkey*
Müge İnanir, *Turkey*
Ozgur Bezgin, *Turkey*
Mete Erdemgil, *Turkey*

Webmaster

Eugene Dubinin, *Russia*

FRIENDS of TC207

Regina Dashko, *Russia*
Anna Shidlovskaya, *Russia*

TABLE OF CONTENTS

Kari Avellan & Belopotocanova Erika
Soil deterioration, slope failure in relation to trenching, trench pipe design and public safety.....1

Talal Awwad & Donia Modar
The geotechnical effect of existence high permeable thin soil layer at different depths in the foundations of an embankment dam.....9

Alexandra Ene, Dragos Marcu & Horatiu Popa
Complete Approach of Deep Excavations.....19

Nuno M. C. Guerra, Cláudia M. S. Josefino & Armando N. Antão
Overall stability of anchored retaining walls: revisiting Brom's method.....25

Chris Haberfield
Foundation considerations for two tall towers.....33

Hemanta Hazarika & Netra Prakash Bhandary
Overview of the Damage and Lessons Learned from the 2015 Nepal Earthquake.....46

Juan Manuel Fernandez Vincent, Freddy Lopez Loayza & Sergio Diaz Casado
Monitored deep excavation in the Ripio de Santiago de Chile.....62

Rolf Katzenbach & Steffen Leppla
Tunnelling in the vicinity of sensitive structures.....68

A.K.M. Lam & J.W.C. Sze
Piled Raft Foundation Design for a Supertall Tower Underlying by Complex Ground Condition.....75

S. Marchetti
Flat dilatometer (dmt). Applications and recent developments.....83

S.S. Nimbalkar & D. Choudhury
Design of earth retaining structures and tailing dams under static and seismic conditions.....93

N.K. Samadhiya & A.K. Singh
Influnce of seepage force on active and passive thrust for design of a rigid cut-off wall.....103

Ikuo Towhata
Construction of underground walls in urayasu to mitigate liquefaction damage and in Fukushima no. 1 nuclear power plant to stop radioactive leakage.....128

V.M. Ulitsky, A.G. Shashkin & M.B. Lisyuk
Use of piles in complex reconstruction of cities 133

Shi Zheng, Fang Liu, Mingjing Jiang, Haoyu Sun, Yutai Liu, Hiroaki Nakayama, Shinji Taenaka & Atsushi Kato
Evolved earth pressure during excavation against a combined sheet pile wall enhanced by H sections: Centrifuge test.....147

Soil deterioration, slope failure in relation to trenching, trench pipe design and public safety

Avellan Kari & Belopotocanova Erika
KAREG Consulting Engineers, Helsinki, Finland

Abstract: Deterioration is one of the major factors governing the stability of slopes in stiff overconsolidated clays and clay shales. It is always a predisposing factor responsible for a time-dependent weakening of the soil. When combined with other factors such as human activity, it can cause a slope collapse. Excavation and trenching are among the most hazardous construction operations. Trench collapses can occur in any soil and account for a large number of worker deaths each year. It is crucial to identify soil types, its condition, and understand the challenges of trenching. Suitable design is key to trench integrity and needs to be considered early within construction projects so that adequate costs and schedule are allowed for construction, and guarantees the safety of the workers.

Keywords. soil deterioration, slope collapse, trench pipe design, fissured clay, unbraced trench, public safety

1. GEOLOGICAL BACKGROUND

The natural environment has been undergoing changes for millions of years. Earthquakes, volcanic action, glaciers, floods, wind action and climatic factors, variable erosion, depositions produce the soil cover on the Earth´s crust, which is derived from the underlying rock. Aside natural forces, human activity has also vastly contributed into ever changing form and shape of the landscape.

1.1. Relations between soil deterioration and slope failure

Although the above-mentioned natural factors together with human activities are considered the main cause of landslides, the slope failure, on the other hand, especially in hard clays and clay shales, it may occur suddenly without an apparent reason. It is assumed that the most common trigger is the increase in pore pressure (or decrease in suction) caused by rainfall since the majority of landslides occur during the wet seasons.

That does not necessarily mean that the consequence is instant or happens within a short period of time from the cause. Often, the process is initiated in the past. In some cases, it could have been set off undetected by damaging the soil structure as the after-effect of local failure. If the process involves the entire volume of soil above the assigned depth, the mechanical parameters provided by relatively recent tests are likely consistent with the actual safety factor of the slope. On the other hand, if the process is relatively fast, the data collected even recently can provide misleading information. If the deteriorated zone is limited to a particular part of the slope or of the trench only, the risk that in-situ and laboratory tests do not provide reliable data for the slope analysis is much higher.

2. MECHANISM, CAUSES AND EFFECTS OF SOIL DETERIORATION

For simplicity, the process of soil deterioration is classified into two main categories: mechanical and physio-chemical.

2.1. Mechanical process of deterioration

Mechanical deterioration is caused by stress changes and associated shear and/or volumetric plastic strains that cause breaking of bonds, increase of water content and possible modification in the arrangement of soil particles. Mechanical deterioration may also include formation of fissures and cracks. Plastic sheer strains can be responsible for a radical change in soil structure. So-called “sheer zones” represent weak zones in overconsodidated clay deposits.

The mechanism of deterioration set off by shear is also known as strain-softening. Firstly, it

causes destructuring and consequently vanishing of the true cohesion (Figure 1).

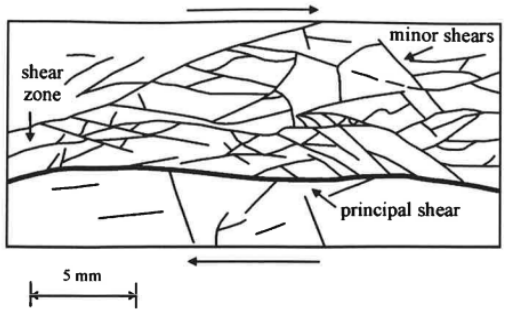

Figure 1. Shear zone (Skempton &Petley 1967).

2.2. Physio-chemical process of deterioration

Any change in pore fluid composition can greatly influence the mechanical behavior of clay soils. In particular, a reduction in pore water salinity can produce a dramatic decrease in shear strength. Remarkable effects of such a decrease are exhibited by landslides in quick clays. These are sensitive marine clays deposited at the end or after the last glaciation (Figure 2).

Figure 2. General location of European glaciation.

In Europe the most dangerous quick clays are situated on the Atlantic coast of Norway and southern Sweden. As a result of the uplift caused by the retreat the glaciers, some deposits were subjected to freshwater leaching and consequently to the decrease in ion concentration of pore solution. In the middle Finland there are clay layers consisting of stiff Anculys-clay layer ($c_u >$ 40kN/m^2) on soft Yoldia-clay ($c_u \leq$ 20kN/m^2). The reason of stiff figured Anculys-clay is due to ice time and due to rising of the earth (Figure 3).

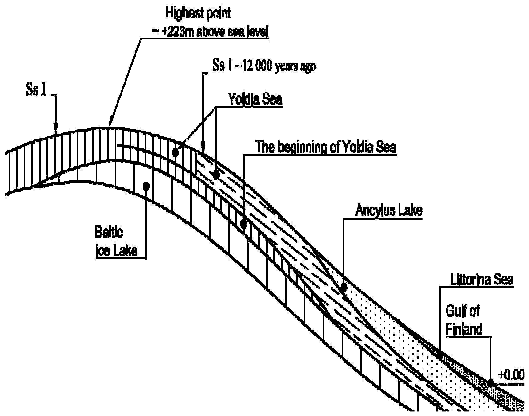

Figure 3. Stratigraphic distribution of clays in South Finland. Ss I – the Yoldia clay is homogenous or sedimentary while north of Ss I is diatactic.

2.3. Soil types, properties and condition

Different soil types behave differently, depending on the immediate condition of the soil. The type of the soil determines the strength and stability of trench walls. Identifying soil types requires knowledge, skill and experience. This knowledge must include awareness that soil types and conditions can change over very short distances. Even hard soil may contain faults in seams or layers that make it unstable when excavated.

3. TRENCH PIPE DESIGN

There are many types of trench, suited to different purposes and soil conditions. Geotechnical aspects of pipeline trench design include:

- Trench base stability
- Trench wall stability
- Influence of spoil pile
- Influence of equipment track pressure
- Minimum required width of right of way arising from trench depth, width and spoil heap
- Trench width

3.1. Trench wall stability design

The main factors influencing trench side slope stability include:

- Ground water level
- Trench width undrained shear strength, or soil angle of friction
- Trench depth and side slope inclination
- Distance between toe of the spoil pile to the top edge of the trench and the height (or surcharge) of the spoil
- Equipment track pressure together with the distance from the track to the trench
- Dynamic vibration impact from equipment
- Season that work is being carried out in (wet, dry, frozen ground, season)

Based on clay soils as an example, for a clay soil with the average of undrained shear strength of about 12 kPa, unstable conditions may occur unless the trench has a slope inclination of greater than 45º, and if the spoil is located approximately 1 m away from the edge of the trench.

The angle and the height of the spoil pile also needs to be adequately designed and specified to ensure that spoil does not collapse towards the trench thus comprising the trench itself.

When the upper slope material is stiff clay, the compatibility between overlying stiff clay and underlying soil material has to be assessed (Subchapter 4.1.1).

Common engineering practice is to predict possible tension cracks in slope-stability engineering for predicting safety factor of existing slope or to calculate safety factor for new excavation (Figure 4 and 5).

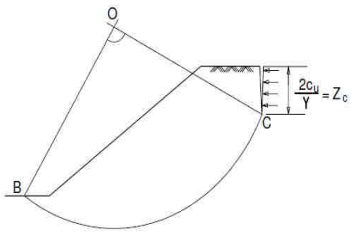

Figure 4. Tension cracks, existing slope.

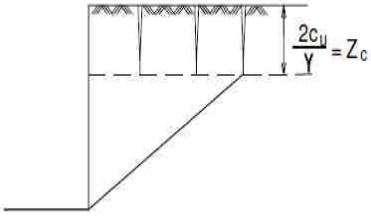

Figure 5. Tension cracks, new trench

Calculation examble of the author on unbraced pipe trench can be found in reference (2).

3.2. Trench width design

A number of factors guide the trench width, such as safety, soil characteristics, outer pipe diameter, trench depth, minimum available width of excavator bucket, type of crossings, and any special purpose requirements. In turn, the trench width affects the loading on the pipe.

Together with the trench depth and characteristics of the fill over the pipe, the trench width will produce the load which must be supported by the pipe and its bedding. Generally speaking, the wider the trench, the greater the load on the pipe. Beyond a certain point this effect stops and widening the trench further does not impact the loading on the pipeline anymore.

3.3. Trench depth design

Pipelines are often buried under locations where human activity is intense. In areas where vehicle crossing is likely or certain (under a road or track, or under farm land), it can be necessary to bury the pipe at an increased depth.

The load exerted on the pipeline by the soil cover can be beneficial for the pipeline system as it can be used to lock the pipe into place and mitigate adverse pressure and temperature effects. The load on a buried pipe is created by the weight of the soil lying above it as well as the above-ground loading. Increasing the trench depth increases the soil load but reduces the traffic load, as illustrated in Figure 6.

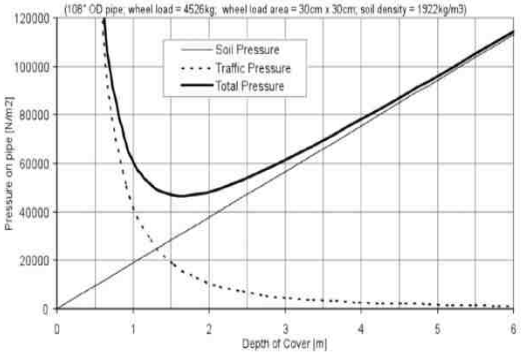

Figure 6. Soil and traffic loading pressure Vs cover depth to top of pipe.

Trench design is key to trench integrity and needs to be considered early within construction projects, so that adequate costs and schedule are allowed for pipeline construction.

Guaranteeing the trench integrity is essential for the safety of the workers in and around the trench as well as being necessary for the completion of construction.

4. TRENCH PIPE INSTALLATION AND CHALLENGES

In most instances, problems arise during open cut trench excavation work due to unfavorable soil and groundwater conditions, excavation procedures, foundation and bedding requirements, or backfill compaction requirements.

4.1. Trench excavation problems

Trench excavation can be undertaken, without significant problems in most types of soil, provided the water table is below the trench base. On the other hand, where excavation is attempted below a high water table, the considerations are very different. Before attempting to excavate, the location of the groundwater level and the soil type should be determined. It is very important to define these two parameters during a borehole investigation and test pit or trial excavation before the design and construction stages.

In consolidated clayey soils, the groundwater level for normal service pipe installation is not important. Since the soil is virtually impervious, even with a high groundwater level, excavation will be relatively straightforward, since negligible or no groundwater will enter the excavation area.

In sand, it is normally accepted that excavation to the groundwater level will be straightforward. In most instances, it should be possible to excavate approximately 300 mm below the groundwater level using perimeter ditches and filtered sump pumps. If the sand is very fine, then the temporary excavation may be extended to approximately 600 mm below the groundwater level.

Under these circumstances, it is suggested that the installation be undertaken in as short a section as practical, i.e. short trench length excavated, the service pipe installed and then backfilled before the next section is excavated.

Attempts to excavate trenches more than 300 mm below the groundwater level in a sandy soil is a problem. At many sites, the natural groundwater level is 1 to 2 m below ground surface. Thus excavation in wet sands to depths in excess of about 2 to 3 m require either wellpoints or sheeting. Wellpoints lower the groundwater level and therefore, the wellpoint tips should extend to a depth of at least 2 m below the proposed trench bottom. Sheeting, on the other hand, does not lower the water table. However, it prevents collapse of the trench sides and quick conditions of boiling of the base, when adequately designed and installed. A geotechnical engineer and a specialist dewatering contractor should be retained for this work.

The performance of excavations in wet silts is extremely difficult to predict. Several deep excavations have been undertaken without having to resort to sheeting. Wellpoints are not normally effective in dewatering very fine silts since they have very low permeabilities.

4.1.1. Mechanism of new cracks due to excavation

Figures 7 and 8 visually demonstrate the mechanism of new cracks due to excavation in different types of soil. No cracking occurs provided the overlaying material is either gravel or sand.

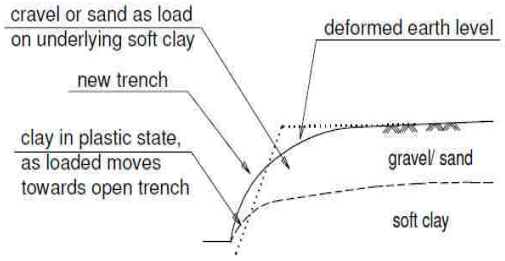

Figure 7. Visual demonstration. Upper layer consists of gravel or sand. No cracking due to excavation.

However, if the upper layer consists of stiff fissured clay that loads the underlying soft clay, new cracks are likely to develop (Figure 8).

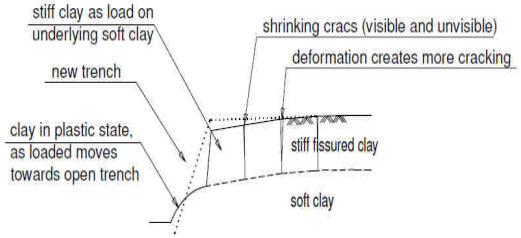

Figure 8. Visual demonstration. Overlying material stiff clay. New cracks due to excavation.

4.2. Trench stabilization

The need for stabilization to firm up the base of a service trench prior to placing the pipe bedding is generally a function of the type of soil and the groundwater levels, and to some extent, the expertise of the contractor. In most areas, the soil in trench bases will tend to be easily disturbed, particularly in excavations slightly below the water table in sands without using well points, or in soft clays, or loose wet silts. The disturbance to the soil in trench bases can be increased with the continual passage of workers and equipment, i.e. the trench base in wet silt becomes liverish.

Often, success has been achieved with clear stone, since it is heavy and its angular fragments bind and cement together to produce a firm base. A 50 mm clear stone is suggested for this purpose in most instances. A 150 mm layer is adequate. Well graded Granular A,B or C materials do not normally provide a good material to stabilize the trench base because of the large percentage of finer material which becomes unstable when wet. A common practice is also to use geotextiles and coarse well graded gravel.

4.3. Trench backfill

Trench backfill is compacted in order to improve its properties and, in particular, to increase its strength and supporting properties, as well as reduce its compressibility and thereby minimize settlement.

Trenches are backfilled to the subgrade level with approved excavated native soil previously excavated from the trench to reduce differential heaving.

The effects of non compacted backfill in trenches should be considered. Studies have been performed on the amount of settlement associated with compacted fills. It can be assumed that any fill compacted to a minimum value of 95 percent Standard Proctor density will not result in settlement of any appreciable magnitude. Fill compacted to a lesser degree, say 90 percent may result in settlement as follows:

$$\frac{H}{A}(95\% - \text{actual compaction } \%) \quad (1)$$

where, H = total depth of loose fill, and A = 1 or 2 for various soil types

Pipe trenches, which cross both peat and bedrock require adequate transition zones to minimize differential settlement of pipes.

5. DANGERS OF TRENCHING

Excavation and trenching are among the most hazardous construction operations.

Trench collapses can occur in any soil and account for a large number of worker deaths each year.

In Finland around 40% of deadly work accidents occur in the field of civil engineering. There are reported between 1-3 deadly accidents per year caused by collapsed trenches (Figure 9). Number of serious accidents is much higher.

A safe trench or excavation must adhere strictly to all plans and specifications. Soil conditions must be monitored for changes and location of all existing utilities is mandatory.

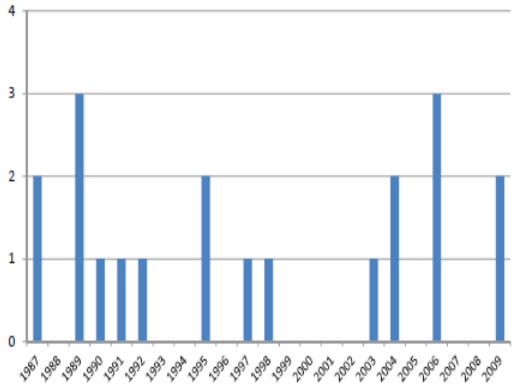

Figure 9. Reported deadly accidents in trenches in Finland.

6. ACCESS AND SAFETY

Trench safety is of paramount importance to ensure that those working in the trench are safe and protected from trench collapse and trench flooding. Like all construction activities, pipeline construction can potentially be dangerous to workers.

If the walls of the trench are not supported there is the possibility that the walls will collapse and trap the workers in the trench. However, very high safety standards can prevent most accidents and result in a very safe working environment. Safety codes on the national, regional or municipal level as well as training and education greatly contribute to high safety standards and prevent injuries and accidents.

6.1. Unbraced trench guidelines and regulations

European countries have their own regulations or codes concerning human risks, risk-to-life categories in unbraced pipe trenches. The codes however refer to general guidelines, such as height of trench, soil-material, slope angle, distance of excavator from upper slope rand, workload of excavator, the type of excavator, weight of stored material near the rand slope etc.

An example of one of the most comprehensive codes is DIN 4124 (Germany), where most of the above-mentioned parameters are clarified in a practical way (Figure 10).

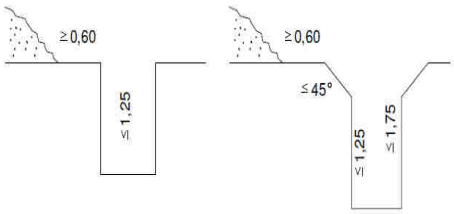

Figure 10. Extract from German code DIN 4124.

This Code, for example, specifies that the maximum height of the unbraced trench is 1.75 m provided that undrained shear strength is > 25 kPa.

For trenches between 1.5 m and 6.0 m deep, shoring, by sheeting, by trenchboxes, by sheet-walls or by sloping by benches are acceptable protective measures.

In Finland, regulations concerning risks in trenches state that every trench with height > 2.0 m must be "braced", but the bracing system can consist of slopes and berms (Table 1). The trench must be designed by a geotechnical engineer. If there are workers in the trench, then the overall safety factor must be more than 1.5.

Table 1. Table 16200;T2. InfraRYL 2010, Finnish Code Of Building practice, Infrastructure.

Table 16200;T2. Unbraced, temporary trench. Maximum depth and slope angle. Su =undrained shearstrength

earth basis		slope angle					
		5:1	3:1	2:1	1:1	1:2	1:3
		maximum depth m					
IV	Very soft clay (Su=7...<10 kPa)	-	-	-	1,7	1,9	2,1
V	Soft clay (Su=10...<20 kPa)	1,6	1,7	1,9	2,3	2,5	2,7
VI	Stiff clay (Su ≥20 kPa)	2,0	2,5	3,0	3,2	3,7	4,0

Trench has to be predesigned if there is any risk of collapse and always when the depth is >2,0m.

6.2. Sloping and stepping

All trenches have what is known as a stand-up time. It is a function of the ratio between depth and width of trench.

At greater depths or in unstable soil, shoring, sloping, or stepping is required to improve the stability of the trench and its stand-by time. T-shaped sloping and stepping drastically increases the width of the trench at ground level as the depth of the trench increases.

6.3. Use of shoring, sheetwalls and trench boxes

Typical collapsing behaviors are shown in Figure 11 for different types of soft soils. Sandy soil will tend to collapse straight down, wet clays and loams tend to slab off the side of the lower trench. Firm, fairly dry clay tends to crack some distance from the trench wall. Wet sands and gravels tend to slide into the excavation at about a 45-degree angle.

In excavations where the open ditch method is not sufficient, trench walls likely to collapse must be supported by proper shoring to mitigate the risk of cave-in.

Shoring jacks, with or without sheeting, are a quick and efficient shoring system. For deep trenches and unstable ground, the best shoring system is either braced sheetwals or trench boxes depending on the stability of the trenchboxes an the ground water level (Figure 12). The primary concern is for safety, and all applicable regulations should be strictly observed.

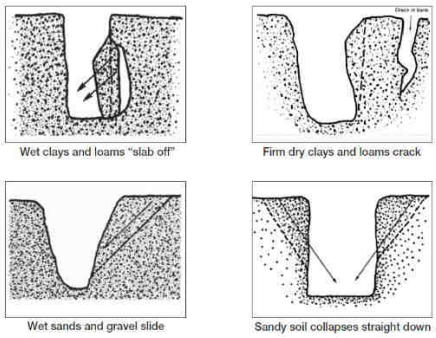

Figure 11. Collapsing of trench walls in soft soil.

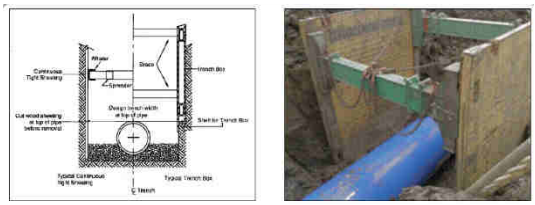

Figure 12. Shielding. Typical trench box.

6.4. Use of trench boxes, braced sheetwalls and professional responsibility

The public has become increasingly aware that industrial progress often has negative side effects. The place of engineers in protecting the public from these negative effects is a controversial issue.

The use of trench boxes on construction sites illustrates this debate. A trench box may be placed in the trench to prevent trench failures from injuring workers. Due to the added expense of using the trench box, many contractors are reluctant to use them.

When a construction project requires a large excavation, such as digging the foundation for a tall building, the support structure for the excavated walls should be specified in the plans. The main problem occurs in cities, when water or sewer lines are being installed or repaired. The engineer usually does not specify the support structure for the trench on the plans, but leaves that to the contractor.

7. SOCIAL RESPONSIBILITY VS LEGAL LIABILITY

Litigation associated with engineering design has escalated enormously over the last few decades, and has increased the intensity of debates over whether engineers and their companies should give priority to social responsibility or legal liability.

Liability is complicated by the fact that law typically lags behind social costs associated with failed design. This phenomenon has become particularly critical regarding litigation involving engineering design and product liability.

The responsibility of engineers in protecting the public from these side effects is the focus of a lively debate. This is intensified by the fact that legal liability and social responsibility may not always coincide.

7.1. Social responsibility for public safety

We strongly stand behind the statement that safety is a social, not a legal obligation, and that engineers and their managers must always keep their obligations to the public welfare at the fore when making design and management decisions.

Sometimes a cost/benefit analysis is not enough, especially when lives are at stake. The same duties apply to engineering design and management. Quality engineering is a necessity. This means there is a need for creative engineering and ethical corporate practice. When engi-

neers, managers, corporate owners, contractors, subcontractors and inspectors take pride in, and responsibility for their designs the entire engineering profession benefits.

8. SUMMARY AND CONCLUSIONS

Deterioration is always a predisposing factor that is responsible for a time-dependent weakening of the soil which, combined with other factors such as human activity, can cause a slope collapse, but in some cases it is the only factor that can explain sudden failures that are otherwise unexplainable.

Different soil types behave differently, depending on the immediate condition of the soil. The type of the soil determines the strength and stability of trench walls. Identifying soil types requires knowledge, skills and experience.

Trench design is key to trench integrity and needs to be considered early within construction projects, so that adequate costs and schedule are allowed for pipeline construction.

Excavation and trenching are among the most hazardous construction operations. Trench collapses can occur in any soil and account for a large number of worker deaths each year.

Trench safety is of paramount importance to ensure that those working in the trench are safe. High safety standards can prevent most accidents and result in safe working environment.

We firmly believe that safety is a social, not a legal obligation, and engineers and their managers must always keep their commitments to the public welfare a priority when making design and management decisions.

9. REFERENCES

Avellan, K. *Internal archive, Projects Database.* Helsinki: 2015.

Avellan, K. *UNBRACED PIPE TRENCH, STIFF FISSURED CLAY LAYER ON SOFT CLAY, ECSMGE 2015*, Edinburgh. Available at: http://www.kareg.com/konferenssi/ECSMGE-2015-TC-207_Kari_Avellan-16_9.pdf (Accessed: 3 October 2015).

Calcaterra, D. & Parise, M. 2014. *Weathering as a predisposing factor to Slope movements*. London: The Geological Society.

Donner, J. 1978. *Suomenkvartaali – geologia*. Helsingin yliopisto, pp. 100 -104.

Eronen, M. 1991. Jääkausien jäljillä. Helsinki: Tähtitieteellinen yhdistys Ursa.

German Code DIN 4124. 2012. *German National Code.* Berlin: Beuth.

Henley, G. & Hachfeld, E. 2011, 2012. Pipeline trench design. *The Road to Success.* Vol. 1 & 2.

Moorman, K. 1989. Does Ethical Engineering Practice Affect Creativity? *Civil Engineering (American Society of Civil Engineers).* Vol 59, pp 68-69.

Nesteruk, J. 1991.The ethical significance of Corporate Law. *Journal of Business Ethic.* Vol 10, No 9, pp. 723-727.

Picarelli, L. & Di Maio, C. 2014. Deterioration processes of hard clays and clay shales. *Geological Society, Engineering Geology.* Special Publication No 23, pp. 15 -32.

Rantanen, E. & Harju, M. & Norokorpi, L. & Uusitalo, J. 2013. Danger lurks underground - research project on excavation safety. *Investment steering. Finnish Transport Agency.* Vol. 9, pp. 4 – 11.

Sarafinchin, M. 2010, 2011. *Earth Engineering: Perspectives, Principles and Practices.* Bloomington: iUniverse.

Stone, D. 1975. *Where the Law Ends: The social control of corporate Behavior.* New York: Harper&Row.

The geotechnical effect of existence high permeable thin soil layer at different depths in the foundations of an embankment dam

Awwad Talal [*] [a], Donia Modar [b]

[*]Corresponding Author Email: *dr.awwad@ymail.com* (Dr. Awwad)

[a] *Department of Geotechnical Engineering, Faculty of Civil Engineering, Damascus University, Syria*
[b] *Ministry of water resources, Damascus, Syria.*

Abstract :

Many dam problems appeared in Syria during the last few years. These problems include differential subsidence, vertical cracks and full failure (Zeyzoun Dam 2002). The lack of Geotechnical investigations is the primary cause of these problems. That reason emphasizes the importance of analyzing the effects of lithological strata in dam foundations on dam stability. This paper is concerned with studying the effect of high permeable thin soil layer at different depths in the foundations of an embankment dam (Zeyzoun dam), taking into account that this layer reaches a minimum depth at failure sections of the dam. Geo-studio software is a Geotechnical program that is based on finite element method and analyzes numerical models of seepage, stresses, and slope stability. The results illustrate an increasing in fluxes in clay core and permeable soil layer, rising of phreatic line level in dam body, decreasing in factor of safety for slope stability, along with decreasing of permeable layer depth. These results confirm the influence of the change of permeable soil layer's depth on the downstream slope stability of the dam.

Key words: Slope stability, Seepage, Geo-studio, Safety factor, embankment dam.

NOMENCLATURE			
Layer 3-1	Permeable foundation layer	ϕ	friction angle
Layer 3-2	other foundation soils	ν	Poisson ratio <0.49
E	Young'Modulus (kpa)	ψ	Dilation angle
C	Cohesion (Kpa)	γ	bulk unit weight ($KN/m^{3)}$
K_o	Lateral earth pressure at rest	$PWP_{(i)m}$	Pore-water pressure when layer3-1 exists at the depth (i)

1. Introduction

In this paper, a seepage analysis in embankment dam and its foundations, has been performed for three study cases of coefficient of permeability to evaluate the influence of permeability coefficient, which are k= (1×10^{-4}, 4.5×10^{-5}, 4.5×10^{-6} m/s), the third one is the real case. Those values are related to the thin foundation soil layer with high permeability (layer3-1), thus seepage analysis aimed to investigate the relation between the phreatic line level in the dam body, the depth and permeability of layer3-1. Pore-water pressure obtained from the real case of permeability was included in a stress analysis to calculate the total and effective stresses in dam body and foundations. Consequently, the pore-water pressure and stresses are used to calculate slope stability factor of safety for different depths of the permeable layer using the finite element method. The results of the methods of Bishop, Janbu and Morgenstern-Price are used for comparison purpose only.

2. Seepage analysis

General seepage conditions have been assumed to perform the model. The conditions include that the reservoir head remains constant for a sufficient time to result in a stable flow regime (steady state condition), a total head difference of 36 m is the boundary condition of the seepage model, three coefficient of horizontal conductivity are adopted for the layer 3-1, these

coefficients varies from high permeable to moderate permeable case. The three cases of permeability help to give a good sense about the influence of conductivity factor on the values of flux and the level of phreatic line. The foundation layers are assumed to remain in the saturated status, thus a constant conductivity factor could be assigned for each layer. However the materials of the dam body are in the saturated/unsaturated status therefore a function of suction pressure and conductivity factor has been assigned to the materials of dam using Van Genuchten method, Figure (1).

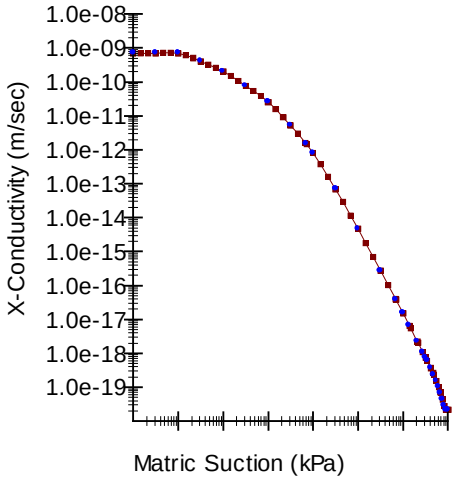

Fig (1) conductivity function of the clay core .

The analysis formulated on the basis that the flow of water through both saturated and unsaturated soil follows Darcy's Law which states that: Q=K*I

Where Q is the specific discharge, K is the hydraulic conductivity and I is the gradient of the total hydraulic head. Under steady-state conditions and for both saturated and unsaturated conditions, the governing differential equation used in finite element formulation, is:

$$\frac{\partial}{\partial x}\left(k_x \frac{\partial H}{\partial x}\right) + \frac{\partial}{\partial y}\left(k_y \frac{\partial H}{\partial y}\right) + Q = m_w \gamma_w \frac{\partial H}{\partial t} \quad \textbf{(1)}$$

By Applying the Galerkin method of weighed residual to the governing differential equation, the finite element equation for two-dimensional seepage, is:

$$[K]\{H\} + [M]\{H\},t = \{Q\} \quad \textbf{(2)}$$

Where:

[K]: the element characteristic matrix.

[M]: the element mass matrix.

{Q}: the element applied flux vector.

{H}: the vector of nodal heads.

t: time.

For a steady-state analysis, the head is not a function of time and, consequently, the terms {H} and t vanishes, reducing the finite element equation to the abbreviated finite element form of the fundamental seepage equation, Darcy's Law:

$$[K]\{H\} = \{Q\} \quad \textbf{(3)}$$

A seepage analysis was conducted for three study cases. Each study case includes a different coefficient of permeability K (1E-4 ,4.5E-5, 4.5E-6)m/Sec, that are assigned to the high permeable layer (layer3-1) located at different depths (32, 24, 16, 12, 8, 4, 2, 0) m, Figure(2). Figure (3) illustrates a simplified longitudinal section of the dam.

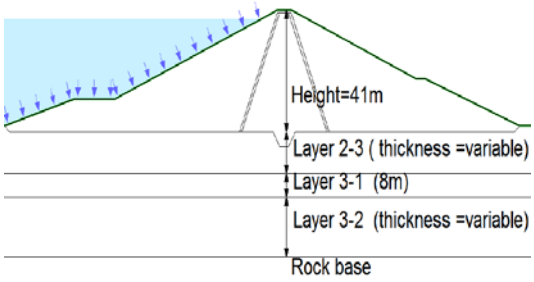

Fig (2) foundation strata of the dam .

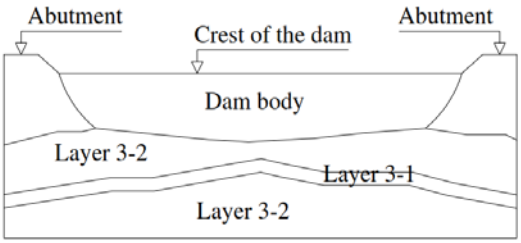

Fig (3) simplified longitudinal section of the dam and foundation.

The purpose is to estimate fluxes in clay core and layer 3-1 for each case and depth. The results showed that flux in the clay core increased along with decreasing of layer 3-1 depth for each study case.

There are no significant changes in clay core fluxes for different study cases, Figure (4). Fluxes in layer 3-1 increased along with decreasing in its depth until the depth of 4m, where the flux drops off to a value near zero at depth 0m. This observable fact can be justified by the function of the cut-off under dam clay-core, which approximately stops seepage in layer 3-1 at the depth of 0 m.

There are big changes in layer 3-1 fluxes for different study cases, Figure (5). Also phreatic line level rises along with decreasing of layer 3-1 depth (at a vertical section located at 45.5 m downstream of the dam), Figure (6).

The phreatic line level drops off at depth 0m due to the function of the cut-off, which means that this case does not present a good sense about the problem.

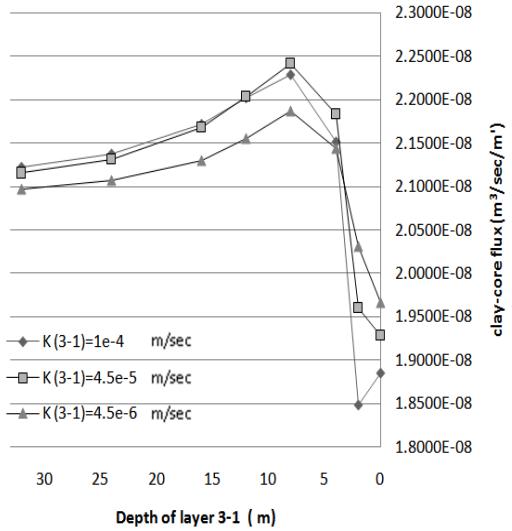

Fig (4) fluxes of the clay core VS layer 3-1 depths.

Therefore the case of layer3-1 at depth 0m will be ignored in the next analysis since it doesn't give reliable results for this paper. At the depth 2 m phreatic line level increases approximately by (11, 3.3, 1.8) m, for the study cases (K=1×10-4, K=4.5×10-5, K=4.5×10-6) m/s respectively. Phreatic line level increased due to increase of pore-water pressure in dam body and foundations. For example figure (7) shows phreatic line level in the case of layer3-1 at depths 32m and 2m.

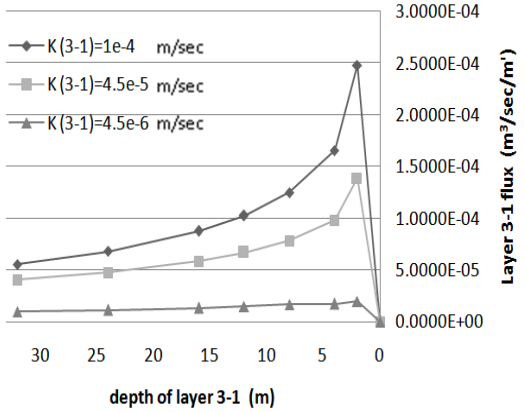

Fig (5) fluxes VS depths of layer 3-1.

Figure (8) indicates a comparison of pore water pressure distribution in a vertical section that is located at 17m down-stream the dam axis, between the three study case of permeability and for the layer3-1 located at the depth of 2m.

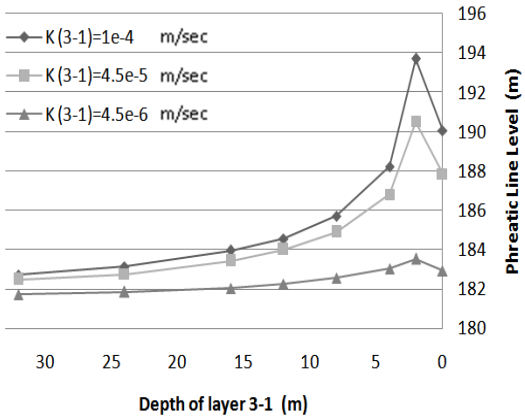

Fig (6) phreatic line level in the clay core VS layer 3-1 depths.

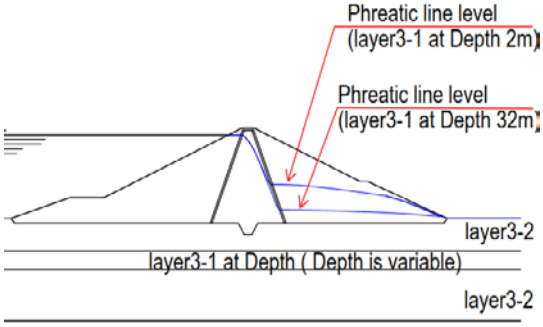

Fig (7) phreatic line level in the case of layer3-1 exists at the depths of 32m and 2m, K= 1e-4m/S.

The highest pore-water pressure values induced when layer 3-1 located at depth 2m. This figure shows that, pore-water pressure values increased in dam body and foundations when the coefficient of conductivity of layer3-1 augmented.

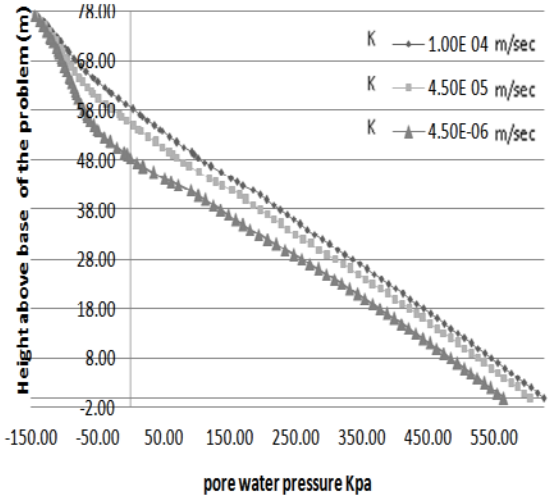

Fig (8) pore-water pressure VS the height, layer 3-1 locates at depth 2m

3. Stresses analysis

This analysis is performed taking into consideration the following: no external loads are applied in the initial analysis whereas the weight of the water in the reservoir is included in the later load/deformation analysis. Linear-elastic method is used for the initial analysis while linear-elastic and elastic-plastic methods are used for the load/deformation analyses. Boundaries conditions include fixed displacements in the horizontal and vertical directions for the base of the problem and fixed displacements in the horizontal direction for the lateral boundaries. The angle ϕ_B is used to make the cohesive strength a function of negative pore water pressure. Infinite regions are modeled at the both ends of the problem. These infinite regions make it possible to greatly extend the position at which the boundary conditions are effective. The problem of this paper is two-dimensional plane strain, thus the used software considers all elements to be of constant thickness t. the finite element is developed for stress/deformation analysis using potential energy, the finite elements equation is:

$$[K]\{a\} = \{F\} = \{F_b\} + \{F_s\} + \{F_n\} \qquad \textbf{(4)}$$

Where:

[K]:the element characteristic (stiffness) matrix.
([K]= t $\int$A ([B]^T [C] [B]) dA ,for plain strain problems).

{a}: nodal incremental displacements.

{F}: applied nodal incremental force which is made up of the following:

{F_b}: incremental body forces.

{F_s}: force due to surface boundary incremental pressures,
({Fs}= Pt $\int$L (N)^T dL ,for two-dimensional analysis).

{Fn}: concentrated nodal incremental forces.

t: time.

P: incremental surface pressure.

A: area along the boundary of an element.

(N): row vector of interpolating functions.

[B]: strain-displacement matrix.

[C]: constitutive matrix.

The used software will solves this finite element equation to obtain the displacements and calculates the resultant stresses and strains. It then sums the results of the initial analysis and load/deformation analysis, and reports the summed values in the output files.

Table 1. Geotechnical data

	E	C	ϕ	ϕ_B	ν	γ	γ	K_o	P_{wv}	P_{Dv}	P_{B1}	P_{B2}	P_{D1}	P_{D2}
clay-core	38000	73	11.5°	15	0.39	0-11.5°	20.3	0.64	0.5975	0.4833	0.0016	0.0519	0.0172	0.0233
Fill	27500	11.2	29°	15	0.238	0-29°	20	0.31	0.4820	0.4847	0.0034	0.0819	0.0212	0.0476
filter	3000	2	28°	15	0	0-28°	20.6	0	0.4660	0.4799	0.0055	0.1191	0.0264	0.0743
Layer 2-3	13000	39	15.43°	15	0.4	0-15.43°	17.7	0.67	0.3493	0.4749	0.0080	0.1641	0.0322	0.1054
Layer 3-1	32500	23	18°	15	0.31	0-18°	18.6	0.45	0.3322	0.3697	0.0111	0.2179	0.0381	0.1434

Initial analysis is very important to define initial total and effective stress distribution throughout the dam and foundations, and used as the initial status for the stress analysis.

Due to the simplicity of this analysis, it's useful and easy to check the accuracy of the obtained results, which is consequently valid for the following analysis. For total and effective stresses at 189m upstream the dam axis, the total stresses are the effective stresses plus the pore-pressure which is: U= 44m x9.81=431.64 Kpa. At the base of the problem:

σ_h = 284.04 x 0.67+ 70.32 x 0.45 + 431.64 = 653.59 Kpa.

σ_v = (17.7 – 9.81) x 36+ (18.6 – 9.81) x 8 + 431.64 = 786 Kpa.

Small differences exist between previous calculation and the values illustrated in figure (9) due to the weight of the embankment in the vicinity of the section. In the linear-elastic analysis and elastic-plastic analysis and in the case of vertical effective stresses calculation, pore-water pressure was subtracted from vertical total stresses under phreatic line (s'=s_t-u) ,and added to vertical total stresses above phreatic line (s'=s_t-(-u)) as illustrated in fig(10) , which is corresponded to the case of (K=4.5e-6 m/s-depth 32m) at a level of 204m .it can be noticed that vertical effective stresses are bigger above phreatic line.

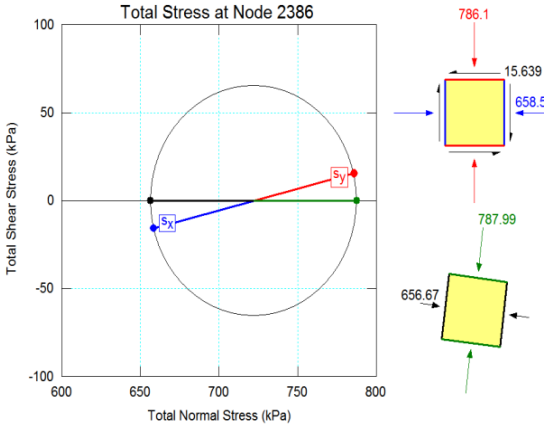

Fig (9) Mohr circle at the base of problem

by ignoring vertical effective stresses values in the range of x=(240 ► 260) m, which are related to another material (clay-core) with another bulk unit weight ,it can be noticed that effective stresses at level 204m are bigger above phreatic line than effective stresses under phreatic line, which is conform with the criterion mentioned above.

Comparison of vertical effective stresses data, for load/deformation analyses and for two depths of layer (3-1), shows that vertical effective stresses before (x=240) do not change with the change in layer 3-1 depth. However after(x=268), vertical effective stresses decreased along with layer3-1 depth decreasing, fig (11).

This will affect the stability factor of safety of the dam' downstream, as it will be shown later in slope stability analysis.

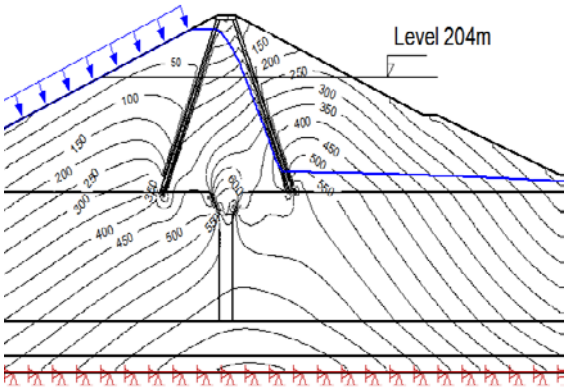

Fig (10) vertical effective stresses at level 204m. load/deformation analysis.

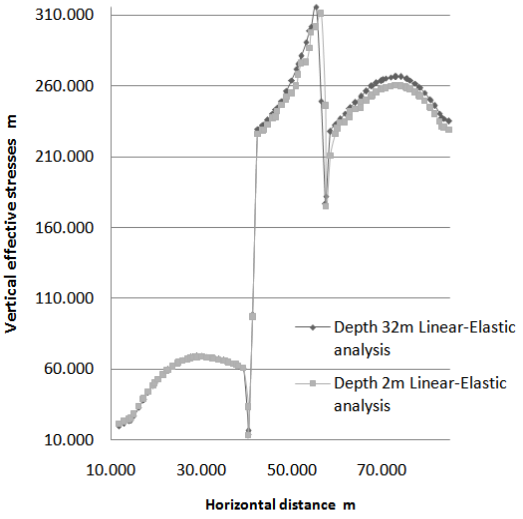

Fig (11) vertical effective stresses at level 204m VS distance, linear-elastic analysis.

4. Slope stability analysis

Slope stability analysis is performed taking into consideration the Weight of the water of the reservoir in addition to body loads. The pore water pressure is imported from the seepage analysis that is corresponded to the conductivity factor of K=4.5×10-6 m/s. The Stresses are imported from elastic-plastic load/deformation analysis to include it in the finite elements slope stability analysis. The stability factor (S.F) by the finite element stress method is defined as the ratio of the summation of the available resisting shear force S_r along the slip surface, to the summation of the mobilized shear force S_m along the slip surface In equation form. The stability factor (S.F) is expressed as:

$$S.F. = \frac{\Sigma S_r}{\Sigma S_m} \quad \textbf{(5)}$$

The available resisting force of each slice is calculated by multiplying the shear strength of the soil at the base centre of the slice with the base length, fig (11). Therefore, from the modified form of the Mohr-Coulomb equation for an unsaturated soil the available resisting force is:

$$S_r = s\beta = \left(c' + \left(\sigma_n - u_a\right)\tan\phi' + \left(u_a - u_w\right)\tan\phi^b\right)\beta \quad \textbf{(6)}$$

Where:

S = effective shear strength of the soil at the base centre of a slice.

b = base length of a slice.

s_n = normal stress at base centre of a slice.

Similarly, the mobilized shear force of each slice is calculated by multiplying the mobilized shear stress (τ_m) at the base centre of the slice with the base length.

$$S_m = \tau_m \beta \quad \textbf{(7)}$$

A local stability factor of a slice can also be obtained when the available resisting shear force of a slice is compared to the mobilized shear force of a slice.

$$Local\ S.F. = \frac{S_r}{S_m} = \frac{s\beta}{\tau\beta} \quad \textbf{(8)}$$

The normal stress (σ_n) and the mobilized shear stress (τ_m) are computable values from the previous load/deformation analysis. A comparison is made later between the results of the finite elements slope stability and the limit equilibrium analyses. The purpose of this paper is to detect the effects of phreatic line level changes due to decreasing depth of layer 3-1, on the factor of safety of slope stability. Therefore any interference of other parameters such as shear strength of layer 3-1, could provide

misleading results taking into account that Shear strength of layer 3-1, is bigger than shear strength of other soils (layer2-3) .To avoid this misleading results, a fully specified slip surface passing through the dam body and above foundations surface, is used to calculate the factor of safety for different depths of layer 3-1 and for the different analyzing method. As mentioned earlier in stresses analysis, vertical effective stresses are calculated from vertical total stresses and pore-water pressure, under phreatic line ($\sigma'=\sigma_t-u$), and above the phreatic line ($\sigma'=\sigma_t-(-u)$). This criterion means that positive values of pore water pressure under (phreatic line) have a destabilizing effect on the sliding mass. On the other hand negative values of pore water pressure (suction) have a stabilizing effect on the sliding mass above phreatic line. When depth of layer 3-1 decreased, phreatic line level increased as illustrated in seepage analysis, and Due to fixed slip surface a larger part of the sliding mass become under phreatic line, as it's shown in fig(12).

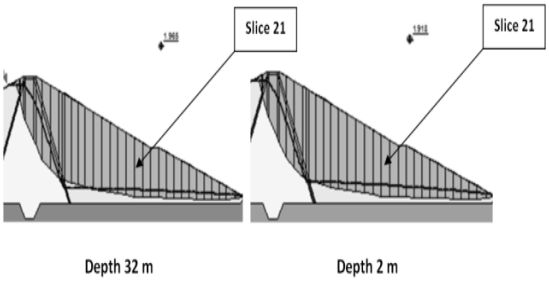

Fig (12) the sliding mass of the layer 3-1 when it exists at the depth of 32m and 2 m .

Fig (12) illustrates that larger part of the sliding mass become under phreatic line, thus pore-water pressure will generate a bigger destabilizing forces and smaller stabilizing forces. Taking as an example slice21 located at 84m downstream of dam axes, the inter-slice forces are: the normal and shear forces acting in the vertical faces between slices, the cohesion force which is cohesion strength multiplied by base length. A comparison of the forces shows increasing in destabilizing forces (pore water force), and decreasing in stabilizing forces (side shear forces- base shear resistance force- base normal fore), however weight remains invariable. (Results at depth 0m are not significant due to the influence of cut-off under dam base), fig (13) fig 14(a-b-c-d).

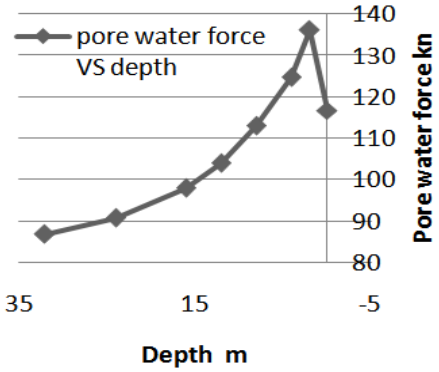

Fig (13) pore water force VS Depth.

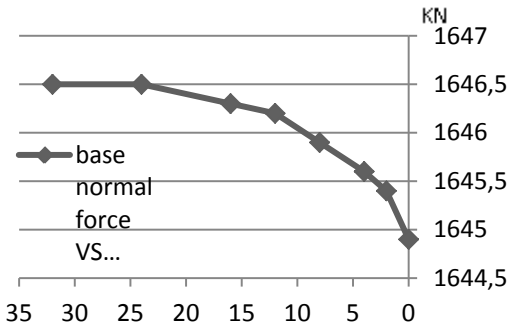

Fig (14-a) Base normal force VS change in depth of layer 3-1.

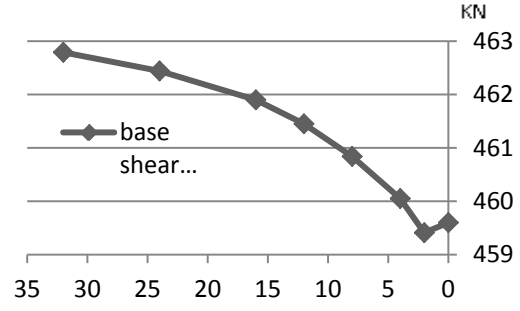

Fig (14-b) Base shear force VS change in depth of layer 3-1.

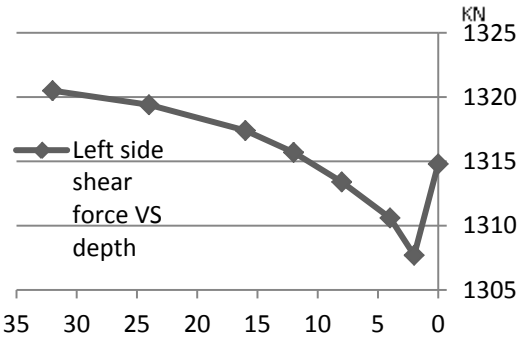

Fig (14-c) Left side shear force VS change in depth of layer 3-1.

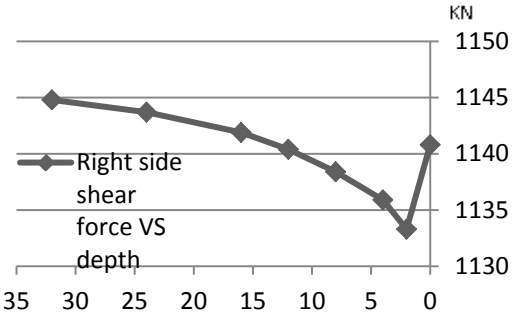

Fig (14-d) Right side shear force VS change in depth of layer 3-1.

The changes of forces applied on slices of sliding mass due to decreasing of layer 3-1 depth, results in reduction of factor of safety of slope stability.

FS values at depth of 0m are insignificant due to the influence of cut-off, Fig 15(a-b-c-d). It can be noticed from figure (15-a) - FS finite element method, that slope stability factor of safety increased when depth changes from 32 m to 24m, then decreased gradually along with depth decreasing.

This phenomenon showed-up only in FEM method due to soil stresses inclusion in slope stability analysis, while they are not included in other analysis method. Hence, when the depth of layer 3-1 decreased from 32m until 24m, only a small change can be noticed in phreatic line level, however when depth decreased from 24m until 16m the changes in phreatic line level will be bigger ,fig(6).

Depending on the last ideas, it's important to compare the differences in PWP (positive PWP-under phreatic line) ,and suction (negative PWP-above phreatic line) for the cases of depth changing from 32m to 24m (PWP_{32m}-PWP_{24m}), and from 24m to 16m (PWP_{24m}-PWP_{16m}), at a vertical section passing through slice 21 figure (12).

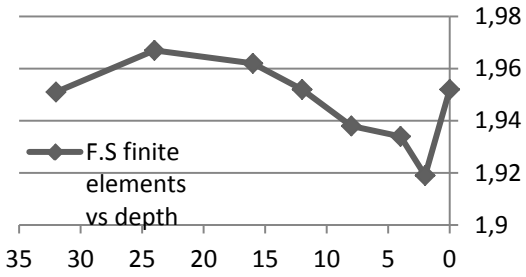

Fig (15-a) Finite elements factors of safety VS layer 3-1 depth.

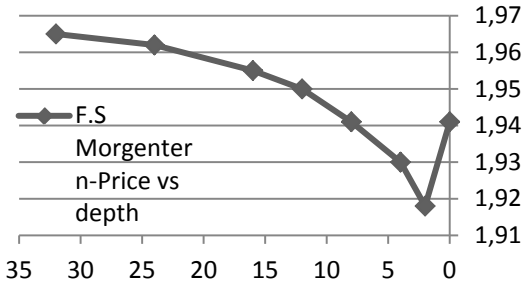

Fig (15-b) Morgenstern-Price factors of safety VS layer 3-1 depth.

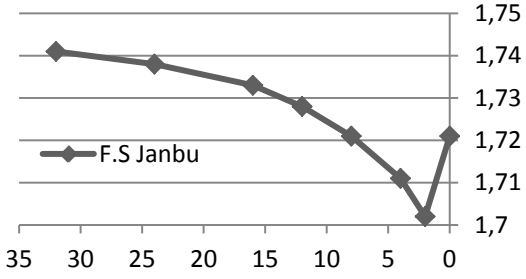

Fig (15-c) Janbu factors of safety VS layer 3-1 depth.

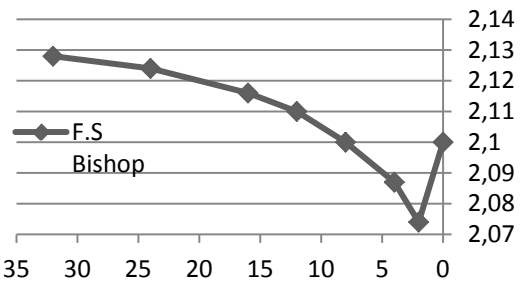

Fig (15-d) Bishop factors of safety VS layer 3-1 depth.

It is useful to compare differences of PWP values under an approximated level of 181.5m (where PWP has positive values) and the values above 181.5m (where PWP has negative values-suction), figure (16).

It can be noticed that values of (PWP_{32m}-PWP_{24m}) are lesser than (PWP_{24m}-PWP_{16m}) under phreatic line level, this means that the increasing in destabilizing forces in the case (PWP_{32m}-PWP_{24m}) is lesser than the case (PWP_{24m}-PWP_{16m}), Which is contrary to the case above phreatic line level. This is the reason that F.S of slope stability increased for depth changes from 32m to 24m then decreased steadily along with depth decreasing.

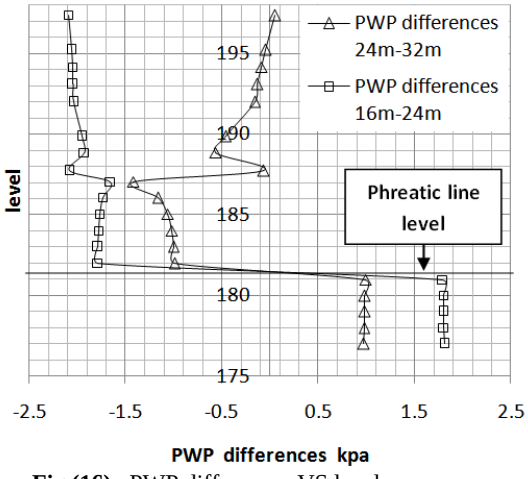

Fig (16) PWP differences VS level.

5. Conclusion

In embankment dam design, it is important to take into account the existence of a high permeable soil layer in dam foundations due to its significant effects on dam stability. The study proves that:

(1) Phreatic line level rises in the dam body because of decreasing in permeable layer depth, which is resulting in two effects. The first is increasing in total fluxes, pore-water pressure, and destabilizing forces in dam body. The second is decreasing in stabilizing forces and factors of safety.

(2) The minimum FS is more than /1.7/.

(3) The results substantiate the negative effect of the existence of a high permeable soil layer in Zeyzoun dam foundations on its stability under static conditions, although it is not the main cause of dam failure.

6. References

1. Bathe, K-J. 1982. Finite Element Procedures in Engineering Analysis. Prentice-Hall.
2. Bishop, A.W. and Morgenstern, N., 1960. Stability coefficients for earth slopes. Geotechnique, Vol. 10, No. 4, pp. 164 169.
3. Bettess, P. 1992. Infinite Elements. Penshaw Press.
4. Childs, E.C., and Collis-George, N., 1950. The Permeability of Porous Materials. Proceedings of the Royal Society, pp. 392-405.
5. Janbu, N. 1954. Applications of Composite Slip Surfaces for Stability Analysis. In Proceedings of the European Conference on the Stability of Earth Slopes, Stockholm, Vol. 3, p. 39-43.
6. Hasani, H., Mamizadeh, J., and Karimi, H. 2013. Stability of Slope and Seepage Analysis in Earth Fills Dams Using Numerical Models (Case Study: Ilam DAM-

Iran). World Applied Sciences Journal 21 (9): 1398-1402.
7. Morgenstern, N.R., and Price, V.E. 1965. The Analysis of the Stability of General Slip Surfaces. Geotechnique, Vol. 15, pp. 79-93.
8. Kokaneh, S.P. et al. 2013. Seepage evaluation of an earth dam using Group Method of Data Handling (GMDH) type neural network: A case study. Scientific Research and Essays Vol. 8(3), pp. 120-127.
9. Van Genuchten, M. Th. 1980. A closed-form equation for predicting the hydraulic conductivity of unsaturated soils. Soil Science Society of America Journal 44:892-898.

Complete Approach of Deep Excavations

Alexandra Ene & Dragos Marcu
POPP & ASOCIATII INGINERIE GEOTEHNICA, Romania

Horatiu Popa
TECHNICAL UNIVERSITY OF CIVIL ENGINEERING BUCHAREST, Romania

Abstract: The present paper presents the logical relation between the activities and competences necessary for the geotechnical designer today in order to offer efficient solutions. The process is however an iterative one and it involves deep understanding, involvement and also gathering a large experience based on accurate and complete input data from ground investigations, numerical and experimental models, field registers and monitoring data.

The authors propose a working manner they achieved during the time for a complete approach of deep excavations.

Keywords. deep excavations, soil-structure interaction, efficient design, models, monitoring data, database, back-analysis

1. INTRODUCTION

1.1. Scope of the paper

The geotechnical design process involves gathering comparable experience within similar parameters: soil conditions, execution technologies, natural hazards etc.

Throughout the time, based on a large experience on design of deep excavations, the authors understood that in order to identify good quality and feasible solutions it is necessary to adopt a complex approach, starting with good identification of the geotechnical parameters, understanding the behavior of the structure and the possible actual situations, choosing the appropriate numerical and soil model, receiving actual information during execution by actively assisting on site and through monitoring works.

All the above should lead to comparisons between theory and reality, interpretations on the actual behavior, re-calculations of the structure and re-consideration of the input data.

Hence the authors present the concept of *complete approach of deep excavations* that they consider it should be followed by as many practitioners designing deep excavations and other geotechnical works in order to achieve more accurate results, more rational and economical design without increasing the risks associated with the design and execution of deep excavations.

1.2. Brief description of the working team

Popp & Asociatii is one of the most famous company in the structural design field in Romania with a vast portfolio of civil buildings, representative for our country, some of them awarded at the National and European level.

Figure 1. Photographs of representative buildings designed by Popp & Asociatii

Because most of these buildings are concentrated in a dense populated urban area, they are often tall and require several basements performed in deep excavations. Throughout the

time, for an effective design of the deep excavations, the company felt the necessity of a specialized team, focused on geotechnical design field. This is now *Popp & Asociatii Inginerie Geotehnica* (PAIG).

Figure 2. Examples of deep excavations designed by Popp & Asociatii Inginerie Geotehnica

Popp & Asociatii Inginerie Geotehnica has become one of the most important company of consultancy and design of geotechnical works.

Throughout the design activities we rely on close collaboration with specialists, researchers and academic professors of different specializations including geotechnical engineering. Research is also an important part of design through internal or public technical papers, participation at national and international conferences.

Today, *PAIG* activity is not limited to design, but includes also ground investigations and monitoring works which, together with the experimental works and back-analysis calculation lead to a *Complete approach of (the design) deep excavations*.

2. COMPLETE APPROACH OF DEEP EXCAVATIONS

Needless to say that the geotechnical design is very complex due to the large variability of soil conditions, available execution technologies, design approaches and models, natural hazards etc. For this reason, the geotechnical designer is most motivated to receive accurate input from the ground investigations and also needs to validate the calculation by feedback from execution, tests and measurements.

Tasks should be assigned to the people who have the greatest motivation to achieve high quality data. (Dunnicliff, 2015).

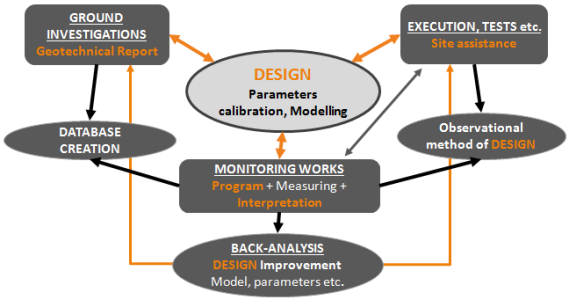

Figure 3. Diagram representing the concept of Complete Approach of Deep Excavations

The geotechnical design is an iterative process, leading to more effective and realistic design we all tend to achieve.

2.1. Design of deep excavations

The design of deep excavations should give a complete and detailed documentation for the execution of the retaining structures and also for the necessary works associated with the performance of deep excavations, such as dewatering project and specifications, detailed monitoring program, field tests specifications etc. These principles are also stated in the Romanian norm for deep excavations NP 120-2010 which assesses the requirements for design and execution of such works in accordance with their influence on the neighboring structures.

For an effective design there is necessary to use advanced soil models. When the main criteria is limiting the displacement for safety of neighboring buildings, the model used and the associated soil parameters are of most importance. Some of the complex soil parameters defining non-linear behavior, plasticity criterion and their variation are highly sensitive for the results of the computation. The soil-structure interaction phenomena are very complex and difficult to control by theoretical modeling. Using more advanced constitutive laws for the soil does not necessarily ensure more realistic results, especially if there are uncertainties on the geotechnical parameters.

For this reason, a database with the results of the investigations determining these parameters on several similar sites is of great importance resulting in comparable experience.

2.2. Ground Investigations/Geotechnical Report

First of all, the number and type of tests must be in correlation with the model used for design, with the calculation method, soil behavior model (e.g. unloading behavior, stiffness variation with depth, small strain parameters etc.).

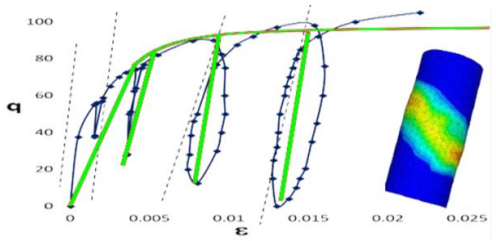

Figure 4. Example of correlation between the tests performed and the soil model used for design

Secondly, number and depth of the investigations must be in relation with the geometry and loads of the structure.

The Romanian normative for ground investigations NP 074-2014, which is related to the Eurocode 7, adopted in Romania as SR EN 1997-1:2004, indicates the minimum geotechnical investigations in relation with the project, site and geotechnical category of the structure.

However, most of the times, these indications are not sufficient and a detailed scope of works for the geotechnical investigations must be given for the Geotechnical Report by the same entity that will actually use these data. This must comprise location and number of the ground investigations, detailed specifications for the required tests etc. As it can be observed from the Figure 5 below, the number, depth and type of the geotechnical investigations were indicated in relation with the future designed deep excavation and structure.

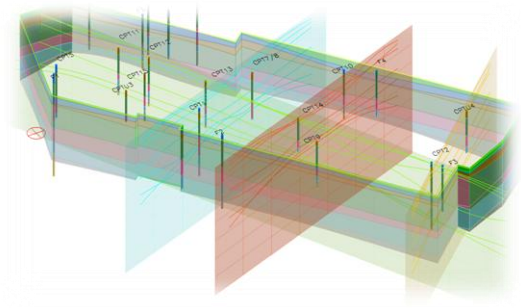

Figure 5. Example of correlation between the location and number of tests performed and the structure

What is more, changes are often required due to the actual site conditions. For example, it might result necessary to perform denser or deeper investigations in some areas where the information is not complete (doubts regarding the embedding layer, high alternation of layers, thin layers with little soil sampling, high variability of soil parameters etc.).

The choice of characteristic values for the geotechnical parameters must be a cautious estimation of the mean values determined by tests and must be complemented by comparable experience, as indicated in the Romanian normative NP 122-2010.

Also, after implementing these into calculations, the results must also be compared with previous measurements from similar projects and carefully adapt the values for the geotechnical parameters – choosing the right ones.

2.3. Site assistance during execution

A good coherence between design and execution lead to greater quality and easier execution. Design and execution should not be seen as two separate stages of a project, but they should be in close relation.

Figure 6. Images from work sites assisting for encountered conditions

Even with good planning and quality design and execution of geotechnical works, changes are often required due to unexpected site conditions, technological capability, errors etc. It is vital that the designer controls and verifies the design assumptions based on the actual performance during execution.

What is more, prescriptive design methods are, generally, too cautious and it results in non-economical solutions. Or, even when there are several more advanced design methods, due to

the complexity of the soil-structure interaction parameters that are involved, there are differences between calculation and experiments.

Therefore, field tests performed in actual site conditions and with the same technology used for construction must be the base of the final design leading to more reliable and even more economical solutions.

For example, in Figure 7 it can be noticed that two out of six ground anchors performed on the same site lead to significant differences due to local ground conditions (Ene et. al, 2014b).

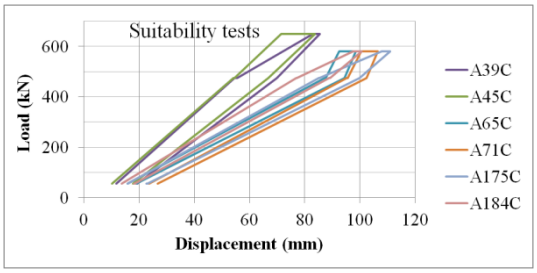

Figure 7. Results of control tests performed on ground anchors

2.4. Monitoring works

Modern practice in design and execution prescriptions requires proper monitoring of the structures both during execution and operational time. The risks of these works are significantly reduced by careful and correct monitoring, preventing if bad evolutions are noticed.

Even by using complex constitutive models, it is difficult to accurately assess the behavior of the designed structures and of the existing neighboring as a result of the excavation and construction works. There are uncertainties from estimating the geotechnical parameters for advanced calculations, from the limitations of the numerical model and even from construction phase when unexpected situations are encountered or the execution technology needs to be adapted.

As in the case of the ground investigations, the scope of works for the monitoring works must be given in accordance with the designed works assessing the type, number and location of the monitoring instruments as exemplified in Figure 8. These are always related to the behavior and mechanism of the structure.

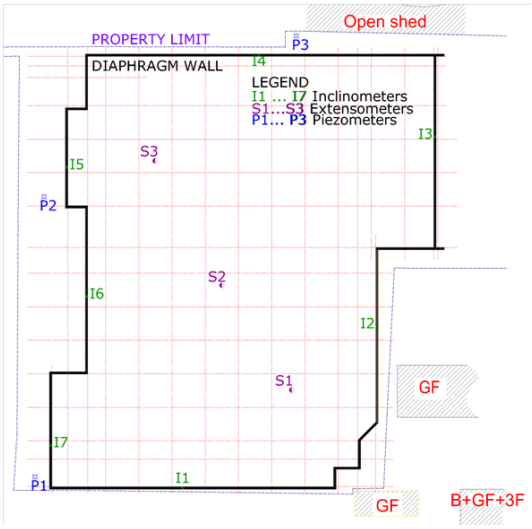

Figure 8. Example of monitoring works planned (Ene et. al, 2014a)

The measurements must be correlated with the execution stages and they must be clearly stated in the monitoring reports.

Also, the interpretation of the data obtained, the identification of the risks and the estimation of the consequences of each risk event must be given at each stage.

Many times, this operation is performed even during execution and it can loosely consider the process as observational method of design.

Figure 9. Images from work site measuring force in ground anchors during tensioning and lock-off

The results obtained from the monitoring activity must be compared with the results from the design and with similar works. These shall be the base for validation and calibration of the design models for improving future calculations through

database creation (see paragraph 2.5) and back-analysis (see paragraph 2.6).

Last, but not least, triggering values of the parameters measured and actions must be given based on the data collected, registers and observations.

All these actions must be integrated rapidly during execution and this can be best done by the entity which best knows the behavior and mechanism of the monitored structure.

2.5. Database creation

In order to perform efficient analysis and to calibrate the design models, based on 11 cases of excavations deeper than 10 m, executed in similar lithological and hydrological conditions, we started a database.

Table 1. General information of the analyzed buildings.

Id. Nr.	Short description	D-wall solution	Support System	H (m)	L (m)	t (m)
1	3B+GF+12S Office	SW+SP	3 lvs p-s HS	13.20	19.50	60/90
2	3B+GF+19S Office	SW	IS	9.40	16.80	60
3	3B+GF+15S Office	SP	HS	9.35	17	90
4	4B+GF+11S Office	SW	TD	14.10	22	60
5	(3)4B+GF+3(22)S Office	SW	TD	12.95	25.80	60/80
6	5B+GF+13S Residential	SW	TD	16	30	80
7	4(5)B+GF+15S Office	SW	TD	15	21	60
8	2B+GF+100 m Cathedral	SW	3 lvs A	16	24	80
9	3B+GF+12 S Office	SW	A	12	18	60
10	5B+GF+17S Office	SW	TD	16.35	27	80
11	4B+GF+8/15S Office	SW	TD	15.05	24	80

SW- Slurry Walls; SP - Secant Piles; HS - Horizontal Struts;
IS - Inclined struts; p-s - pre-stressed; A - Anchorages; TD - Top-Down
H - excavation depth; L - DW length (depth); t - DW thickness

This database allows the analysis of some indices, based on several ratios of the geometrical dimensions of the retaining wall, or based on the ratio between the measured values and the previously computed values. (Marcu et. al, 2015)

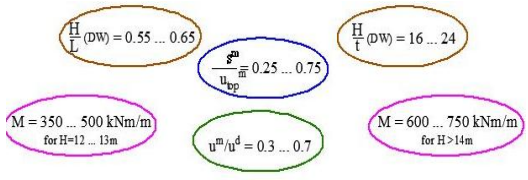

Figure 10. Comparative analysis of the calculated and measured data (Marcu et. al, 2015)

The analysis of this indices allow us to express some guide values, which can become extremely useful in the preliminary dimensioning process, but also for verifying the retaining systems.

2.6. Back-analysis

In the case of the retaining structures for deep excavations, the soil-structure interaction phenomena are very strong. For this reason, a more realistic model of the soil and of its interaction with the retaining structure is essential.

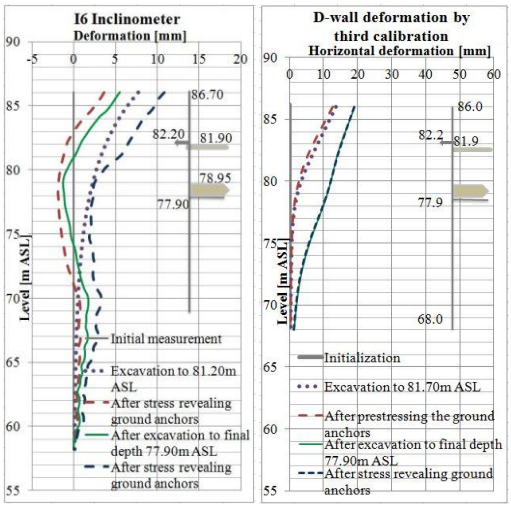

Figure 11. Diaphragm wall deformation measured and calculated after calibration of the model (Popa et. al, 2015).

The comparative calculations proved a high sensitivity of the results in relation to the parameters and it is very easy to fall within an unsafe area if these are not well controlled.

For this, there is one way of controlling the results better: detailed field investigations and calibration and verification computations based on experimental measurements. (Popa et. al, 2015)

The back calculations are also a research activity, a connection to the scientific domain, leading to a better understanding of the interaction phenomena and the influence of several parameters, whether it is the calibration of the materials properties, the design model or the calculation method.

3. CONCLUSIONS

The concept and performance of deep excavations require a complex approach nowadays, following the more daring challenges of the projects, the evolution of the technologies etc. What is more, the requirements today are higher and the performance parameters - feasibility, quality, cost, safety, time - are inseparable.

It is essential that the designer has an overview for identifying the input data, implementing the new technologies, as well as for using advanced calculation and processing methods. Experience and engineering judgment are, therefore, consequences of a complex approach.

It can be observed from the abovementioned, the importance of each activity related to the design of deep excavations and the connections between these activities as presented in Figure 3. Only an integral approach in which all the activities are controlled and connected can lead to better results for safer and economical solutions.

Even if the cost of each described activity is significant, the final result shall be less expensive through the proposed solutions and also through the quality resulted for the ground investigations, design, execution and monitoring works.

The role and professional training of a multidisciplinary design team is therefore essential.

4. REFERENCES

Ene, A. Marcu, D. & Popa H. 2014a. Monitoring of a deep excavation from Bucharest sustained by anchored diaphragm walls, *Conference proceedings of the 15th Danube-European Conference on Geotechnical Engineering*, 1015-1020

Ene, A. Marcu, D. & Popa H. 2014b. Testing of ground anchorages for a deep excavation retaining system in Bucharest, *Conference proceedings of the 15th Danube-European Conference on Geotechnical Engineering*, 1021-1026

Marcu, A., Popa, H., Marcu, D., Coman, M., Vasilescu, A. and Manole, D. (2008). The impact of deep excavations on the existing neighboring buildings (in Romanian). *Revista Constructiilor* No.33/2007 and 34/2008. ISSN 1841-1290, pp. 92-96 / 90-94.

Marcu, D., Ene, A., Popa, H. (2015). Monitoring measurements on retaining walls for deep excavations in similar sites - database creation. *Proceedings of the XVI European Conference on Soil Mechanics and Geotechnical Engineering*, 3577-3582

NP 074 (2014). *Norm regarding the geotechnical documentation for constructions*.

NP 120 (2010). *Norm regarding design and construction of deep excavations in urban areas*.

NP 122 (2010). *Norm regarding the evaluation of the characteristic and design values for the geotechnical parameters*.

Popa, H. (2010). Deep excavations in urban areas – influence on the neighboring structures; numerical modelling and measurements. *Geotechnical Challenges in Megacities - International Geotechnical Conference*, June 7-10, 2010, Moscow, Russia.

Popa, H., Ene, A., Marcu, D. (2015). Back-analysis of an anchored retaining structure of a deep excavation. *Proceedings of the XVI European Conference on Soil Mechanics and Geotechnical Engineering*, 3995-4000

Popp, T., Marcu, A., Marcu, D., Coman, M. (2003). Office building in Charles de Gaulle square (Bucharest). Design and execution (in Romanian). *Buletinul AICPS* Nr.4/2003-1/2004

Dunnicliff, J. (2015). Systematic Approach to Planning Monitoring Programmes (Presentation). *International Course on Geotechnical and Structural Monitoring*.

SR EN 1997-1 (2004)/NB (2007) *Eurocode 7: Geotechnical design. Part 1: General Rules. National bulletin*.

SR EN 1997-1 (2006). *Eurocode 7: Geotechnical design. Part 1: General Rules*.

Overall stability of anchored retaining walls: revisiting Brom's method

Nuno M. C. Guerra, Cláudia M. S. Josefino & Armando N. Antão
UNIC, DEC, FCT, Universidade NOVA de Lisboa, Portugal

Abstract: Kranz and Broms' methods are briefly reviewed and it is shown that they are equivalent, under the same conditions, giving the same results. Broms' method is applied to a relatively wide range of cases of anchored retaining walls with two anchor levels, considering different anchor inclinations, locations of anchor heads, embedded lengths and soil strength parameters. The method is used to determine the length of the top anchor level needed to ensure overall stability, for a given length of the bottom anchor level. Results are compared with traditional simplified procedures. It is shown that for certain cases these simplified procedures does not ensure overall stability.

Keywords: overall stability, Broms' method, limit equilibrium

1. INTRODUCTION

Overall stability is a fundamental stability verification of anchored retaining walls. Classical methods for this analysis are Kranz's (1953) method, Broms' (1968) method and other methods based on Kranz's, such as Ranke and Ostermayer's (1968). However, very frequently in some countries, overall stability is not specifically analysed and only semi-empirical simplified geometrical considerations are used, such as the ones presented in Figure 1. Are these geometrical considerations enough to ensure overall stability?

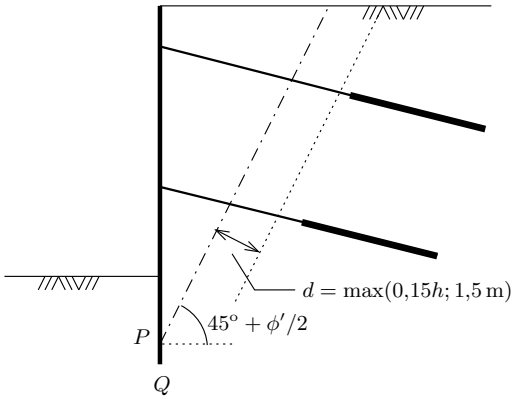

Figure 1. Example of semi-empirical geometrical considerations for the location of anchor bond lengths.

2. KRANZ AND BROMS METHODS

In the present paper Broms' method will be used to answer this question. Broms' (1968) method is compared with Kranz's (1953) (and other methods based in Kranz's) in Figure 2. There are three differences between the two types of methods: 1) location of point C; 2) definition of safety factor and 3) volume involved in the equilibrium.

Location of point C is a difference between the two methods that will not be considered in the present paper. In fact, Broms' method discusses the location of this point whereas methods directly derived from Kranz's method consider point C at the middle of the bond length, but both methods can easily consider any location of point C and in the present paper point C will be considered in the middle.

Safety factors were originally considered in the two methods in quite a different way. Kranz's method assumes the safety factor, FS_K to be defined as $FS_K = F_{a,K}/F_a$, where $F_{a,K}$ is the allowed force applied on the anchor, determined from Kranz's method, and F_a is the force applied on the anchor. Broms' method considers the safety factor, FS_B, as $FS_B = I_p/I_{p,B}$, where I_p is the passive earth pressure that can be mobilized at the from of the wall and $I_{p,B}$ is the passive force needed to ensure equilibrium, determined from Broms' method. These are global safety factors, but instead of such factors, a partial factor ap-

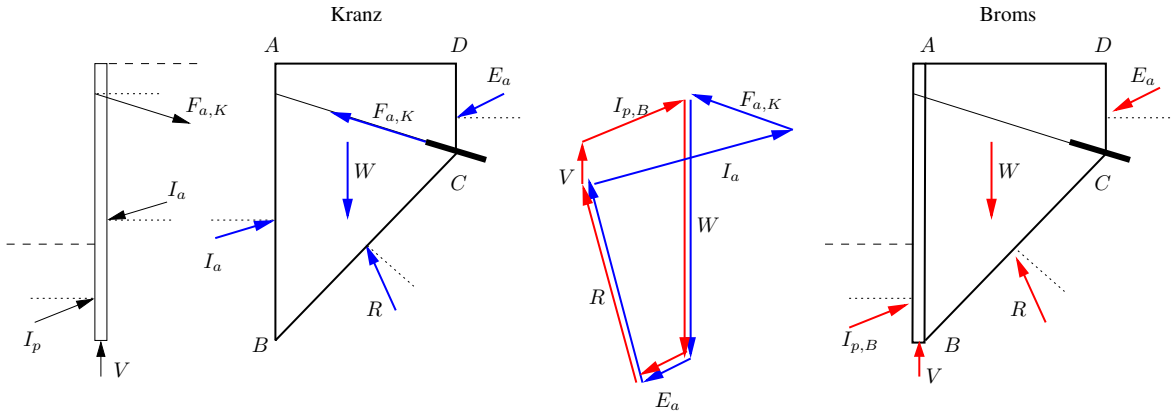

Figure 2. Kranz's and Broms' methods.

proach can be used, using, for example, design valued of the soil properties.

The two methods become equivalent in spite of the differences between these methods concerning the volume involved in equilibrium. In fact, Broms' method considers the equilibrium of both wall and soil mass ABCD whereas Kranz's method considers the equilibrium of the soil mass only. Of course they will be equivalent if all applied forces are in equilibrium and, in particular, if the wall is in equilibrium (Figure 2). In the present paper, Brom's method is used.

3. GEOMETRY OF THE PROBLEM

A very simple geometry (Figure 3) of a retaining wall with two prestressed anchor levels was considered. The soil was assumed homogeneous, with soil angle of strength ϕ'_d and unit weight γ. Anchors make angle α with the horizontal plane and the horizontal components of anchor forces determined using Terzaghi and Peck's apparent diagram with $\sigma_h = 0.65 K_a \gamma h$, where K_a is Rankine's active earth pressure coefficient $(= (1 - \sin\phi')/(1 + \sin\phi'))$. No surcharge at the soil surface was considered and the soil was assumed dry.

4. MECHANISMS. APPLICATION OF BROMS' METHOD

The possible mechanisms involved in Broms' method are shown in Figure 4.

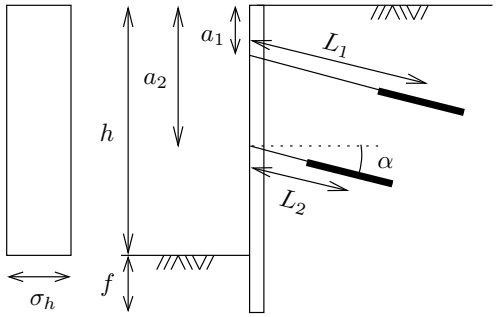

Figure 3. Geometry of the problem

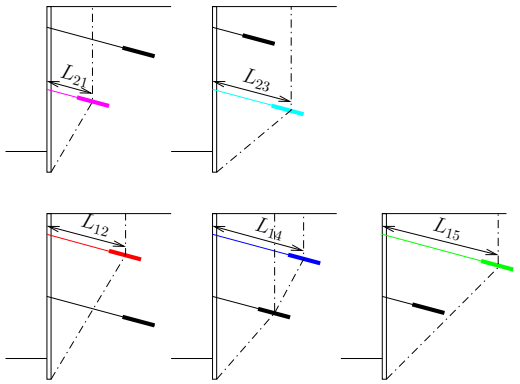

Figure 4. Possible mechanisms using Broms' method

Equations for determining each L_{ij} corresponding to each mechanism of Figure 4 could be obtained in a dimensionless way:

$$\frac{L_{ij}}{h} = f\left(\phi'_d; \alpha; \frac{f}{h}; \frac{a_1}{h}; \frac{a_2}{h}; \frac{\sigma_h}{\gamma h}\right) \qquad (1)$$

The approach was to determine, for a given L_2, the minimum value of L_1 needed to ensure equilibrium, using the mechanisms presented in the figure.

Two problems should, however, be addressed first. The first one is that there is a minimum value of f to ensure vertical stability (see Figure 5), if V is null (or small). This minimum value of f can be quite large and in the present paper only the case on the right of Figure 5 will be considered. Force V was, therefore, considered at the toe of the wall and assumed with the value needed to ensure the vertical equilibrium of the wall, considering the vertical components of the anchor forces, the weight of the wall and the vertical component of the passive force at the left. The resultant of the pressures on the right of the wall was assumed horizontal in these calculations.

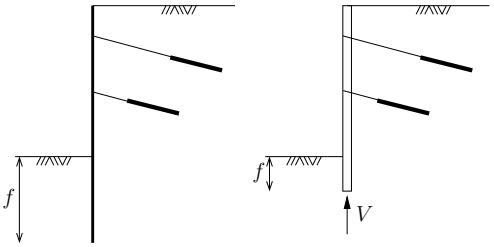

Figure 5. Walls not applying a significant vertical force at the toe (left) and applying such force (right).

The second problem is that in some cases stability of the wall is not ensured when designing the anchor forces with Terzaghi's diagram. Taking, for example, the case of a design value of the soil friction angle, $\phi'_d = 30^o$ (corresponding to $\phi' = 35.8^o$ using a partial factor, $\gamma'_\phi = 1.25$), and $f = 0$, the minimum value of $(F_{a1} + F_{a2}) \cos\alpha$ to ensure stability would be the design value of the active earth force, I_{ad}, equal to $0.5 K_{ad} \gamma h^2$, which leads to an average normalized pressure $\sigma_{hd}/(\gamma h) = (F_{a1} + F_{a2}) \cos\alpha/(\gamma h^2)$ equal to 0.1667. Terzaghi and Pecks value would be $0.65 K_a = 0.1702$, which is greater than the minimum value. For other cases, however, the minimum force (and normalized pressure) is greater than Terzaghi and Peck's value. The calculations presented next will consider the greatest of the two values.

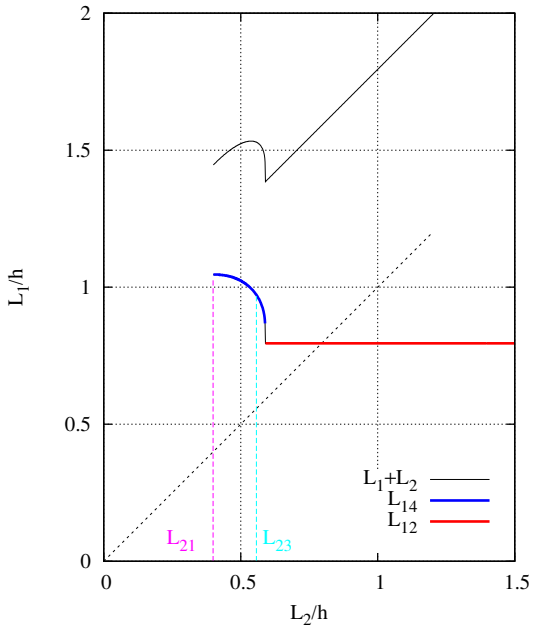

Figure 6. Values of L_1/h needed to ensure equilibrium as a function of L_2/h for the case $\phi'_d = 30^o$, $a_1/h = 0.25$, $a_2/h = 0.75$, $f/h = 0.2$ and $\alpha = 15^o$.

5. EXAMPLE. CHOICE OF THE SET (L_1, L_2)

A simple case study of the geometry presented in Figure 3 was considered, with $\phi'_d = 30^o$, $a_1/h = 0.25$, $a_2/h = 0.75$, $f/h = 0.2$ and $\alpha = 15^o$. For different values of L_2, Broms' method was used to determine the minimum value of L_1 needed to ensure equilibrium. Results are presented in Figure 6. In this figure it can be seen both values of L_{21} and L_{23} (Figure 4) and also that there are no values of L_1 for $L_2 < L_{21}$; in fact, equilibrium is not possible in this situation, no matter what the length L_1 might be. It can also be seen that for the lower values of L_2, the mechanism conducing to the minimum value of L_1 needed for equilibrium is the one corresponding to L_{14} and, beyond a certain value of L_2, the mechanism changes to the one corresponding to L_{12} (see Figure 4).

It can therefore be concluded that any solution on the blue and red line or above it is a possible solution and so the question that arises is: which solution to adopt? A solution on the line would be a solution which would correspond to a minimum

design value of both lengths, but which point of the line? A reasonable choice from an engineering point of view would be the most economical one, the one that would minimize $L_1 + L_2$. This sum is represented by the black line in Figure 6. It can be seen that this point corresponds to the transition between the blue line and the red one. Choosing this point would therefore mean that a small error in L_2 would lead to a significant increase in L_1, as the blue line shows large increases of L_1 when L_2 decreases slightly. This would not be acceptable unless a geometrical safety margin was considered. In the present paper, the solution that will be adopted will be the value of L_2 that corresponds to the minimum and the value of L_1 in the middle of the blue line, where the effect of a sudden increase is no longer significant.

6. INFLUENCE OF THE ANCHOR INCLINATION

Figure 7 shows the same results presented previously as well as those obtained using the same procedure for different values of the anchor inclination with the horizontal plane, α. It can be seen that the same type of results is obtained, with longer lengths L_1 being needed for lesser values of α for the same L_2 and a wider range of L_2 for which case L_{14} is relevant for lesser values of α. It can also be seen that for $\alpha = 30^o$ and 45^o for the shorter L_2 the minimum values of L_1 correspond to L_{15} (green line).

7. INFLUENCE OF THE NORMALIZED EMBEDDED LENGTH

Figure 8 shows the same results for other values of f/h, from 0 to 0.3. It can be seen that for small values of f/h, an increase of this length leads to an increase of both L_1 and L_2. In fact, for small values of f/h, the increase in the embedded length results in a small increase in the passive force but a large increase in the soil weight and therefore equilibrium requires longer anchor lengths. For larger values of f/h the increase in the passive force is much greater and the needed anchor length start to decrease. For $f/h = 0.3$ the mechanisms involved are no longer translational (as assumed in Broms' method) and become rotational. The lengths in

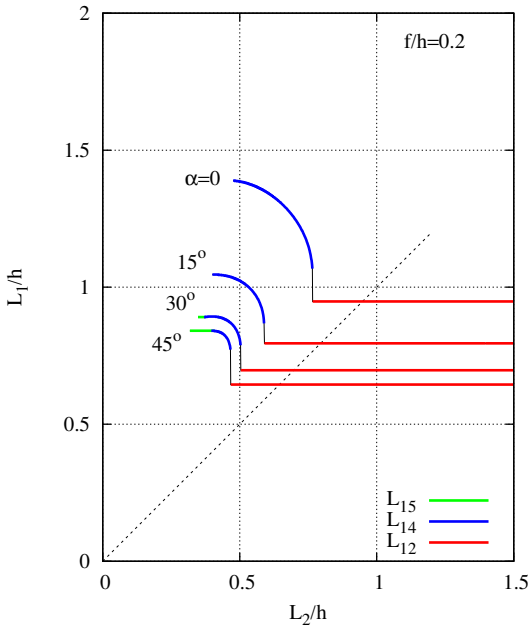

Figure 7. Values of L_1/h needed to ensure equilibrium as a function of L_2/h for the case $\phi'_d = 30^o$, $a_1/h = 0.25$, $a_2/h = 0.75$, $f/h = 0.2$ and different values of α.

Figure 8 for $f/h = 0.3$ were determined considering these type of mechanisms.

Using the criteria described in 5 for the choice of the set $(L_1; L_2)$ results in Figure 9. It can be seen, as expected, that values of the anchor length decrease with the soil friction angle and anchor inclination. It can also be seen that, as expected, values of L_1 are greater than values of L_2.

The results shown in Figure 9 can also be obtained for other values of f/h and can be represented in a more interesting way in a transversal cut of the wall. This is done in Figure 10. In this figure the results are presented for $a_1/h = 0.25$ and $a_2/h = 0.75$, but also for $a_1/h = 0.25$, $a_2/h = 0.60$ and for $a_1/h = 0.10$, $a_2/h = 0.60$.

It is interesting to notice that the points representing both L_1/h and L_2/h are aligned more or less rectilinearly except when the mechanisms become rotational, above a certain value of f/h (this can be seen for the first time for $\phi'_d = 40^o$ and $f/h = 0.2$) or when anchor are no longer needed for equilibrium (which can be seen for $\phi'_d = 40^o$

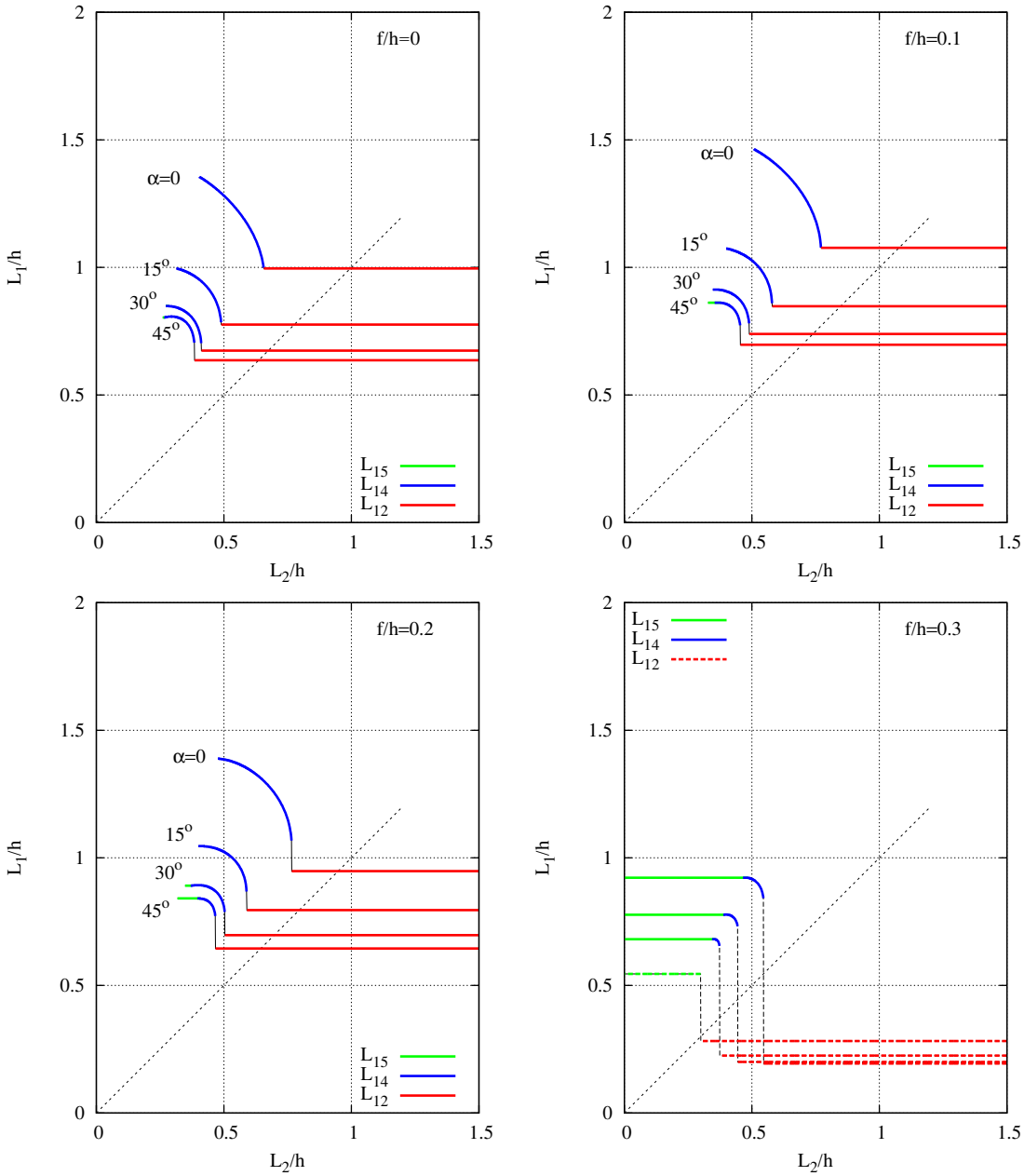

Figure 8. Values of L_1/h needed to ensure equilibrium as a function of L_2/h for the case $\phi'_d = 30^{\circ}$, $a_1/h = 0.25$, $a_2/h = 0.75$ and different values of f/h and α.

and $f/h = 0.4$).

8. COMPARISON WITH THE SIMPLIFIED PROCEDURE

Results shown in Figure 10 cannot be directly compared with the line represented in Figure 1. In fact,

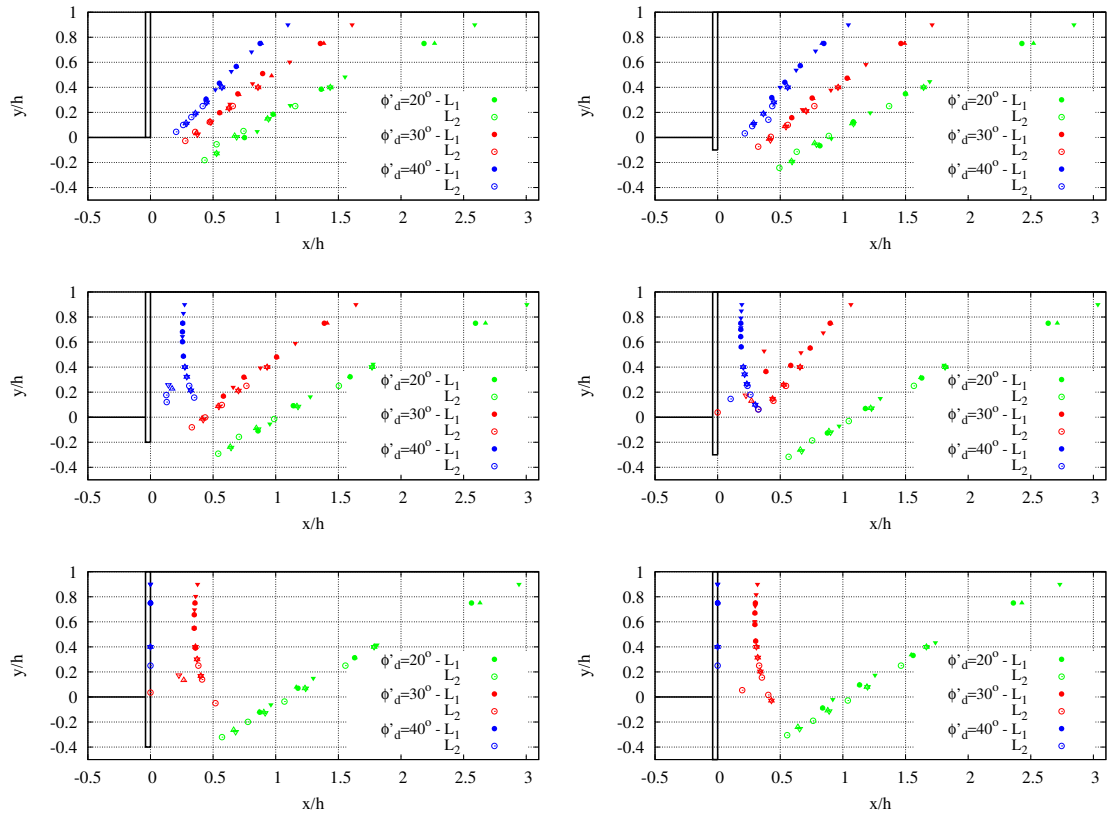

Figure 10. Set of L_1/h and L_2/h using criteria of section 5, for different values of ϕ'_d, α and f/h from 0(top-left) to 0.5 (bottom-right), and for $a_1/h = 0.25$, $a_2/h = 0.75$ (round symbols), $a_1/h = 0.25$, $a_2/h = 0.60$ (upward triangular symbols) and $a_1/h = 0.10$, $a_2/h = 0.60$ (downward triangular symbols).

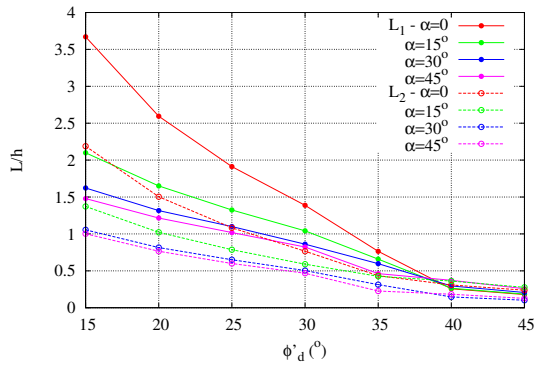

Figure 9. Anchor lengths using criteria of section 5, for $a_1/h = 0.25$, $a_2/h = 0.75$, $f/h = 0.2$ and different values of ϕ'_d and α.

the line in this figure represents the limit beyond which the bond length can be placed, whereas the lines defined by the dots in Figure 10 represent the location of the center of the bond length. Comparison between the two can therefore only be made if the bond length is defined. Figure 11 allows this comparison for the case $\phi' = 30°$, $f/h = 0.2$. In this figure the line in Figure 1 is represented and corresponds to a theoretical case of $L_b = 0$; in the same figure other lines correspond to other values of L_b/h. These (curved) lines can now be compared with the line defined by the red dots also represented in the figure.

It can be seen that the inclination of the lines are different and that the simplified procedure leads to shorter anchor lengths for the lower values of L_b/h. This is particularly true for the top anchor level, where the results obtained from Broms' method seem to need a specially longer length than the one specified by the simplified procedure; the

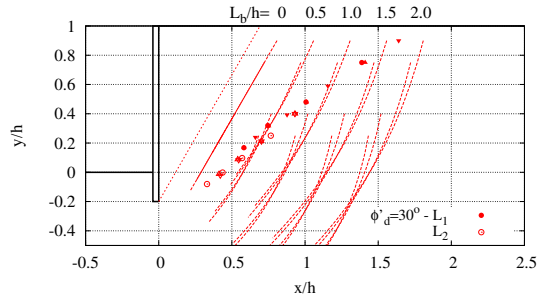

Figure 11. Comparison between the location of the bond lengths obtained from the simplified procedure and from Broms' method, for the case $\phi'_d = 30^o$ and $f/h = 0.2$ and for different bond length ratios L_b/h.

oposite occurs to the lower anchor level. So, taking into account that the dots represented in Figure 11 resulted from a choice of the set of lengths that was described, the question that might arise is if the values from the simplified procedure could still be safe. To answer this question, Figure 12 was prepared. In this figure, obtained for $f/h = 0.2$ and for $\phi' = 30^o$ (top) and $\phi' = 20^o$ (bottom) the lines previously seen in figures such as Figure 8 are again represented and the dots are now the results from the simplified procedure. Comparable cases are represented in the same color and a dot below the line of the same color means that the simplified procedure does not verify Broms' method. There are not many cases for $\phi' = 30^o$, but there are quite a few for $\phi' = 20^o$. They seem to occur, therefore, for smaller values of the friction angle, for the shorter bond lengths and the smaller values of the anchor inclinations.

This can be seen in Figure 13, where the color dots represent the cases where the simplified procedure lead to shorter anchor lengths than Broms' method.

9. FEM VERIFICATION

Finite Element Method code Plaxis and its $c - \phi$ reduction feature that allows determining the strength parameters for the colapse situation were used for comparison with Broms' method. An example of this is presented in Figure 14. For the case $f/h = 0.2$, a set of calculations with a fixed L_2 and different values of L_1 were performed, and another

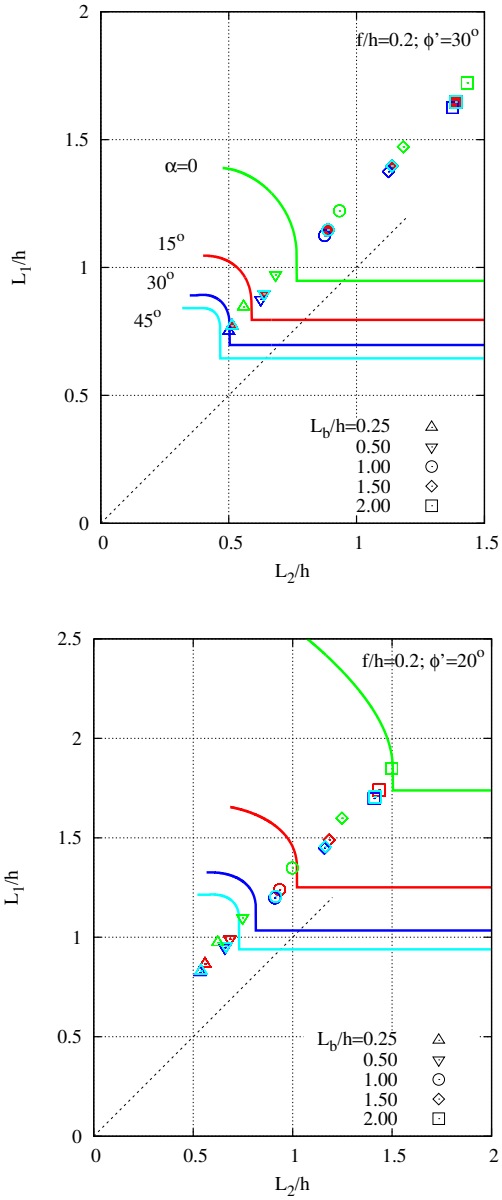

Figure 12. Location of the bond lengths obtained from the simplified procedure and from Broms' method, for $f/h = 0.2$, $\phi'_d = 30^o$ (top) and $\phi'_d = 20^o$ (bottom).

set of calculations was performed using constant L_1 and different values of L_2. The soil friction angle in the collapse situation was determined.

FEM calculations are represented in Figure 14 by the color dots. Each dot shoud be compared

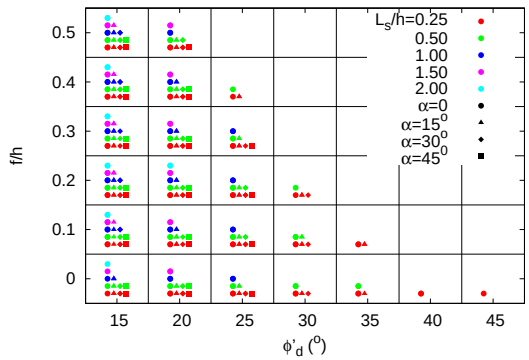

Figure 13. Cases for which Broms' method leads to greater anchor lengths than the simplified procedure.

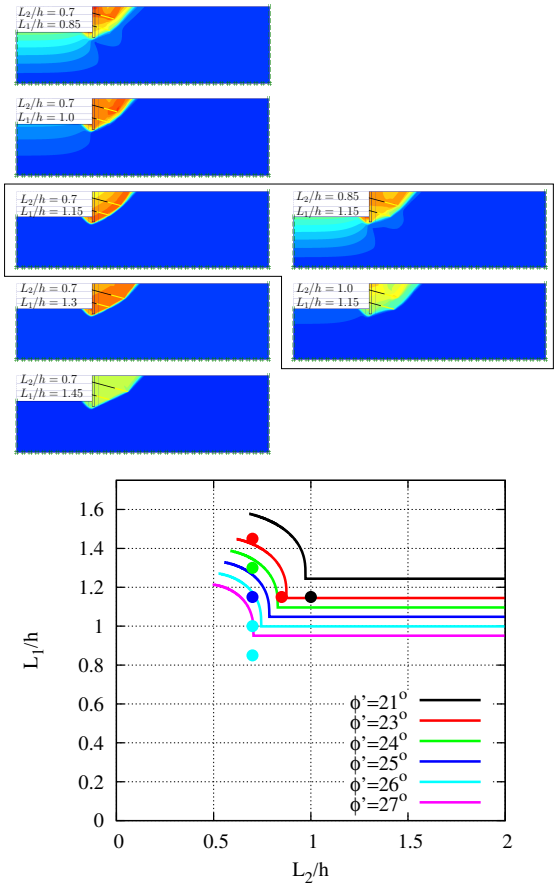

Figure 14. Mechanisms and results obtained from FEM method for $f/h = 0.2$; comparison with Broms' method.

with the line with the same color (same friction angle). Results do not cover a wide range of cases and the study needs to be completed, but the available results show similar values obtained from FEM and Broms' values.

10. CONCLUSIONS

Kranz's and Broms' methods are equivalent and give the same results (for the same geometry and definition of the safety factor).

A simplified procedure to define the location of anchor seals was compared with the traditional method (Broms' method) to analyse the overall stability a retaining walls with 2 level of anchors. A proposal for defining the anchor lengths based on Brom's method amongst the possible solutions was presented.

Comparison with the simplified procedure showed that this procedure can lead to results less safe than the ones from Brom's method. These cases correspond to the situations with low friction angles, anchors with low inclination and lower seal lengths.

Comparison with f.e. results was started but needs further development.

REFERENCES

Broms, B. B. (1968). Swedish tieback system for sheet pile walls. In *Proc. 3rd Budapest Conf. Soil Mech. Found. Eng*, pages 391–403.

Kranz, E. (1953). *Uber die Verankerung von Spundwander*. Wilhelm Ernst & Sohn. In German.

Ranke, A. and Ostermayer, H. (1968). Beitrag zur stabilitatsuntersuchung mehrfach verankerter baugrubemumschlie. *Die Bautechnik*, 45(10):341–350. In German.

50th IGC
IGS Pune chapter
50th INDIAN GEOTECHNICAL CONFERENCE
17th – 19th DECEMBER 2015, Pune, Maharashtra, India
Venue: College of Engineering (Estd. 1854), Pune, India

FOUNDATION CONSIDERATIONS FOR TWO TALL TOWERS

Dr Chris Haberfield, Golder Associates Pty Ltd, Melbourne, Australia, chaberfield@golder.com.au

ABSTRACT: This paper presents design considerations and analysis of the foundations of two tall towers in two very different geological settings. The first involves the redevelopment of a 24 level building into a 74 level tower using the existing structural frame and footings (which found in Sydney sandstone). The second tower comprises 108 levels and when constructed will be the tallest tower in Australia. The ground conditions which comprise 20 m of very soft to soft clay at the surface pose significant problems with respect to foundation and building performance under wind loading.

INTRODUCTION

This paper presents design considerations and analysis of the foundations of two tall towers in two very different geological conditions.

The first tower involves the redevelopment of an existing 24 level building into a 70 level tower using the existing structural frame and footings. The existing 24 level building on the site is supported on belled bored piles founding in competent Sydney sandstone. It is planned to strip the existing building back to the steel frame and then rebuild a 70 level building using the same building frame and foundations. To complicate matters further, located adjacent to the site are 4 railway tunnels as well as an easement for future railways tunnels, the construction of which could potentially impact on the proposed tower. Through an extensive series of soil structure interaction analyses it was demonstrated that the existing footings only required relatively minor augmentation to support the new building , saving millions of dollars and months of construction time to the project.

The second tower comprising 108 levels, when constructed will be the tallest tower in Australia. The foundations comprise large diameter bored piles founding at 40 m depth in weathered rock. A major consideration in the design of the foundations was the 20 m of very soft to soft clay at the surface, which only has a very limited ability to carry lateral wind and earthquake loads. An extensive series of three dimensional soil structure interaction analyses were carried out in combination with structural analysis of the building to enable the foundation system to be confidently designed.

PART 1 - ADDING 46 LEVELS TO AN EXISTING TOWER

Background

It is planned to redevelop an existing 24 level, steel framed building located in the CBD of Sydney, Australia into a 70 level residential tower by the addition of 46 levels. The structural frame of the existing 24 level building is to remain and be utilised in the structural frame of the proposed 70 level tower (refer Figure 1). Investigation and analysis were undertaken to assess whether it was practical to use the existing footings to support the taller building.

Others had carried out three phases of geotechnical investigation at the site incorporating a relatively large number of boreholes. However testing of the subsurface material was limited to point load strength index testing of the underlying rock. No direct measurement of the modulus of the subsurface materials was undertaken. Preliminary design of footings for the new tower were carried out by others and resulted in recommendations that augmentation of the footings was required. Initially the footing augmentation comprised installation of bored piles and pile caps. This was

later replaced by a grid of large strip footings (4 m deep and 4 m wide). The cost of the proposed footing augmentation was expensive in terms of cost (many millions of dollars) and time (months of construction time).

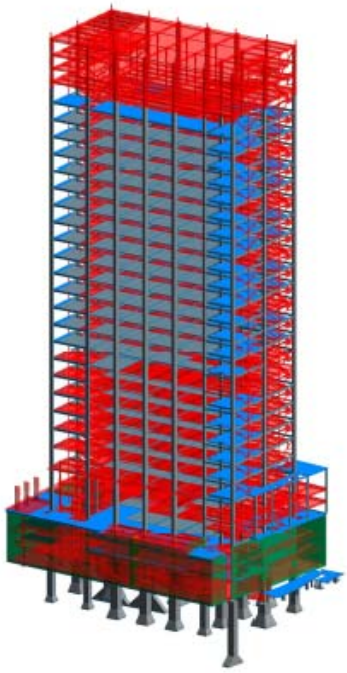

Figure 1 Existing building frame and footings

To make matters more complicated, the building is adjacent to both existing and planned railway tunnels and there is a requirement that the building does not impact on the existing tunnels or on the future construction of railway tunnels within the easement. For this reason, detailed three dimensional finite element analyses to assess the potential impacts of the proposed redevelopment on nearby railway tunnels and easement were undertaken. The results of this analysis show that the form of the footings does not have a significant impact on either the existing or planned railway tunnels.

On the basis of the geotechnical reports by others, it would appear that no detailed geotechnical analysis of the footings for the proposed building had been undertaken and the pile and footing design recommendations set out in the geotechnical report were based on traditional values adopted in Sydney for the shale and sandstone. These traditional values are widely accepted and are usually conservative. It was concluded that significantly higher rock properties (in particular stiffness) and bearing pressures than those recommended in the geotechnical report would likely be applicable, and the adoption of such values may allow the extent of the footing augmentation to be significantly reduced or eliminated for some columns.

Ground Model

The subsurface materials underlying the site comprise relatively homogeneous, flat bedded sandstone with occasional thin interbeds of shale (Figure 2). There appears to a normal fault with strike towards N-NE on the eastern side of the site. This feature may be associated with the Martin Place Joint Swarm.

The geotechnical reports also identified a second fault on the western side of the site, with small offset. Our assessment of the borehole reports was that they do not appear to show a significant zone of fracturing associated with this fault and it is not inferred to be of significance to the engineering properties of the rock mass. Nevertheless, the rock mass in this area appeared to be of poorer quality than elsewhere on the site and this should be considered in the design of the footings in this area.

The sandstone underlying the site has been weathered to a relatively shallow depth, with highly to moderately weathered rock typically extending to a maximum depth of about 5m below the existing basement level.

Figure 2 indicates five geotechnical zones that have been designated on the basis of defect concentration (RQD and defect frequency), material strength (point load strength index - $Is_{(50)}$ and degree of weathering) and material composition (shale versus sandstone).

The larger existing footings are inferred to be supported on slightly or less weathered sandstone, with RQD greater than 90% (volume shaded yellow in Figure 2). Some of the smaller and higher footings may be supported on shale.

The material underlying the existing basement and extending to about 5 m below the underside of the

basement is typically highly to moderately weathered sandstone (volume shaded red in Figure 2). On the eastern side of the site, in the vicinity of the fault, the defect frequency at shallow depth is greater, with RQD typically less than 50% (volume shaded green in Figure 2).

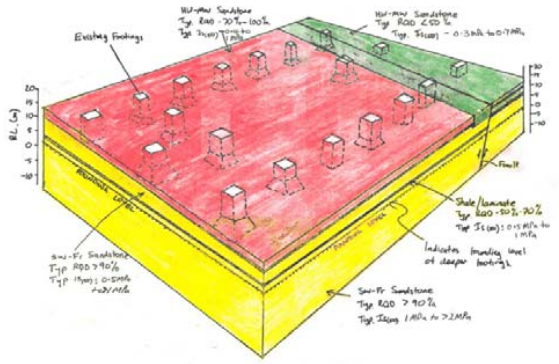

Figure 2 Ground model for analysis

Rock Mass Properties

As explained below, in our assessment of the rock mass properties for the site, we chose not to adopt the rock mass classification system proposed by Pells et. al. 1988 [1] as is commonly adopted in Sydney, but have instead assessed the rock parameters based on the parameters set out above (defect frequency and characteristics, material strength and rock type) and on published information and information from our archives.

The rock mass modulus obtained from this process were compared with those obtained by applying the Pells et. al., classification system, and from this comparison, a range of design Young's modulus values applicable to the design of footings for the site were developed.

Sandstone

The borehole reports provide detailed information on the fractures within the rock mass. The borehole reports indicate that for the majority of the site the sandstone (represented by the red and yellow volumes in Figure 2) contains less than 1.5 % clay or crushed seams. In addition, fracture spacing is generally greater than 300 mm, with only about 20 % of the borehole core length logged with a fracture spacing of less than 300 mm. Many of the fractures are clean and tight with no staining, indicating that they may be drilling breaks along bedding (and not fractures at all).

The exceptions to the above occur at the eastern end of the site in the vicinity of the inferred fault shown in Figure 2 (the green shaded volume in Figure 2) and at the south western corner of the site. The sandstone over the upper 10 m below the basement at these locations is of poorer quality with typically greater than 2 % clay or crushed seams and/or significant lengths of core with fracture spacing less than 300 mm.

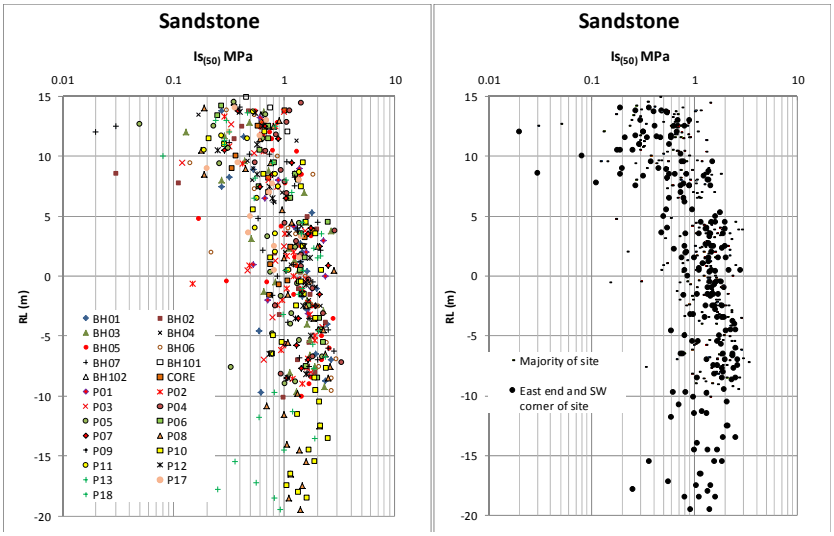

Figure 3 Point load strength index versus elevation

An indication of the strength of the sandstone can be obtained from the results of the point load index testing set out in the geotechnical reports. Figure 3 plots the point load index test results ($I_{s(50))}$ for sandstone in the axial direction with elevation. The results have been plotted according to borehole and location on the site (i.e. grouped results from the east end and south west corner of the site and from the rest of the site).

Whilst there are occasional lower and higher values, the point load index test results generally indicate the following for each sandstone zone:

Upper Zone: Between RL 15 and RL 10: $I_{s(50)}$ = 0.3 MPa to 0.7 MPa (east end and south west corner of site)

$I_{s(50)}$ = 0.4 MPa to 1 MPa (remainder of site)

Mid Zone: Between RL 10 and RL 5: $I_{s(50)}$ = 0.5 MPa to >1.0 MPa

Lower Zone: Below RL 5 m; $I_{s(50)}$ = 1 MPa to >2.0 MPa.

In the absence of other strength testing (such as unconfined compressive strength testing) the point load strength index test results have been used to estimate unconfined compressive strength (UCS) of the rock with depth using multipliers of 15 and 20 between $I_{s(50)}$ and UCS, Pells, 2004[2]. Applying this same process to the 5 rock units identified above, along with the fracture spacing and description of each of the rock units, an estimate of the geotechnical strength index (GSI) for each rock unit was made. From this, estimates of the strength properties (cohesion and friction angle) and a range of mass Young's modulus values for each zone of the sandstone were made.

The approximations made in undertaking the above process are acknowledged, and as a result prudent estimates were adopted in making this assessment. The above process provides an upper and lower estimate of strength and modulus for each of the zones and essentially assumes the entire zone comprises the lowest strength/quality sandstone (lower estimate) or the highest (upper estimate). This provides a rather broad range of modulus values (strength is less important as the quality of the rock is such that strength is not a critical factor for the footing augmentation design). To reduce this range of modulus values a more detailed estimate of the mass modulus of the sandstone zones in each borehole was made using the following process:

i) Based on the rock and fracture descriptions in the borehole reports the stratigraphy at each borehole location was subdivided into a

number of layers with similar rock description and fracturing;

ii) an average UCS and fracture spacing was assessed for each layer;

iii) a multiplier between UCS and modulus of between 50 and 300 was applied to each layer depending on fracture spacing and description. A multiplier of 50 applies to highly fractured rock masses with fracture spacing typically less than 100 mm, whilst the multiplier of 300 applies to rock masses with wide fracture spacing (> 1m). These factors are based on experience with weak to strong rock and are based on the results of plate load tests, pressuremeter tests, pile load tests and back estimates from settlement monitoring undertaken for a range of building projects Benson and Haberfield (2003) [3];

iv) for each sandstone zone and each borehole, the estimated modulus values were added together in series to calculate an overall mass modulus for the zone

This process resulted in a narrower range of rock mass modulus values from which were assessed design best, upper and lower estimates of modulus for each sandstone zone.

Siltstone/shale/Laminite

The borehole reports provide information on seams of shale, laminite and siltstone that were encountered within the sandstone. In general these seams are relatively thin and where tested have a similar axial point load strength index to the adjacent sandstone. A prominent seam of siltstone/shale with an average thickness of about 1.5 m is present within the Mid Zone between about RL 5 m and RL 7.5 m. The point load strength index tests in this material (see Figure 4) indicate similar results to the adjacent sandstone. The siltstone/shale/laminite is generally described as massive with widely spaced joints and very few seams. Design properties of this material were assessed to be in the same range as assessed for the sandstone in the Mid Zone. Our analysis therefore did not explicitly include these seams in the model, but instead included them in the assessment of modulus for the various rock zones as appropriate.

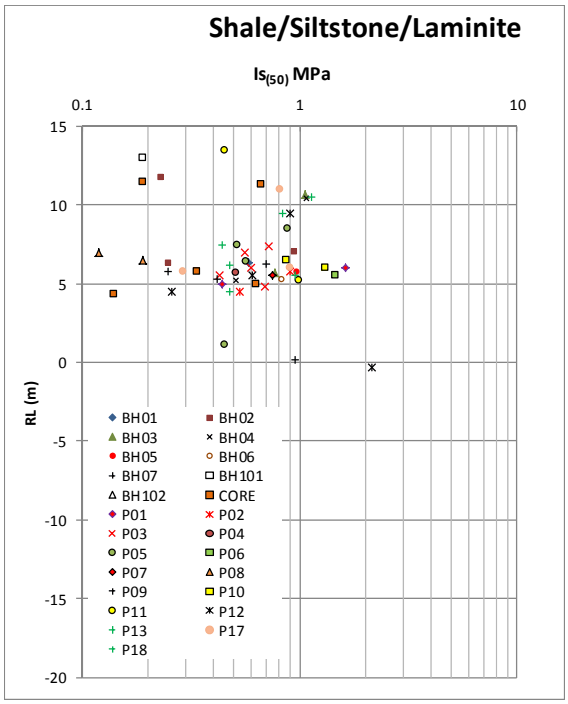

Figure 4 Point load index test results in shale/siltstone/laminite

Design Rock Mass Properties

Using the processes set out above an estimate of the design mass properties for each rock zone as set out in Table 1 were made. Best estimate design Young's modulus values are provided with suggested range (minimum and maximum design estimates) in brackets.

Table 1 Suggest design rock properties

Zone	Elevation range RL (m)	Young's modulus (MPa)	Cohesion (kPa)	Friction angle (deg)
Upper	15m to 10m	1400 (1000 to 2000)	330	53
Mid	10m to 5m	2400 (1500 to 3000)	530	57
Lower	Below 5m	5500 (3000 to 6000)	1750	66

As noted above, the strength parameters were assessed using GSI and a relatively low confining stress, resulting in low cohesion and high friction angle values. The strength values are not critical to the assessment of footing performance.

The best estimate design modulus values set out in Table 1 for the Upper Zone is at the upper end of the Pells et. al. (1988) values for Class III sandstone (200 MPa to 1200 MPa) and at about mid-range for Class II sandstone (700 MPa to 2000 MPa). In general we assessed the Upper Zone to comprise a mixture of Class III and Class II sandstone.

Similarly the best estimate design modulus for the Mid Zone is at the upper end of the Pells et. al. values for Class II sandstone and shale (700 MPa to 2000 MPa) and at the lower end for Class I sandstone and shale (> 2000 MPa). In general we assessed the Mid Zone to comprise a mixture of Class II and Class I sandstone and shale.

Our best estimate design modulus for the Lower Zone is significantly higher than the Pells et. al. minimum value of 2000 MPa for Class I sandstone. In general we assessed the Lower Zone to comprise Class I sandstone. The adoption of the higher best estimate design modulus for the Lower Zone will not have a significant impact on the design performance of the footings. In fact, the adoption of a lower modulus for the Lower Zone will result in less load being carried by the existing piles and more load being carried by the proposed footing augmentation set out below.

Suggested Footing Design Philosophy

The proposed redevelopment planned to utilise the existing belled piles which found below about RL 5 m in good quality sandstone (predominantly Class I sandstone in the context of the Pells et al. (1988) classification system). It is also proposed to encase the existing steel columns within new concrete columns which will be eccentric to the existing belled piles resulting in approximately half to two thirds of the new column plan area being outside the plan dimensions of the shaft of the existing piles (see Figure 5).

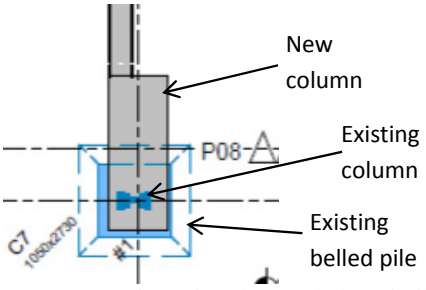

Figure 5 Plan showing existing belled pile and new column

For this reason, it is probable (and practical and prudent) that the portion of each new column not supported directly by the existing pile will need to be supported by a footing.

Had the existing piles not been present, it is likely that the proposed building would have been supported on shallow pad footings founding at just below current basement level (i.e at perhaps RL 12.5 m). Based on the assessment set out above, such pad footings could have been designed for an allowable bearing pressure of 10 MPa to 12 MPa.

For example, the most heavily loaded new column has plan dimensions of 1.16 m x 2.73 m and a design axial working load of 101,000 kN. This column could have been supported on a pad footing with plan dimensions of say 2.66 m x 4.23 m giving a plan area of 11.25 m^2 (i.e. these dimensions correspond to an outstand of 0.75 m around the column).

However, it is proposed that this column will be partially supported on a pile which has shaft plan dimensions of 1.016 m x 1.016 m and bell plan dimensions of 1.6 m x 1.6 m (plan area of 2.56

m^2). Consider for the moment, that the portion of the plan area of the column not supported by the pile is supported by a shallow pad footing which abuts the pile shaft and has say a 1 m outstand from the edge of the column as shown by the red shaded rectangle in Figure 5. The pad footing has plan dimensions of about 3.16 m x 2.73 m and is founded at shallow depth (say RL 12.5 m) compared to the belled pile (which founds at about RL 5 m).

A similar approach (but at a larger scale) was successfully adopted for the core of Eureka Tower (currently Melbourne's tallest building which is in excess of 80 levels). Eureka is supported on piles which found at two different levels and two different rock units – some piles found in an upper, high strength basalt, whilst others found at significant depth in siltstone (Ervin and Finlayson, 2003).

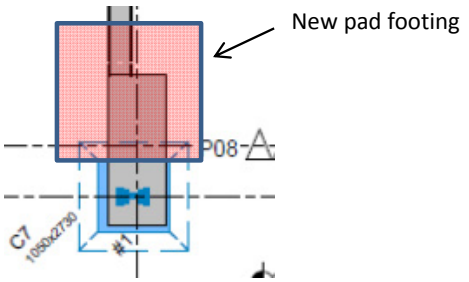

Figure 6 Column with footing augmentation

The total plan area of the belled pile and new pad footing shown in Figure 6 is about 11.2 m^2 which is a similar area to that required to support the column on a pad footing alone.

The different founding levels between the belled pile and new pad footing, and the greater stiffness of the existing pile compared to the surrounding rock, will mean that the existing pile shaft will take most of the column load. The actual distribution of load between the existing pile and the new footing can be calculated using three dimensional analysis as set out below.

The results of the analysis indicate that the axial stress in some pile shafts may be of the order of 30 MPa, which is likely to be in excess of the characteristic compressive strength of the concrete in the pile. However, the characteristic compressive strength of the concrete is measured under unconfined conditions and is not applicable to a situation where the pile is confined in rock of medium to high strength. Under such conditions, the confinement provided by the surrounding rock is significant, and this confinement results in a significant increase in the load the concrete can sustain. In effect, the rock prevents the concrete from crushing as the concrete has nowhere to fail to.

The non-symmetry of the pile/pad footing support may lead to some rotation at the base of the column. However, this rotation is resisted by the column and by the lateral support from the surrounding rock mass. The analyses set out below indicate that the rotation is small. Nevertheless the column will need to be designed to carry the moments resulting from any design rotation.

With respect to the combined pile/pad footing shown in Figure 6, there is no need to structurally join the pad footing to the pile shaft. The pad footing can simply be poured directly up against the cleaned and scabbled surface of the pile shaft. The overlying column needs to be designed to distribute the column load to the pile and pad footing.

Analysis of Footing

Three dimensional analyses of the building core and selected individual footings for the proposed redevelopment have been undertaken using the geotechnical software package PLAXIS3D. The aims of the analysis were to:

i) Calculate the design settlement of the proposed core structure and provide estimates of spring stiffness values for use in structural analysis of the proposed building;
ii) Calculate the performance of selected existing belled piles without footing augmentation under the eccentric loading from the proposed new columns;
iii) Assess the extent of footing augmentation required for the existing belled piles and provide spring stiffness design values for the

piles and footing augmentation for use in structural analysis of the proposed building.

Only isolated footings have been considered in the in analysis. Group settlement effects were considered to be minor as indicated by the results of the three dimensional model which investigated the potential impact of the development on railway infrastructure (assuming a reduced footing augmentation scheme).

The analysis assumed a Young's modulus of any new concrete of 30 GPa. The existing reinforced concrete belled piles were modelled as mass concrete with a modulus of 20 GPa and Mohr Coulomb strength parameters of cohesion of 6 MPa and a fictional angle of 50^{o} (resulting in an effective unconfined characteristic strength of the concrete of about 30 MPa).

The analysis assumes the maximum serviceability loads.

Belled Piles

The analysis of the heaviest loaded column is summarised below. The new column design axial load is 100,798 kN. The performance of other belled piles was also assessed using the same techniques as set out below, but not included herein.

For the case of no pad footing support the base of the new column was assumed at RL 14 m. A maximum frictional resistance of 1000 kPa was assumed for all pile/rock/pad footing interfaces.

For the case where a belled pile is augmented with a pad footing the pad footing was assumed to be constructed immediately north of and in contact with the belled pile shaft with footing dimensions which result in a 1 m outstand from the column plan dimensions. The pad footing was assumed to be 1.5 m deep and found at RL 12.5 m. Figure 7 shows a typical model geometry showing the existing belled pile and new pad footing. The column was assumed to be free standing with no restraint provided by the building.

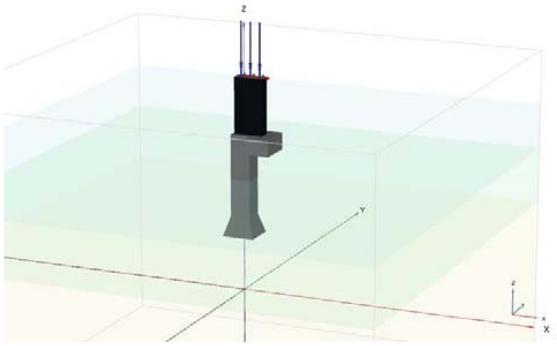

Figure 7 Typical geometry of belled pile and footing augmentation

Figure 8 compares calculated settlement profiles at the base of the new pad footing for a column without pad footing augmentation (best estimate properties) and with pad footing augmentation (lower, best and maximum estimate rock properties). The profile is along the north-south centre line of the pad footing/pile, with the pile shaft centred at 0 m (pile extends between about -0.6 m and +0.6 m) on the horizontal axis. Calculated settlements vary between about 6 mm and 17 mm depending on assumptions. A reduction in maximum interface resistance from 1000 kPa to 500 kPa results in about a 5 mm increase in settlement.

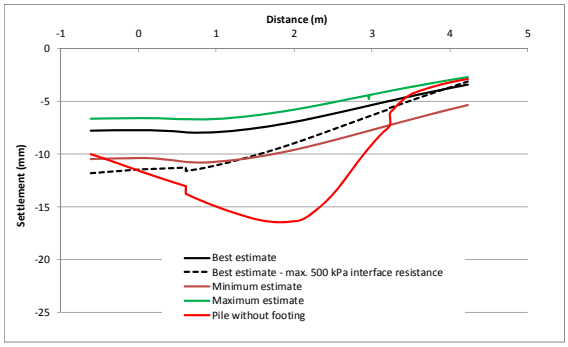

Figure 8 Settlement profiles for pile S13 with and without footing augmentation

The pile without pad footing augmentation shows a significantly higher rotation which, as shown below in Figure 9 impacts significantly on the axial stresses in the pile.

Figure 9 indicates for a pile augmented with a pad footing the maximum calculated axial stress in the pile is about 30 MPa, whilst for the pile alone (without pad footing augmentation) the maximum axial stress in the pile increases to about 60 MPa. Figure 9 also indicates the average bearing stress beneath the pad footing is about 8000 kPa beneath the column and about 2000 kPa outside of the column plan area.

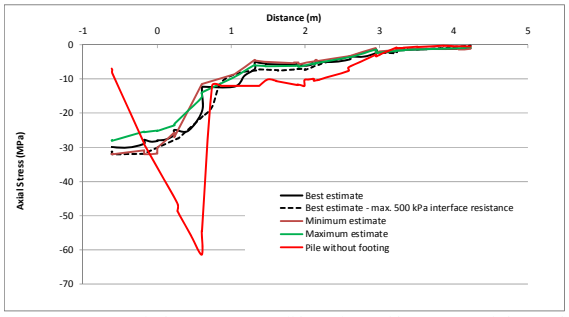

Figure 9 Axial stress profiles for pile S13 with and without footing augmentation

Figure 10 shows contours of calculated settlement and vertical stress at the base of the new pad footing with footing augmentation assuming best estimate rock properties and an interface resistance of 500 kPa. Maximum calculated settlement is about 10 mm.

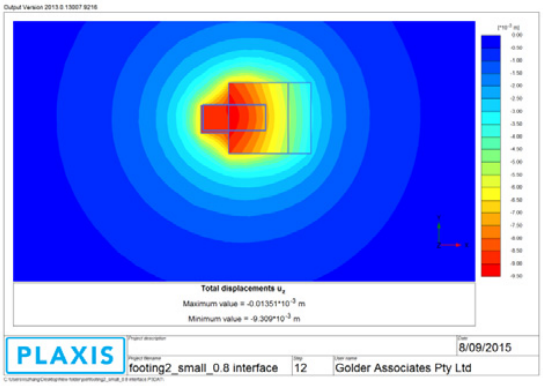

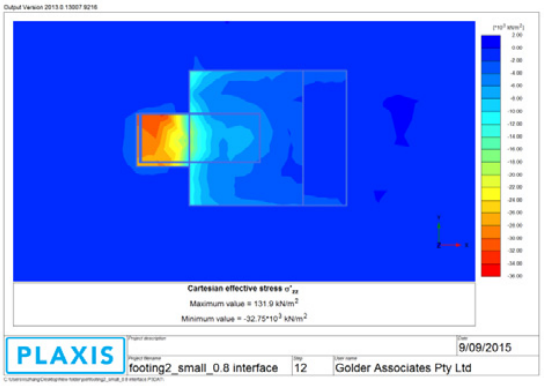

Figure 10 Contours of settlement (top) and vertical stress (bottom) at base of pad footing (RL12.5m)

Table 2 sets out the suggested design spring stiffness values for the pile and pad footing for use in structural analysis of the proposed building frame. Such analysis will also require estimates of horizontal and rotational spring stiffnesses to resist the impact of eccentricity of load on the pad footing.

Table 2 Results of analysis

Rock properties	Average design spring stiffness (kPa/mm)	
	Pile	Pad footing
Minimum estimate	2400	500
Best estimate (interface 1000 kPa)	3100	750
Best estimate (interface 500 kPa)	2700	750
Maximum estimate	3400	1000

Axial Stress in Pile Shaft

The results of the analysis indicate relatively high calculated axial stresses in the pile shafts. However, the characteristic strength of the concrete is not applicable in this situation due to the confinement provided by the rock. For a mass modulus of the Upper Zone of rock of 1400 MPa, we estimate a confining stiffness provided by the rock to the concrete of 1900 kPa/mm. This

confinement should be considered in the structural assessment of the piles.

Summary

On the basis of the results of the analysis undertaken, it was proposed that the new columns for the proposed building be supported on the existing belled piles augmented with a pad footing founded at about RL 12.5 m. From a geotechnical perspective, no structural connection is required between the shaft of the existing pile and the new pad footing.

PART 2 AUSTRALIA'S TALLEST BUILDING

Background

Australia's tallest building at 317 m in height is to be built in Melbourne. The tower will comprise 108 floors with 1105 apartments. Construction has commenced and is expected to be completed in 2020.

The ground conditions at the site are challenging with the upper 20 m of the subsurface stratigraphy comprising uncontrolled fill and soft clay. The tower will be supported on large diameter piles founding in medium strength siltstone at about 40 m depth.

The near surface deposits of soft clay posed a significant challenge to the footing design due to the need to provide sufficient lateral stiffness under design wind loading, especially in respect to the dynamic response of the tower. The dynamic response of the building was found to be relatively sensitive to the design of the foundation system. The structural engineers for the project required accurate input regarding the foundation stiffness for use in the structural analysis of the tower which could only model the footings supporting the columns as springs with axial, lateral and rotational stiffness. The design stiffness values for the footings was computed using the three dimensional finite element analysis package PLAXIS3D[3]. A summary of the approach undertaken is provided below.

Figure 9 Australia's tallest building

Ground Conditions

The subsurface stratigraphy at the site comprises:

Fill: about 2 m thick, variable (a mixture of soft to firm silty clay and loose to medium dense silty sand and sand) fill materials; overlying

CIS (Coode Island Silt): about 18 thick, soft silty or sandy clay, becoming soft to firm and firm with depth; overlying

FBS (Fishermens Bend Silt): about 4 m thick, firm to stiff silty clay; overlying

MSG (Moray Street Gravels): about 8 m thick, medium dense and dense silty sand and stiff sandy silt; overlying

WF (Werribee Formation): about 5 m thick, stiff to very stiff sandy clay; overlying

MF (Melbourne Formation): highly weathered, low strength siltstone becoming less weathered and of medium to high strength with increasing depth.

The water table is located at an elevation of about RL 0 m (or about 2 m below the surface).

Typical properties adopted for the wind load analyses are provided in Table 3. As the performance of the footings under wind loading is a dynamic loading case, short term properties were assessed for each of the subsurface materials.

Table 3 Soil properties

Soil	Cohesion (kPa)	Friction angle (deg)	Young's Modulus (MPa)
Fill	0	28	10
CIS	15+1.5z	0	4.5+0.45z
FBS	5	28	30
MSG	8	30	80
WF	10	30	30
MF	500	43	1000

Stability System to Resist Wind Loading

Figure 10 shows the pile layout of the primary support foundation elements which resist wind loading (referred to as the stability system). The stability system comprises three levels.

The lowest level of the core is the lift over-run pit which is supported on 16 No. 1800mm diameter bored piles founding in the MF with floating 600mm diameter secant piles between adjacent 1800 mm diameter piles. The 1800 mm and 600 mm diameter piles also form the retention system for the lift over-run pit. A 1.9 m wide capping beam connects these piles and forms a structural connection to the core wall. The lift over-run pit has a 1.5 m thick raft foundation at the base of the core which is connected structurally to both the 1800 mm diameter piles and secant pile wall.

The intermediate level of the core is supported on 600 mm, 900 mm and 2100 diameter piles (with pile caps) founding at depth in the MF. These piles/pile caps are connected to the core capping beam by a 300 mm thick slab and walls.

The upper most level of the stability system is at ground surface level and is supported by bored piles ranging in diameter from 600 mm to 2100 mm which found in the siltstone. These are connected to the intermediate and lowest levels of the stability system by 250mm concrete slabs and walls.

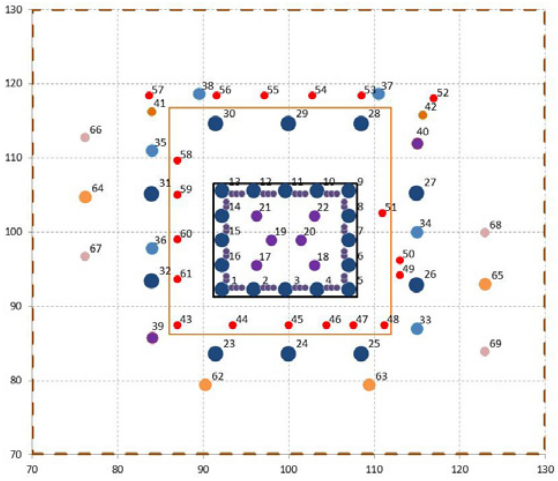

Figure 10 Pile layout of the foundation system

Throughout the foundation structure interaction analysis process, the pile arrangement (including pile caps) and pile diameters were modified to obtain an optimal solution.

Analysis Model

A commercial Geotechnical non-linear finite element program, PLAXIS3D was adopted as primary tool for the geotechnical analysis of the footing stability system.

An example PLAXIS 3D model (including the mesh) is presented in Figure 11. The overall model size is 200 m x 200 m x 85 m (length x width x depth). Footings within a radius of about 30 m from the centre of the building (which were not part of the stability system) were also included in the analysis. This was so that the structural actions in these elements (bending moments, shear forces etc) resulting from the displacement of the stability system under wind loading could be computed.

The mesh comprised in excess of 60,000 soil elements and 90,000 nodes. A finer mesh was used around the core area and gradually graded to larger elements (about 5 m dimension) used outside the core.

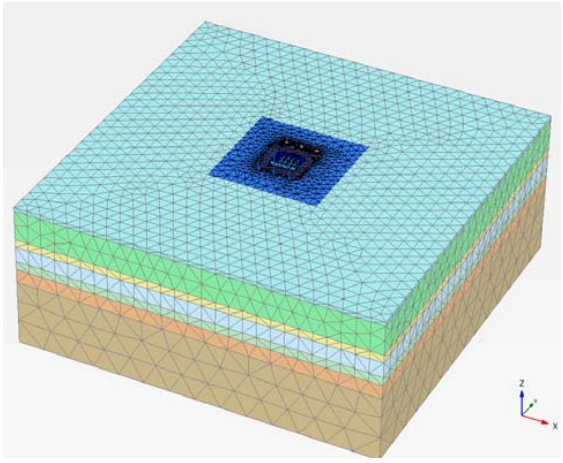

Figure 11 PLAXIS 3D model

Figure 12 shows the PLAXIS 3D model of the foundation system (for clarity the ground floor slab is not shown).

All piles were modeled as embedment piles and the external and internal core walls and ground floors were modelled by plate elements. Pile caps and raft footing of the lift over-run pit were modeled as concrete blocks to better capture the lateral resistance provided by these elements.

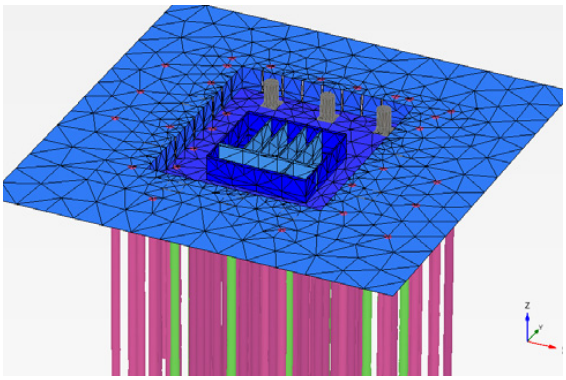

Figure 12 PLAXIS 3D model of stability system

Interaction between Geotechnical/Structural Engineers

In excess of ten loading cases for serviceability and ultimate limit state wind and earthquake conditions were carried out.

The aim of the analyses was to optimize the foundation type both in terms of practicality and economy of construction and to minimize the pile numbers and size of piles, whilst maintaining satisfactory performance under wind and earthquake loading.

Following an initial meeting between structural and geotechnical engineers and some preliminary advice with respect to the likely foundation system, the structural engineers provided a preliminary footing layout for the stability system. The geotechnical engineers provided some preliminary stiffness values for each foundation element and the structural engineers conducted preliminary analysis for the perceived worst loading condition. From the results of this analysis a first estimate of structural reactions at each level of the stability system were provided to the geotechnical engineers. These reactions were then applied in the PLAXIS3D model. The output from the PLAXIS3D analysis was interpreted to provide profiles of displacements of the stability system, structural actions within the piles and interconnecting structural units (walls, floor and raft) and updated spring stiffnesses for each foundation element. Based on these results, pile, wall, raft and slab sizes were revised and the structural analysis undertaken on the revised stability system. New reactions were then provided to the geotechnical engineers and the above process repeated. This iterative process was undertaken a number of times until a reasonable match between the vertical and horizontal displacements computed from the structural and geotechnical analyses was obtained.

Once a satisfactory footing solution was obtained for the worst wind load case, other wind and earthquake cases were undertaken. The earthquake loading cases were found to be less critical than the wind load cases.

The iterative process was complicated significantly by the torsional forces acting on the stability system and by the three different levels of the stability system.

An example of a typical match between the calculated horizontal displacements from both geotechnical and structural analysis are presented in Figure 13.

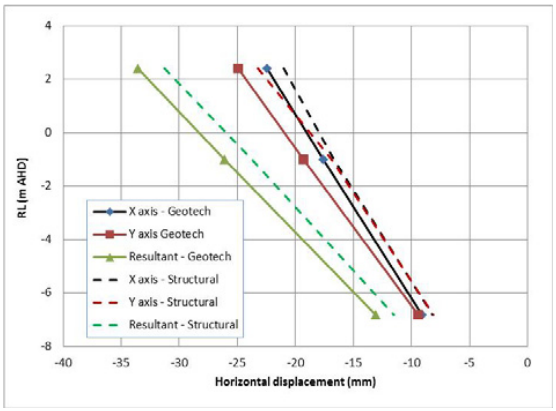

Figure 13 Comparison of calculated lateral displacements from geotechnical and structural analyses

Summary

The close interaction between structural and geotechnical engineers and careful foundation structure interaction analysis was instrumental in developing and optimising a foundation system for Australia's tallest building. The stability of the building under wind loading in particular was a challenge due to the significant thickness of soft clay at the site.

CONCLUSIONS

Two tall tower case studies involving the analysis and design of footing systems using foundation structure interaction analyses have been presented.

The first case study showed the value in foundation structure interaction analysis to better understand the likely performance of eccentrically loaded existing piles. This resulted in significant savings in cost and time to the project.

The second case study again showed the value in foundation structure interaction analysis to allow development and optimisation of the footing system for Australia's tallest building which is to be located on a site where ground conditions were challenging especially in respect to the performance of the building under wind and earthquake loading.

REFERENCES

1. Pells, PJN, Mostyn, G. and Walker, B.F. (1998). "Foundations on sandstone and shale in the Sydney region". Australian Geomechanics, No 33, Part 3, Dec 1988, pp. 17 to 29
2. Pells, PJN (2004). "Substance and mass properties for the design of engineering structures in Hawkesbury sandstone". Australian Geomechanics, Vol 39, No. 3 September 2004, pp. 1 -21.
3. Benson, N. and Haberfield, C.M. (2003). "Assessment of rock mass modulus". 10th International Congress on Rock Mechanics, Johannesburg, Sth Africa.
4. Ervin, M.C. and Finlayson, J.E. (2003). "Deep footing solution for Eureka Tower Project, Melbourne, Australia". BGA International Conference on Foundations Dundee, Scotland. Thomas Telford, pp 269-281
5. PLAXIS 3D Reference Manual (2013), plaxis nl.

Overview of the Damage and Lessons Learned from the 2015 Nepal Earthquake

Hemanta Hazarika
Department of Civil Engineering, Kyushu University, Fukuoka, Japan

Netra Prakash Bhandary
Graduate School of Science and Engineering, Ehime University, Matsuyama, Japan

Abstract: This paper discribes the damage brought by the 2015 Nepal earthquake to urban infrastructures, modern and traditional buildings as well as some word heritage sites in and around Kathmandu city. The paper also focuses on a disaster brought to a hydropower plant by the compound action of a previous landslide and this time earthquake. Some of the possible reasons for such damage were brought to light, and challenges of the geotechnical community towards the retrofitting and recovery of the devastated structures were discussed.

Keywords. 2015 Nepal earthquake, amplification of motion, world heritages, landslide, compound disaster

1. INTRODUCTON

The Nepal Gorkha earthquake (moment magnitude, Mw=7.8) struck at 11:56 NST on 25 April 2015 with epicenter at Barpak village of Gorkha district, which is located 77 km northwest of Kathmandu, the capital city of Nepal (Fig. 1). This was the largest earthquake in Nepal's history since 1934 Bihar–Nepal Earthquake. The recent report by the Government of Nepal indicates that the recorded death toll has reached close to 9,000. Immediately after the earthquake a Japanese expert team from three professional societies was sent for quick survey of the damage area. The professional societies were: the Japanese Geotechnical Society (JGS), Asian Technical Committee of ISSMGE on Geotechnical Natural Hazards (ATC3), Japan Society of Civil Engineers (JSCE) and Japan Association for Earthquake Engineering (JAEE). The authors were a part of the team, and surveyed some areas in and around the city of Kathmandu.

A recently submitted post-disaster need assessment (PDNA) report by the National Planning Commission of Government of Nepal, has estimated the total economic loss in 15 different sectors to be about US$7 billion, and the reconstruction cost to be about US$6.2 billion. The highest economic loss has been in the building structures and human settlements sectors, which show nearly half the total economic loss.

This paper summarizes the damage brought by the devastating earthquake especially to urban infrastructures, the historical monuments, modern and traditional buildings as well as some word heritage sites in and around Kathmandu city. The paper also focuses on a compound disaster brought to a hydropower plant by a previous landslide and subsequently by the earthquake. Finally, the paper also divulges possible reasons for such damage and geotechnical challenges towards the retrofitting of structures and reconstructions of the devastated areas.

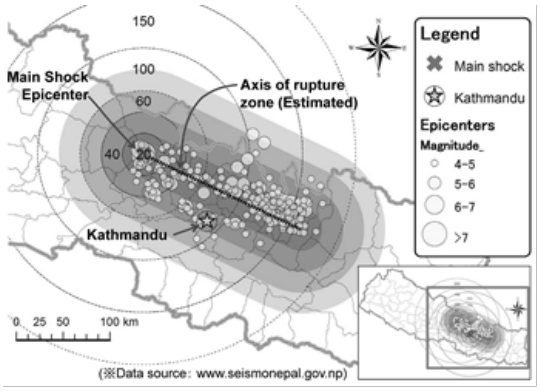

Figure 1. Epicenter of the earthquake and distribution of aftershocks.

2. TECTONICS OF KATHMANDU VALLEY AND MECHANISM OF THE EARTHQUAKE

2.1 Past earthquakes in Nepal

The record of historical earthquakes in the Nepal Himalaya dates back to the 13th century, but no clear documentation of the damage that occurred is available in the literature. Tabulated data on the historical earthquakes in Nepal and peripheral areas, as compiled by NSET and GHI (1999), indicate that a large earthquake occurs in the Nepal Himalaya roughly every 100 years. Since the last large earthquake in 1934 (i.e., Bihar–Nepal Earthquake, M8.1), 81 years have passed and it was widely estimated that a large earthquake was going to occur in the Nepal Himalaya within 100 years from 1934. During the last 35 years, three heavily damaging earthquakes and several damaging earthquakes have struck Nepal. The heavily damaging earth-quakes include the 1980 far western region earthquake (M6.5, Darchula), the 1988 eastern Nepal earthquake (M6.5, Udayapur), and the 2011 earthquake (M6.9, Nepal–India border) while damaging earthquakes of <M6.0 were recorded almost every year from 1993 until 2003. In addition, there is a long list of minor earthquakes that occur almost every month in and around the Nepal Himalaya. These earthquake data indicate that Nepal is situated in a highly earthquake-prone plate tectonic zone of the Himalayas.

2.2 Mechanism of the earthquake

The occurrence of earthquakes in the Himalayan region is primarily due to the collision between the Indian plate and the Eurasian plate (sometimes also referred to as the Tibetan plate in local or regional scale). As indicated in Fig. 2, the Indian plate moves northward and subducts underneath the Eurasian plate creating a zone of plate-tip squeezing at the Himalayas. This plate movement has resulted in the formation of the Himalayan Mountains, the uplift of which occurs at an estimated rate of 2 cm per year (Bilham et al., 1995). Moreover, the area-wide compression and uplift of the Himalayan region has resulted in extensive distribution of regional and local faults. Some of these faults generate major earthquakes, such as the 2008 Sichuan Earthquake during which nearly 88,000 people died. So far, however, the major earthquakes in and around the Nepal Himalaya have been mostly generated at the subduction zone of the Indian plate underneath the Eurasian plate (Fig. 2). The depth of the 2015 Nepal Earthquake has been estimated to be about 15 km, which makes it clear that this earthquake was generated exactly at the depth of subduction plane. The exact mechanism involved in the generation of this earthquake is yet to be clearly known, but a general interpretation is that the strain energy stored in the rupture zone due to the northward gently inclined thrust of the Indian plate was released with slipping of Eurasian plate-tip below the Main Boundary Thrust (MBT; Fig. 2).

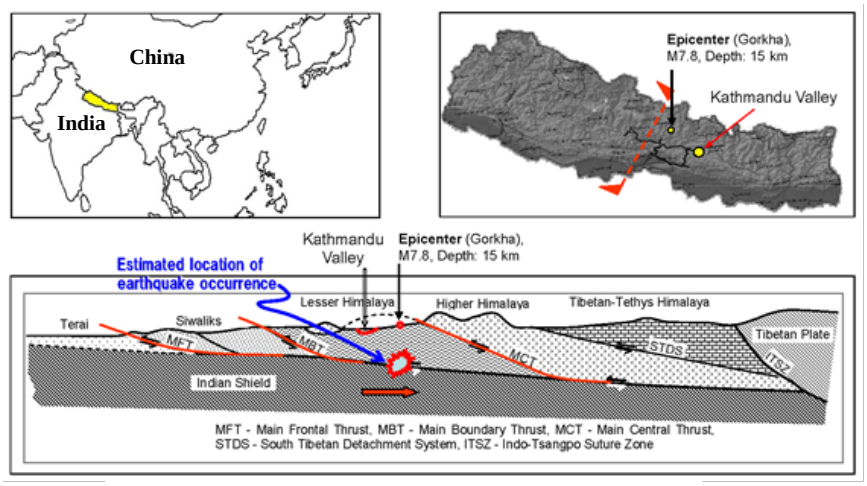

Figure 2. Mechanism of the earthquake.

3. DAMAGE TO URBAN INFRASTRUCTURES

9.142 km segment of the Kathmandu-Bhaktapur Road section of the Araniko Highway was upgraded by expanding the previous two-lane road to four lanes through JICA (Japan International Cooperation Agency) funded project. The road is also known as Nepal-Japan friendship road. The Kathmandu-Bhaktapur Road is designed to serve not only as a road to ensure smooth transportation of goods and people between Kathmandu and Bhaktapur, but also to play an important role linking the Kathmandu Valley with the Eastern Terrain via the Araniko Highway and the Sindhuli Road (which connects Dhulikhel-Sindhuli-Bardibas of the East-West Highway). Furthermore, this road section also improved the connection of the Kathmandu Valley with the north via the Araniko Highway, which is a vital physical infrastructure for Nepal in terms of connectivity to China and India (JICA, 2007). A part of the road was damaged due to the earthquake. This section summarizes the damage of the road and the surrounding infrastructures during the earthquake as well as the geological and geotechnical information available close to the area.

3.1 Damage to the road and surrounding infrastructures

Our survey focused only on the damage of the road located near the Lokanthali area (Fig. 3), covering a length of about 400 m. The state of the road before and after the earthquake is shown in Fig. 4. The various locations of the surveyed area were are shown in Fig. 5. In the Kathmandu side, heaving and subsidence of the road, slope failures in the main road and in the access road, ground fissuring, retaining wall damage and damage to the residential buildings close to the access road were observed. Similarly, in the Bhaktapur side, heaving and subsidence of the main road, slope failures in the access road and ground fissuring were observed.

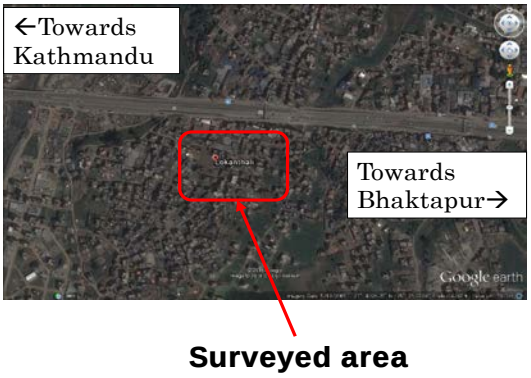

Figure 3. Kathmandu-Bhaktapur road (URL Source: http://www.earth.google.com).

(a) Before the earthquake

(b) After the earthquake

Figure 4. State of the road before and after the earthquake.

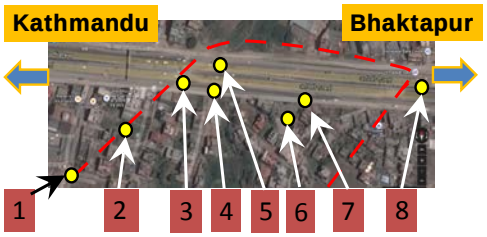

1: Ground fissuring
2: Ground fissuring
3: Slope failure and road damage
4: Retaining wall and building damage
5: Settlement of the road embankment
6: Sinking of the access road
7: Slope failure and road damage
8: Settlement of road

Figure 5. Locations of the damaged area in the main road and the access road (Source map URL: http://www.maps.google.com).

Slope failure in location 3 is shown in Fig. 6. As seen in the figure the traffic police box was tilted by about 12 degree due to slope failures and settlement of the road. In the Bhaktapur side (location no. 7) subsidence of the main road was observed (Fig. 7a). Also, slope failure took place in the access road (Fig. 7b). In location 5, huge settlement of the access road in the Kathmandu side was observed (Fig. 8a). An apartment building close to this sinking road was found to be settled and tilted as seen in Fig. 8b.

In location 4, two types of retaining walls exist: One is the reinforced retaining wall and the other is the gravity retaining wall. As seen from Fig. 9(a), in the joint between the two walls, damage was observed. Also, in some parts of the gravity retaining wall, cracks were observed along the same line in which ground fissuring of the access road was observed Fig. 9(b). Ground fissuring extended up to the residential areas along the road. Two residential buildings located along this fissure were found to be heavily damaged (Fig. 10). According to the owner the building with exposed brick structure, whom the authors happened to meet, the building settled by about more than 1 m towards the road and tilted. Many ground fissuring were also observed in the surrounding of the two buildings.

Figure 6. Slope failure in the Kathmandu side

(a) Main road

(b) Access road

Figure 7. Slope failure and subsidence (Bhaktapur side).

(a) Subsidence of the access road

(b) Tilted apartment building

Figure 8. Slope failure and subsidence (Bhaktapur side).

Ground fissuring was also observed in many lo-cations around the residential area surrounding the access roads. Fig. 11a shows one of those having a maximum width of 20 cm. Ground fissuring in 30° azimuth towards the east was observed. Such ground cracking was observed not only in the road embankment but also continued within a wide area both towards the left and right side of the road embankment. The angle of ground fissuring is almost the same in both sides of road embankment and of was 400 m in length towards the south west (Fig. 11b).

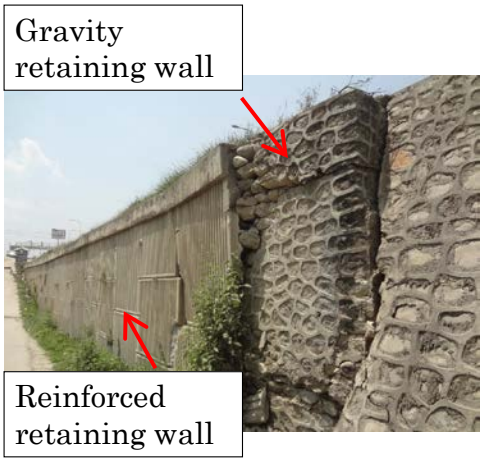

(a) Damage to retaining walls

(b) Ground cracks

Figure 9. Retaining wall damage and ground fissuring.

Figure 10. Settlement and tilting of buildings resulting from ground fissuring.

(a) Observed ground fissuring

(b) Fissure orientation in the area

Figure 11. Ground fissuring in the surveyed area.

3.2 Geological and geotechnical characteristics of the area

No detailed geotechnical information about the soil characteristics in the Lokanthali area is available. The closest information available is from the three borehole locations near 84m long Manahara bridge (Fig. 12) which is located less than 1 km from Lokanthali (JICA, 2007). Fig. 13 shows the geological profile of the borehole no. 3 (location close to Lokanthali).

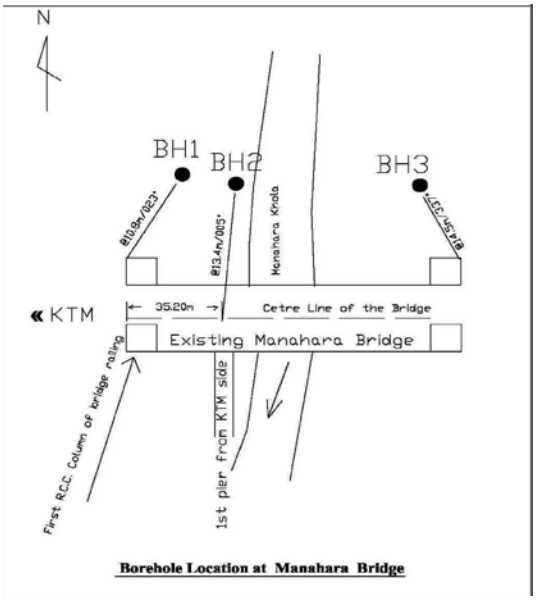

Figure 12. Borehole locations around Manahara bridge (JICA, 2007).

From Fig. 13 it is clear that the area is mostly dominated by very thick layer of compressive clay. Settlement of this clay deposits and possible amplification of motion may have resulted in such localized damage in this part of the Kathmandu-Bhaktapur road. However, detailed borehole information adjacent to the site and other geotechnical survey results are necessary to arrive at a definite conclusion.

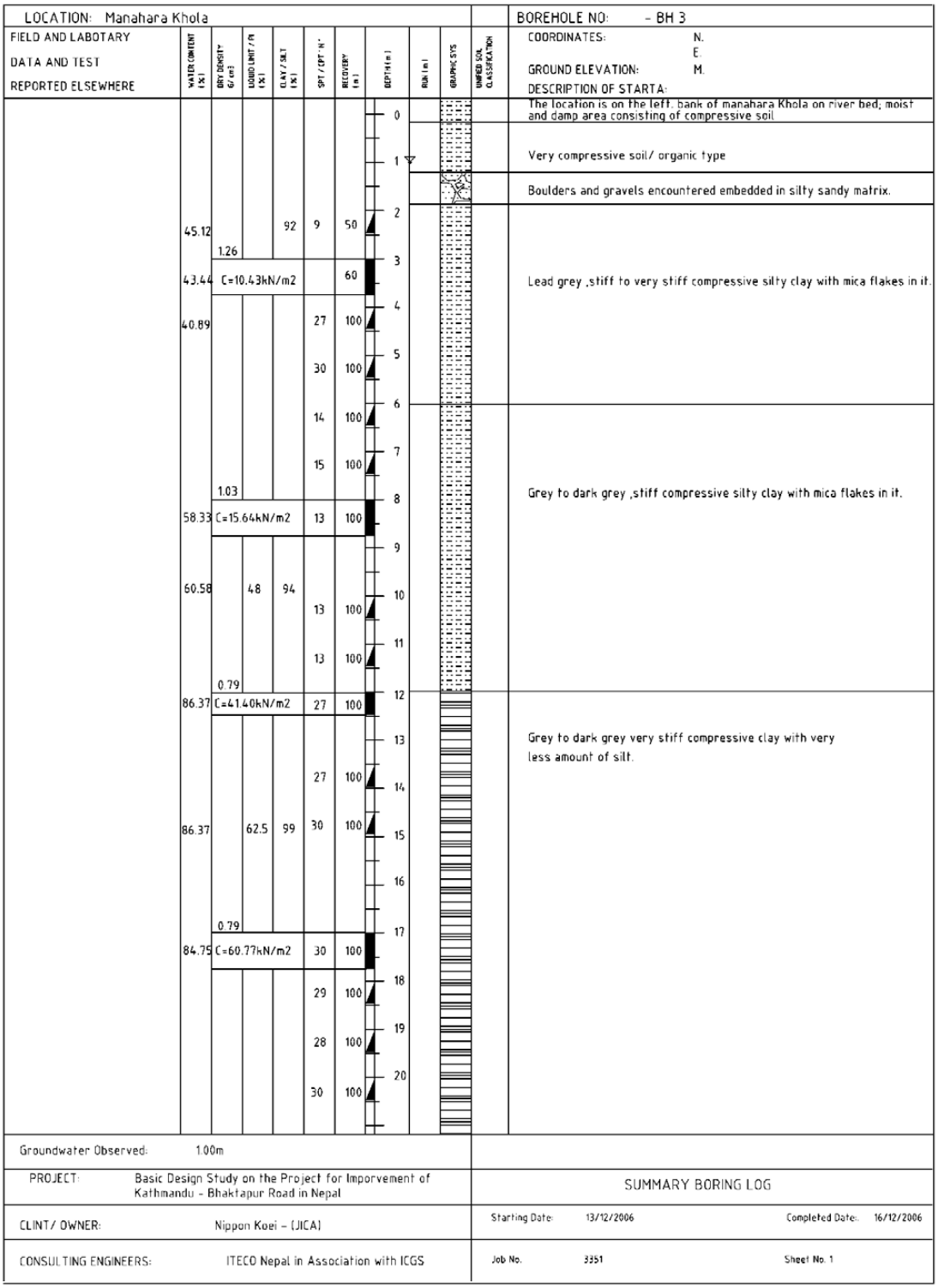

Figure 13. Soil profile at borehole no. 3 (JICA, 2007).

4. DAMAGE TO HISTORICAL SITES

Nepal is nonetheless home to eight UNESCO World Heritage cultural sites. That includes three royal cities and several Hindu and Buddhist sites within the Kathmandu Valley, as well as Lumbini, the legendary birthplace of the Buddha, all of which are in the area affected by the earthquake. Many of those centuries-old buildings and monuments were destroyed in the Kathmandu Valley, including some at the Kathmandu Durbar Square, the Patan Durbar Square, the Bhaktapur Durbar Square, the Changu Narayan temple and the Swayambhunath temple. In the following subsections few examples of damage inflicted on those historical buildings and monuments, word heritage sites and historic town are discussed.

4.1 Damage at Kathmandu durbar square

Several pagodas on Kathmandu Durbar Square, a UNESCO World Heritage Site, collapsed. The Dharahara tower in that square, built in 1832, completely collapsed leading to death of at least 180 people including honeymoon couples. Fig. 14 show the states of the tower before and after the earthquake.

Figure 14. State of damage of Dharahara tower.

4.2 Damage at Patan durbar square

Patan, famous as the oldest city in Kathmandu valley, is also known as the city of fine arts. Another name of Patan, is Lalitpur. The exquisite artworks and architectural buildings, scattered in and around Patan Durbar square, are from 16th century and onwards. In 1979 they were listed in the world heritage monument. It is probably one of the oldest Buddhist Cities in the world. The city is situated on a plateau across Bagmati River. In Patan, the Char Narayan Mandir, the statue of Yog Narendra Malla, a pati inside Patan Durbar Square, the Taleju Temple, the Hari Shankar, Uma Maheshwar Temple and the Machhindranath Temple in Bungamati were destroyed during the earthquake.

Fig. 15 is a 2010 photo of the intact temples. Several of the tiered temples appear to have collapsed. Fig. 16 shows the Harishankar temple, built in 1706 and one of the most outstanding temples in Patan before and after the earth-quake.

Figure 15. Patan square before the earthquake (Photo courtesy: Narendra Shrestha).

Figure 16. Harishankar temple before and after the earthquake.

4.3 Damage at Bhaktapur durbar square

In Bhaktapur durbar square, several monuments, including the Fasi Deva temple, the Chardham temple and the 17th century Vatsala Durga Temple, were fully or partially destroyed. Fig. 17

shows the famous Hindu temple (Vatsala Durga temple) before the earthquake. Built in 1672, this beautiful stone building was a favorite for many people to sit out on and watch the sunset in Bhaktapur durbar square. It is no more than rubble now (Fig. 18). Few other temples (Fig. 19) in the square were also seriously damaged including a school building which completely collapsed (Fig. 20).

Figure 17. Vatsala Durga temple before the earthquake.

Figure 18. Vatsala Durga temple after the earthquake.

Figure 19. States of other temples and buildings in Bhaktapur square.

Figure 20. Collapsed school building (only the gate remains) in Bhaktapur square.

4.4 Damage to Changu Narayan temple

One of the oldest Hindu temples in Nepal, Changu Narayan is believed to have been built in the 5th century A.D. Located on a hilltop east of Kathmandu, the two-tiered pagoda (Fig. 21) is considered one of Nepal's most unique architectural monuments. Constructed on a single slab of stone, the Changu Narayan temple had withstood the large earthquake of 1934 Bihar-Nepal Earthquake. This time earthquake inflicted some damage to this main temple as seen from the scaffolding of the temple after the earthquake (Fig. 22). Two of the four temples on the premises of Changu Narayan square have been reduced to rubble by the earthquake (Fig. 23 shows one of them).

Figure 21. Two-tiered pagoda in Changu Narayan.

Figure 22. Two-tiered pagoda after the earthquake protected by scaffolding.

Figure 23. One of the collapsed temples in Changu Narayan.

4.5 Damage to Sayambhunath temple

Comprising temples, shrines and the iconic stupa which bears the painted-on eyes of the Buddha, the 150-year-old Swayambhunath (also known as monkey temple) is not only a revered location for locals, but also one of the most-visited tourist destinations in the capital (Fig. 24). Swayambhunath temple complex in the Kathmandu Valley suffered heavy damage due to the earthquake. Few structures within the temple complex suffered damage (Fig. 25).

4.6 Damage to historic town of Sankhu

Sankhu is the ancient town, with predominant Newari culture, located in the north-eastern corner of Kathmandu Valley in about 17 km from the capital city Kathmandu. Sankhu is probably the worst affected historical town, where 80 to 90% of the buildings were completely col-lapsed.

Fig. 26 shows the view of the buildings in the town before the earthquake. Fig. 27 shows the state of the same buildings after the earthquake. Total collapse of many structures in the city were observed here and there (Fig. 28).

Figure 24. Sayambhunath temple complex.

Figure 25. Damage in Sayambhunath temple complex.

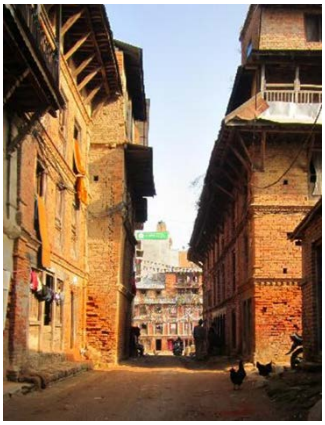

Figure 26. View of Sankhu town before the earthquake.

Figure 27. View of the spot in Fig. 15 after the earthquake.

Figure 28. Few selected collapsed structures in the town.

5. DAMAGE TO MODERN BUILDINGS

Not only the historical monuments and old brick masonry buildings, but many recently built and comparatively well-engineered buildings including multistory business complexes and apartment buildings were also heavily damage. In recent years, especially during the last one decade, Kathmandu valley has had a sharp rise in the number of multistory business complexes and apartment buildings, mainly constructed of reinforced concrete framed structure with brick masonry infill. Most modern residential and commercial buildings also follow the similar construction practice, but a large number of these buildings have been constructed without adequately incorporating the seismic design criteria. Even within the Kathmandu valley, which is the most densely populated urban settlement of the nation, most peripheral areas enjoyed waiver of the administrative process of construction permit up until a couple of years ago. Moreover, in many occasions, manipulation of the design data and use of substandard material quality have also added to poor seismic capacity of the buildings.

The trend of damage to reinforced concrete buildings during this earthquake can be categorized into two main patterns: 1) column breakage and severe structural tilting or complete collapse in comparatively short buildings (i.e. 3-6 story), as in Fig. 29 and 2) massive shaking and heavy damage to non-structural elements, such as brick masonry partition walls, in comparatively tall buildings (i.e., >10 story), as in Fig. 30. Leaving aside a few cases of complete collapse in other locations, damage to short buildings was concentrated in some pocket areas, such as Gongbu, Swayambhu, Sitapaila, and Kapan (Fig. 31). However, most such buildings in central core were not affected much except for a few cracks in the walls. On the other hand, out of more than 50 tall buildings in Kathmandu and Patan, more than 40 were found to have sustained medium to heavy damage, mainly in non-structural parts (Fig. 30).

Kathmandu valley is filled with soft sediment deposit composed primarily of lacustrine material, that goes as deep as 500 meters in the center. Borehole logs of different times are also evident that a larger part of the sediment deposit is composed of organic clayey material. Despite the fact that the bearing capacity of this clayey sediment is extremely weak, most buildings in Kathmandu valley have been constructed on isolated or raft footing foundation. Some of the tall buildings were found to have been tilted, which is due to poor bearing capacity of the foundation soil.

Figure 29. A typical case of damage to comparatively short buildings.

Figure 30. A typical case of damage to tall buildings.

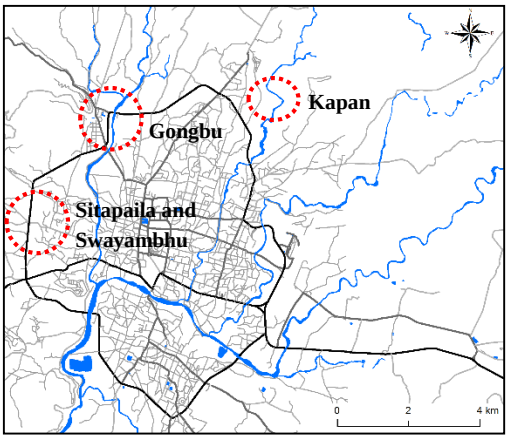

Figure 31. Core Kathmandu and Patan area.

6. COMPOUND DISASTER IN SUNKOSHI AREA

6.1 Jure landslide

A massive landslide occurred at around 02.30am, local time on August 2, 2014 at Jure village in Sindhupalchowk district of Nepal. The landslide killed 156 people, injuring 27 and displacing 436 people.

The massive landslide blocked Sunkoshi River creating a high dam across the river (Fig. 32). A river gauging station of the Department of Hydrology and Meteorology (DHM) at Pachuwarghat downstream of the landslide dam showed a rapid decline in water flow three hours after the landslide, after which the flow of water completely stopped for approximately 12 hours. An inflow of about 160 m^3/sec of water quickly created a large lake behind the dam. Within 13 hours the newly formed lake , which rapidly grew to a volume of an estimated 7 million cubic meters, extended about 3 km upstream, completely submerging the 2.6 MW Sanima hydropower station (Fig. 33).

Figure 32. Landslide in Jure (*Courtesy: Sanima Hydropower Ltd., Kathmandu*)

Figure 33. Submerged power station (*Courtesy: Sanima Hydropower Ltd., Kathmandu*)

The landslide-dammed lake also has created havoc amongst the local residents and people living in the downstream and upstream riverside areas. The landslide completely obstructed the Araniko Highway, and it was not possible to pass through the landslide further to the north, disrupting the transportation network to China,

and braking the national daily revenue of about 30 million Nepali Rupees.

6.2 Damage to Sanima Sunkoshi Power Plant due to landslide

The landslide at Jure has swept away two gates of the Sunkoshi power house headworks. The power house was also submerged after damage to the project's penstock. The powerhouse and the camp house lied at the sediment deposition zone. The lake inundated most of the equipment/materials in powerhouse and camp house. Figs. 34 (a)-(b) show the state of the damage before and after the landslide.

Private development firm (Sanima Hydropower Plant) undertook the repair and reconstruction works of the dam and it was ready for commissioning on May 1, 2015.

(a) Before the landslide

(b) After the landslide

Figure 34. State of the power station before and after the landslide (*Courtesy: Sanima Hydropower Ltd., Kathmandu*)

6.3 The Compound disaster

However, there is big blow to the works by the earthquake of April 25, 2015. The power house was damaged at various places by the earthquake as seen in Figs. 35(a) - 35(d). The earthquake also induced shallow landslides on the upstream and right bank of the power station as shown in Figs. 36(a) - 36(b).

(a) Wall collapse on riverside

(b) Rupture of reinforcement bar

(c) Operator's camp at headworks

(d) Machine floor

Figure 35. Earthquake induced damage to the power station

(a) Landslide in the upstream of intake

(b) Landslide in the right bank of Headworks

Figure 36. Earthquake induced landslide

The landslide related loss to the power plant amounts to 148 million Nepali Rupees. The earthquake damage was estimated to be 34 million Nepali Rupees. Total damages from this compound disaster stand at 203 million Rupees.

7. POSSIBLE REASONS OF THE DAMAGE AND LESSONS LEARNED

The acceleration, velocity, displacement profiles (Fig. 37) and spectral distribution (Fig. 38) of the earthquake reveal that the maximum acceleration (about 182 Gal) is not that high. However, the velocity, which is a barometer for generated earthquake energy, is rather high. Also, the spectral distribution of acceleration reveals that it was a long-period motion.

Most of the damage can be contributed to the non-engineered structures (combination of sunburnt brick and clay mortar), which have negligible resistance to earthquake type loading. Also, damage were mostly localized, which indicate the possibilities of resonance due to ground motion amplification in Kathmandu valley, which basically compose of soft alluvial deposits in old rivers and lakes (Fig. 39). The Kathmandu valley comprises of thick semi-consolidated fluvio-lacustrine Quaternary sediments on the top of basement rocks. Piya (2004) reports that the maximum thickness of the valley sediments reaches up to 550 m at the central part of the valley. The shear wave velocity of the soft sedimentary deposits ranges between 167 m/s and 297 m/s, and ground amplification may be ranging between 1.9 and 7.9 according to Chamlagain and Gautam (2015). Due to complicated geology of the Kathmandu valley two levels of resonance are expected (Paudyal et al., 2012).

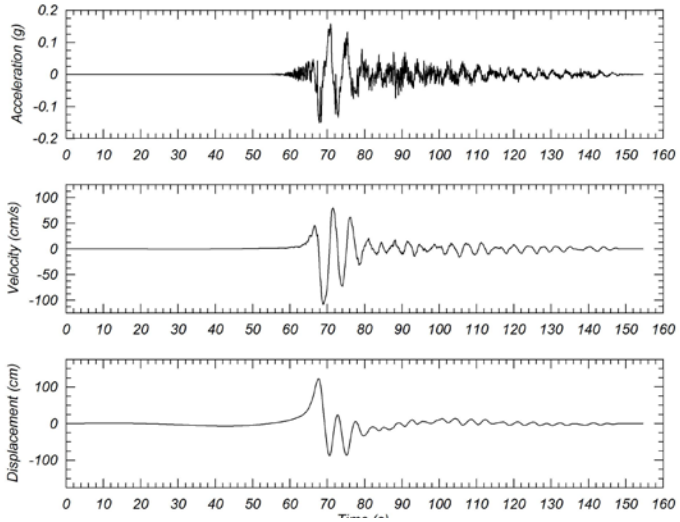

Figure 37. Acceleration, velocity and displacement profiles of the earthquake (Source: USGS).

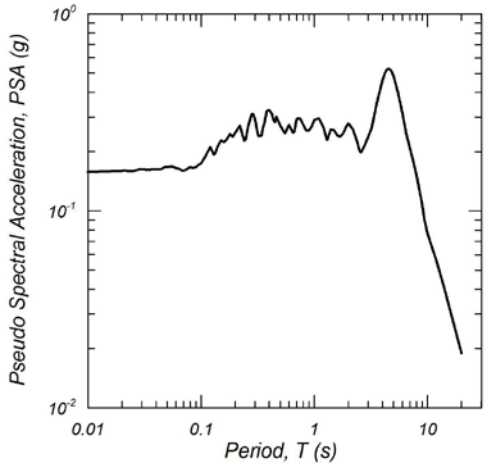

Figure 38. Spectral distribution (Source: USGS).

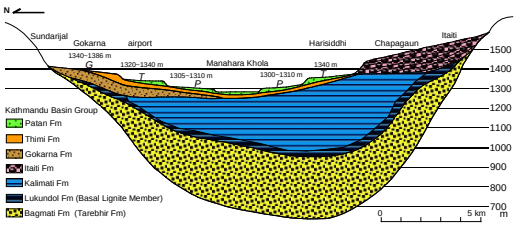

Figure 39. Schematic geological cross section of Kathmandu valley along N-S (Sakai, 2001).

8. CONCLUSIONS AND RECOMMENDATIONS

The following conclusions and recommendations could be made based on this preliminary survey of the earthquake damage of the structures.

(1) The damage to newly built building structures was concentrated at particular pocket areas and more specifically in newly developed sub-urban areas of the Kathmandu city core.

(2) Most old brick masonry buildings were heavily damaged throughout the valley, and the destruction was particularly found to be concentrated in Bhaktapur city core and Sankhu area of Kathmandu.

(3) One typical characteristic of the damage pattern found this time was that, comparatively little damage to hospital buildings and lifeline infrastructures including power line, water pipes, communication network, and roads. The only international airport in Nepal was reported to be totally undamaged.

(4) Immediate geotechnical and geological investigations of the soils in the vicinity of historical monuments are required.

(5) Reconstruction and retrofitting measures to be adopted considering acceleration amplification in future earthquakes.

(6) It is very important to take into the account the effect of soil stratum (surface and lower layers) and the velocity distribution profiles based on geotechnical data base.

(7) New approaches in the geotechnical design and retrofitting of foundations, which are cost-effective and locally available, require immediate attention.

(8) Use of information technology and local participation towards disaster mitigation also need attention.

(9) Rebuilding the historical sites this time around, especially the older ones, will be no easy task. In the retrofitting of the historical monuments in the Kathmandu valley, it is very important to collect information regarding the foundations of those structures. That is definitely going to be a challenging task for geotechnical engineers and researchers in the years to come.

ACKNOWLEDGEMENT

The authors would like to express their sincere gratitude to all the members of the survey group for their help while conducting the survey. The first author also would like to acknowledge the financial support provided by Kyushu University towards the survey.

9. REFERENCES

Bilham, R., Bodin, P., and Jackson, M. (1995). Entertaining a Great Earthquake in western Nepal: historic inactivity and geodetic tests for the present state of strain. Journal of Nepal Geological Society, Vol. 11, No. 1, pp. 73-78.

Chamlagain, D., and Gautam, D (2015). Seismic hazard in the Himalayan Intermontane Basins: An example from Kathmandu Valley Nepal. Mountain Hazards and Disaster Risk Reduction, pp. 73-103.

JICA (2002). The study of earthquake disaster mitigation in Kathmandu valley, Kingdom of Nepal. Japan International cooperation Agency, Final Report, Vol. I, II, III, IV.

JICA (2007): Planning for improvement of Kathmandu-Bhaktapur road in the Kingdom of Nepal, Japan International cooperation Agency, Report on the preliminary design and investigation.

NSET and GHI (1999). Earthquake Scenario, product of the Kathmandu Valley Earthquake Risk. Management project, National Society for Earthquake Technology-Nepal (NSET-Nepal) and GeoHazards International (GHI).

Paudyal, Y.R., Yatabe, R., Bhandary, N.P., and Dahal, R.K. (2012). A study of local amplification effect of soil layers on ground motion in the Kathmandu valley using micro tremor analysis. Earthquake Engineering and Engineering Vibration, Vol. 11, No. 2, pp. 257-268.

Piya, B.K. (2004). Generation of a geological database for the liquefaction hazard assessment in Kathmandu valley. MSc Thesis, International Institute for Geo-Information Science and Earth Observation, Enschede, The Netherlands.

Sakai, H. (2001). Stratigraphic division sedimentary faces of the Kathmandu basin group, Central Nepal. Journal of Nepal Geological Society, Vol. 25, Special Issue, pp. 19-22.

Sakai, H., Sakai, H., Yahagi, W., Fuji, R., Hayashi, T. and Upreti, B.N. (2006). Pleistocene rapid uplift of the Himalayan frontal ranges recorded in the Kathmandu and Siwalik basins, Palaeogeography, Palaeoclimatology, Palaeoecology, Vol. 241, No. 1, pp. 16–27.

Monitored deep excavation in the Ripio de Santiago de Chile

Juan Manuel Fernandez Vincent
Regional Technical Manager, Pilotes Terratest S.A., Chile

Freddy Lopez Loayza
Project Engineer, Pilotes Terratest S.A., Chile

Sergio Diaz Casado
Project Engineer, Pilotes Terratest S.A., Chile

Abstract: The typical retaining wall system used to execute the excavations carried out in Santiago corresponds to a discontinuous wall consisting on reinforced concrete piles, laterally braced with ground anchors.This paper presents a traditional contiguous wall system designed for a 21m deep excavation in the "Ripio de Santiago", and presents the results of the geotechnical monitoring carried out in the construction site for a typical section, consisting on inclinometer and anchor load measurements.

Keywords. Deep excavations, Ripio deSantiago, ground anchors, monitoring

1. INTRODUCTION

The city of Santiago de Chile, the country's capital with more than six million inhabitants, has been developing its buildings and underground spaces, changing the standard excavation in the year 2000 from 10-15m up to 20-30meters nowadays. Ground anchors took a big part as a technological tool to aid in that task, being introduced in the building industry in 1996 by this company. The accumulated expertise gained over the years and improved knowledge of the performance of the deep excavations of the time, was also fundamental.

The typical retaining wall system used to execute the excavations carried out in Santiago corresponds to a discontinuous wall consisting on reinforced concrete piles, laterally braced with ground anchors. The piles can be dug manually (usually in a rectangular shape), or drilled by a rig. The square piles initially were of one meter side and its separation was about 2,0-2,2m. Then the section turned rectangular and more efficient and with separations of 3,0-3,5m with up to 5,0m recorded.

2. GEOLOGICAL CONDITIONS

Santiago lies in the central part of an 80-km-long and 30-km-wide basin, a large bowl-shaped valley at the northern end of the central depression of Chile, which was caused by tectonic movements in the Tertiary of an area between two major faults parallel to two mountain chains running north-south. Volcanic activity dated between the upper Oligocene and lower Miocene is believed to have formed the basement of the Santiago basin. The basin itself is covered by sediments, most of which have been transported from the Andes mountains by a branched river system (Valenzuela 1978). The thickness of the sedimentary cover varies over short scales and can exceed more than 550 m. The sediments are mainly composed of gravel, sand and clay. Some deposits are believed to result from volcanic mud flows or glaciers.

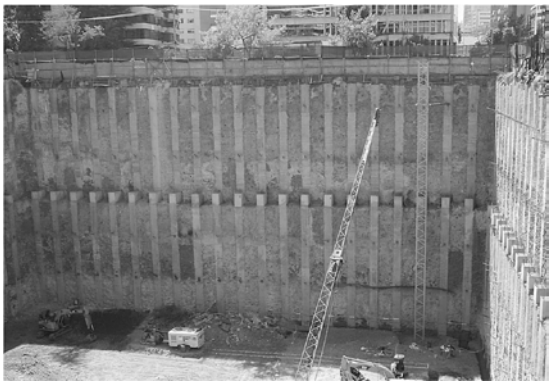

Figure 1. Deep excavation of 33 meters

3. GEOTECHNICAL CONDITIONS

The Santiago gravel is a Quaternary fluvial-glacial deposit, associated to the main drainage systems existing in the area: the Mapocho and the Maipo Rivers. The so called "Ripio de Santiago" presents excellent geomechanical characteristics.

From the surface down to a depth of 5–7 m, the gravel contains low-plasticity silty fines, with a cohesion of about 20kPa, and an angle of internal friction as high as 45º. This upper gravelly layer is known as the Second Deposition of the Mapocho River. This stratum is underlaid by the First Deposition of the Mapocho River. The first deposition is denser than the second one, but it has a similar granulometry. The following parameters for this deposition are commonly accepted: γ = 22,5kN/m3; c´= 20 – 37kPa; φ´=45°; E´=200-250 MPa.

Hydrological conditions are also favourable and the ground water level is at a depth of 70-80m below ground surface. The occurrence of water infiltration is associated to existing water bearing layers, leaking tubes and surface water percolating through the permeable gravel layers.

Figure 2. Deep excavation of 26,5m.

4. DESIGN ISSUES

The norm NCh3206.Of2010 defines the requirements that an excavation have to deal with. Usually, the key issue for the design of a deep excavation is its deformation. Often this is done by modelling the excavation and its construction phases, defining the most suitable earth pressure redistribution diagrams (i.e. after the EAB 2012 or own experience), and increased earth pressure coefficients, where applicable. Also, as a highly active tectonic region, the seismic verification plays an important role in the design and it is approached with a pseudo-static analysis, such as the proposed by Kuntsche (EAU 1990) or Mononobe-Okabe.

A basic acceleration of Ao=0,30g applies to this site (Zone II, after NCh433.Of2009). For temporary works, it can be reduced in function of the level of expected post-seismic plastic deformation (in function of characteristic of neighbour structure to protect or level of risk to assume). For a very stiff soil as the "Ripio de Santiago", usually a reduction factor of 0,50 applies to streets and 0,60 to neighbour structures.

The ground anchors length is dealt either by the simplified method of the seismic wedge analysis or by the Ranke-Ostermeyer deep seated stability analysis.

5. MONITORING PARQUE ORIENTE

Pilotes Terratest decided to monitor one of its projects in which its own Engineering design was to be executed in the Parque Oriente Building. Bored cased piles were executed in order to guarantee a minimum deviation of the wall due to the big boulders usually present.

Figure 3. Bored cased piles being executed

The typical section was 21,2m depth, and the monitored one was on the vicinity of the avenue Alonso de Cordova. An inclinometer casing was disposed in one pile attached to the reinforcement cage in its full length, and the two rows of ground anchors were instrumented with load cells when the sequence of construction applied. The inclinometer restriction in depth probed, after numerical analysis, not to influence more than 1mm the final stage readings because of the soil great rigidity.

Piles of 880 mm diameter were arranged every 3,20 m. In the monitored section, the first row of ground anchors was placed at 4,50 m depth and the second one at 13,0 m depth. The service loads of each anchor were 880 kN (275 kN/m) and 1245 kN (389kN/m) for the first and second row respectively.

Figure 4. Installation of the pile reinforcement cage with the inclinometer tube attached

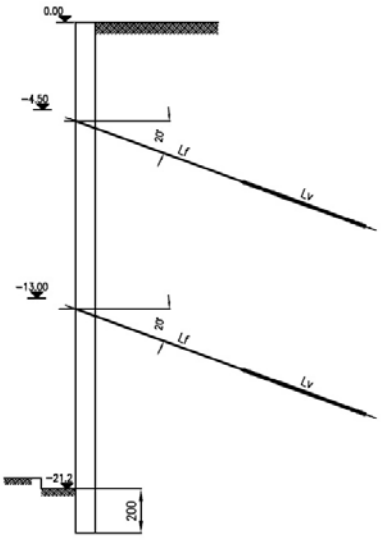

Figure 5. Cross section of the anchored pile wall.

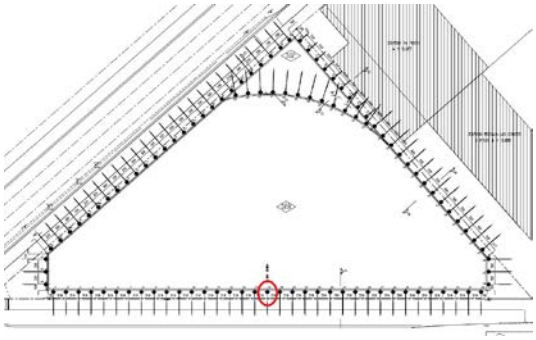

Figure 6. Excavation layout and monitored pile.

5.1. Construction sequence

The first excavation stage was carried to 5,50 m depth where the first row anchors were executed.

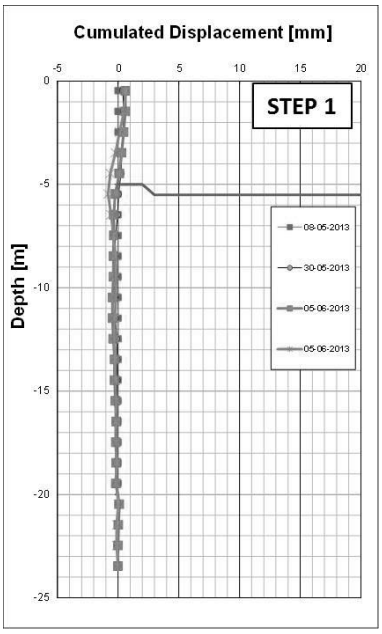

Figure 7. Horizontal deformations of stage 1.

The horizontal deformation of the pile in a cantilever behavior was of 1,3mm, and also was measured just before and after the anchor was tensioned and the wall moved 0,75mm backwards, and in the second row it was 0,45mm.

The second excavation stage was carried to 13,50 m depth where the second row anchors where executed. The excavation continued to 15,50 m depth before tensioning the anchor. A berm was left in front of the piles to allow the tensioning works.

The third excavation stage was carried to the maximum excavation depth. A maximum horizontal deformation of 15mm was measured at maximum excavation depth.

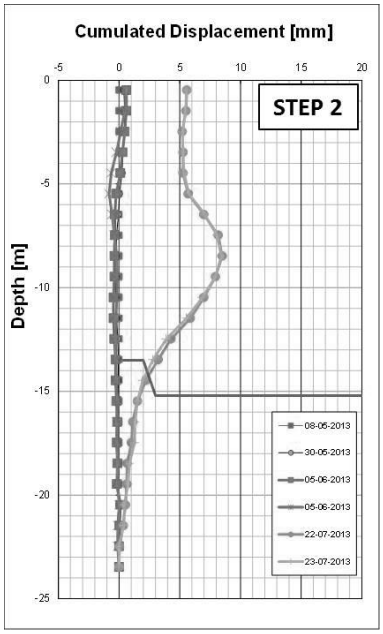

Figure 8. Horizontal deformations of stage 2.

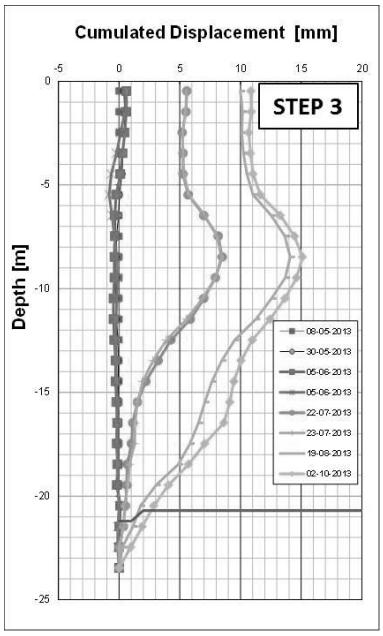

Figure 9. Horizontal deformations of stage 3.

The anchors loads were also measured at the mentioned stages. The anchor load variation behaviour was coherent with the expected very low creep value (ks) of the set soil-grout-steel and the measured deformation of the pile wall, related to its free length (specific deformation)

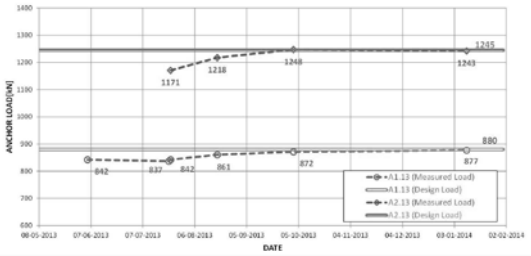

Figure 10. Ground anchor loads measured.

6. CONCLUSIONS

The monitoring of the jobsite verified the expected deformation perfomance of the wall and ground anchors behavior, and it helps the development of a robust expertise to safely approach deeper excavations in the future in order to provide the solutions that society demands from the a specialist geotechnical contractor.

7. REFERENCES

Boldrini, S. & Lopez, F. 2014.Design and Instrumentation of an Excavation with a contiguous pile Wall in the Santiago Gravel. *Proceedings of the VIII Chilean Geotechnical Engineering Congress*.

German Geotechnical Society 2012.Recommendations on Excavations (EAB 2012). 2nd Edition Berlin: Ernst &Sohn

German Geotechnical Society 1990.Recommendations of the Working Committee for Waterfront Structures (EAU1990). 8th Edition Berlin: Ernst &Sohn

INN-Chile 2010. NCh3206.Of2010 Geotecnia – Excavaciones, entibaciones y socalzados – Requisitos. NCh433.Of2009. Diseño Sísmico de Edificios.

Ranke-Ostermeyer. 1968. Bautechnik (Construction Engineering), Issue 10.

Valenzuela, G. 1978. Suelo de fundacion de Santiago. *Instituto de Investigaciones Geologicas*, Boletin No.33.

Figure 11.Deep excavation of 28 meters.

Figure 12. Inclinometer and load cell readings.

Figure 13.Parque Oriente building excavation completed.

Tunnelling in the vicinity of sensitive structures

Rolf Katzenbach,
Technische Universität Darmstadt, Germany, katzenbach@geotechnik.tu-darmstadt.de

Steffen Leppla,
Technische Universität Darmstadt, Germany, leppla@geotechnik.tu-darmstadt.de

Abstract: The growing size and population density of metropolitan areas is accompanied by a higher traffic demand. To ensure the growing requirements the construction of large infrastructure projects is necessary. In many cases these infrastructure projects are close to sensitive properties. Especially the influence on existing (underground) structures in conjunction with the construction of new underground structures and the deconstruction of existing structures must be taken into consideration. The experiences of two large projects from Spain and Germany will be presented in the paper. The first of the presented projects is the new tunnel of the Spanish high speed railway line under the city center of Barcelona, Spain. The tunnel with a diameter of 11.55 m passes adjacent to buildings belonging to the World Heritage Properties of the UNESCO. The second project is a tunnel from the high speed railway line Cologne-Rhine/Main next to Frankfurt am Main airport, Germany. The motorway interchanges Frankfurt has to be crossed under by several tunnels. The experiences made in the planning and construction phases of these complex projects are explained and for new inner urban projects recommendations are given.

Keywords. soil-structure interaction, in-situ testing, observational method, World Heritage Properties

1. INTRODUCTION

Due to the continuously growing traffic volume in most metropolitan areas large infrastructure projects are accomplished, mainly in order to improve the public transport (bus, metro, train, tram) and the individual traffic (cars, pedestrians).

In almost every big city in Europe underground constructions in high density urban areas like metro, tram, road and railway tunnels are realised, for example the metro in Vienna [1], the metro in Rom [2], the metro in Budapest [3], the road tunnels of the M-30 in Madrid [4], the metro and railway tunnels in Berlin and the high speed railway line in Barcelona.

Concerning the location in urban sites, these underground constructions have to be realised in a context of a sensitive neighbourhood [5], for example World Heritage Properties like the Sagrada Familia in Barcelona. Therefore the requirements on those infrastructure projects with regard to precision and the minimization of impacts on the heritage properties are extremely high. The interaction between existing buildings, the tunnelling process, groundwater and subsoil is very complex. The quantity of the impacts cannot be easily predicted, even with the existing state of the arts calculation methods [6].

High-level soil investigations, a comprehensive analytical analysis and numerical simulations in conjunction with a qualified, construction supervision and the consistent application of the Observational Method can guarantee for the safety and serviceability of new underground structures and neighbouring structures.

2. DISPLACEMENTS RELATED TO EPB TUNNELLING

In order to reduce the subsidence risk, earth pressure balanced shield machines are a good solution in an urban environment in comparison to other tunneling methods [7].

Settlements are evoked by changes in the stress conditions or changes in pore water pressure [8]. With an active support pressure of the face, of the gap between shield and surrounding soil and of the gap behind the tail of shield, these changes can be reduced to a minimum [8].

Nevertheless, settlements or ground subsidence occur in every tunnel construction process.

In order to characterize the settlement trough evolution in width and depth over a tunnel section, the volume loss factor V_1 can be used. V_1 describes the volume of the settlement trough related to the theoretical tunnel volume [9], [5] (Figure 1).

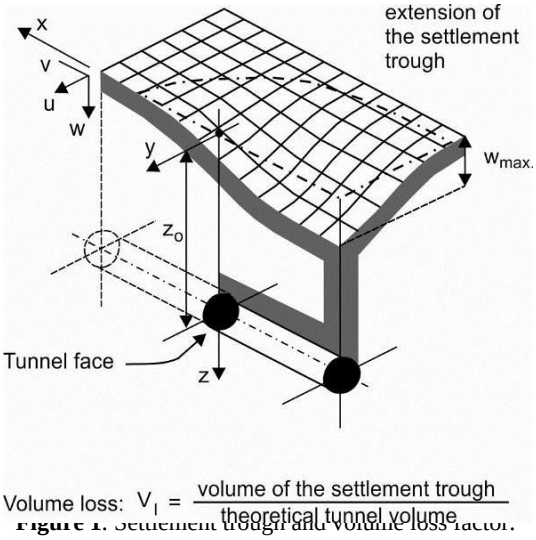

Figure 1. Settlement trough and volume loss factor.

As shown in Figure 1, V_1 is an instantaneous value, changing with the position of TBM and the analyzed tunnel section. The final V_1 usually ranges from 1% to 2% for tunnels excavated with the conventional method. In the case the tunnel is constructed using an earth pressure balance shield lower values can be observed, sometimes below 0.5% [5].

The factor influencing the shape, the depth and the length of the settlement trough related to EPB tunneling are numerous. Basically, they can be divided into geotechnical, geometrical and operational parameters of the TBM [10].

2.1. Geotechnical parameters

The boundary conditions for the tunnelling process are given with the geotechnical parameters, i.e. the soil characteristics as for example rigidity, friction angle, cohesion, deformability, permeability and abrasiveness. Based on a good soil investigation, the choice of the tunnelling method and the specification of operational parameters can be done efficiently. Good knowledge of ground parameters and groundwater conditions enables realistic calculations and then the possibility to define requirements and adequate thresholds for the operational parameters of the TBM.

2.2. Geometrical parameters

The geometrical tunnel parameters are essentially the depth of the tunnel, the diameter of the tunnel and the lining geometry, meaning the thickness and shape of the lining and the width of the gaps.

Besides the geometry of the tunnel, the distance and geometry of adjacent buildings and structures have a significant influence on the magnitude of settlement [11]. This might be for example pile foundations, another tunnel or – like in Barcelona – a protection wall influencing the settlement behaviour.

Also the geometry of the TBM itself influences the development of settlement; especially the conical shape of the shield has to be mentioned in this context [5].

2.3. Operational parameters

Numerous operational parameters of tunnel boring machines with earth pressure balanced shields exist, all influencing the reaction of the soil around the TBM. The following 10 TBM parameters were identified as having the greatest influence on the magnitude of surface settlement [10]:

- Face pressure
- Pressure and volume of filling the gaps
- Torque on the cutting wheel
- Total thrust force
- Power excavating 1 m³
- Back filling pressure
- Grouted volume of mortar
- Rate of advancement
- Time for boring and installing 1 ring
- Change in vertical angle of the TBM
- Change in horizontal angle of the TBM

With a numerical study Vanoudenheusden [12] identified that essentially the rate of advancement, the torque on the cutting wheel, the face pressure and the change in vertical angle of the TBM could be correlated to surface settlement.

3. CONSTRUCTION WORK NEXT TO SENSITIVE HISTORICAL BUILDINGS

Performing construction adjacent to historical building very often implements special difficulties already in the design phase of the new project. The structural elements, especially foundation elements, of ancient buildings are not or not exactly know [5]. Drawings very often do not exist or do not give enough details. Former structural calculations cannot be reconstructed any more.

Usually, careful and extensive site investigations are needed to analyse the structure and the foundation of historical buildings.

During the construction of new structures displacements, vibrations or changes in groundwater conditions may occur and create difficult situations for sensitive historical buildings.

4. TUNNELLING CLOSE TO WORLD HERITAGE PROPERTIES

4.1. Project overview

In 2010 to 2012 a double tracked tunnel with a length of 5.6 km was constructed under the city centre of Barcelona as a part of the new Spanish high speed railway line (AVE) connecting Madrid, Barcelona and Paris.

The tunnel of the high speed railway line passed directly next to the famous church Sagrada Familia and the famous building Casa Milà, both belonging to the world Heritage Properties of the UNESCO.

The tunnel has an outer diameter of 11.55 m. The bottom of the tunnel Is located in a depth of about 40 m under the ground surface.

The tunnel was built by a tunnel boring machine (TBM), using an earth pressure balance shield (EPB). The TBM was working and monitored continuously 24 hours a day. With the chosen EPB shield, the soil was conditioned with water and foam injections at the cutter head. The homogenized, excavated earth slurry was used as support medium [13]. The gap between the TBM and the excavated soil was injected with bentonite [8]. The gap behind the tail of the shield was permanently grouted with mortar to provide a compensation grouting procedure [5].

4.2. Soil and groundwater conditions

The location of the project is the comparatively plain area in the City Centre of Barcelona.

Most of the soil layers passed by the tunnel boring machine are tertiary layers (Figure 2). In the first kilometre of the tunnel the TBM passed through the tertiary clay followed by a section of tertiary silty sands. In this section the world heritage properties Sagrada Familia and Casa Milà have been passed.

The soil and groundwater characteristics in the vicinity of Sagrada Familia and Casa Milà are given as follows:

- 0 m to 2 m: filling
- 2 m to 12 m: quaternary layers
- 12 m to 60 m: tertiary silty sands
- Below 60 m: tertiary clays
- Groundwater level is about 16.5 m below the surface

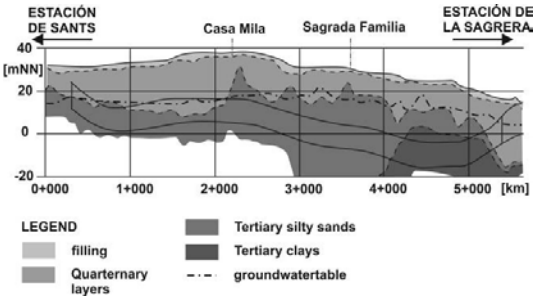

Figure 2. Geotechnical longitudinal section.

4.3. Tunnel construction close to Sagrada Familia

The basilica of Sagrada Familia is a church still under construction. It was designed by the architect Antoni Gaudí. The construction of the outstanding building began in the year 1882 and the end of the construction works is currently planned for 2026. The parts of the church built in Gaudí's lifetime belong to the World Heritage Property of the UNESCO since 1984.

Antoni Gaudí planned a church with a 50 m high main nave with a length of 90 m and at large 18 steeples, from which the highest is planned with a height of 170 m.

The church of Sagrada Familia has a pile foundation. The piles under the main nave are estimated to have a depth of approx. 20 m.

The AVE tunnel lies in a horizontal distance of only 4 m parallel to the Glory façade, the bottom of the tunnel in a depth of approx. 37 m as shown in Figure 3.

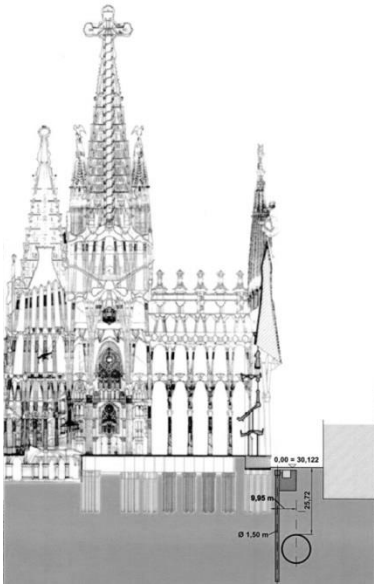

Figure 3. Cross section at Sagrada Familia.

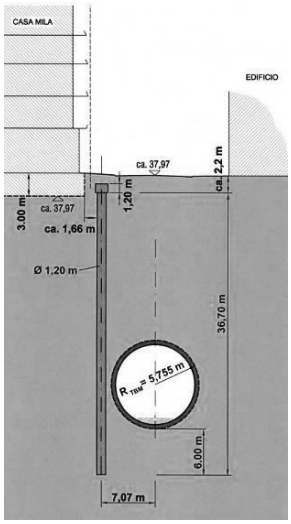

Figure 4. Cross section at Casa Milà.

In order to guarantee the safety of Sagrada Familia and to avoid settlements soil improvements (grouting, soil exchange) were executed and a bored pile wall was constructed between Glory façade of Sagrada Familia and the AVE tunnel. The diameter of the piles is 1.5 m. They have an axial distance of 2 m and a length of approx. 40 m.

4.4. Tunnel construction close to Casa Milà

The other World Heritage Property of the UNESCO that was passed by the TBM is the Casa Milà. It was also designed by the architect Antoni Gaudí and built from 1905 to 1910.

The AVE tunnel has a minimal horizontal distance approx. 30 m (Figure 4).

In order to fulfil the special requirements in control and construction of the AVE tunnel, between Casa Milà and the AVE tunnel a bored pile wall has been installed. The diameter of the piles is 1.2 m with a depth of 37 m. The drilling works for this redundant safety margin have been complitacated due to the form of the balconies of the building.

The settlement due to the construction process of the bored pole wall was about 0.1 cm. The TBM passed in February 2011 and induced additional settlement of less the 0.1 cm.

4.5. Monitoring results

In order to ensure a safe construction of the AVE tunnel and to give the maximum possible safety for the sensitive buildings in vicinity the construction works had to be executed under special control and supervision requirements following the observational method according to Eurocode EC 7 [14]. The monitoring in Barcelona was realized with a dense grid of geodetic and geotechnical measurement devices in the surrounding of the tunnel on the one side and with a permanent monitoring of the most important operational parameters of the TBM on the other side. With regards to [12] an observation of the geometrical, geotechnical and operational parameters was implemented. For example the correlation between the geotechnical parameters and the settlements are shown in Figure 5.

The measured surface settlements do not exceed 0.5 cm over the whole tunnel length. The volume loss factor V_l is in the range of only 0.1%. The biggest settlement occurred at the start of the TBM between PK 5+800 and PK 4+700 in the tertiary clay. It is possible to explain the decrease of the settlement over the tunnel length by the adaptation of the gained experience of the soil and tunneling conditions during the first part of the tunneling process concerning the definition of adequate thresholds and limits for the TBM operation.

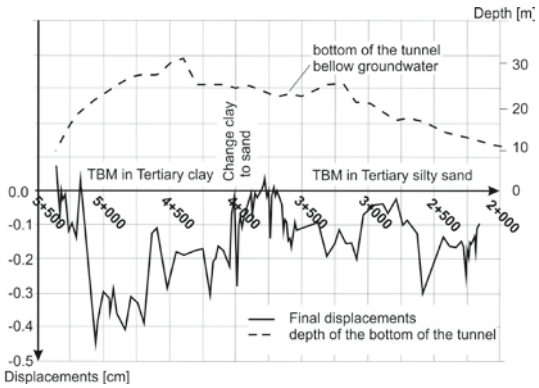

Figure 5. Surface settlements and geotechnical parameters.

Small heaving of less than 0.1 cm occurred between PK 4+200 and 4+300, directly after the change from tertiary clay to tertiary silty sands. The settlements in the tertiary clay are up to 0.4 cm. in the tertiary silty sand the settlements are up to 0.3 cm.

An influence of the groundwater height over the bottom of the tunnel on the displacements cannot be noted.

In all reflections about the magnitude of the displacements the measurement accuracy for the surface leveling of approx. 0.1 cm has to be taken into consideration.

5. TUNNELLING UNDER INFRASTRUCTURES

5.1. Project overview

To realize the construction of the new high speed railway line between Cologne and the Rhine/Main area, Germany, including the new railway station at Frankfurt airport a motorway intersection had to be crossed by tunnels.

Because of the higher depth and to achieve a minimal disturbance of the road traffic the construction of the southern tunnel was done by conventional tunneling. The northern tunnel section was constructed by a cut-and-cover construction method respectively by a dig-and-cast construction method.

To construct the tunnel by conventional methods a jet grouted roof cover and a jet grouted floor cover were necessary. The roof cover was necessary for the stabilization. The floor cover was necessary to seal the tunnel against the groundwater. The tunnel face was stabilized by a support core. The construction scheme is shown in the Figure 6 and 7. The tunnel was constructed from both sides in alternating steps.

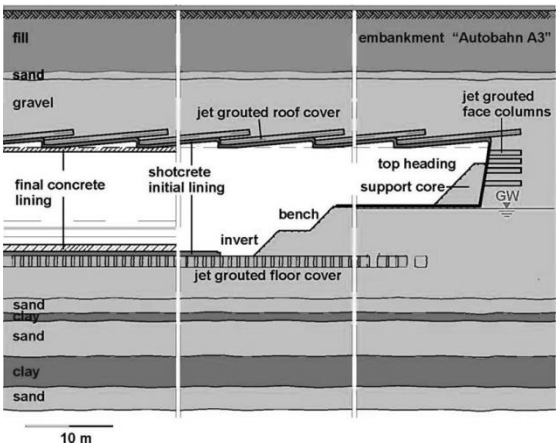

Figure 6. Longitudinal section.

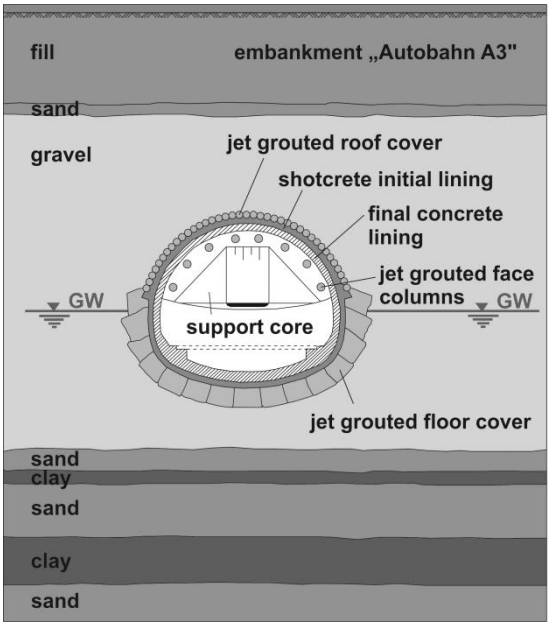

Figure 7. Cross section.

5.2. Soil and groundwater conditions

The project is located in the northern Upper Rhine Valley Fault particularly in the area of the Kelsterbacher Tiefscholle. Most of the soil layers passed by the tunnels are lower pleistocene soils which consist of alternating layers of dense sand

and gravel. This condition is typical for the area and is called Kelsterbacher Terrasse.

In bigger depth clay layers have been found, alternating with the sand and gravel layers.

The groundwater level is about 15 m to 16 m below the surface.

5.3. In-situ tests

Due to the complex soil-structure interaction at this project the originally design had to be verified to achieve a safe and optimized solution. Therefore the results of the laboratory tests had to be checked as well.

In addition to the laboratory tests large scale in-situ tests have been carried out to detect the shear strength parameters in the location of the tunnel. Therefore two series of shear tests were performed in the calotte of the tunnel. The in-situ shear tests have been carried out in the breaks of the alternating construction steps without hindering the construction progress.

For the in-situ test a 1 m x 1 m quadratic shear frame with hydraulic jacks for the vertical loading and the horizontal displacements including the necessary measurement devices have been installed close to the tunnel face. Figure 8 shows the test setup with the steel beam construction which transfers the loads to the top of the tunnel as abutment.

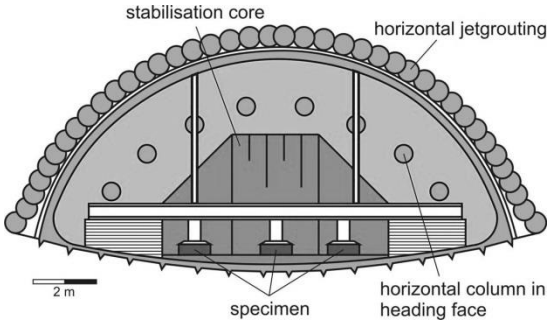

Figure 8. Test setup at the tunnel face.

The occurring very big loads had to be carried by the steel frame and the construction of the tunnel roof. Density tests in-situ detected a density $\rho = 2.08$ g/cm³ of the sandy gravel. As the result of one of the in-situ shear tests Figure 9 shows the τ-σ-diagram.

The results of the in-situ shear tests confirmed the results of the laboratory tests. This knowledge is part of the safety concept of this tunnel construction project.

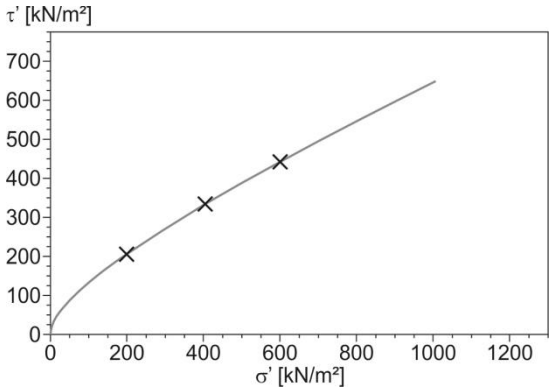

Figure 9. Result of an in-situ shear test.

5.4. Measured settlements

Regarding to the complex soil-structure interaction the construction works have been monitored according to the means of the observational method [15].

For safety reasons of the ongoing road traffic the settlements of the surface have been measured. The overview of the project area and the measured settlements are shown in Figure 10. The maximum settlements were about 4 cm. The main tracks of the motorways had settlements of up to 2 cm.

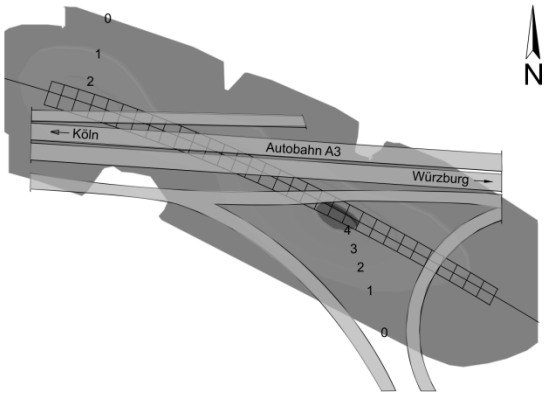

Figure 10. Measured settlements in [cm].

6. CONCLUSION

The two examples from Barcelona and Frankfurt show that a careful and well planned and moni-

tored construction process enables tunnel construction projects even in the direct vicinity of sensitive structures. The application of the observational method with its special requirements in design, construction and monitoring is a tool of safety and quality assurance. The main aspects for a safe and optimized construction of underground structures close to sensitive structures are as follows:

- For the precise prediction of the soil-structure interaction extensive numerical, non-linear analysis are necessary.
- Based on the principle of the observational method a geodetic and geotechnical monitoring program has to be developed and installed.
- The 4-eye-principle has to be guaranteed. An independent peer review should be installed in an early planning phase [16].
- For extreme situations an emergency and contingency program has to be developed concerning the aspects of stability and serviceability.

7. REFERENCES

[1] Moritz, B. & Koining, J. 2011. *Geotechnische und messtechnische Herausforderungen beim Auffahren großer, oberflächennaher Querschnitte im Lockergestein*, Taschenbuch für den Tunnelbau, pp. 105-142.

[2] Hofmann, A., Cresto, A., Kraft, O.: Mechanized Tunnelling for two new Metro lines in Rome, *Tunnel 2/2010*, pp. 30-35.

[3] Bäppler, K. 2009. EPB Shields for Building Metro Line 4 in Budapest/H, *Tunnel 3/2009*, pp. 20-24.

[4] Marqués, M. F. & Lorenzo Romero, J.: Modelization, back-analysis and sensitivity analysis of the north tunnel of the M-30 south bypass (Madrid), *Ingeniería Civil 159/2010*, pp. 19-31.

[5] Kastner, R., Emeriault, F., Dias, D. 2010. Assessment and control of ground movements related to tunnelling, *International Conference GEOMOS*, Geotechnical Challenges in Megacities, Moscow, Russia, 2010, pp. 92-119.

[6] Knitsch, H.: Steering Supporting Measures for Urban Tunnelling, *Tunnel 2/2010*, pp. 43-49.

[7] Saczynski, T. M., Pearce, M., Elioff, A. 2007. Monitoring Earth Pressure Balance Tunnels in Los Angeles, FMGM: *Seventh International Symposium on Field Measurements in Geomechanics*, Boston MA, 2007, ASCE

[8] Maidl, B., Herrenknecht, M., Maidl, U., Wehrmeyer, G. 2011. *Maschineller Tunnelbau im Schildvortrieb*, Berlin: Ernst and Sohn Verlag.

[9] Burghignoli, A., Di Paola, F., Jamiolkowski, M., Simonacci, G. 2010. New Rome metro line C: approach for safeguarding ancient monuments. *International Conference GEOMOS*, Geotechnical Challenges in Megacities, Moscow, Russia: pp. 55-78.

[10] Boubou, R., Emeriault, F., Kastner, R. 2008. Correlation between TBM parameters and ground surface settlements, neural network method, *ISSMGE TC 28*, Budapest, Hungary: presentation slides.

[11] Mair, R. J., 2005. *TC28 – tunneling: reflections on advances over 10 years.* Geotechnical Aspects of Underground Construction in soft ground, London: Bakker et al. (Eds), pp. 81-86.

[12] Vanoudheusden, E., Petit, G., Robert, J., Emeriault, F., Kastner, R., Lamballerie, J.-Y., Reynaud, B. 2006. *Analysis of movements induced by tunnelling with an earth-pressure balance machine and correlation with excavating parameters*. Geotechnical Aspects of Underground Construction in soft ground, London: Bakker et al (eds), pp. 81-86.

[13] Göbl, A. 2010. The interaction of ground, TBM and segment lining with closed shield machines, *Geomechanics and Tunnelling 3*, 2010, pp. 491-500.

[14] Katzenbach, R. & Strüber, S., 2003. Schwierige Tunnelvortriebe im Locker- und Festgestein – Anforderungen an Erkundung, Planung und Ausführung. Geotechnik 4, pp. 224-229.

[15] Katzenbach, R., Bachmann, G., Leppla, S., Ramm, H. 2010: Chances and limitations of the observational method in geotechnical monitoring. 14th Danube-European Conference on Geotechnical Engineering, Bratislava, Slovakia, 13p.

[16] Katzenbach, R., & Leppla, S. 2013: *Qualified soil investigation and the 4-eye-principle as basis for safety and serviceability of geotechnical constructions*. 1st International Conference on Foundation and Soft Ground Engineering Challenges in Mekong Delta,Thu Dau Mot University, Binh Duong City, Vietnam, pp. 19-26.

Piled Raft Foundation Design for a Supertall Tower Underlying by Complex Ground Condition

A.K.M. Lam and J.W.C. Sze
Ove Arup & Partners Hong Kong Limited, China

Abstract: This Paper presents a supertall tower in South Korea resting on soft rock with complex geological setting as a case history to illustrate the geotechnical design process of a piled raft foundation to ensure that the movement performance of the tower is being met. The specialties are attributed by the way in establishing the possible geological models, three dimensional soil-structural interaction analyses and non-linear stiffness adopted in the analyses to better represent the non-linearity of the ground response under the tower loads. The findings of the three dimensional soil-structural interaction analyses using Arup in-house program GSRAFT computer models and a cross-checking exercise using PLAXIS 3-D model will be discussed.

Keywords. supertall, piled-raft, soil-structural interaction, non-linear stiffness

1. INTRODUCTION

The combination of raft and pile foundations as a unified supporting system to support super high-rises involves soil-structure interactions amongst the raft, piles and the underlying soil. The estimation of the load sharing among the raft and the piles and the degree of mobilization of the pile capacity are the key challenges for a piled raft design. Normally, a safety factor of 2 and 3 are applied to the design of the pile and the raft foundations respectively. When the raft alone does not possess adequate safety factor, the piles are introduced to reduce the bearing pressure of the raft. However, as the piles are much stiffer than the soil, if the conventional safety factor is adopted, most of the load will be taken by the piles and the contribution from the raft under the piled raft system is substantially decreased. In some situations, the raft alone possesses adequate safety factor against bearing failure and the piles can be designed as settlement reducers solely to control the settlement and/or differential settlements of a raft.

This Paper presents a supertall tower in South Korea resting on soft rock with complex geological setting as a case history to illustrate the geotechnical design of a piled raft foundation using the concept of piles as settlement reducers. These piles are mainly to ensure the movement performance of the tower.

2. DESIGN PHILOSOPHIES

The design philosophies with respect to piled raft foundation have been clearly defined by Randolph (1994) and summarized by Poulos (2001a) as follows: -

(a) the "conventional approach", in which the piles are designed as a group to carry the major part of the load, while making some allowance for the contribution of the raft, primarily to ultimate load capacity;
(b) "creep piling", in which the piles are designed to operate at a working load at which significant creep starts to occur, typically 70 to 80% of the ultimate load capacity; sufficient piles are included to reduce the net contact pressure between the raft and the soil to below the pre-consolidation pressure of the soil.
(c) differential settlement control, in which the piles are located strategically in order to reduce the differential settlements, rather than to reduce the overall average settlement substantially.

Design philosophy (a) is predominately governed by the pile group behavior. Design philosophy (b) is considered to be effective to control the raft settlement with piles designed with a lower safety factor. Design philosophy (c) is believed to be the most cost effective piled raft system as the piles are designed to fully utilize

their ultimate capacity. It is however difficult to precisely predict the load sharing between the piles and the raft in view of the complex soil-structural interaction of a pile group, the non-linear stiffness behavior of the soil and the actual pile deformation behavior in practice.

As far as the overall stability of a piled raft system is concerned, the most effective application of such system is that the raft alone can provide adequate load bearing capacity and the piles are only designed to control the settlement and/or differential settlements of the raft. In this regard, the piles can be treated as settlement reducers or part of the ground stiffening element and a lower safety factor can be adopted. This design concept is acceptable to most design engineers as the overall stability is also increased in associated with the introduction of the piles. Nevertheless, the structural design of the piles shall comply with the respective design code in order to prevent any structural damage. Taking the design philosophy (b) as discussed above but with the raft alone being capable to provide adequate safety factor against bearing failure, piles are designed with factor of safety of about 1.3 to 1.4 against the geotechnical capacity. With this design concept, Davies et al (2009) applied the piled raft system to control the settlement and the differential settlement for a high-rise development and discussed its financial benefits.

3. DESIGN PROCESS AND METHOD

The movement performance of the raft is dominated by the geological condition and the ground stiffness parameters beneath the raft. The geological model is usually inferred from the borehole data and for the case of raft foundation bearing on rock (i.e. soft rock) with complex geological setting, rock face mapping is essential to establish a credible geological model. Sometimes, several geological models are developed for design in respond to the variability of the ground.

Apart from the geological model, the stiffness of the ground is another critical factor that influences the analysis results. Soil and soft rock are well known as non-linear materials but in routine foundation designs they are usually treated as elastic material to facilitate an easier computational analysis. However, the ground with complex geological setting renders difficult estimation of a reasonable average stiffness of the ground. In addition, the use of non-linear soil and/or rock stiffness do not require a well-defined rigid boundary beyond which the settlement becomes minimal. The degradation curve of the non-linear modulus for sandy soils can be referred to Seed & Idriss (1970) and Pappin et al (1989). The initial modulus at very small strain (i.e. about 0.0001%) can be correlated with the in-situ shear wave velocities measurement whilst the modulus at higher strain values (i.e. about 0.01% to greater than 1%) can be correlated with the deformation modulus obtained from the small strain triaxial tests or Pressuremeter tests for soil and Goodman Jack tests for rock. The radial strain measured from these tests were converted into axial strain based on the relationship of $\varepsilon_{axial} = 2\ \varepsilon_{radial} / \sqrt{3}$ as proposed by Jardine (1992).

With the raft, corewall and mega column layout and the established credible geological models, preliminary raft analysis can be carried out to identify areas with excessive bearing stress and settlement. The piles can then be strategically located at areas with high concentrated loads and large settlement. However, over provision of piles on areas with small load and settlement shall be placed with cautious as this may cause adverse differential settlement. Also, the geological model shall be refined and calibrated as far as possible with the interim face mapping results along with the excavation for the raft construction so that the pile layout and length can be further optimized. Sensitivity analysis based on other possible geological models and the envisaged ranges of ground stiffness parameters shall also be carried out to check the robustness of the raft performance.

The essential part of a piled raft design is soil-structure interaction. Katzenbach et al (1999) described the interactions amongst different elements of a piled raft design, which is much more complex than the traditional raft foundation design. These included raft-pile interaction, raft-soil interaction, pile-soil interaction and pile-pile interaction. Poulos (2001b) described different methods of analysis for piled raft foundations. Amongst these methods, numerical analysis using the plate-on-springs approach and 3D finite element analysis are potentially the most accurate method available. It is however very time consuming to carry out a 3D finite element analysis.

Arup has developed an in-house program namely GSRaft, which is part of the General Structural Analysis (GSA) program, using similar concept of plate-on-springs approach with consideration of the soil-structure interac-

tion by conducting iterative process to achieve the compatibility of settlement between the structural elements and the underlying soil elements. The program takes into account the structural stiffness of the raft, piles as well as the stiffness of the underlying soils. The interaction between the raft and the soil is simulated by a group of springs at the base of the raft while the interaction between the pile and the soil is simulated by a group of soil interaction springs as illustrated in Figure 1 and the level of these springs can be defined as the base of an equivalent raft level of the piles, which is usually taken as two-third of the pile depth for pile friction developed linearly with depth or half of the pile depth for constant pile friction. Since the pile in GSRaft is modelled as elastic beam element, when the pile approaches its ultimate capacity, the pile spring stiffness may be overestimated. Therefore, GSRaft is primarily applicable for design philosophies (a) & (b). Furthermore, the assigned equivalent raft level of the piles will affect the results and in layered soil strata and soil with varying stiffness, it is not easy to determine the appropriate level.

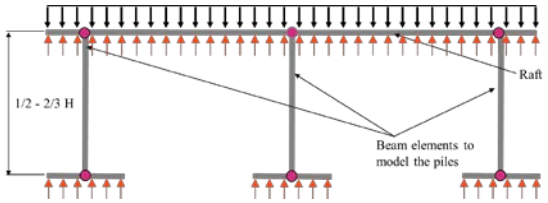

Figure 1. GSRaft Conceptual Model

4. CASE HISTORY

4.1. The project

The site is located at Jamsil-dong of Seoul, South Korea with a footprint of 87,000m^2 and to be developed into an integrated commercial, residential and entertainment complex. A landmark development comprising a 123-storey 555m high supertall tower with a 6-level basement is situated at the western end of the site. The initial ground investigation boreholes at the Tower were sunk in early 2006 to provide the basic geotechnical information for the design of the Tower foundation. The Tower was subsequently replanned and Arup was appointed as the geotechnical engineer of the international design team to provide the geotechnical designs for the newly planned tower in view of the suspected complex ground condition as revealed from the initial boreholes.

4.2. Structural form

The Tower has a footprint of approximately 72m x 72m. The structural form comprises concrete core wall with 8 peripheral mega columns to resist both the gravity and lateral forces. To enhance the structural rigidity, two belt trusses are positioned at 218m and 347m from the base of the raft. The total serviceability gravity load is around 6,700MN.

4.3. Ground investigations and geological conditions

There were three phases of borehole investigation carried out at the Tower location. The first phase was carried out in early 2006 and consisted of 16 numbers of boreholes accompanied by in-situ Pressuremeter/Goodman Jack tests and laboratory strength tests. Most of these boreholes were terminated at around 20m below the foundation level, which were relatively short comparing to the Tower footprint. Additional ground investigation consisted of 7 numbers of deep boreholes were sunk in mid 2009 with depth as deep as 80m and signs of faults running underneath the Tower were identified. With the mega-column locations and the corewall dimensions became more certain, the third phase boreholes, which consisted of 10 numbers of boreholes, was carried out in late 2009 accompanied by additional in-situ Pressuremeter tests and Goodman Jack tests to further supplement the existing borehole information. Figure 2 illustrates the variability of the rock quality and strength at distances underneath the foundation level.

Figure 2. A sample rock core

The ground investigation works revealed that the bedrock at the Tower consisted of Gyeonggi

Gneiss complex overlaid by Quaternary colluvium and alluvium deposits. The Gneiss had banded structures and medium grain to coarse grained texture. Hydrothermal intrusions were observed along fractures resulted from faulting. Due to the variability of the rock strength over the depths underneath the Tower, for engineering purpose, the rockmass could be classified into several categories using Geological Strength Index (GSI) classification suggested by Hoek et al (1995) and the corresponding rockmass modulus, E_m, could be estimated as shown in Table 1.

Table 1. GSI Classification of the rockmass

Rockmass Category	GSI/E_m (GPa)		
	Upper Bound	Lower Bound	Average
Banded Gneiss A	50/8.7	35/3.7	42/5.5
Banded Gneiss B	36/3.2	21/1.3	30/2.2
Brecciated Gneiss at Shear Zone	31/2.1	13/0.8	23/1.3
Fault Zone	18/0.5	5/0.3	13/0.4

Another indicator of rock condition is the value of Rock Quality Designation (RQD), which measures the rock mass integrity based on the condition of the rock core samples. Figure 3 illustrates the distribution of RQD values under the Tower footprint. RQD values range from 0 to 100%. High RQD value indicates high percentage of good rock within a borehole and vice versa.

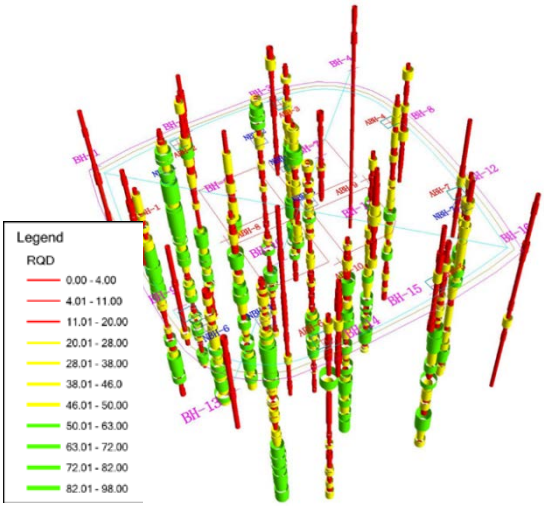

Figure 3. Perspective view of RQD value under the Tower footprint

The rock condition at the excavation face of around 10m above the foundation level was inspected and mapped by the Korea Society of Engineering Geology (KSEG) in late 2009 and reviewed by Arup, in order to better infer the rock condition over the footprint of the Tower. The rock face mapping at the final formation level is shown in Figure 4.

4.4. Proposed foundation system

In view of the loading condition of the Tower and the bearing capacity of the ground even assuming lower conservative parameters, a single raft foundation was considered to be a technically feasible after an initial assessment. Compared to individual footings, a single 6.5m thick raft foundation over the Tower footprint was more robust in tolerating local weak spots due to its high stiffness. However, the presence of faults, shear zones and highly foliated soft to hard rock would have a significant influence on the total and differential settlements of the raft, which were carefully considered in order not to impair the Tower performance. The uncertainties associated with the estimation of raft foundation settlement included: -

1. The rock conditions were highly variable. The stress and strain levels were concentrated locally at the good rock areas under the core and mega columns. According to the Pressuremeter test results, the difference of elastic modulus between good and poor rocks could be varied by a factor greater than 20. The risk of unacceptable differential settlement would be high especially under lateral forces.
2. The geology condition beneath the formation level was highly complex. It would be difficult to develop a full or complete geological model to represent the ground. The uncertainty of the geological model would impose a high risk in predicting the actual response of the ground under the applied pressure.
3. Computation analysis, irrespective to the degree of sophistication, involved simplifications and the inferred geological models could not be fully reflected in the analysis.

To mitigate such ground risk and enhance the performance of the raft foundation, ground stiffening piles were placed at strategic locations to balance the foundation cost, ground variation and the building performance. Using different credible geological models and after several rounds of studies, a total of 108 nos. 1m diameter

Percussion Rotary Drilling (PRD) piles were designed to be positioned underneath the perimeter corewall and inner zones as shown in Figure 4. PRD pile was selected due to its readily easy maneuvering and quick installation upon bulk excavation had reached 1 to 2m above the foundation level. The piles did not require a temporary steel casing to be used and the down-the-hole hammer drilling could be applied directly to enable a fast construction. These piles had a net length of 20m and 30m located at the highly stressed influence zone and distributed based on the inferred geological setting. Figure 5 shows a typical section showing the extent and depth of the proposed ground stiffening piles across the Tower footprint.

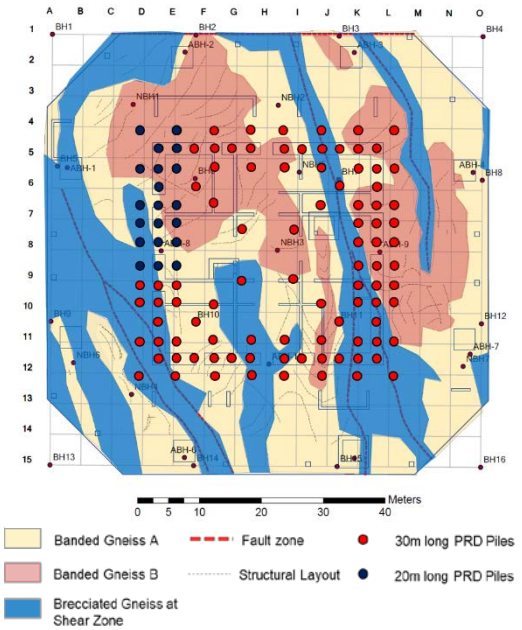

Figure 4. Final rock face mapping with ground stiffening piles

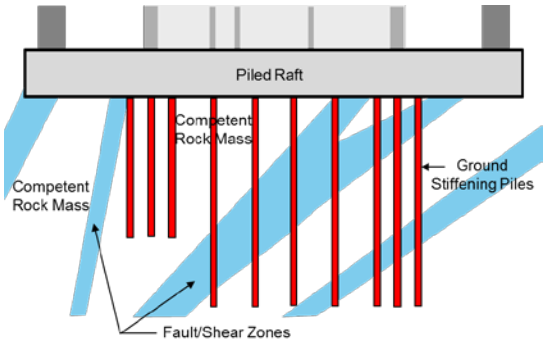

Figure 5. Typical geological section

4.5. Design parameters & models

Non-linear stiffness of the banded Gneiss and brecciated Gneiss (shear zone) were applied in order to better reflect the strain dependent behaviour of these rockmasses, as shown in Figure 6. The initial moduli at very small strain was correlated with the in-situ shear wave velocities measurement whilst the moduli at higher strain values were correlated with the deformation moduli obtained from the Pressuremeter and Goodman Jack tests. In view of the ground variation risk, a lower bound design line was adopted for design and prediction of the Tower performance. For fault zones, since the long term creeping of the highly weathered soil dominated the non-linear behaviour rock, linear deformation modulus was adopted in the design.

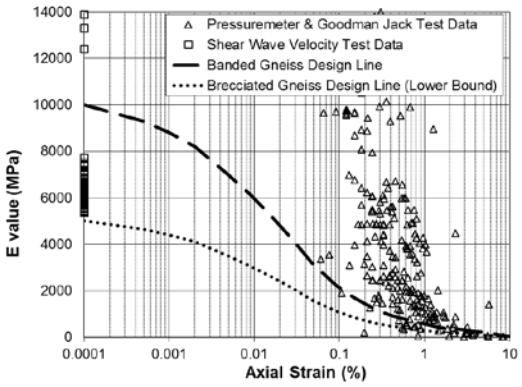

Figure 6. Non-linear modulus design curves

With different phases of borehole information and the rock face mapping at 10m above the foundation level during the bulk excavation, two possible geological models were established to be the most credible for the design purpose. One of the simplified geological models is shown in Figure 7. In the GSRaft analysis, the raft was modelled as grillage and the cross points formed the common nodes to iterate with the soil model. Piles could also be attached to these nodes. The piles were modelled as bar elements with axial stiffness only and the top of the piles were pin-jointed to the raft. Soil-pile interaction springs were placed at the end of the equivalent length of the piles. The loads were simulated as patches of pressure loading over the mega columns and core walls footprint. A number of GSRaft models were set up to carry out sensitivity check based on a range of design parameters and different load cases. A GSRaft model is shown in Figure 8, which was coupled with the soil model as

shown in Figure 7 during the analysis. To further enhance the overall rigidity of the raft, core walls above the raft with high bending stiffness were also simulated in the GSRaft model. This will certainty reduce the differential settlement of the raft within the core.

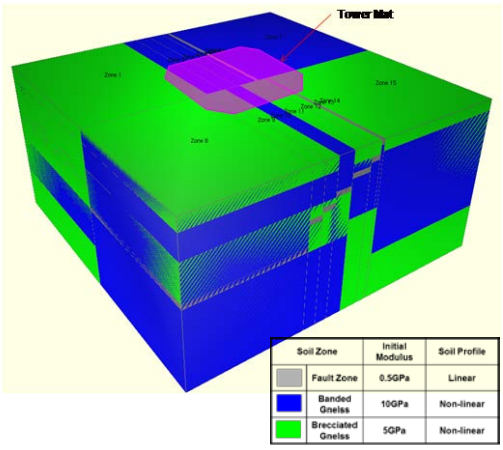

Figure 7. Geological model for GSRaft input

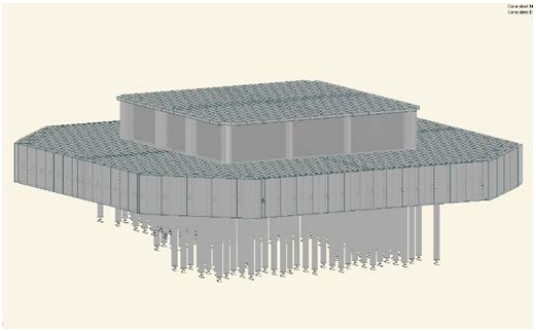

Remark: Half-length of piles modelled in GSRaft to reflect the pile-soil interaction level

Figure 8. Raft and piles in GSRaft Model

The result of analysis along one section at a particular load case of the proposed raft is shown in Figure 12. The maximum and differential settlements can be derived accordingly from the displacement at individual node. The corresponding spring constant could also be derived by dividing the reaction by the displacement at each node for individual load case and a spring contour map could be produced for the use of the Project Structural Engineer for the detailed structural analysis and design of the raft foundation using structural programs such as ETABS and structural SAFE models. A cross-checking shall be carried out to ensure that the raft deformation between the GSRaft and the structural models are compatible.

In addition, from the GSRaft models, the envelope of reaction forces at individual ground stiffening piles could be obtained. As discussed above, the raft foundation alone could sustain the total tower load. The inclusion of the ground stiffening piles was to reduce the raft settlement and to bridge over fault zones or localized weak zones. In this regard, these piles were allowed to settle plastically relative to the surrounding soil (i.e. creeping) such that the exceptionally high load could not be developed in piles. In order to allow the pile settled plastically relative to the surrounding soil/rock following the design philosophy (b) as mentioned in Section 2, a factor of safety of 1.3 was adopted for the derivation of allowable geotechnical capacity of the ground stiffening pile. A trial pile with load testing was carried out prior to the commencement of the working pile construction and a bond capacity between the concrete and the brecciated Gneiss was proven to be 400kPa. Since the piles were generally socketed into banded Gneiss and/or brecciated Gneiss, with such a high bond capacity, the pile capacity was not governed by the geotechnical capacity. Instead, the structural design governed the pile capacity. The structural design of the pile complied with the Korean Building Code (KBC) - Structural 2009. The ground stiffening piles had a concrete cylinder strength of 60MPa, which had the same concrete strength as the raft after considering a tremie factor of 0.85.

A key feature of these piles was the pile heads being disconnected from the raft, with a 200mm soil cushion as shown in Figure 9, which separates the piles entirely as part of the ground.

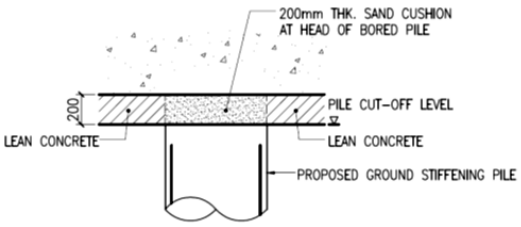

Figure 9. Pile head soil cushion

This reduced the maximum pile reaction by 30% as the load from the raft was transferred to the ground before reaching the pile but with about 10% increase in raft settlement. This also allowed the load from the raft to transfer more

uniformly into the ground instead of forming extremely hard spots at the individual pile locations.

When the excavation approached around 1 to 2m above the foundation level, a final rock mapping was carried out and the geological model was finalized. The GSRaft analysis was then refined and further compared with a 3-D Plaxis model. The mesh set-up, the ground model and the raft simulation are shown in Figure 10.

Non-linear moduli of the rockmass were also adopted in the Plaxis model. Based on the results of the analysis, similar peak settlement was found in both 3-D Plaxis and GSRaft models but the predicted differential settlement by 3-D Plaxis was about 17% smaller than that predicted by GSRaft model. It might be explained by the fact that the raft in Plaxis was modelled as "solid continuum" element, which allowed dispersion of load through the physical dimension of the elements resulting in more uniform load distribution beneath the raft while the raft in GSRaft was modelled as "shell" element with no physical thickness despite the stiffness equivalent to the raft was incorporated.

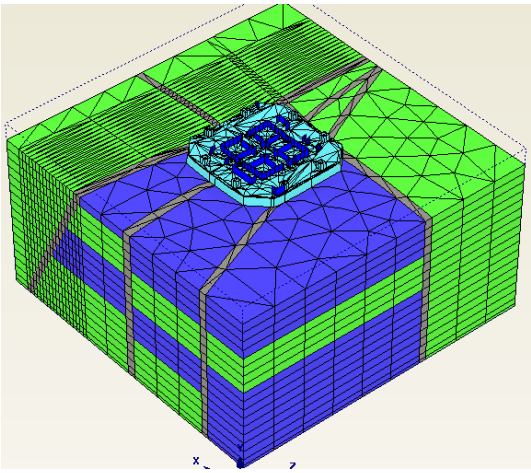

Figure 10. 3-D Plaxis Model

4.6. Construction stage support

It is a common practice in South Korea that the construction supervisor was independent from the design team and the supervision team might have limited knowledge on the geotechnical design. In view of the variability of the rock condition, the active input from the Designers during the construction phase apart from the routine supervision by the Construction Supervisor is a critical element to promptly review if the actual ground condition matches with the design assumptions. Periodic site supervisions were conducted by Arup's designer and engineering geologist to carry out rock face mapping and to verify or update the geological models at the interim stages of excavation and before the final formation level was reached.

When excavation approached around 1 to 2m above the foundation level, a final rock face mapping over the floor at the Tower footprint was carried out. This provided another set of geological information to project the geological condition of the ground beyond the foundation level and to refine the adopted geological model. Local weak spots, which might affect the performance of mat foundation, could also be identified at the final rock face mapping and remedial measure by shallow replacement by mass concrete could be designed at specific areas.

Another important issue is the potential blast induced damage to the rockmass immediately beneath the raft, which may result in undue settlement during recompression of the opened joints under the imposition of the building loads. It is therefore advised that no blasting shall be applied to the rockmass within 1m above the foundation level.

The construction of the PRD took around 3 months to complete. The pile head trimming on the completed piles, sand cushion provision and the preparation of the final foundation floor including shallow replacement of local weak spots by mass concrete is shown in Figure 11.

Figure 11. Trimming of PRD pile head

4.7. Tower health performance

Monitoring of the raft response during the imposition of loads throughout the construction

phase is important to verify the design assumptions and hence to secure the Tower performance. Instrumentations at raft foundation level included the strain gauges in selected ground strengthening piles, earth pressure cells underneath the raft, extensometers in rockmasses and settlement markers at the top of the raft. The bearing stress, settlements and hence the differential settlements obtained from the site were compared to the prediction at different stages of the Tower construction. The Tower is still under construction at the time of preparing this Paper. Figure 12 shows the measured settlement of the raft when the Tower construction was up to about 95% of the total building height comparing with the design prediction.

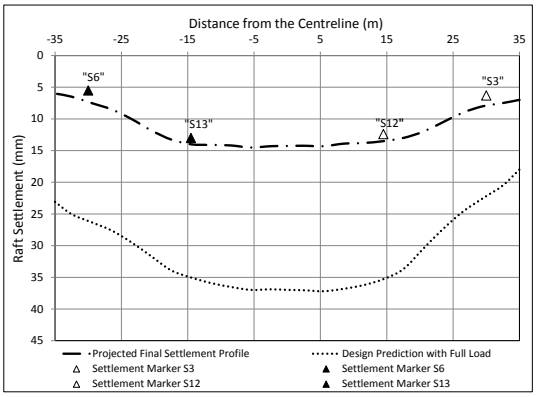

Figure 12. Comparison of measured, predicted and projected settlement of the Tower

The projected settlement when the total building load is applied is also estimated and is well within the design prediction. This reflects that the assumed ground stiffnesses are reasonably conservative and the actual ground stiffness may be close to the average ground stiffness as shown in Figure 6. Besides, the bearing stress measured by the earth pressure cells underneath the mega column was found to be slightly less than the theoretical value. This may be due to the actual concrete stiffness of the raft being higher than the design prediction to spread the column load.

5. CONCLUSIONS

The use of piles as settlement reducers (i.e. ground stiffening pile) to control the settlement and/or differential settlement of a raft foundation is geotechnically viable. Using the modern computer modelling tools, the soil-structural interaction among the raft foundation, the ground stiffening piles and the ground can be efficiently analysed. Furthermore, with the consideration of non-linear ground stiffness, a cost-effective piled raft foundation solution can be derived. The case history presented in the paper has demonstrated the successful application of ground stiffening piles for the raft foundation design in a complex ground condition to support a high super tall landmark tower in Seoul. The Designers' involvement to calibrate the ground models throughout the construction process is one of the essential elements for the success of the project.

6. REFERENCES

Davies J., Lam K.L.A. & Junaideen S.M. 2009. Piled Rafts to Support High Rise Developments, Proceedings of The 3rd Asian Seminar on ATC 18 Mega Foundation: "Recent Advance of Deep Excavation and Foundations", Bangkok, Thailand.

Hoek E., Kaiser P.K. and Bawden W.F. 1995. Support of underground excavations in hard rock, Rotterdam, Balkema, 213pp.

Jardine R.J. 1992. Nonlinear stiffness parameters from undrained pressuremeter tests, Canadian Geotechnical Journal, Vol. 29, pp. 436-446.

Katzenbach R., Schmitt A. and Turek, J. 1999. Cooperation Between Geotechnical and Structural Engineers – Experience Gained from Projects in Frankfurt, COST Action C7, Soil-Structure interaction in urban civil engineering Proceedings of the Workshop in Thessaloniki, 1./2. Oct. 1999

Pappin J.W., Heidenbrecht A.C., Henderson P. and Naumoski N. 1989. Site response study – soil modeling, McMaster University, EERG Report 89-02, 52pp.

Poulos, H.G. 2001a. Piled Raft Foundations – Design and Applications. Geotechnique, Vol. 50, (2): 95-113.

Poulos, H.G. 2001b. Methods of Analysis of Piled Raft Foundations. A Report Prepared on Behalf of Technical Committee TC18 on Piled Foundations.

Randolph, M.F. 1994. Design Methods for Pile Groups and Piled Rafts. S.O.A. Report, 13 ICSMFE, New Delhi, 5: 61-82.

Seed H.B. and Idriss I.M. 1970. Soil moduli and damping response analysis. EERC Report No. 70-10, Berkeley, California.

Proceedings of Indian Geotechnical Conference IGC-2015
December 17-19, 2015, PUNE, India

FLAT DILATOMETER (DMT). APPLICATIONS AND RECENT DEVELOPMENTS

S. Marchetti, Prof., L'Aquila University – Italy, silvano@marchetti-dmt.it

ABSTRACT : Many designers, today, consider an investigation composed by CPT and DMT adequate for day-to-day jobs. The DMT, introduced 40 years after the CPT, is the most recent penetration probe. Its use has been spreading fast. DMT is currently used in over 70 countries. The main applications of the DMT are :
Settlement prediction. Many top experts worldwide consider DMT the best presently available tool for predicting settlements, notoriously not well predicted by conical probes.
Compaction control. DMT has been recognized to be more than twice more sensitive than CPT to compaction. For this reason before-after DMTs are increasingly used to monitor the gain in modulus and the gain in OCR due to the compaction.
Liquefaction. A chart has been recently (2015) developed to estimate the liquefaction resistance CRR based at the same time on CPT and DMT. An estimate of CRR based on two parameters is expected to be better than estimates based on just one parameter.
Detecting slip surfaces in clay slopes. Values of Kd ≈ 2 found in a slope indicate the presence of slip surfaces in the slope, active or quiescent.

INTRODUCTION

The Flat Dilatometer (DMT) is an in situ testing tool developed some 40 years ago [1]. The DMT is currently used in practically all industrialized countries. It is standardized in the ASTM [2] and the Eurocode [3]. The DMT has been object of a detailed monograph by the ISSMGE Technical Committee TC16 [4]. ISO/CEN is currently working on a Flat Dilatometer standard.

Some key features of the DMT are:

- The DMT is a penetration test. As such, it has the advantage of not requiring a borehole.
- The DMT, being a load-displacement test, provides information on soil stiffness, an information unobtainable by penetration tests, that essentially measure "rupture" characteristics, i.e. strength. Moreover the insertion distortions caused by the DMT blade are substantially less than the distortions caused by conical probes.
- The DMT equipment is robust, easy to use and remarkably operator-independent and repeatable.
- The DMT provides information on Stress History, which has a dominant influence on soil behaviour. In particular information on Stress History permits better estimates of settlements and of liquefaction resistance.

As to the SDMT, the add-on module has added to the parameters measurable by DMT the shear wave velocity V_S. V_S is today increasingly measured because of:

- More frequent requirement of seismic analyses, for which V_S is a basic input parameter.
- The newly introduced Eurocode 8 seismic regulations prescribe the determination of V_S in the top 30 m at all construction sites located in seismic zones.
- SDMT provides both the small strain shear modulus $G_0 = \rho V_S^2$ and the stiffness at operative strains (as represented by the constrained modulus M_{DMT}). Such two stiffnesses may offer guidance when selecting the G-γ curves, i.e. the decay of the shear modulus G with the shear strain γ.

DILATOMETER TEST (DMT)

The flat dilatometer consists of a steel blade having a thin, expandable, circular steel membrane mounted on one face. When at rest, the membrane is flush with the surrounding flat surface of the

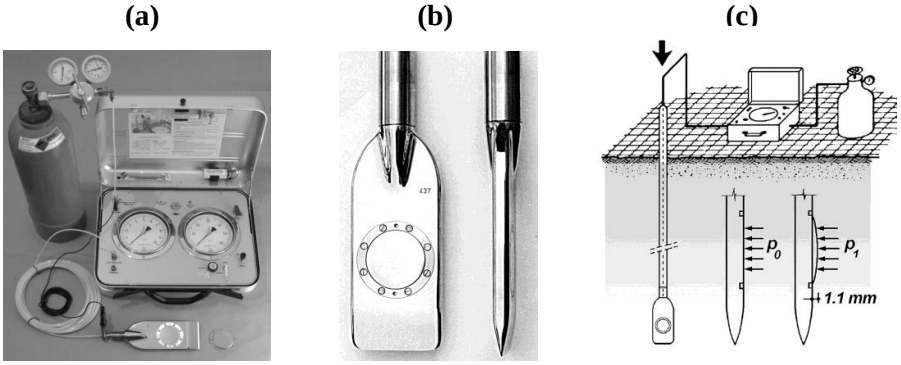

Fig. 1 Flat Dilatometer: (a) Equipment (b) Dilatometer Blade (c) Schematic layout of the seismic dilatometer test.

blade. The blade is connected, by an electro-pneumatic tube running through the insertion rods, to a control unit on the surface (Fig. 1).

The control unit is equipped with pressure gauges, an audio-visual signal, a valve for regulating gas pressure (provided by a tank) and vent valves. The blade is advanced into the ground using common field equipment, i.e. penetrometers normally used for the cone penetration test (CPT) or drill rigs. The DMT can also be driven, e.g. using the SPT hammer and rods, but statical push is preferable. Pushing the blade with a 20 ton penetrometer truck is most effective (up to 80 m of profile per day). The test starts by inserting the dilatometer into the ground. When the blade has been advanced to the desired test depth, the penetration is stopped. Without delay the operator inflates the membrane and takes, in about 30 sec, two readings: the A pressure, required to just begin to move the membrane (lift-off pressure), and the B pressure, required to expand the membrane center 1.1 mm against the soil. A third reading C (closing pressure) can also optionally be taken by slowly deflating the membrane soon after B is reached. The blade is then advanced to the next test depth, with a depth increment of typically 20 cm.

The interpretation proceeds as follows. First the field readings are converted into the DMT intermediate parameters I_D, K_D, E_D (Material index, Horizontal stress index, Dilatometer modulus). Then I_D, K_D, E_D are converted, by means of commonly used correlations [4] to: constrained modulus M, undrained shear strength Cu, K_0 (clays), OCR (clays), friction angle ϕ' (sands), bulk unit weight γ. Consolidation and permeability coefficients may be estimated by performing dissipation tests [4]. The C-reading, in sand, approximately equals the equilibrium pore pressure. An example of the profiles obtained by DMT is shown ahead in the paper in Fig. 3, where:

- I_D is the material index, that gives information on soil type (sand, silt, clay)
- M is the vertical drained constrained modulus (at geostatic stress)
- Cu is the undrained shear strength
- K_D is the Horizontal Stress Index. The profile of K_D is similar in shape to the profile of the overconsolidation ratio OCR. $K_D \approx 2$ indicates in clays OCR = 1, $K_D > 2$ indicates over-consolidation. The K_D profile often provides, at first glance, an understanding of the Stress History of the deposit.

More detailed information on the DMT equipment, test procedure and all the interpretation formulae may be found in the DMT 2001 Report by the ISSMGE Technical Committee TC16 [4]. A comprehensive update of the above DMT Report, including information on developments in the last 15 years, has recently been published (Marchetti 2015 [5]).

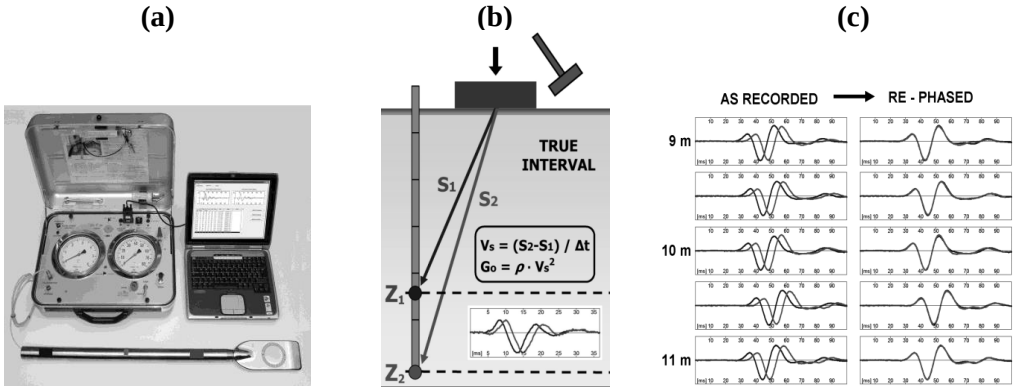

Fig. 2 Seismic Dilatometer: (a) DMT blade and seismic module (b) Schematic layout of the seismic dilatometer test. (c) Example of seismograms as recorded and rephased

SEISMIC DILATOMETER TEST (SDMT)

The SDMT is the combination of the flat dilatometer with an add-on seismic module for the measurement of the shear wave velocity [6-9]. The seismic module (Fig. 2a) is a tubular element placed above the DMT blade, equipped with two receivers located at 0.5 m distance. When a shear wave is generated at surface, it reaches first the upper receiver, then, after a delay, the lower receiver. The seismograms acquired by the two receivers, amplified and digitized at depth, are transmitted to a PC at the surface, that determines the delay. V_S is obtained (Fig. 2b) as the ratio between the difference in distance between the source and the two receivers (S2 - S1) and the delay Δt from the first to the second receiver. The true-interval test configuration with two receivers avoids possible inaccuracy of the "zero time" at the hammer impact, sometimes observed in the pseudo-interval one-receiver configuration.

Moreover, the couple of seismograms recorded by the two receivers at a given test depth corresponds to the same hammer blow. The repeatability of the V_S measurements is remarkable (observed V_S repeatability ≈ 1 %, i.e. a few m/s).

Fig. 2c shows an example of seismograms obtained by SDMT at various test depths at the site of Fucino. Fig. 3 shows an example of SDMT results. The fifth diagram is the V_S profile obtained by the seismic module. It can be seen that the repeatability of V_S is similar to the repeatability of the other four DMT parameters.

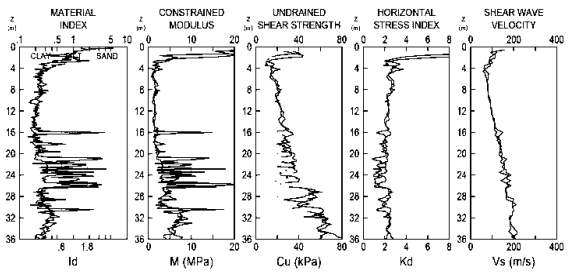

Fig. 3 Example of SDMT results (from two nearby SDMTs)

SENSITIVITY OF K_D TO STRESS HISTORY

It is well established that the DMT's K_D parameter is considerably more sensitive to Stress History than penetration resistance. The higher sensitivity to Stress History of K_D has been observed by numerous researchers, either in the large calibration chamber (e.g. [10]) and in the field (e.g. [11], [12]).

As an example Fig. 4 shows results [13] from a recent calibration chamber research carried out in Korea, comparing the reactivity of CPT and DMT to Stress History. Forty large specimens of Busan silica sand were preconsolidated to OCR in the range 1 to 8. Then half of the specimens were tested by CPT, the other half by DMT. As it can be seen in Fig. 4 OCR produces a substantial increase

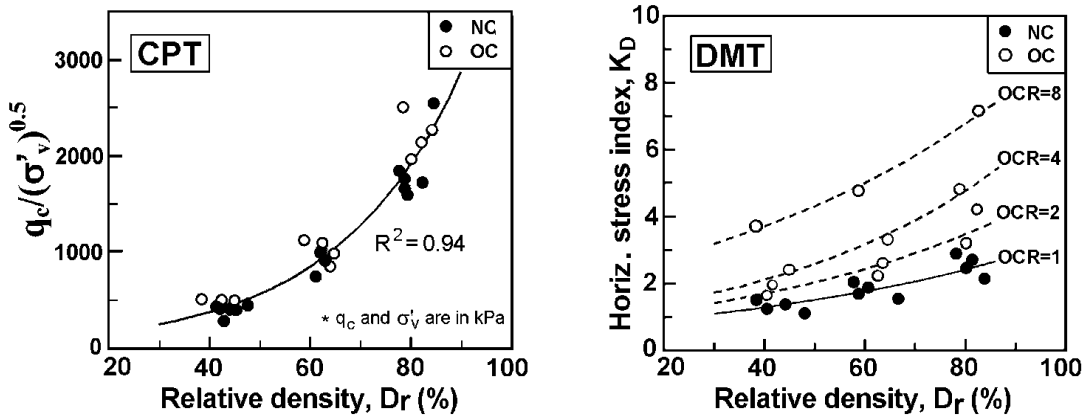

Fig. 4 Sensitivity of CPT and DMT to Stress History (Lee et al. 2011 [13])

of K_D but an almost negligible increase of q_c. The two diagrams in Fig. 4 confirm that K_D is considerably more reactive to OCR than the normalized tip resistance $Q_{cn.}$ To the same Q_{cn} correspond many values of K_D. K_D permits to distinguish sands with Stress History, penetration tests much less.

Sensitivity to Stress History is important because not many in situ methods are available to sense it. On the other hand Stress History is fundamental for realistic estimates of settlements and liquefaction resistance, it makes the soil much "stronger". If Stress History is not sensed, and therefore ignored, the benefits are wasted. Stress History is a substantial economical resource, permitting a more economical design.

ESTIMATING V_S FROM MECHANICAL DMT (NON SEISMIC) RESULTS.

If V_S has not been measured directly, approximate estimates of V_S and G_0 can be obtained from the three DMT parameters I_D, K_D, M_{DMT} obtained by mechanical DMT (i.e. plain, non seismic DMT). Once K_D and M_{DMT} have been determined by mechanical DMT, Fig. 5 provides estimates of G_0 and then of V_S. Note that the ratio G_0/M_{DMT} on the vertical axis is the ratio between the small strain modulus and the operative modulus. It can be seen that such ratio varies in a quite wide range , say from 0.5 to 25. Fig. 5 negates the possibility, sometimes suggested, to estimate the operative modulus by dividing G_0 by a constant, considering that the "constant" varies in the range 0.5 to 20.

The experimental relationship in Fig. 5 is quite stable, having been constructed using SDMT results from 34 different sites world-wide in a variety of soil types [9]. Obtaining datapoints in Fig. 5 does not require a specific research. Datapoints are obtained whenever a SDMT is executed, because SDMT provides routinely at each test depth either K_D, I_D, M_{DMT} and G_0.

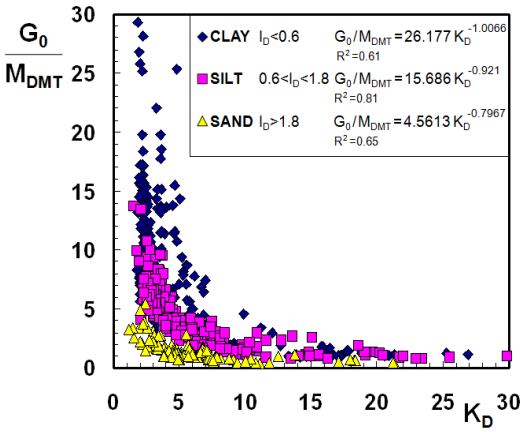

Fig. 5 Ratio G_0 /M_{DMT} vs. K_{D} (OCR) for various soil types [8]. It can provide estimates of G_0 (and V_S) from the results of the "mechanical" DMT

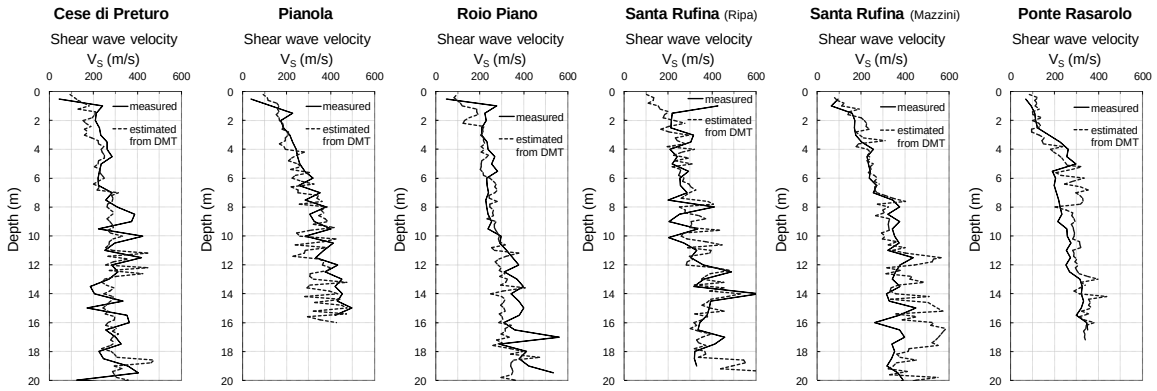

Fig. 6 Comparison of profiles of V_S measured by SDMT and estimated from mechanical DMT data, by use of the correlations in Fig. 5, at six sites in the area of L'Aquila (Monaco at al. 2013 [14])

The V_S comparisons shown in Fig. 6 indicate a fair agreement between the V_S values determined by SDMT (solid lines) and the V_S values inferred by entering K_D, I_D, M_{DMT} in Fig. 5 (dashed lines in Fig. 6). The relative error, calculated as (V_S measured – V_S estimated) / V_S measured, is about 20% on average.

Amoroso et al. (2013) [15] compare the DMT correlations for estimating V_S with the similar correlations by CPT. Amoroso concludes that V_S estimates based on DMT are closer to the measured V_S and attributes the better quality V_S by DMT to the fact that DMT is a genuine two parameter test.

TESTABLE SOILS

The soils that can be investigated by DMT range from extremely soft to hard soils to soft rocks. The DMT readings are accurate even in nearly liquid soils. On the other hand the blade is very robust and can penetrate even in soft rock. Clays can be tested from *Cu* = 2-4 kPa up to 1000 kPa (marls). The range of measurable moduli *M* is from 0.4 MPa up to 400 MPa.

The DMT blade can be inserted by a variety of penetration machines. Truck-mounted penetrometers are the fastest. A drill rig is also usable, with the "Torpedo" configuration [4], though at a lower productivity. Penetration by percussion, e.g. using the SPT hammer (Fig. 7), is also possible. Though dynamic insertion using an SPT rig is not the preferred way, in some countries, e.g. Switzerland, driving is the most common insertion method.

APPLICATIONS TO ENGINEERING PROBLEMS

Design via Parameters

In most cases the DMT estimated parameters, in particular the undrained shear strength *Cu* and the constrained modulus *M*, are used with the common design methods of Geotechnical Engineering for evaluating bearing capacity, settlements etc.

Fig. 7 DMT blade advanced by an SPT rig

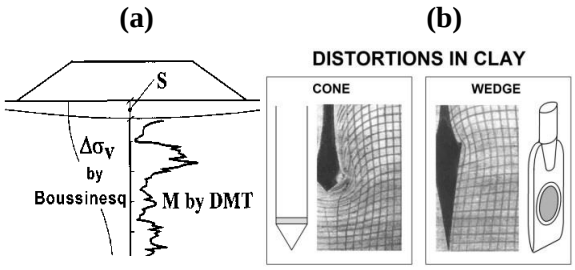

Fig. 8 (a) Settlement prediction by DMT (b) Soil distortions caused by tips of different shape (Baligh & Scott 1975 [16])

However, for a number of applications, specific comments may be opportune.

Settlements of Shallow Foundations

Predicting settlements of shallow foundations is probably the No. 1 application of the DMT, especially in sands, where undisturbed samples cannot be retrieved. Settlements are generally calculated by means of the one-dimensional formula (Fig. 8a) :

$$S_{1-DMT} = \sum \frac{\Delta\sigma_v}{M_{DMT}} \Delta z \quad (1)$$

with $\Delta\sigma_v$ calculated according to Boussinesq and M_{DMT} constrained modulus estimated by DMT. The validity of the method has been confirmed by a large number of observed agreement between measured and DMT-predicted settlements. Fig. 8b compares the insertion distortions caused by probes of different shape.

Laterally Loaded Piles

Methods have been developed for deriving P-y curves from DMT results [17,18]. A number of independent validations (NGI, Georgia Tech and tests in Virginia sediments) have indicated that the two methods provide similar predictions, and that the predictions are in quite good agreement with the observed behavior. Note that all methods are for the case of first time monotonic loading.

Detecting Slip Surfaces in OC Clay

The $K_D \approx 2$ method [4] permits to detect active or old slip surfaces in overconsolidated (OC) clay slopes, based on the inspection of the K_D profiles. In essence, the method consists in identifying zones of normally consolidated (NC) clay in a slope which, otherwise, exhibits an OC profile. The NC clay bands, remoulded by the sliding, then reconsolidated under the weight of the overlying soil, are recognized by using $K_D \approx 2$ as the identifier of the NC zones. Note that the method involves searching for a specific numerical value ($K_D \approx 2$) rather than for simply weak zones, which could be detected just as easily by other in situ tests. The $K_D \approx 2$ method permits to detect even quiescent surfaces, which could reactivate e.g. due to a cut.

Compaction Control

DMT has been found to be more than twice more sensitive than CPT to compaction. For this reason before-after DMTs are increasingly used to monitor the gain in modulus and the gain in OCR due to compaction. Schmertmann (1986) [11] found that the compaction produced on average an M_{DMT} gain 2.3 times the q_c gain. A similar trend was observed by Jendeby (1992, [12]) who found, upon compaction of a loose sandfill, an increase of the ratio M_{DMT} / q_c from a pre-compaction M_{DMT} / q_c ≈5-12 to a post-compaction M_{DMT} / $q_c \approx$ 12-24 (Fig. 10a). The fact that M_{DMT} / q_c increases with compaction - which is a way of applying stress history - confirms that OCR increases M_{DMT} at a faster rate than q_c. The higher sensitivity of DMT to compaction has been confirmed by many researchers, e.g. Balachowski (2015 [19]) : "The mean increase of M_{DMT} within the compacted sandy layer is about 2.3 times higher than corresponding increase of q_c ".

Many designers like to know not only the gain in M, but also the gain in OCR due to compaction. OCR in granular soils can be estimated, before and after compaction, from the ratio M_{DMT} / q_c using the Monaco et al. (2014 [20]) equation :

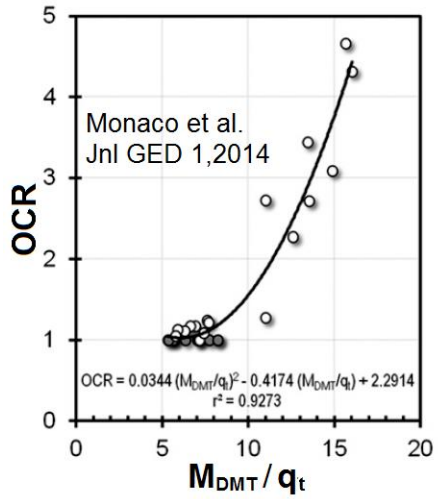

Fig. 9 Correlation OCR= f(M_{DMT} / q_c) for Sandy layers (Monaco et al. 2014 [20])

$$OCR = 0.0344\ (M_{DMT}/q_c)^2 - 0.4174\ (M_{DMT}/q_c) + 2.2914 \quad (2)$$

or its graphical equivalent Fig. 9.

It is noted that, in order to estimate OCR, both CPT and DMT are necessary, because both q_c and K_D increase with D_r and Stress History - though in a different proportion. Dr and Stress History are two unknowns, it is therefore impossible to estimate OCR in granular soils from CPT or DMT alone.

Profiles of OCR - or of its proxy M_{DMT} / q_c - are often plotted (Fig. 10) by designers wishing to confirm the gain in OCR of the compacted fill.

In 1986 Schmertmann [11] observed that, since the primary objective of the ground improvement is to limit settlements, it appears more rational to establish the acceptance criterion in terms of minimum modulus rather than of minimum D_r , as modulus relates more closely to the objective than D_r. In the job described by Schmertmann the designers replaced the q_c to D_r criterion to a minimum M_{DMT} acceptance criterion. Similarly Balachowski (2015,[19]) describes a compaction job where "the minimum average M_{DMT} = 80 MPa was fixed as an acceptance criterion for the post-treated subsoil".

A collateral advantage of using the minimum M_{DMT} acceptance criterion is avoiding the in situ D_r determination, often problematic, because there is no unique mapping q_c to D_r applicable to all sands (e.g. Robertson and Campanella 1983 [21]).

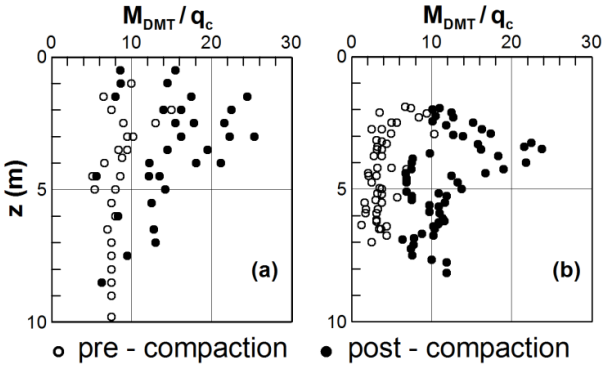

Fig. 10 M_{DMT}/ q_c ratio before/ after compaction. (a) Jendeby (1992) [12] (b) Balachowski and Kurek (2015 [19])

Subgrade Compaction Control

DMT has been used for verifying the compaction of the natural ground surface (i.e. the subgrade) to support the road superstructure [22]. DMT has been used as an economical production tool for quality control of the compaction, with only occasional verifications by the originally specified methods.

Estimating liquefaction resistance CRR from the DMT's parameter K_D

In the last decades various CRR-K_D correlations have been developed. They appear to converge towards a narrow central band. Much of the interest on the CRR-K_D correlation derives from the fact that the Stress History increases significantly CRR and K_D, but only slightly the normalized tip resistance Q_{cn} (Fig. 4). Hence it is possible that a correlation K_D-CRR will be stricter than Q_{cn} - CRR. A collection of recent CRR-K_D correlations is shown in Fig. 11.

As today (end of 2015), the recommended CRR-K_D correlation is the correlation composed by the two equations combined:

$$CRR = \exp[(Q_{cn}/540) + (Q_{cn}/67)^2 - (Q_{cn}/80)^3 + (Q_{cn}/114)^4 - 3] \quad (3a)$$

with $Q_{cn} = 25\ K_D$ (3b)

Eq. (3a) is the Idriss and Boulanger (2006 [23]) correlation to estimate CRR from Q_{cn}.
Eq. (3b) is the Robertson (2012 [24]) average interrelationship $Q_{cn} \approx 25\ K_D$.
The recommended CRR-K_D correlation, defined analytically by the combination of Eqs. (3a) and (3b), is plotted in Fig. 11, identified with the label RIB.
If both DMT and CPT results are available, it is possible to obtain two independent estimates of CRR, one from CPT using Eq. (3a), the second one from DMT using Eq. (3a) and Eq. (3b) combined. The two above mentioned CRR estimates are however obtained each one by one-to-one correlations, one providing CRR just from DMT, the second one providing CRR just from CPT. A recent chart (Marchetti 2015 [25]), rather than providing two CRR estimates from two distinct one-to-one CRR correlations, presents a correlation providing just one estimate of CRR, based at the same time on Q_{cn} & K_D, in the form CRR=f(Q_{cn},K_D), as shown in Fig. 12.

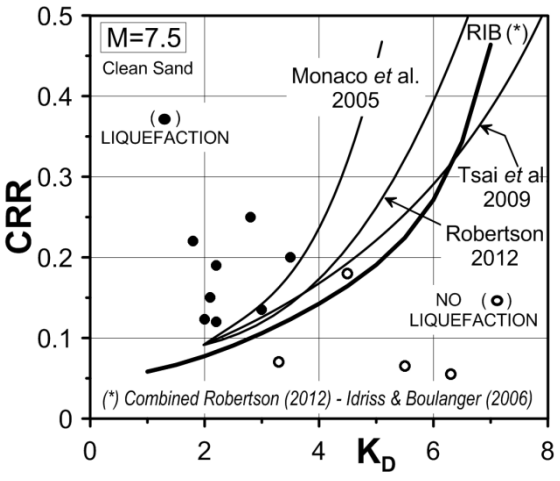

Fig. 11. Recent clean sand K_D – CRR correlations

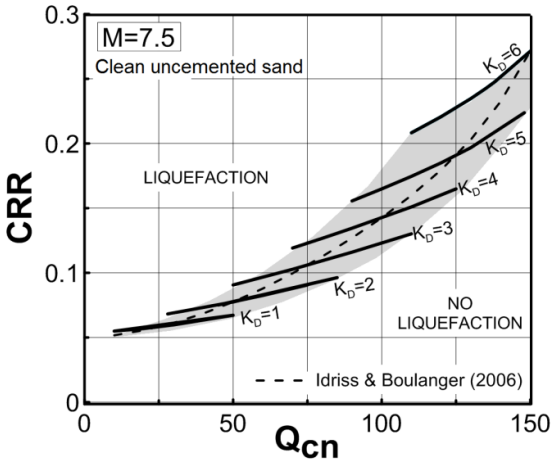

Fig. 12 Correlation for estimating CRR based at the same time on Q_{cn} and K_D - for clean uncemented sand (Marchetti 2015 [25])

A numerical example. For Q_{cn} =100 and K_D = 4, Fig. 12 provides CRR = 0.14. However, for the same Q_{cn} =100, if K_D =5, Fig. 12 provides CRR = 0.17. In other words, for the same Q_{cn}, Fig. 12 provides CRR estimates which are higher if K_D is more than average (i.e. > Q_{cn}/25) , are lower if K_D is less than average.

The Seafloor Dilatometer

The seafloor dilatometer (Fig. 13) has been developed to execute DMT soundings from the seabed. It is composed by an upper pushing section, whose weight is 60-80 Kg, easily transported and a lower heavy section, that can be ballasted 3 to 7 tons, easy to construct locally. The two sections can be quickly solidarized using 4 bolts. The seafloor dilatometer can operate up to a waterdepth of 100 m. The maximum test depth depends on soil consistency – it is the depth penetrable with 7 ton push. Six or seven pushrods are already charged vertically on top, before lowering the machine. More rods can be added by keeping the string vertical, sustaining the rodstring with a buoy - or a trestle fixed to the top of the ballast.

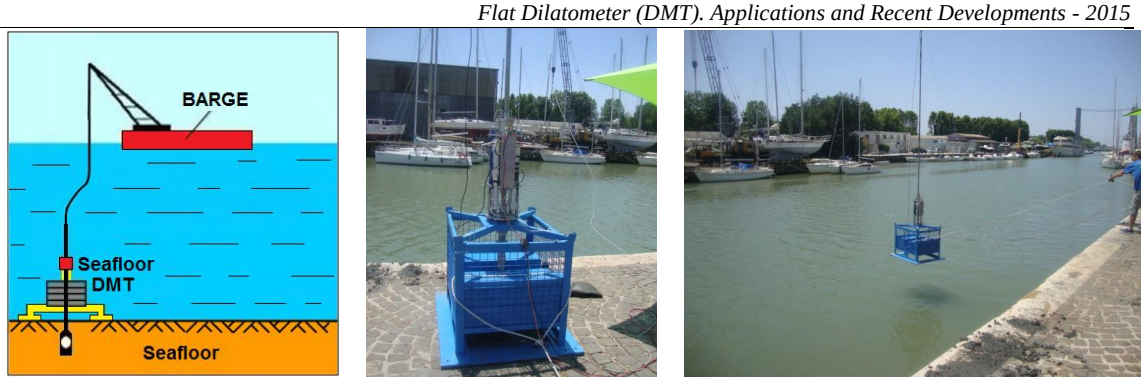

Fig. 13 Seafloor Dilatometer for executing DMT or SDMT from the seafloor

CONCLUSIONS

The Flat Dilatometer and the Seismic Dilatometer are relatively recent in situ tests. They provide estimates of a variety of design parameters. They are fast and simple to operate, and the measurements are reproducible and operator independent. The DMT most frequent application is to predict settlements. Other applications have been briefly described in the paper. The test is standardized in the ASTM and the Eurocode.

REFERENCES (°)

1. Marchetti, S. (1980), In Situ Tests by Flat Dilatometer, *Jnl GED, ASCE*, 106, GT3, 299-321.
2. ASTM D6635-01 (2001 & 2007), Standard Test Method for Performing the Flat Plate Dilatometer, *Book of Standards*, 14 pp.
3. Eurocode 7 (1997 & 2007), Geotechnical Design - Part 2, *Ground Investigation and Testing*, EN 1997-2:2007.
4. TC16 (2001), The Flat Dilatometer Test (DMT) in Soil Investigations, A *Report by the ISSMGE Committee TC16*. May 2001, 41 pp. Reprinted in Proc. 2nd Int. Conf. on the Flat Dilatometer, Washington D.C. 2006, 7-48.
5. Marchetti, S. (2015), Some 2015 Updates to the TC16 DMT Report 2001, , *Proc. 3rd Int. Conf. on the Flat Dilatometer DMT'15*. Roma, Italy, 43-65.
6. Monaco, P., Marchetti, S., Totani, G. & Calabrese, M. (2005), Sand liquefiability assessment by Flat Dilatometer Test (DMT), *Proc. XVI ICSMGE*, Osaka, 4, 2693-2697.
7. Monaco, P. & Marchetti, S. (2007), Evaluating liquefaction potential by seismic dilatometer (SDMT) accounting for aging/stress history, *Proc. 4th Int. Conf. on Earthquake Geotechnical Engineering ICEGE*, Thessaloniki, 12pp.
8. Marchetti, S., Monaco, P., Totani, G. & Marchetti, D. (2008), In Situ Tests by Seismic Dilatometer (SDMT), *Proc. from Research to Practice in Geotechnical Engineering, ASCE Geotech. Spec. Publ. No. 180* (honoring J.H. Schmertmann), 292-311.
9. Monaco, P., Marchetti, S., Totani, G. & Marchetti, D. (2009), Interrelationship between Small Strain Modulus G_0 and Operative Modulus, *International Symposium IS-Tokyo 2009 on Performance-Based Design in Earthquake Geotechnical Engineering*, 8 pp.
10. Jamiolkowski, M. and Lo Presti, D.C.F. (1998), DMT Research in Sand. What can be learned from calibration chamber tests, *1st Int. Conf. on Site Characterization ISC'98*, Atlanta. Oral presentation.
11. Schmertmann, J.H., Baker, W., Gupta, R. and Kessler, K. (1986), CPT/DMT Quality Control of Ground Modification at a Power Plant, *Proc. ASCE Spec. Conf. on Use of In Situ Tests in Geotechnical Engineering In Situ '86*, Virginia Tech, Blacksburg. ASCE Geotech. Spec. Publ. No. 6, 985-1001.

12. Jendeby, L. (1992), Deep Compaction by Vibrowing, *Proc. Nordic Geotechnical Meeting NGM-92*, 1, 19-24.
13. Lee, M., Choi, S., Kim, M. and Lee, W. (2011), Effect of Stress History on CPT and DMT results in Sand, *J .Engineering Geology, Elsevier*, 117, 259-265.
14. Monaco P., Totani G., Amoroso S., Totani F., Marchetti D. (2013), Site Characterization by Seismic Dilatometer (SDMT) in the City of L'Aquila, *Rivista Italiana di Geotecnica*, Year 47, 3, 8-22.
15. Amoroso, S. (2013), Prediction of the Shear Wave Velocity Vs from CPT and DMT, *5th Int. Young Geot. Engineering Conference* - 5iYGEC'13.
16. Baligh, M.M. & Scott, R.F. (1975), Quasi Static Deep Penetration in Clays, *ASCE Jnl GE*, 101, GT11 , 1119-1133.
17. Robertson, P.K., Davies, M.P. & Campanella, R.G. (1987), Design of Laterally Loaded Driven Piles Using the Flat Dilatometer, *Geot. Testing Jnl*, Vol. 12, No. 1, 30-38.
18. Marchetti, S., Totani, G., Calabrese, M. & Monaco, P. (1991), P-y curves from DMT data for piles driven in clay, *Proc.* 4th *Int. Conf. on Piling and Deep Foundations*, *DFI, Stresa*, Vol. 1, 263-272.
19. Balachowski, L. and Kurek, N. (2015), Vibroflotation Control of Sandy Soils, *Proc. 3rd Int. Conf. on the Flat Dilatometer DMT'15*. Roma, Italy, 185-190.
20. Monaco et al. (2014), Overconsolidation and stiffness of Venice Lagoon Sands and Silts from SDMT and CPTU, *Jnl Asce GGE*. Jan 2014, 215-227
21. Robertson, P.K. and Campanella, R.G. (1983), "Interpretation of Cone Penetration Test, *Canad. G. Jnl*, 20, p. 722.
22. Marchetti, S. (1994), An example of use of DMT as an help for evaluating compaction of subgrade and underlying embankment, *Internal Technical Note*, 4pp.
23. Idriss, I.M. and Boulanger, R.W. (2006), Semi-empirical procedures for evaluating liquefaction potential during earthquakes, *Soil Dynamics and Earthquake Engineering*, 26, 115-130.
24. Robertson, P.K. (2012), Mitchell Lecture. Interpretation of in-situ tests - some insight, *Proc.4th Int. Conf. on Site Characterization ISC-4*, Porto de Galinhas - Brazil, 1, 3-24.
25. Marchetti S. (2015), Incorporating the Stress History Parameter K_D of DMT into the Liquefaction Correlations in Clean Uncemented Sands, *Jnl Asce GGE*, published online Aug. 2015

(°) Many of the references can be downloaded from the site www.marchetti-dmt.it

50th IGC
IGS Pune chapter
50th INDIAN GEOTECHNICAL CONFERENCE
17th – 19th DECEMBER 2015, Pune, Maharashtra, India
Venue: College of Engineering (Estd. 1854), Pune, India

DESIGN OF EARTH RETAINING STRUCTURES AND TAILING DAMS UNDER STATIC AND SEISMIC CONDITIONS

S. S. Nimbalkar, Research Fellow, University of Wollongong, Australia, email: sanjayn@uow.edu.au
D. Choudhury, Professor, Indian Institute of Technology Bombay, India, email: dc@civil.iitb.ac.in

ABSTRACT: In this paper the seismic active earth pressure is determined by using pseudo-dynamic method. Mononobe-Okabe method by pseudo-static approach gives the linear distribution of seismic earth pressure behind retaining wall in an approximate way. A rigid vertical retaining wall supporting cohesionless backfill material with horizontal ground has been considered in the analysis with planar rupture surface. Results highlight the non-linearity of seismic earth pressures distribution. Applications of pseudo-dynamic method for stability assessment of gravity dams and tailing dams are presented. A new simplified method to include soil arching effect on determination of earth pressures is also proposed.

INTRODUCTION

Study of dynamic active earth pressure is essential for the safe design of retaining wall in the seismic zone. As pioneering work in this area, the theory of dynamic lateral earth pressure based on pseudo-static analysis was proposed, commonly known as Mononobe-Okabe method [1,2]. But this method using pseudo-static approach gives the seismic active earth pressure value in a very approximate way. To Rectify the shortcomings of the pseudo-static approach, a pseudo-dynamic method has been recently developed to address this problem [3-5]. Effects of both the horizontal and vertical seismic accelerations can be considered to provide more realistic results [6-9].

In one of pioneer studies [10], soil arching was also found to affecting the nonlinear distribution of the active earth pressure acting on the rigid walls in contrast to the assumption made by both Coulomb [11] and Rankine [12] theories. A method for calculating the active earth pressures assuming Coulomb slip was proposed [13]. The seismic active earth pressure acting on the retaining walls were evaluated using the pseudo static [14], more recent pseudodynamic [4,6,15-17] as well as modified pseudodynamic methods of analyses [18]. However, none of these studies considered the stress trajectory caused by soil arching effect, a common phenomenon in geotechnical engineering.

The design and behavior of retaining wall under seismic conditions is very complex and many researchers have discussed on this topic. A classical seismic design method by using Mononobe-Okabe method for the design of earth retaining structures [19]. Caltabiano et al. [20] determined the seismic stability of retaining wall with surchage using Mononobe-Okabe method along with the soil-wall inertia effect by considering pseudo-static seismic acceleration in horizontal direction. Although several researchers in the past highlighted the limitations and drawbacks of the pseudo-static approach, there are very limited studies being reported worldwide for the seismic stability assessment of dams and embankments.

Seismic stability of tailings dams and embankments is an important topic which needs the special treatment by researchers as it is mainly governed by the safety concerns. Many researchers in the past have attempted to investigate the seismic stability of dams and embankments by using pseudo-static method of analysis. Semi empirical stability charts [21] are often used to obtain a preliminary estimate of the permanent, earthquake induced deformation of earth dams and embankments.

In recent past, methods for determination of active earth pressure considering the soil arching effects have been proposed [22,23]. However, these methods were limited to non-cohesive soils. Considering this, a simplified method for calculating the active earth pressure acting on a rigid retaining wall undergoing translation is proposed.

PSEUDO-DYNAMIC METHOD

Consider the fixed base vertical cantilever wall of height H as shown in Fig. 1. The wall is supporting a cohesionless backfill material with horizontal ground. The shear wave and primary wave are assumed to act within the soil media due to earthquake loading. For most geological materials, $V_p/V_s = 1.87$ [24]. The period of lateral shaking, $T = 2\pi/\omega$, where ω is the angular frequency is considered in the analysis. Consider a planer rupture surface inclined at an angle, α with the horizontal.

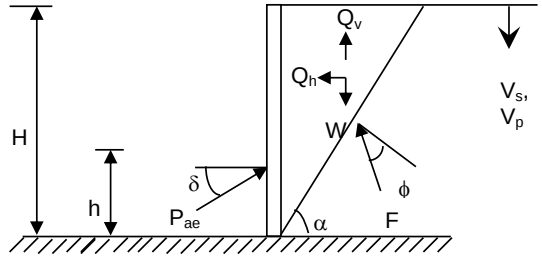

Fig. 1 Model retaining wall considered for computation of pseudo dynamic active earth pressure

Let us assume that the base of the wall is subjected to harmonic horizontal seismic acceleration of amplitude $a_h g$, and harmonic vertical seismic acceleration of amplitude $a_v g$, where g is the acceleration due to gravity.

The acceleration at any depth z and time t, below the top of the wall can be expressed as,

$$a_h(z,\ t) = a_h \sin\left[t - \frac{H-z}{V_s}\right] \tag{1}$$

$$a_v(z,\ t) = a_v \sin\left[t - \frac{H-z}{V_p}\right] \tag{2}$$

The mass of an elemental wedge at depth z is

$$m(z) = \frac{\gamma}{g}\frac{H-z}{\tan\alpha}dz \tag{3}$$

where, γ is the unit weight of the backfill. The total horizontal inertial force acting within the failure zone can be expressed as,

$$Q_h(t) = \int_0^H m(z)a_h(z,\ t)dz$$

$$= \frac{\lambda\ \gamma\ a_h}{4\pi^2 g\tan\alpha}\left[2\pi H\cos w\zeta + \lambda(\sin w\zeta - \sin wt)\right] \tag{4}$$

where, $\lambda = TV_s$ is the wavelength of the vertically propagating shear wave and $\zeta = t\text{-}H/V_s$. And, total vertical inertial force acting within the failure zone can be expressed as,

$$Q_v(t) = \int_0^H m(z)a_v(z,\ t)dz$$

$$= \frac{\eta\ \gamma\ a_v}{4\pi^2 g\tan\alpha}\left[2\pi H\cos\omega\psi + \eta(\sin\omega\psi - \sin\omega t)\right] \tag{5}$$

where, $\eta = TV_p$, is the wavelength of the vertically propagating primary wave. And $\psi = t - H/V_p$. The total (static plus dynamic) active thrust can be obtained by resolving forces on the wedge and can be expressed as,

$$P_{ae}(t) = \frac{W\sin(\alpha-\phi) + Q_h(t)\cos(\alpha-\phi) - Q_v(t)\sin(\alpha-\phi)}{\cos(\delta+\phi-\alpha)} \tag{6}$$

The seismic active earth pressure distribution can be obtained by differentiating the total active thrust as,

$$p_{ae}(t) = \frac{\partial P_{ae}(t)}{\partial z} = \frac{\gamma\ z}{\tan\alpha}\frac{\sin(\alpha-\phi)}{\cos(\delta+\phi-\alpha)} + \frac{k_h\gamma z}{\tan\alpha}\frac{\cos(\alpha-\phi)}{\cos(\delta+\phi-\alpha)}\sin\left[w\left(t-\frac{z}{V_s}\right)\right] - \frac{k_v\gamma z}{\tan\alpha}\frac{\sin(\alpha-\phi)}{\cos(\delta+\phi-\alpha)}\sin\left[w\left(t-\frac{z}{V_p}\right)\right] \tag{7}$$

Results and Discussion

In the case of cohesionless soils, to avoid the phenomenon of shear fluidization for the certain combinations of k_h and k_v [25] the values of ϕ considered in the analysis are to satisfy the relationship given by,

$$\phi \succ \tan^{-1}\left[\frac{k_h}{1-k_v}\right] \tag{8}$$

Fig. 2 shows the comparison of normalized pressure distribution behind rigid retaining wall obtained by the present study with that by Mononobe-Okabe method. It reveals nonlinear seismic active earth pressure distribution behind retaining wall in a more realistic manner compared to the pseudo-static method.

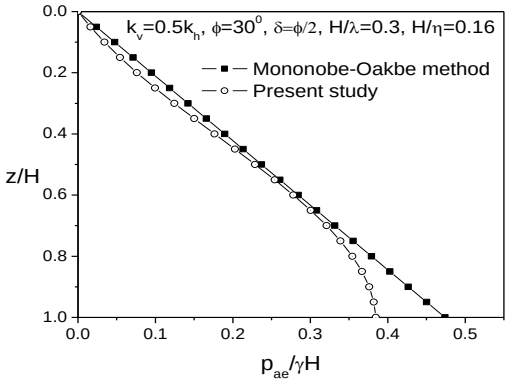

Fig. 2 Comparison of results for $k_v = 0.5k_h$, $\phi = 30^0$, $\delta = \phi/2$, $H/\lambda = 0.3$, $H/\eta = 0.16$

SEISMIC STABILITY OF DAMS

In this section, pseudo-dynamic method is applied for the seismic design of the retaining wall with respect to the stability of the wall against sliding, by considering both the soil and wall inertia effect due to both shear and primary waves propagating through both the backfill and the wall with time variation.

Consider the rigid vertical gravity wall of height H and width b_w, supporting horizontal cohesionless backfill. Using D'Alembert's principle [26] for inertial forces acting on the wall,

$$N_b = P_{ae}(t)\sin\delta + W_w(t) - Q_{vw}(t) \quad (9)$$

$$F_b = P_{ae}(t)\cos\delta + Q_{hw}(t) \quad (10)$$

where, N_b and F_b are the normal and tangential components of the reaction at the base of the wall respectively.

At sliding [27], $F_b = N_b \tan\phi_b$ (11)

where, ϕ_b is the friction angle at the base of the wall. Thus,

$$P_{ae}(t)\cos\delta + Q_{hw}(t) = \left[P_{ae}(t)\sin\delta + W_w(t) - Q_{vw}(t)\right]\tan\phi_b \quad (12)$$

Weight of the wall is given by,

$$W_w(t) = P_{ae}(t)C_{IE}(t) \quad (13)$$

where, $C_{IE}(t)$ is the dynamic wall inertia factor given by,

$$C_{IE}(t) = \frac{\cos\delta - \sin\delta\tan\phi_b}{\tan\phi_b} + \frac{Q_{hw}(t) + Q_{vw}(t)\tan\phi_b}{P_{ae}(t)\tan\phi_b} \quad (14)$$

The relative importance of the two dynamic effects (i.e., the increased seismic active thrust on the wall due to pseudo-dynamic soil inertia forces on the sliding wedge and the increase in driving force due to time dependent inertia of the wall itself) can be seen by normalizing them with regard to the static values. Thus defining soil thrust factor, F_T as

$$F_T = \frac{K_{ae}}{K_a} \quad (15)$$

and wall inertia factor, F_I as

$$F_I = \frac{C_{IE}(t)}{C_I} \quad (16)$$

where,

$$C_I = \frac{\cos\delta - \sin\delta\tan\phi_b}{\tan\phi_b}$$

Considering the product of the soil thrust and wall inertia factors as a safety factor applied to weight of the wall to consider both the effects of soil inertia and wall inertia, the combined dynamic factor, F_w proposed for the design of the wall is defined as,

$$F_w = F_T F_I = \frac{W_w(t)}{W_w} \quad (17)$$

where, W_w is the weight of the wall required for equilibrium against sliding under static condition.

Results and Discussions

Fig. 3 shows variation of combined dynamic factor, F_w with k_h for different values of vertical seismic acceleration coefficient (k_v). From the plot, it may be seen that the combined dynamic factor, F_w increases with the increase in vertical seismic acceleration. For k_h = 0.2, F_w increases by 15 % when k_v changes from 0 to 0.5k_h and 14 % when k_v changes from 0.5k_h to k_h. Though usually the effect of vertical seismic acceleration on stability of retaining wall is hardly considered in the analysis by many researchers, but the present study reveals the significant influence of vertical seismic acceleration on the stability of retaining wall.

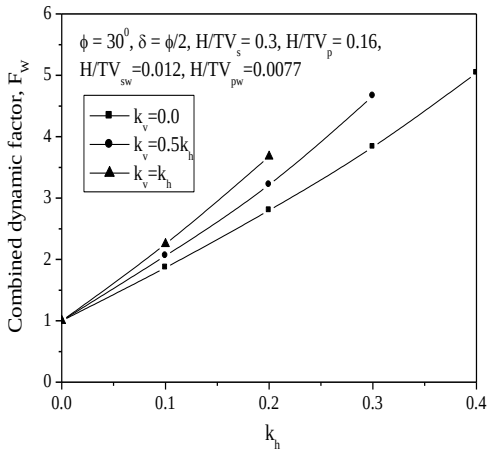

Fig. 3 Effect of vertical seismic acceleration coefficient (k_v) on combined dynamic factor, F_w

SEISMIC STABILITY OF TAILING DAMS

In this section, the seismic stability of the tailings dam by using horizontal slice method considering pseudo-dynamic inertia forces along with other seismic input parameters.

Proposed Analytical Model

The tailings dam, of height H, supporting the compacted tailings overlaid by tailings pond is shown in Fig. 4. The phase of both the horizontal and vertical seismic accelerations are varying along the depth of the dam.

The total horizontal inertia force $q_{hi}(t)$ acting on the i^{th} slice can be expressed as,

$$q_{hi}(z, t) = m_i(z).a_h(z, t) \quad (18)$$

Again, the total vertical inertia force (q_{vi}) acting on the i^{th} slice can be expressed as,

$$q_{vi}(z, t) = m_i(z).a_v(z, t) \quad (19)$$

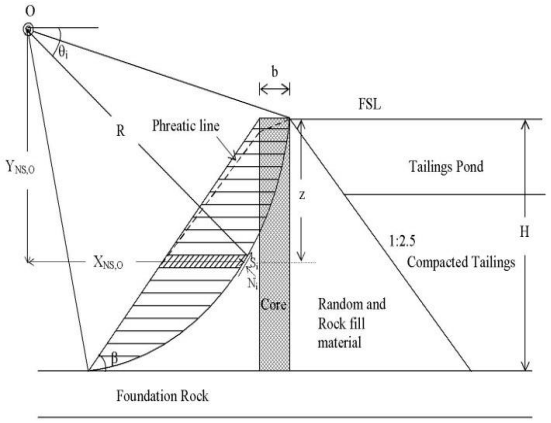

Fig. 4 Tailings dam section considered in the analysis

Detailed mathematical treatment of $q_{hi}(t)$ and $q_{vi}(t)$ can be found elsewhere [8,9]. Similar to the 2N+1 formulation [28], equilibrium equations can be written as

$\sum F_y = 0$ (for each slice) gives

$$V_{i+1} - V_i - W_i - q_{vi} + S_i \sin\alpha_i + N_i \cos\alpha_i = 0 \quad (20)$$

where, V_i and V_{i+1} are vertical inter-slice forces calculated by integration of overburden pressures on horizontal border of slice.

Again, $\tau_r = \frac{\tau_f}{FS}$ (for each slice) yields

$$S_i = \frac{1}{FS}\left(cb_i + N_i \tan\phi\right) \quad (21)$$

Substituting for S_i from equation (21) into equation (20),

$$N_i = \frac{V_i - V_{i+1} + W_i + q_{vi}(z,t) - \frac{cb_i}{FS}\sin\alpha_i}{\frac{\tan\phi}{FS}\sin\alpha_i + \cos\alpha_i} \quad (22)$$

$\sum M_O = 0$ (for the whole wedge)

$$\sum_{i=1}^{m}\begin{bmatrix} q_{hi}(z,t)(Y_{G,O1} + R\sin\theta_i) \\ -(W_i + q_{vi}(z,t))(X_{G,O1} + R\cos\theta_i - l_i) \\ -(S_i\sin\alpha_i + N_i\cos\alpha_i)(X_{NS,O}) \\ -(S_i\cos\alpha_i - N_i\sin\alpha_i)(Y_{NS,O}) \end{bmatrix} = 0 \quad (23)$$

Here, the assumption is made that the normal (N_i) and shear (S_i) forces act at the mid-point of base of each slice and thus,

$$\left.\begin{aligned} X_{NS,O} &= R\cos\theta_i - \frac{h_i}{2\tan\alpha_i} \\ Y_{NS,O} &= R\sin\theta_i + \frac{h_i}{2} \end{aligned}\right\} \quad (24)$$

Substitute S_i and N_i in equation (23) to obtain the factor of safety (FS). The slip circle is assumed as circular in this analysis for the sake of simplicity.

Results and Discussion

The values of factor of safety for tailings dam are reported for both the tailings pond empty and full water conditions.

Fig. 5 shows the effects of both horizontal and vertical seismic acceleration coefficients (k_h and k_v) on factor of safety (FS) for tailings dam empty and full water condition respectively. It is evident from Fig. 5 that, the required value of FS shows significant decrease with increase in horizontal and vertical seismic acceleration coefficients (k_h and k_v).

Referring to the tailings dam empty condition, for $k_v = 0.5k_h$, when k_h changes from 0 to 0.1, required factor of safety (FS) of decreases by about 22.6%. Also when k_h changes from 0.1 to 0.2, required factor of safety (FS) decreases by about 21.5%. Similarly when k_h changes from 0.2 to 0.3, required factor of safety (FS) decreases by about 21%. Also for $k_h = 0.2$, when k_v changes from 0 to $0.5k_h$, the required factor of safety (FS) decreases by about 6.2% and when k_v changes from $0.5k_h$ to $1.0k_h$, required factor of safety (FS) decreases by about 8%.

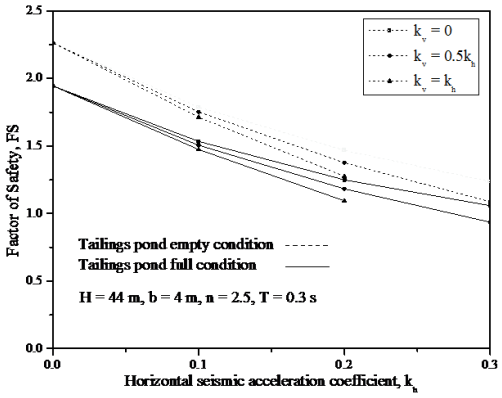

Fig. 5 Effect of horizontal and vertical seismic acceleration coefficients on factor of safety, FS

Similar trend is observed for the tailing dam full water condition. Thus, effects of both horizontal and vertical seismic acceleration coefficients (k_h and k_v) are significant in the computation of stability of the tailings dam. The results reported in the present paper are compared with the pseudo static based slope stability analysis of the tailings dam. Figure 6 shows such a comparison of the results of slope stability analysis using both of these methods of analysis for the case of tailings pond empty and full water condition respectively. It is evident that for the static case, both the methods report similar results.

For finite values of k_h and k_v, factor of safety (FS) computed by pseudo-dynamic method of analysis is more than that by pseudo-static method. The pseudo-static based approach seriously underestimates the stability of dam due to conservative use of constant seismic accelerations throughout the height of dam. Also as the seismic increases, the results computed by using pseudo-dynamic method of analysis deviates more from those of pseudo-static method of analysis.

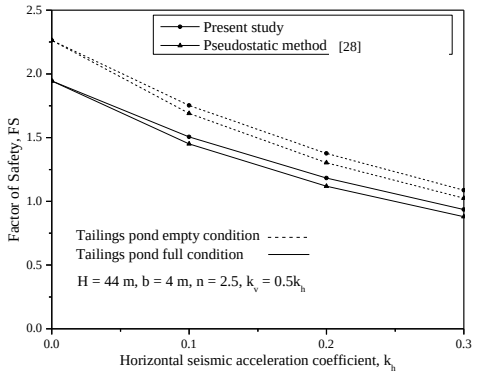

Fig. 6 Comparison of factor of safety (FS) obtained by pseudo-dynamic results with those by pseudo-static results [28] with $k_v = 0.5k_h$.

EFFECT OF SOIL ARCHING ON STABILITY OF RETAINING STRUCTURES

The retaining wall is considered to be rigid and the backfill soil is considered to be cohesive. A planer failure surface is considered in accordance with previous studies [29-34]. The analysis of lateral active earth pressure in cohesive soils is carried out using horizontal flat element method. In this method [35], the failure wedge is divided into a number of horizontal flat elements. Each flat element derives the wall-soil adhesion resistance along the vertical boundaries and the internal frictional resistance induced from the direction of the principal stresses acting on the horizontal boundaries (Fig. 7). For the sake of simplicity, similar to an earlier method reported [22], it is assumed that the trajectory of minor principal stresses takes the form of an arc of a circle.

Analytical Model

Considering the effects of soil arching and wall-soil friction, a new coefficient of lateral active earth pressure (K_{aw}) is defined as:

$$K_{aw} = \frac{1+\frac{1-\sin\phi}{1+\sin\phi}\cot^2\left(\frac{1}{2}\arcsin\left(\frac{\sin\delta}{\sin\phi}\right)-\frac{\delta}{2}\right)}{\csc^2\left(\frac{1}{2}\arcsin\left(\frac{\sin\delta}{\sin\phi}\right)-\frac{\delta}{2}\right)-\frac{2\sin\phi}{3(1+\sin\phi)}} \tag{25}$$

From Equation (1), it is established that when the wall surface is smooth (i.e. δ = 0), $K_{aw} = K_a = \tan^2(45°-\phi/2)$ which coincides with Rankine's active earth pressure coefficient. The lateral active earth pressure at the back of the wall can be calculated as:

$$\sigma_h = K_{aw}\left[\left(q+\frac{\gamma H}{1+\chi}+\frac{c}{\tan\phi}\right)\times\left(1-\frac{y}{H}\right)^{-\chi}-\gamma\left(\frac{H-y}{1+\chi}\right)\right]-\frac{c}{\tan\phi} \tag{26}$$

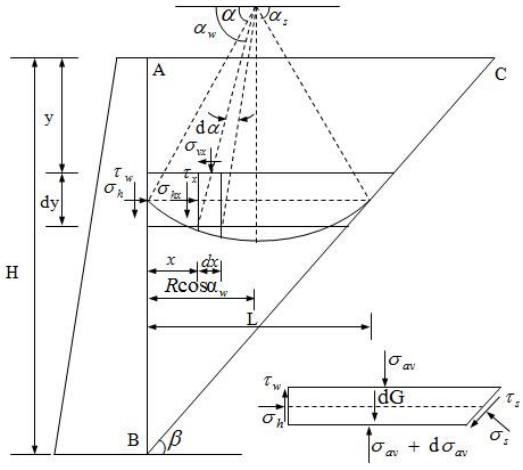

Fig. 7 Trajectory of principal stresses and forces of differential flat element ([35], With permission from ASCE)

If cracks do not appear in the backfill surface, integrating Equation (10) with respect to *y*, the active thrust can be obtained:

$$E_h = \int_0^H \sigma_h dy = \xi\left(qH+\frac{\gamma H^2}{2}\right)-(1-\xi)\frac{cH}{\tan\phi} \tag{27}$$

where

$$\xi = \frac{\sin\left(\lambda-\frac{\phi+\delta}{2}\right)\cos\delta}{\cos\left(\lambda-\frac{\phi+3\delta}{2}\right)\tan\left(\lambda+\frac{\phi-\delta}{2}\right)} \tag{28}$$

From the analysis of Equations (27) and (28), it is observed that when the wall surface is smooth (i.e.

$\delta = 0$), $\xi = K_a = \tan^2(45° - \varphi/2)$ which coincides with the Rankine's active earth pressure coefficient, and the active thrust is equal to that computed by Rankine's theory [12].

If a crack papers at a given the depth (H_c) within the backfill surface, the lateral earth pressure within this depth is assumed to be as zero. By integrating Equation (26) with respect to y from h_c to H, the lateral active earth pressure force can be obtained as follows:

$$E_h = \int_{H_c}^{H} \sigma_h dy$$
$$= \xi(H - H_c)\left[q\left(1 - \frac{H_c}{H}\right)^{-\chi} - \left(\frac{\eta_c c}{\tan\phi}\right) + \eta_r \gamma\left(\frac{H - H_c}{1+\chi}\right)\right] \quad (29)$$

where

$$\eta_c = \frac{1}{\xi} - \left(1 - \frac{H_c}{H}\right)^{-\chi}$$

$$\eta_r = \left(1 - \frac{H_c}{H}\right)^{-1-\chi} - \left(\frac{1-\chi}{2}\right)$$

Results and Discussion

Figure 8 shows the lateral active earth pressure distribution along the normalised height (y/H) of a translating rigid wall with cohesive backfill soil for various values of soil cohesion. It is evident that the lateral active earth pressure distribution along the rigid wall exhibited nonlinear shape for all the values of soil cohesion. With the increase of the soil cohesion c, the lateral active earth pressure decreases significantly, while it is interesting to note that the normalised height of the point of application of active thrust increased marginally. In addition, the depth of tension crack from the surface of the cohesive backfill soil is developed significantly, attributed to the increasing values of soil cohesion.

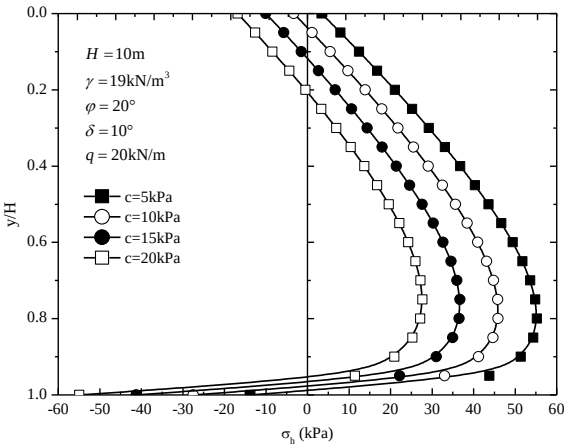

Fig. 8 Variation of active earth pressure distribution with the cohesion of backfill soil ([35], With permission from ASCE)

Figure 9 shows the lateral active earth pressure distribution along the normalised height (y/H) of a translating rigid wall with cohesive backfill soil for various friction angle (ϕ). It is apparent that the lateral active earth pressure decreases significantly with the increasing value of internal friction angle of cohesive soil, while the shape of the lateral active earth pressure distribution remained unchanged.

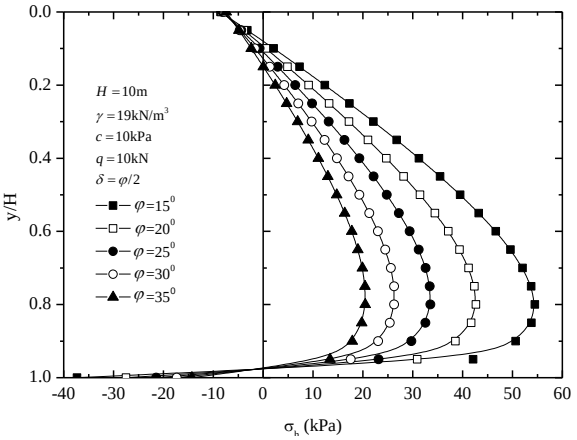

Fig. 9 Variation of active earth pressure distribution with soil friction angle ([35], With permission from ASCE)

The normalised height of the point of application of the active thrust from the base of the wall increased marginally. Moreover, as ϕ increases, the depth of tension crack from the surface of the cohesive soil increases significantly.

Comparison with Other Studies

In order to check the applicability of the proposed formulations, the predictions from the derived equation are compared with experimental results [36], where the distribution of the active earth pressures acting on the translating rigid retaining wall with the height of 4 m were measured. Figure 10 shows the comparison of the non-dimensional distributions of the active earth pressure with other studies [11,12,28].

It is evident that the results obtained using the proposed equation are in good agreement with the measured values, especially for capturing the salient feature of non-linear distribution of active earth pressures, which cannot be predicted by using the existing Coulomb's [11] and Rankine's theories [12].

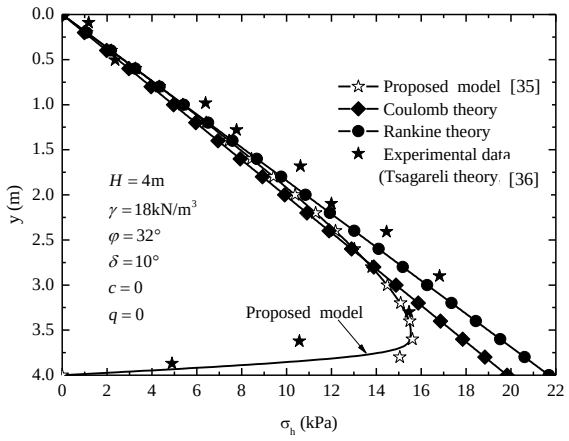

Fig. 10 Comparison between predicted and experimental data ([35], With permission from ASCE)

CONCLUSION

In pseudo-dynamic method by considering the phase change in shear and primary waves propagating in the backfill behind the rigid retaining wall, the seismic active earth pressure distribution as well as the total active thrust behind the retaining wall is altered from that by pseudo-static method. It gives more realistic non-linear seismic active earth pressure distribution behind the retaining wall as compared to the Mononobe-Okabe method.

Pseudo-dynamic method is adopted for the analysis of dam. Seismic stability of dam reduces with increase in the seismic accelerations and phase difference in body waves. Seismic inertia forces acting on the tailings dam are obtained using the pseudo-dynamic method. The results of this study also indicate that, the pseudo-static based procedures conventionally used may underestimate sometimes the stability of tailings dams and embankments under seismic conditions. By using the pseudo-dynamic method, a more rational approach can be adopted for the seismic stability assessment based on correct estimation of dynamic soil properties and accurate prediction of ground motion parameters.

A simplified method for determining the nonlinear distribution of the active earth pressure on rigid retaining walls under translation mode is proposed. The analysis of active cohesive earth pressure is carried out using horizontal flat element method, and analytical expressions for computing active earth pressure distribution, active thrust and its point of application. The general applicability of the proposed method is demonstrated by comparing its predictions with experimental results and other theoretical analyses.

ACKNOWLEDGEMENTS

The authors wish to thank the Australian Research Council (ARC) Centre of Excellence in Geotechnical Science and Engineering.

They also appreciate financial support received from the sponsored project no. AERB/CSRP/31/07 by Atomic Energy Regulatory Board, Mumbai, India for carrying out part of this research.

A significant portion of the contents reported here are described in more detail in a number of scholarly articles listed below. Kind permission has been obtained to reproduce some of these contents in this paper.

REFERENCES

1. Okabe, S. (1926), General Theory of Earth Pressure, *Journal of the Japanese Society of Civil Engineers*, Tokyo, Japan, 12(1).
2. Mononobe, N. and Matsuo, H. (1929), On the determination of earth pressure during earthquakes, *Proceedings, World Engineering Conference*, 9, 176.
3. Steedman, R. S. and Zeng, X. (1990), The influence of phase on the calculation of pseudo-static earth pressure on a retaining wall. *Geotechnique*, 40(1), 103-112.
4. Choudhury, D. and Nimbalkar, S. S. (2005), Seismic passive resistance by pseudo-dynamic method. *Geotechnique* 55(9), 699-702.
5. Choudhury, D. and Nimbalkar, S. S. (2006), Pseudo-dynamic approach of seismic active earth pressure behind retaining wall. *Geotechnical and Geological Engineering* Springer, 24(5), 1103-1113.
6. Choudhury, D. and Nimbalkar, S. S. (2008), Seismic rotational displacement of gravity walls by pseudo-dynamic method. *International Journal of Geomechanics* ASCE, USA, 8(3), 169-175.
7. Nimbalkar, S. S. and Choudhury, D. (2008), Effects of body waves and soil amplification on seismic earth pressures. *Journal of Earthquake and Tsunami*, 2(1), 33-52.
8. Nimbalkar, S. S., Choudhury, D. and Mandal, J. N. (2006), Seismic stability of reinforced soil-wall by pseudo-dynamic method. *Geosynthetics International*, 13(3), 111-119.
9. Choudhury, D. Nimbalkar, S. S. and Mandal, J. N. (2007), External stability of reinforced soil-walls under seismic conditions. *Geosynthetics International*, 14(4), 1-8.
10. Harop-Williams, K. (1989), Arch in soil arching, *Journal of Geotechnical Engineering, ASCE*, 15(3), 415-419.
11. Coulomb, C. A. (1776), Essai sur une application des règles de maximis & minimis à quelques problèmes de statique, relatifs à l'architecture, Mémoires de mathématique & de physique présentés a l'Académie Royale des Sciences par divers savans & lûs dans ses assemblées, 7, 343-382, Paris.
12. Rankine, W. J. M. (1857), On the stability of loose earth. Phil. Trans. R. Soc. London, 147, 9-27.
13. Wang Y. Z. (2005), The active earth pressure distribution and the lateral pressure coefficient of Retaining wall. Rock and Soil Mechanics, 26(7), 1019-1022.
14. Ghosh, S. and Sharma, R. (2012), Seismic active earth pressure on the back of battered retaining wall supporting inclined backfill. *International Journal of Geomechanics, ASCE*, 12(1), 54-63.
15. Ahmad, S. M. and Choudhury, D. (2010), Seismic rotational stability of waterfront retaining wall using pseudodynamic method. *International Journal of Geomechanics, ASCE*, 10(1), 45-52.
16. Choudhury, D. and Katdare, A. D. (2013), New approach to determine seismic passive resistance on retaining walls considering seismic waves, *International Journal of Geomechanics, ASCE*, 13(6), 852-860.
17. Choudhury, D., Katdare, A. D. and Pain, A. (2014), New method to compute seismic active earth pressure on retaining wall considering seismic waves, *Geotechnical and Geological Engineering*, 32(2), 391-402.
18. Pain, A., Choudhury, D. and Bhattacharyya, S. K. (2015), Seismic stability of retaining wall-soil sliding interaction using modified pseudo-dynamic method, *Geotechnique Letters*, 5(1), 56-61.
19. Seed, H. B. and Whitman, R. V. (1970), Design of earth retaining structures for dynamic loads, *ASCE Speciality Conference on Lateral Stresses in the Ground and Design of Earth Retaining Structures*, 103-147.
20. Caltabiano, S., Cascone, E. and Maugeri, M. (2000), Seismic stability of retaining walls with

surcharge. *Soil Dynamics and Earthquake Engineering*, 20, 469-476.
21. Sarma, S. K. (1975), Seismic stability of earth dams and embankments. *Geotechnique* 25: 743–761.
22. Paik, K. H. and Salgado, R. (2003), Estimation of active earth pressure against rigid retaining walls considering arching effects, *Geotechnique*, 53(7): 643-653.
23. Li, J. and Wang, M. (2014), Simplified method for calculating active earth pressure on rigid retaining walls considering the arching effect under translational mode. *International Journal of Geomechanics, ASCE,* 14(2), 282-290.
24. Das, B. M. (1993), *Principles of soil dynamics*. PWS-KENT Publishing Company, Boston, Massachusetts.
25. Richards, R., Elms, D. G. and Budhu, M. (1990), Dynamic fluidization of soils, *Journal of Geotechnical Engineering, ASCE,* 116(5), 740-759.
26. D'Alembert, J. (1758), *Puirk de Dynumique* (Second Edition).
27. Richards, R. and Elms, D. G. (1979), Seismic behavior of gravity retaining walls, *Journal of Geotechnical Engineering Division, ASCE,* 105(4), 449-464.
28. Fakher, A. Nouri, H. and Shahgholi, M. (2002), Limit equilibrium in reinforced soil walls subjected to seismic loads. *In: Proceedings of the Third Iranian International Conference on Geotechnical Engineering and Soil Mechanics*, Tehran, vol. 3: 281-286.
29. Nimbalkar, S. and Choudhury, D. (2010), Effect of amplification on seismic stability of tailings dam, *GeoShanghai International Conference* (GeoShanghai 2010), Shanghai, China, 1-6.
30. Choudhury, D. and Nimbalkar, S. (2009), Seismic stability of tailing dam by using pseudo-dynamic method, *17th International Conference on Soil Mechanics and Geotechnical Engineering* (17ICSMGE), Edited by M. Hamza et al., IOS press, Alexandria, Egypt, 1542-1545.
31. Nimbalkar, S. and Choudhury, D. (2008), Computation of point of application of seismic passive resistance by pseudo-dynamic method, *12th International Conference of International Association for Computer Methods and Advances in Geomechanics* (IACMAG 2008), Goa, India, 2636-2643.
32. Choudhury, D. and Nimbalkar, S. (2007), Determination of point of application of seismic active thrust on retaining wall, *4th International Conference on Earthquake Geotechnical Engineering* (4ICEGE-2007), Thessaloniki, Greece (in CD).
33. Choudhury, D., Nimbalkar, S. and Mandal, J. N. (2006), Influence of soil-wall interface friction on pseudo-dynamic earth pressure, *8th US National Conference on Earthquake Engineering* (8NCEE-2006), USA (in CD).
34. Choudhury, D. and Nimbalkar, S. (2004), Seismic active earth pressure by pseudo-dynamic method, *Proceedings of Indian Geotechnical Conference*, IGC-2004, 199-202.
35. Rao, P., Chen, Q., Zhou, Y., Nimbalkar, S. and Chirao, G. (2015), Determination of active earth pressure on rigid retaining wall considering arching effect in cohesive backfill soil, *International Journal of Geomechanics, ASCE* doi: 10.1061/(ASCE)GM.1943-5622.0000589.
36. Tsagareli, Z. V. (1965), Experimental investigation of the pressure of a loose medium on retaining wall with vertical backface and horizontal backfill surface, *Soil Mechanics and Foundation Engineering*, 91(4): 197-200.

INFLUNCE OF SEEPAGE FORCE ON ACTIVE AND PASSIVE THRUST FOR DESIGN OF A RIGID CUT-OFF WALL

N. K. Samadhiya[1] and A. K. Singh[2]

ABSTRACT: Terzaghi (1954) has suggested a simplified approach for the design of cut-off walls considering average seepage force. In Terzaghi's approach, the unbalanced water pressure around the cut-off wall is coupled with the active earth pressure and the resultant thrust is determined by subtracting the passive thrust from the combined active thrust. The value of passive earth pressure coefficient has been assumed to correspond with a downstream failure wedge having an angle of $\left(45^0 - \bar{\phi}_1 / 2\right)$ with the horizontal, where $\bar{\phi}_1$ is the effective angle of shearing resistance of the foundation soil. In this paper, it is shown that under steady state flow conditions for a flexible levee base, failure does not take place always at this angle. Considering exact seepage forces and applying the laws of equilibrium, active and passive earth pressures acting on a rigid sheet pile cut-off wall on an impervious levee have been determined. The weight of the levee has been considered in the computation of active thrust. The design procedure of a rigid cut-off wall is also explained.

---

1 *Professor, Deptt. of Civil Engineering; Indian Institute of Technology, Roorkee – 247667 (India) nksamfce@iitr.ac.in*

2 *Associate Professor, Deptt. of Civil Engineering;NIT Jamshedpur aksnitjsr@rediffmail.com*

INTRODUCTION

Failure resulting from a quick condition and piping in foundation soils due to high seepage pressures is highly dangerous in water retaining structures. Seepage through the hydraulic

structures and its foundation is controlled by two approaches, which are generally used in combination (Peter, 1982). The first approach involves reduction of the quantity of seepage, which may be achieved by providing anti-seepage elements of passive protection e.g., sheet pile (steel, wooden) cut-off wall, slurry trench, clay sealing, upstream impervious blanket, grout curtain, concrete wall, diaphragm wall, etc. The second approach involves providing a safe outlet for seepage water, which still enters the hydraulic structure or the foundation. This may be achieved by providing anti-seepage elements of active protection such as filters, drains, sand drains, stone columns, ditches and relief wells (Sherard et al., 1963; Peter, 1982).

Provision of a sheet pile cut-off wall is one of the common anti-seepage measures taken in water retaining structures such as dams, reservoirs, levees, floodwalls, weirs, irrigation and power generation canals, etc. to ensure stability against sand boiling and piping (Terzaghi, 1954). Sheet pile cut-off walls may be flexible or rigid. Thin steel or concrete sheet pile cut-off walls are treated as flexible, where as, thick steel or reinforced concrete sheet pile cut-off walls are treated as rigid one. Steel sheet piling can provide the best underseepage barrier (Lane and Wohlt, 1961) in pervious soils. When the depth of sheet pile cut-off walls exceeds about 9 to 15 m, it is less expensive to drive steel sheet piling than other provision for seepage control. Steel sheet piles can be driven up to a depth of 38 m (Creager et al., 1968). The importance of the seepage force in the computation of total thrust in the design of sheet pile cut-off walls has been discussed in U. S. Army Corps of Engineers manual (EM 1110-2-2504, 1994).

Terzaghi (1954) analyzed the forces acting on a cut-off wall, such as water pressures in the upstream and downstream side in addition to the active and passive earth pressures. He suggested graphical method for the computation of the active earth pressure, flow net for the determination of water pressure and analytical method for the passive earth pressure. The graphical method suggested by Terzaghi pertains to a retaining wall with vertical drainage

layer, which, during a rainstorm, acts as a surface of seepage (water pressure is zero on the face of the vertical wall). As described by Terzaghi, it is not necessary to compute the seepage force acting on the failure wedge separately. In case of a cut-off wall, there is always water pressure acting on either side and seepage force in the triangular wedge is to be computed exclusively. Terzaghi used submerged unit weight of the soil reduced by the average seepage pressure per unit volume of the mass of soil as the unit weight of the soil for the computation of the passive earth pressure. He combined the unbalanced water pressure between upstream and downstream sides with active earth pressure. The resultant thrust acting on the cut-off wall was obtained by subtracting the passive thrust from the combined unbalanced water pressure and active thrust. In the proposed method, the seepage force acting on the soil wedge is calculated accurately in both upstream and downstream sides. The magnitude and direction of the seepage force changes with the volume of the critical soil wedge. The seepage force is likely to change the angle of the failure plane of the soil wedge also. Computation of active and passive thrusts and their angle of failure plane without considering the actual seepage force is not justified and needs verification.

In the present study, the active and passive thrusts acting on a rigid cut-off wall have been quantified considering limiting equilibrium of forces, including the exact seepage force acting on a trial triangular failure wedge. An equi-potential function (ϕ) and pore water pressures in the flow domain are obtained through conformal mapping (Harr, 1962). The exact seepage force has been determined both graphically and analytically using the boundary pressure method (Cedegren, 1989). The passive thrust acting on the sheet pile cut-off wall is compared with that obtained by Terzaghi's simplified approach. The present study deals with rigid cut-off walls and flexible levee base only.

STATEMENT OF THE PROBLEM

A levee with a rigid sheet-pile cut-off wall at its downstream toe resting on a homogeneous, isotropic permeable foundation of infinite depth is shown in Fig. 1. The bottom width of the levee is b; the height of levee is h_L; the top width of levee is b_T; the depth of sheet pile cut-off wall is d; the upstream pondage depth of water is h_1. Depth of tail water h_2 is nominal. Flow is in a steady state condition. It is required to find the resultant thrust acting on the rigid cut-off wall.

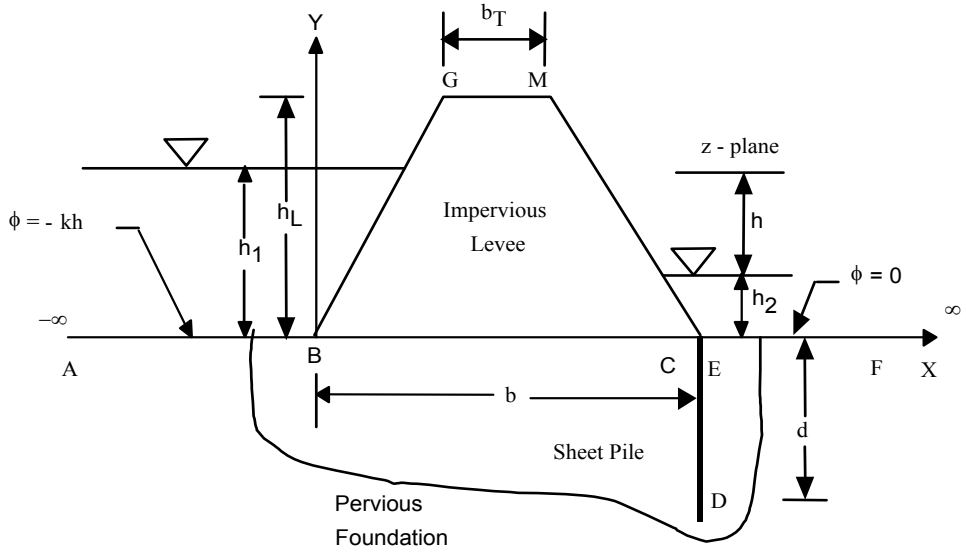

Fig. 1. Layout of levee with rigid cut-off wall

FORCES ON THE WEDGE

A trial triangular failure wedge in the upstream side including the levee body and another triangular failure wedge in the downstream side of a sheet pile cut-off wall are considered for the computation of active and passive earth pressures as shown in Figs. 2(a, b, c); and 3 respectively.

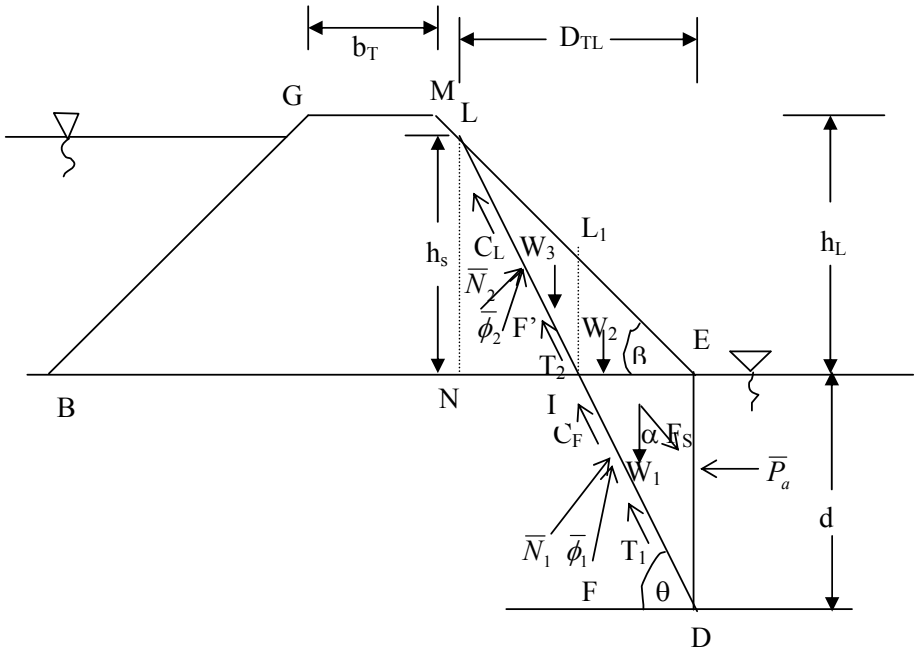

Fig. 2(a). Free body diagram of wedge for case -I in upstream side

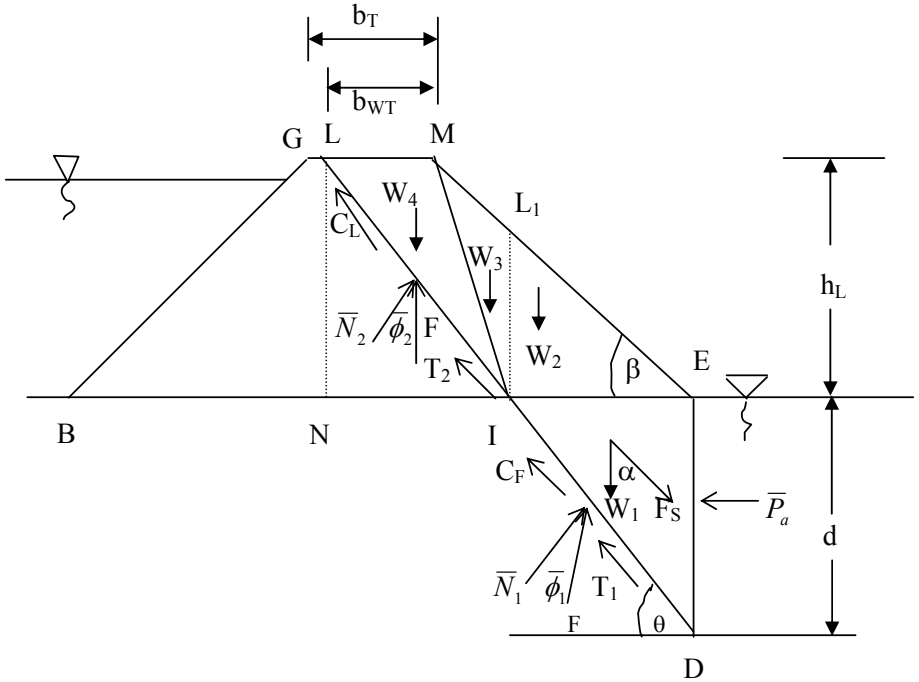

Fig. 2(b). Free body diagram of wedge for case - II in upstream side

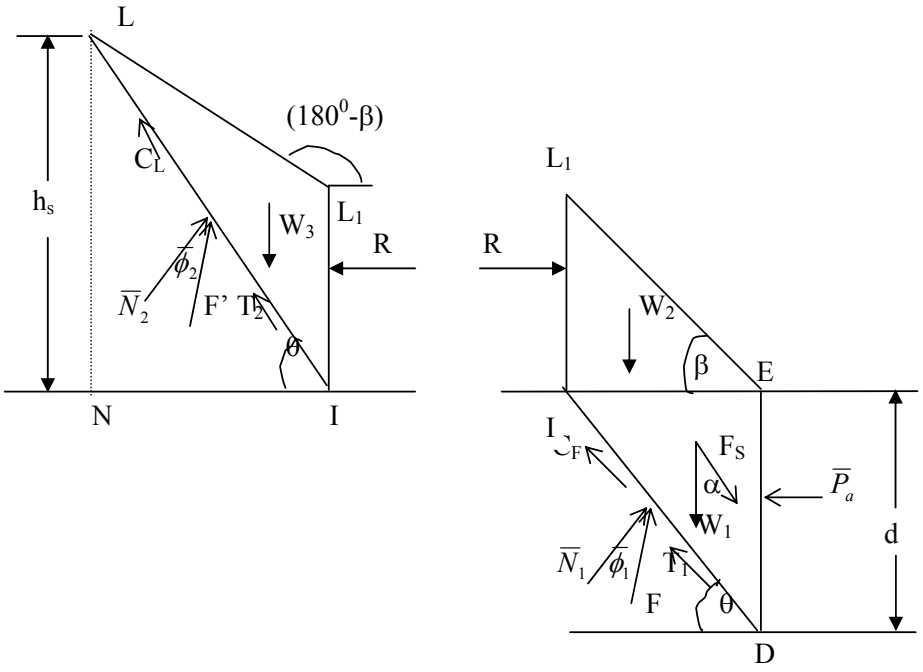

Fig. 2(c). Free body diagram of wedge W_3 and wedge (W_1+W_2) combined for evaluation of force at face L_1I in upstream side

Under the influence of wall friction, the surface of sliding is curvilinear at the lower part near the wall and is planer at the upper part. The shape of the curved part is assumed to be either a logarithmic spiral or an arc of a circle. Terzaghi (1954, p-108) has computed passive earth pressure for sand using logarithmic spiral method. The equations, which have been derived by Karman (1926), Jaky (1938), and Ohde (1938) considering wall friction, are too complicated for practical use. Considering wall friction, Coulomb (1776) has derived co-efficient of passive earth pressure assuming entire surface of sliding as a plane surface. If angle of wall friction is smaller than one third of angle of internal friction of soil, the difference between real surface of sliding and Coulomb's plane surface is very small. The wall friction of a cut-off will get reduced due to lubricating effect of water (Jagla, 2004). Therefore, in the

present analysis, wall friction is neglected in computation of earth pressure. The other forces acting on the trial wedge are as follows:

1. Weight of the Wedge; Tangential Force; and Cohesive Force

(i) Upstream side

If h_s is the height of the point of intersection (L) of failure plane of upstream failure wedge and the downstream side slope (Fig. 2a), θ is the angle of failure plane with horizontal which is discussed subsequently, and β is the angle of downstream side slope with the base of the levee, then

$$h_s = \frac{d}{\frac{\tan\theta}{\tan\beta} - 1} \tag{1}$$

Horizontal distance of the point of intersection (L) from downstream toe (D_{TL}) as shown in Fig. 2 (a) can be determined as

$$D_{TL} = (d + h_L)\cot\theta \tag{2}$$

Weight of the wedge (W_1) in upstream side in foundation is given by (Lambe and Whitman, 1979):

$$W_1 = \frac{1}{2} d^2 \gamma_b \cot\theta \tag{3a}$$

where γ_b is the buoyant unit weight of the foundation soil.

Case – I : When failure plane intersects downstream slope

If h_s computed from Eq. (1) is less than height of levee (h_L) or D_{TL} computed from Eq. (2) is less than horizontal extent of downstream triangular portion of levee ($h_L/\tan\beta$) and γ_{sat} is the saturated unit weight of the compacted levee soil (assuming complete saturation of levee soil), then the weight of the wedges W_2 and W_3 in levee structure (Fig. 2a) are given by

$$W_2 = \frac{1}{2}\gamma_{sat}(d\cot\theta)^2 \tan\beta \tag{3b}$$

$$W_3 = \frac{1}{2}(d\cot\theta)\left(\frac{\tan\beta}{\tan\theta}\right)h_s\,\gamma_{sat} \tag{3c}$$

Total cohesive forces C_F and C_L acting on the failure plane of the wedge in foundation and levee respectively are given by

$$C_F = \frac{\bar{c}_1\, d}{\sin\theta} \tag{4a}$$

$$C_L = \frac{\bar{c}_2\, h_s}{\sin\theta} \tag{4b}$$

where $\bar{c}_1$ and $\bar{c}_2$ are the effective cohesions acting along failure plane in foundation and levee soils respectively.

Tangential forces T_1 and T_2 on the failure plane in foundation and levee respectively can be given by

$$T_1 = \bar{N}_1 \tan\bar{\phi}_1 \tag{5a}$$

$$T_2 = \bar{N}_2 \tan\bar{\phi}_2 \tag{5b}$$

where $\bar{N}_1$ and $\bar{N}_2$ are the normal forces acting on the failure plane in foundation and levee respectively; and $\bar{\phi}_1$ and $\bar{\phi}_2$ are the effective angles of internal friction of foundation and levee soils respectively.

The normal force $\bar{N}_1$ is the component of weight ($W_1 + W_2$) whereas the normal force $\bar{N}_2$ is the component of weight W_3 (Fig. 2b). The normal force $\bar{N}_2$ and reaction R (Fig. 2b) can be obtained by considering limiting equilibrium of the wedge LL_1I and considering summation of forces zero, in vertical as well as horizontal directions i.e., $\sum F_V = 0$ and $\sum F_H = 0$. Friction and cohesion between wedges at face L_1I is neglected. In ($c - \phi$) soil

$$W_3 - \overline{N}_2 \cos\theta - (T_2 + C_L)\sin\theta = 0 \tag{6a}$$

$$\overline{N}_2 \sin\theta - R - (T_2 + C_L)\cos\theta = 0 \tag{6b}$$

In cohesionless soil, the normal force $\overline{N}_2$ and reaction R can be obtained by substituting $C_L = 0$ in Eqs. 6(a) and 6(b).

Case – II : When failure plane intersects crest of levee

If D_{TL}, computed from Eq. (2) is greater than $h_L/tan\beta$, and less than ($h_L/tan\beta + b_T$) then the weight of wedges W_1 and W_2 will be the same as obtained from Eqs. (3a) and (3b). Whereas the weight of wedges, W_3 and W_4 (Fig. 2c) are obtained by keeping $h_s = h_L$ as

$$W_3 = \frac{1}{2}(d\cot\theta)\left[h_L - (d\cot\theta)\tan\beta\right]\gamma_{sat} \tag{7a}$$

$$W_4 = \frac{1}{2} b_{WT}\, h_L\, \gamma_{sat} \tag{7b}$$

where b_{WT} is the base width (LM) of wedge W_4 (Fig. 2c) and can be expressed as

$$b_{WT} = h_L\left[\frac{1}{\tan\theta} - \frac{1}{\tan\beta}\right] + \frac{d}{\tan\theta} \tag{8}$$

Total cohesive force C_F is obtained by using Eq. (4a). In the levee portion, the total cohesive force C_L can be calculated by substituting $h_s = h_L$ in Eq. (4b).

$$C_L = \frac{\overline{c}_2\, h_L}{\sin\theta} \tag{9}$$

The normal force $\overline{N}_1$ is the component of weight ($W_1 + W_2$) as in the case - I whereas the normal force $\overline{N}_2$ is the component of weight ($W_3 + W_4$). The normal

force $\overline{N}_2$ and reaction R can be obtained by taking limiting equilibrium of the wedge LL_1I (Fig. 2c). Reaction R can be computed by using Eqs. (6a) and (6b) by substituting ($W_3 + W_4$) in place of W_3.

Case – III : When failure plane intersects upstream slope

If D_{TL} is greater than ($h_L/tan\beta + b_T$) then the weight of wedges W_1 and W_2 will be the same as obtained from Eqs. (3a) and (3b). Whereas the weight of wedges, W_3, W_4 and W_5 can be obtained as:

$$W_3 = \frac{1}{2}\left[d\left(1+\frac{\tan\beta}{\tan\theta}\right) + h_L\left(1-\frac{\tan\theta}{\tan\beta}\right)\right]\left[\frac{h_L}{\tan\beta} - d\cot\theta\right]\gamma_{sat} \qquad (10a)$$

$$W_4 = \frac{1}{2}\left[2h_L\left(1-\frac{\tan\theta}{\tan\beta}\right) + 2d - b_T\tan\theta\right] b_T\,\gamma_{sat} \qquad (10b)$$

$$W_5 = \frac{1}{2}\frac{\gamma_{sat}}{(\tan\theta+\tan\beta)}\left[h_L\left(1-\frac{\tan\theta}{\tan\beta}\right) + d - b_T\tan\theta\right]^2 \qquad (10c)$$

Total cohesive force C_F is obtained by using Eq. (4a). In the levee portion, total cohesive force C_L can be calculated by

$$C_L = \frac{\bar{c}_2}{\sin\theta}\left[h_L - \left\{ h_L\left(1-\frac{\tan\theta}{\tan\beta}\right) + d - b_T\tan\theta\right\}\left\{\frac{\tan\beta}{\tan\theta+\tan\beta}\right\}\right] \qquad (11)$$

The normal force $\overline{N}_1$ is the component of weight ($W_1 + W_2$) as in previous cases whereas the normal force $\overline{N}_2$ is the component of weight ($W_3 + W_4 + W_5$). The normal force $\overline{N}_2$ and reaction R can be obtained by considering limiting equilibrium of combined wedge ($W_3 + W_4 + W_5$). Reaction R can be computed by using Eqs. [6(a) and 6(b)] replacing W_3 by ($W_3 + W_4 + W_5$).

Weights (W, W_1, W_2, W_3, W_4 and W_5), tangential forces (T_1, T_2) and total cohesive forces (C_F, C_L) are an integral part of the estimation of active thrust.

(ii) Downstream side

Weight of the wedge (W) and total cohesive force (C_F) in downstream side are obtained by using Eqs. 3(a) and 4(a) respectively. Total tangential force (T) can be written as

$$T = \overline{N} \tan \overline{\phi}_1 \tag{12}$$

These forces W, C_F and T are an integral part of the estimation of passive thrust.

2. Seepage Force, F_S

Magnitude and direction of seepage force (F_S) are calculated by boundary pressure method (Cedergren, 1989). Details of computation of boundary pressure are given in appendix I.

TERZAGHI APPROACH (PASSIVE THRUST)

As per Terzaghi (1954), the passive earth thrust in the downstream side of cut-off wall in $(c-\phi)$ soil can be estimated as:

$$P_p = \frac{1}{2}\gamma'' d^2 \tan^2\left(45^0 + \frac{\overline{\phi}_1}{2}\right) + 2\overline{c}_1 d \tan\left(45^0 + \frac{\overline{\phi}_1}{2}\right) \tag{13}$$

where P_P is passive thrust, and γ'' is the submerged unit weight (γ_b) of the soil reduced by the average seepage pressure per unit volume of the mass of soil.

In cohesionless soil, passive thrust can be estimated by substituting $\overline{c}_1 = 0$ in Eq. (13).

PROPOSED APPROACH

Estimation of Active Thrust

The procedure for the calculation of active thrust is as follows:

(i) A trial soil wedge in the upstream side of the rigid cut-off wall is considered as a free body. The resultant of the distributed stresses $\overline{P}_a$, which must exist between this free body and the wall, is found by writing the equations of equilibrium for the free body as a whole.

(ii) All forces acting on the soil wedge are evaluated as shown in Figs. 2(a) to 2(c) for different cases.

(iii) The seepage force is superimposed over the soil wedge where forces are to be analyzed for equilibrium condition.

(iv) In the limiting equilibrium condition, summation of forces in vertical as well as horizontal directions must be zero i.e., $\sum F_V = 0$ and $\sum F_H = 0$. Incorporating all forces in the horizontal and vertical directions for $(c-\phi)$ soil, yields

$$W - (C_F + T_1)\sin\theta - \overline{N}_1 \cos\theta + F_S \cos\alpha = 0 \tag{14}$$

$$\overline{N}_1 \sin\theta - (C_F + T_1)\cos\theta - \overline{P}_a + R + F_S \sin\alpha = 0 \tag{15}$$

where W is the summation of weights W_1 and W_2, F_S is seepage force, α is angle made by seepage force with vertical and $(\overline{P}_a)$ is resultant of distributed stresses between the soil and the wall acting on the upstream side of the cut-off wall.

(v) $\overline{P}_a$ may be calculated by solving Eqs. (14) and (15).

(vi) In cohesionless soil, $\overline{P}_a$ can be calculated by substituting $C_F = 0$ in Eqs. (14) and (15).

(vii) The above procedure is repeated for calculating $\overline{P}_a$ for various angles θ, at suitable intervals ranging from an angle of internal friction of the soil ($\overline{\phi}_1$) to 90^0 in which value of $\overline{P}_a$ will be the maximum.

(viii) A graph is plotted between $\overline{P}_a$ and angle θ. There is an angle (θ) for which the $\overline{P}_a$ is maximum. The maximum $\overline{P}_a$ is the active thrust (P_a).

Estimation of Passive Thrust

The forces acting on a trial failure wedge for the passive case are shown in Fig. 3.

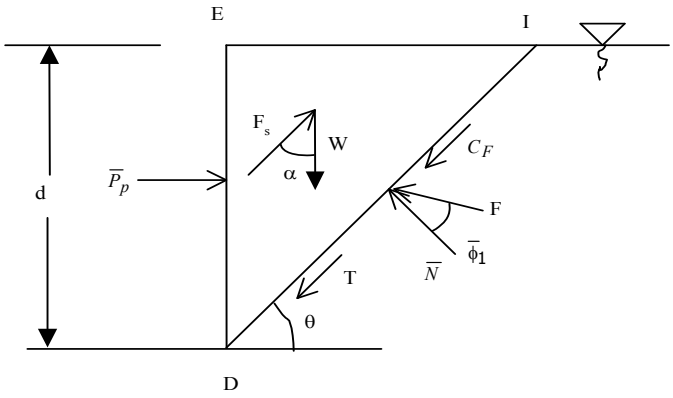

Fig. 3. Free body diagram of wedge in downstream side

Passive thrust can be obtained using following steps:

(i) A trial triangular soil wedge in the downstream side of a rigid cut-off wall is considered as a free body. The resultant of the distributed stresses ($\overline{P}_p$), which must exist between this free body and the wall, is found by writing the equations of equilibrium for the free body as a whole.

(ii) Magnitude and direction of seepage force is obtained as calculated for active case.

(iii) The steps (ii) and (iii) for the active case are repeated here also.

(iv) For equilibrium condition, incorporating all forces in the vertical and horizontal directions for $(c-\phi)$ soil, yields

$$W + (C_F + T)\sin\theta - \overline{N}\cos\theta - F_S\cos\alpha = 0 \tag{16}$$

$$\overline{P}_p - \overline{N}\sin\theta - (C_F + T)\cos\theta + F_S\sin\alpha = 0 \tag{17}$$

where $(\overline{P}_P)$ is the resultant of the distributed stresses between the soil and wall acting on the downstream side of the cut-off wall.

(v) $\overline{P}_P$ may be calculated by solving Eqs. (16) and (17).

(vi) In cohesionless soil, $\overline{P}_P$ can be calculated by substituting C_F = 0 in Eqs. (16) and (17).

(vii) The process is repeated for calculating $\overline{P}_p$ for various angles of θ ranging from $\left(45^0 - \overline{\phi}_1/2\right)$ to 45^0 at suitable intervals.

(viii) A graph is plotted between $\overline{P}_p$ and angle θ. There is an angle (θ) for which the $\overline{P}_P$ is minimum. The minimum $\overline{P}_P$ is the passive thrust (P_p).

Unbalanced Water Force

The unbalanced water force (F_{uw}) is the force developed due to the difference of water pressure acting on the upstream and downstream sides of a cut-off wall and it may be expressed as follows:

$$F_{uw} = F_1 - F_2 \tag{18}$$

where forces F_1 and F_2 are developed due to water pressure in the upstream and downstream sides respectively. Water pressure is determined through conformal mapping (Harr, 1962).

Resultant Thrust

For the design of a rigid cut-off wall, one needs to compute the resultant thrust. The resultant thrust (T_r) is the summation of the unbalanced water force and the difference between the active and passive thrusts (Fig. 4).

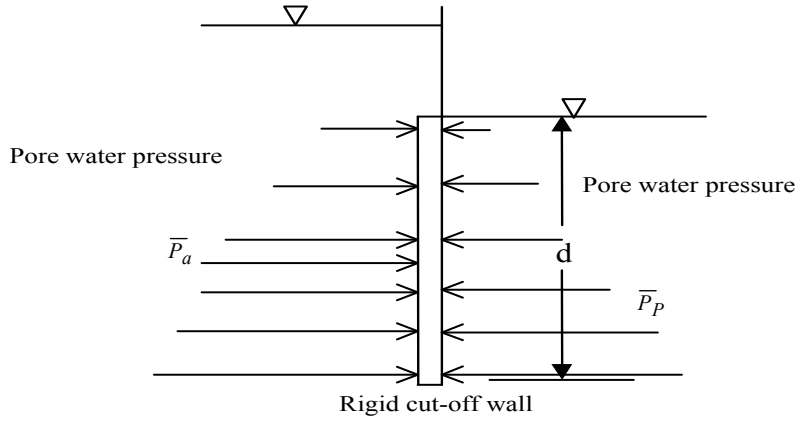

Fig. 4. : Free body diagram of a rigid cut-off wall

Mathematically, it can be written as

$$T_r = F_{uw} + (P_a - P_p) \tag{19}$$

The resultant thrust acts in the direction of the downstream side and causes bending of a cut-off wall. The flexural strength of the sheet pile cut-off wall will resist the bending moment developed due to the resultant thrust (T_r).

ILLUSTRATIVE EXAMPLE

An illustrative example is considered to assess the design implications and to compare the results of Terzaghi's method with the one proposed in this work. The relevant data are given in Table 1. The foundation soil is assumed to be cohesionless. The void ratio (e) and specific

gravity (G) of levee soil and foundation soil are taken to be the same for simplicity. The equi-potential function (ϕ) and pore water pressure distribution in the flow domain under a levee with a sheet pile cut-off wall resting on pervious foundation of infinite depth have been obtained for given data at all boundaries through conformal mapping as shown in Fig. 5. For the present example, it is assumed that the angle of failure plane (comprising wedge) with respect to the horizontal is 40^0.

Table 1. Data for Illustrative Example

b (m)	b_T (m)	h_L (m)	d (m)	h_1 (m)	h_2 (m)	$\bar{c}_1, \bar{c}_2$ kN/m^2	$\bar{\phi}_1, \bar{\phi}_2$ (Deg.)	G	e = e_1	Side Slope
65	5	20	4	19	0	2, 10	25, 18	2.6	0.40	1V: 1.5H

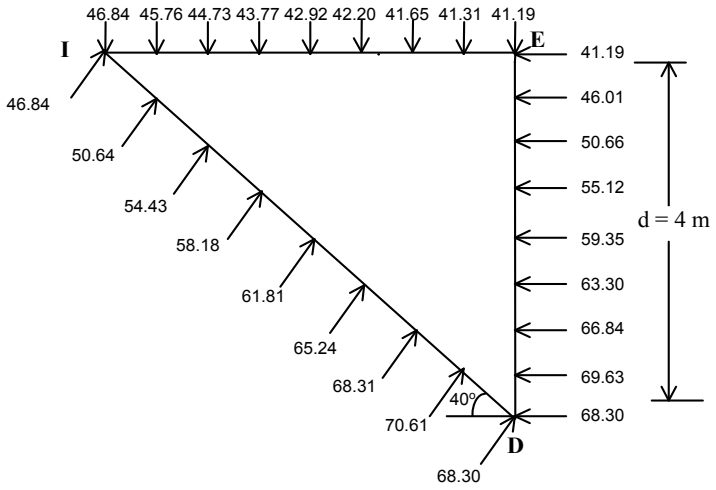

Fig. 5. Pore water pressure distribution around triangular soil wedge

Pore water forces acting in triangular soil wedge are shown in Fig. 6.

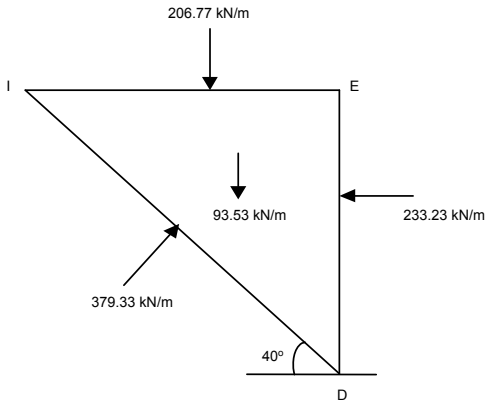

Fig. 6. Pore water force on triangular wedge

The magnitude and direction of the seepage force is determined by force polygon method as shown in Fig. 7.

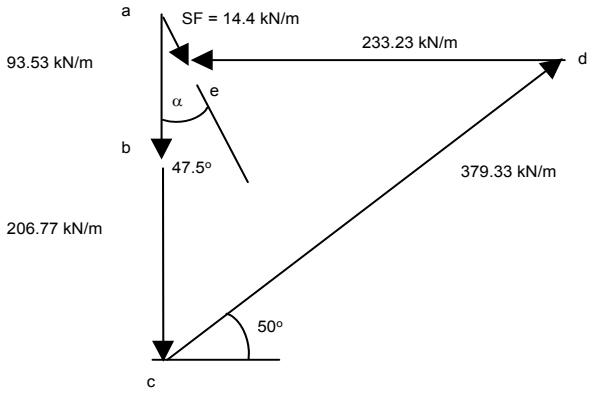

Fig. 7. Pore water force polygon

One can superimpose the seepage force on wedge of soil skeleton as shown in Fig. 2 and the active thrust may be determined. The resultant of the distributed stresses between the soil and wall ($\overline{P}_a$) for different wedges having different failure plane angles is calculated and the results are shown in Table 2. A graph between $\overline{P}_a$ and angle (θ) is drawn as shown in Fig. 8.

Table 2. Seepage Force and $\overline{P}_a$ for Different Angle θ (Proposed Approach)

Sl. No.	Angle θ with Horizontal (Degree)	Seepage Force (F_S) (kN/m)	Angle α with Vertical (Degree) Counterclockwise	$\overline{P}_a$ (kN/m)
1	28	24.79	58.45	399.9
2	29	23.60	57.54	417.84
3	30	22.49	56.63	424.11
4	31	21.44	55.71	418.92
5	32	20.46	54.8	402.45
6	33	19.54	53.90	374.82

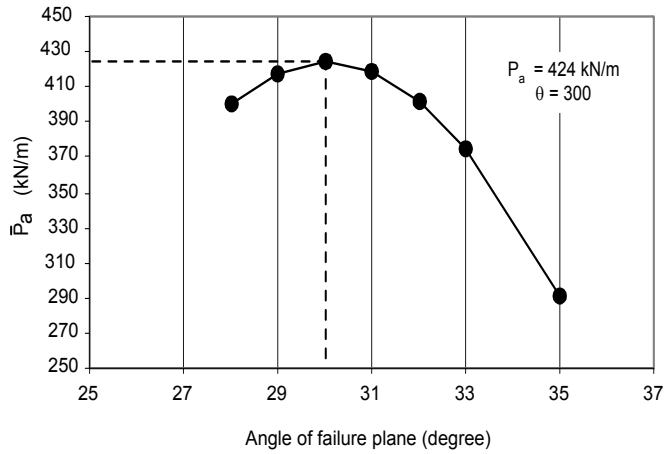

Fig. 8. $\overline{P}_a$ versus angle of failure plane

In the downstream side, the seepage force is calculated in similar way as that in the case of upstream side for different wedges having different angle of failure plane. The resultant of distributed stresses between the soil and the cut-off wall in the downstream side ($\overline{P}_p$) for different angles (θ) are calculated and tabulated in Table 3. A graph between $\overline{P}_P$ and angles (θ) is drawn as shown in Fig. 9.

Table 3. Seepage Force and $\overline{P}_P$ for Different Wedge Angles (Proposed Approach)

Sl. No.	Angle θ with Horizontal (Degree)	Seepage Force (F_S) (kN/m)	Angle α with Vertical (Degree) Clockwise	$\overline{P}_P$ (kN/m)
1	36	55.23	5.24	143.90
2	35	56.96	5.33	143.62
3	34	58.75	5.42	143.59
4	33	60.61	5.51	143.78
5	32	62.54	5.60	144.19

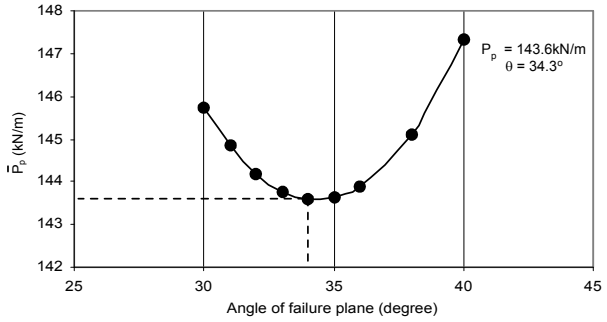

Fig. 9. $\bar{p}_p$ versus angle of failure plane

The maximum active thrust, and minimum passive thrust, unbalanced water force, and the resultant thrust causing bending of the rigid sheet pile cut-off wall are presented in Table 4.

Table 4. Results of Proposed Approach and Terzaghi's Approach

Approach	Active Thrust (kN/m) (i)	Angle θ (Active Case)	Passive Thrust (kN/m) (ii)	Angle θ (Passive Case)	Unbalanced Water Force (kN/m) (iii)	Resultant Thrust (kN/m) [(i) + (iii) - (ii)]
Proposed Approach	424.11	30^0	143.59	34^0	109.754	390.27
Terzaghi's Approach			160.61	32.5^0		

RESULTS AND DISCUSSION

It is obvious from Table 4, that there is a difference of 17.02 kN/m length in the passive thrust obtained from both the approaches (Terzaghi, 1954 and the proposed method). It may also be noted that the wedge angle in downstream side is not necessarily equal to $\left(45^0 - \bar{\phi}_1 / 2\right)$, as inherent in Terzaghi approach. Thus the assumption of the correct size of the triangular wedge appears critical to the design of a rigid cut-off wall. In the proposed approach, certain features are worth mentioning. The wedges at both in the upstream and downstream side of sheet pile cut-off wall have been taken for the calculation of active and passive thrust. The weight of the portion of levee likely to fail is also considered and included in the weight of the wedge for the analysis of active thrust. The seepage force has been obtained through boundary pressure method and superimposed on the soil wedge. Equilibrium of forces are considered and the active and passive thrust acting on a cut-off wall under steady state flow condition have been obtained by optimizing the resultant of the distributed stresses between soil and wall and corresponding angle of failure plane.

A detailed parametric study has been undertaken to explore a variety of conditions. The resultant thrust, T_r, obtained by proposed approach with upstream water head, h_1, for $(c - \phi)$ soil in foundation has been presented in Table 5. The seepage force acting on the cut-off wall has been obtained analytically. The resultant thrusts for various b/d ratio, side slopes of levee, effective angle of internal friction of foundation soil are also presented in Table 6. The negative sign of the resultant thrust indicates that the passive thrust is greater than combined active thrust and unbalanced water force. Such a condition indicates that sheet pile is not required beyond that particular length. It can be seen in Tables 5 and 6 that seepage forces in the downstream side reduce the passive thrust.

Table 5. Variation of Resultant Thrust with Upstream Water Level

$h_L = 20$ m $b_T = 5$ m d = 4 m $h_2 = 0$ $\gamma_w = 9.81\,\text{kN/m}^3$

$\bar{c}_1 = 2\,\text{kN/m}^2$ $\bar{\phi}_1 = 30^0$ G = 2.6 e = 0.40

h_1 (m)	Seepage Force U/s side (kN/m)	Max. $\bar{P}_a$ (kN/m)	Seepage Force D/s side (kN/m)	Min. $\bar{P}_p$ (kN/m)	Passive Thrust (Terzaghi) (kN/m)	Unbalance Water Force (kN/m)	Resultant Thrust (Proposed) (kN/m)
$\theta = 33.69^0$			b = 65 m		$\bar{c}_2 = 16\,\text{kN/m}^2$		$\bar{\phi}_2 = 16^0$
10	12.42	278.21	33.98	232.67	243.49	57.76	103.3
15	18.83	283.40	50.96	200.49	216.85	86.65	169.56
18	22.36	286.50	59.25	181.11	200.86	103.97	209.36
20	24.84	288.57	65.83	168.15	190.20	115.53	235.95
$\theta = 26.56^0$			b = 85 m		$\bar{c}_2 = 10\,\text{kN/m}^2$		$\bar{\phi}_2 = 15^0$
10	13.19	171.78	29.94	240.34	249.76	50.60	-17.96
15	19.78	177.28	44.91	212.0	226.25	75.90	41.18
18	23.73	180.58	52.20	195.03	212.14	91.075	76.69
20	26.38	182.78	58.00	183.60	202.74	101.20	100.38

Passive earth pressure considering wall friction for $(c-\phi)$ soil can be derived by modifying the Eqs. (16) and (17) as follows:

$$W + \bar{P}_p \sin\delta + (C_F + T)\sin\theta - \bar{N}\cos\theta - F_s\cos\alpha = 0 \tag{20}$$

$$\bar{P}_p \cos\delta - (C_F + T)\cos\theta - \bar{N}\sin\theta + F_s\sin\alpha = 0 \tag{21}$$

where δ is the angle of wall friction.

After solving Eqs. (20) and (21), one can evaluate the value of $\bar{N}$ and $\bar{P}_p$

$$\bar{N} = \frac{(F_s\cos\alpha - W - C_F\sin\theta) + (F_S\sin\alpha - C_F\cos\theta)\tan\delta}{(\tan\bar{\phi}_1\sin\theta - \cos\theta) + (\tan\bar{\phi}_1\cos\theta + \sin\theta)\tan\delta} \tag{22}$$

$$\bar{P}_p = \frac{\bar{N}(\tan\bar{\phi}_1\cos\theta + \sin\theta) + C_F\cos\theta - F_s\sin\alpha}{\cos\delta} \tag{23}$$

For cohesionless soil $(\bar{c}_1 = 0)$, therefore $\bar{N}$ and $\bar{P}_p$ can be calculated by substituting $C_F = 0$ in Eqs. (22) and (23). Passive earth pressure has been determined for illustrative example by

considering wall friction ($\delta = 0^0, 5^0, 10^0$). Angle of internal friction of foundation soil ($\bar{\phi}_1$) is 25^0.

Table 6. Variation of Resultant Thrust with Side Slope, Effective Cohesion and Angle of Internal Friction of Soil

h_L = 20 m h_1 = 18 m h_2 = 0.5 m b_T = 5 m
G = 2.6 e = 0.40 $\gamma_w = 9.81\,kN/m^3$

m_1, m_2	b/d	Maxim. $\bar{P}_a$ (kN/m)	Minim. $\bar{P}_p$ (kN/m)	Angle of Failure Plane $\bar{P}_p$ (Degree)	Unbalance Water Force (kN/m)	Resultant Thrust (Proposed) (kN/m)	Passive Thrust (Terzaghi) (kN/m)
$\bar{c}_1 = 2\,kN/m^2$			$\bar{\phi}_1 = 30^0$	$\bar{c}_2 = 12\,kN/m^2$		$\bar{\phi}_2 = 15^0$	b = 65 m
1.5, 1.5	32.5	228.95	40.15	32	35.56	224.36	47.67
	16.25	493.29	184.35	32	101.09	410.03	203.52
	10.83	758.0	442.82	31	184.49	499.67	479.09
	8.125	1033.8	823.56	31	283.67	493.91	878.83
$\bar{c}_1 = 2\,kN/m^2$			$\bar{\phi}_1 = 30^0$	$\bar{c}_2 = 12\,kN/m^2$		$\bar{\phi}_2 = 15^0$	b = 85 m
	14.17	311.18	466.59	31	161.76	6.01	498.21
	10.63	542.82	858.46	31	248.99	-66.65	906.68
$\bar{c}_1 = 1\,kN/m^2$			$\bar{\phi}_1 = 35^0$	$\bar{c}_2 = 12\,kN/m^2$		$\bar{\phi}_2 = 15^0$	b = 65 m
1.5, 1.5	32.5	219.11	41.09	30	35.56	213.58	50.53
	16.25	453.27	209.32	29	100.15	344.10	235.73
	10.88	679.23	522.78	29	184.49	340.94	568.48
	8.125	911.66	985.40	29	283.67	209.93	1057.5
$\bar{c}_1 = 1\,kN/m^2$			$\bar{\phi}_1 = 25^0$	$\bar{c}_2 = 12\,kN/m^2$		$\bar{\phi}_2 = 15^0$	b = 65 m
1.5, 1.5	32.5	247.49	27.14	35	35.56	255.91	33.29
	16.25	547.13	137.84	34	101.09	510.38	154.80
	10.88	860.17	344.56	34	184.49	700.1	374.21
	8.125	1190.5	650.12	34	283.67	824.03	694.26
$\bar{c}_1 = 1\,kN/m^2$			$\bar{\phi}_1 = 25^0$	$\bar{c}_2 = 20\,kN/m^2$		$\bar{\phi}_2 = 15^0$	b = 85 m
2.0, 2.0	14.17	100.57	364.60	34	161.76	-102.3	390.41

It could be seen that for a cut-off wall of 4 m length, for small angle of wall friction ($\delta < \bar{\phi}_1/3$), the passive earth pressure increases by 9 % whereas for $\delta > \bar{\phi}_1/3$, the passive earth pressure increases by 26 %.

Table 7. Passive Earth Pressure and Seepage Force For Different Angle of Wall Friction

Sl. No.	Angle of Wall Friction (δ) (Degree)	Angle θ with Horizontal (Degree)	Seepage Force (F_s) (kN/m)	Angle α with Vertical – Clockwise (Degree)	Passive earth pressure (P_p) (kN/m)
1	0	34	58.75	5.42	143.59
2	5	31	64.55	5.69	167.06
3	10	28	71.14	5.95	196.51

It is expected that the approach adopted in this paper may also be helpful in the calculation of resultant thrust acting on the retaining wall, cellular coffer dam etc. under seepage flow condition. Obviously, the illustrative example and results presented in Tables 5 and 6 highlight the difference in passive earth thrust obtained by the Terzaghi approach and the proposed approach. These results also reflect the resultant thrust developed on sheet pile cut-off wall and required length of a rigid sheet pile cut-off wall in given conditions to ensure safety of the of the hydraulic structures.

CONCLUSIONS

A detailed methodology for quantifying the forces to be considered in the analysis of a rigid cut-off wall has been presented herein. It has been observed that the influence of exact seepage force on active and passive thrust can be very significant. The levee has been considered as flexible. It has been observed that the influence of seepage force on active and passive thrust can be very significant. The active and passive thrust must be calculated by solving the equilibrium of forces only after superimposing the seepage force on a soil wedge. Similarly, the effect of the seepage force on the failure wedge has been found to be considerable in both cases of active and passive thrust in the example presented herein. In the downstream side the difference in the angle of failure plane as compared to Terzaghi's method is significant. The

proposed study may be very useful in determination of seepage force and its influence on active thrust, passive thrust, and resultant thrust which is required for design of a rigid cut-off wall.

REFERENCES

Cedergren, H. R.(1989) : " *Seepage, Drainage and Flow Nets*", 3rd Edition, John Wiley & Sons, New York , pp 91-106.

Creager, W. P., Justin, J. D. and Hinds, J. (1968) : " *Engineering for Dams* " Wiley Eastern Private Limited, Vol.(I, II & III), New Delhi, 929.

Coulomb, C. A. (1776) : " *Essai sur une Application des Regles des maximis et Minimis a quelques problems de Statique relatifs* 'a l' Architecture, mem. acad. Roy. Pres. Divers savants, Vol. 7, Paris.

EM 1110-2-2504 (1994) : " *Design of Sheet Pile Walls*", U. S. Army Corps' of Engineers Manual.

Harr, M. E. (1962) : " *Ground Water and Seepage* ", McGraw- Hill Book Company, Inc., New York , 315.

Jagla, E. A. (2004) : "The Interpretation of Water Anomalies in Term of Core–Softened Models", Brazilian Journal of Physics, Vol. 34, No. 1, March, p-17.

Jaky, J. (1938) : "*Die klassische Erddrucktheorie mit besonderer Rucksicht auf die Stutzwandbewegung*", Abhandl. Intern. Verein. Bruckenbau u. Hochbau (Trans. Itern. Assoc. Bridge And Structural Engg.), Vol. 5, pp. 187-220.

Karman, Th. V. (9126) : " *Uber Elastische Grenzzustande*", Proc. Second Congre. Applied mechanics, Zurich.

Lambe, T. W. and Whitman, R. V. (1979) : " *Soil Mechanics* ", Wiley Eastern Limited, New Delhi , 553.

Lane, K. S. and Wohlt, P. E. (1961) : "*Performance of Sheet Piling and Blankets for Sealing Missouri River Reservoirs*", Seventh Congress on Large Dams, Rome, Report 65, Question No. 27.

Ohde, J (1938) : "*Zur Theorie des Erddruckes unter besonderer Berucksichtigung der Erddruck Verteilung,* Die Bautechnik, Vol. 16.

Peter, P. (1982) : " *Canal and River Levees*", Developments in Geotechnical Engineering, Vol. 29, Elsevier Scientific Publishing Company, Amsterdam, 540.

Sherard, J. L., R. J., Gizienski, S. F. and Clevenger, W. A. (1963) : " *Earth and Earth-Rock Dams*", John Wiley & Sons, Inc. New York, 725.

Terzaghi, K. (1954) : " *Theoretical Soil Mechanics*" , Seventh Printing, John Wiley & Sons, New York , 48-53, 100-108, 257-264.

CONSTRUCTION OF UNDERGROUND WALLS IN URAYASU TO MITIGATE LIQUEFACTION DAMAGE AND IN FUKUSHIMA NO. 1 NUCLEAR POWER PLANT TO STOP RADIOACTIVE LEAKAGE

Ikuo Towhata
President of Japanese Geotechnical Society

ABSTRACT

This paper addresses the author's recent two activities on the use of underground walls that are intended to mitigate or prevent disasters related to earthquakes. Both are new challenges of the use of underground walls and are also characterized by their big scales.
Keywords: soil-cement mixing, freezing, underground wall, liquefaction, nuclear plant accident

INTRODUCTION

In the traditional geotechnical engineering, wall has mostly been regarded as a retaining structure that is constructed to support lateral earth pressure. Although this function will not change in future, the expected roll of a wall is increasing. In the present paper, the author addresses two walls that are used for different purposes.

UNDERGROUND WALL FOR MITIGATION OF LIQUEFACTION

The 2011 Tohoku gigantic earthquake (M=9) in Japan gave engineers many lessons. Among them was the finding that mitigation technology for liquefaction was not sufficient for inexpensive structures such as private house foundation, river levee and embedded lifelines despite that liquefaction mitigation technologies for important structures had been well developed since late 1960s. The different situations for inexpensive and important structures came from budgets available for installation of mitigation. Fig. 1 shows a house that tilted and subsided due to subsoil liquefaction. Because even minor distortion makes it very difficult for residents to continue living therein, a substantial amount of expenses was necessary for restoration. Such a damage occurred to tens of thousands of houses during this earthquake and the national government decided to initiate public-private joint projects in which public roads and private residential lands are reinforced together against future liquefaction. Noteworthy is that the earthquake damage of a private house should in principle be repaired by the house owner's money. This principle was changed because the induced damage was so vast. As shown in Fig. 2, the liquefaction in a private land easily affects the public road. Hence, the restoration of liquefied house foundation was decided to be partially paid by the public fund, which is the government.

Fig.1 Liquefaction-induced tilting of house

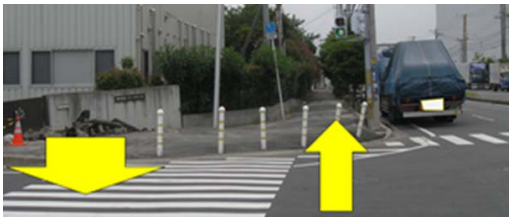

Fig. 2 Subsidence in liquefied private land that induced uplift deformation in public road

Because the public-private joint project is in essence a public project, it is executed on a town block basis in which tens of houses are situated and the living families have to unanimously agree on the project. The most difficult task in such a project is that subsoil has to be improved while houses still exist at the ground surface. Consequently, two existing technologies were considered promising; pumping of ground water and construction of square grid walls around house foundation. When liquefiable subsoil is underlain by a thick deposit of soft clay, ground water pumping is likely to trigger consolidation settlement. Hence, the underground square grid wall became the final candidate technology. The conceptual illustration of this wall is shown in Fig. 3 where existing houses are surrounded by walls. These walls in conjunction with the surface dry and unliquefiable soil crust reduce cyclic shear deformation during earthquakes and consequently prevent the onset of liquefaction. Fig. 4 shows a newly developed small machine for soil-cement mixing that can operate in a very narrow space between two existing houses. This device is able to construct a rigid soil-cement mass of an oval cross section. By connecting such a mass, a continuous underground wall can be constructed (Fig. 5).

The estimated construction cost is about US 50,000 $ per one house in which 50% will be paid by the national government, about 8,000 $ is supported by a local government and the remaining amount should be paid by the house owner. The house owners are requested to make their final decision whether or not to join this project. A unanimous agreement to join the project is required to carry out this public-private project.

Fig. 3 Schematic illustration of underground square grid wall

Fig. 4 Small cement-mixing machine

Fig. 5 Excavated trial underground wall

UNDERGROUND WALL TO PREVENT LEAKAGE OF RADIOACTIVE LIQUID FROM DAMAGED REACTORS OF A NUCLEAR POWER PLANT

The Fukushima No. 1 nuclear plant (abbreviated as F1) was severely damaged by tsunami after the 2011 gigantic earthquake. Because all electric power supply was lost, reactors were not able to be cooled down anymore, nuclear fuel melt and a fatal damage was induced. One of the problems after this accident was leakage of radioactive water from damaged reactors. To prevent this leakage, it has been attempted to lower the ground water level in and around the reactor buildings by surrounding the buildings by walls of frozen soil.

Although in-situ soil freezing had been carried out for many aspects of underground construction (stabilization), all of them were for short-term purposes. In contrast, soil freezing in F1 was intended to last for 7 years and the durability of freezing system was concerned. It is said that more popular slurry wall was not employed because the required permeability was too low for clay to achieve. Fig. 6 indicates the installed pipes and other devices for ground freezing. As per December 5, 2015, the freezing system has not been completed but trial freezing is going on. Ground temperature is monitored to verify that soil is getting frozen. However, water tightness is not verified yet.

Fig. 6 Pipes for ground freezing around nuclear reactor building

Fig. 7 Idea of multiple barriers to prevent leakage of radioactive water (proposed by JGS to IRID)

The Japanese Geotechnical Society (JGS) established a special committee to discuss the geotechnical aspects of the treatment of F1. It is believed that there are many uncertainties underground and, for example, soil freezing may not be so easy as intended. To cope with unexpected situations, the committee proposed to construct more walls around the damaged reactors (Fig. 7). It is believed that geotechnical engineering can play further roles for safe solution of the F1 problem by using the following ideas;

(1) Removal process of molten radioactive fuel is similar to rock coring of ground investigation.
(2) Soil-water mixture is more capable of radioactive shielding than air.
(3) Underground repository seems to be the only possible solution of the radioactive wastes.

CONCLUSION

Underground walls are going to play important roles in mitigation of two seismic damages that were caused by the 2011 gigantic earthquake. One is mitigation of liquefaction damage to houses and walls will be constructed around foundation of existing houses. New construction machines were developed for this purpose. The other is the installation of frozen soil walls around the damaged Fukushima No. 1 Nuclear Power Plant in order to prevent the leakage of radioactive waste water. Because the intended perfect prevention is water-tightness, it is proposed to construct multiple barriers for more reliability.

ACKNOWLEDGMENT

The author expresses his sincere gratitude to the Urayasu City Government, Takenaka Corporation, Maeda Corporation and Prof. H. Komine of Waseda University for their assistance and contribution for the present studies.

Use of piles in complex reconstruction of cities

V.M. Ulitsky
State Transport University, Saint Petersburg, Russia

A.G. Shashkin, M.B. Lisyuk
Georeconstruction Engineering Co, Saint Petersburg, Russia

ABSTRACT: The paper presents examples of use of piles for reconstruction of historical monuments in St. Petersburg. Two important historical monuments are considered - Konstantinovsky Palace and Kamennoostrovsky theatre.

INTRODUCTION

In reconstruction of historical cities piles and pile foundations are used very extensively. We could categorize the use of pile foundations during reconstruction for the following purposes:

1. Strengthening of subsoil and foundation of existing buildings (underpinning of historical buildings using piles).
2. Extension of the existing buildings and structures.
3. Construction of protection walls of underground structures.
4. Reducing pressures on the existing collectors and communications.

One of the brightest examples of the pile foundation application in the 19-th century is the largest cathedral in St. Petersburg – St. Isaac's Cathedral, which is in fact the heaviest building in the city and the largest East Orthodox temple in the world (Fig. 1).

It was constructed in place of the cathedral designed by architect Rinaldi in 1768. August Montferrand, the creator of the new edifice, left foundations of the altar parts and dome pillars of the old building, which were based on 13.000 piles of 10.5 m under the pillars and 8.4 m under the walls. To make a new foundation 5 meter reduced excavation had been provided and from the bottom thereof 24,000 26 cm thick piles were driven being and 8.4 m long under the pillars and 6,3 m under the walls (Dashko, Alexandrova, 2003). In between the piles at the level of 35 cm quarry stone rubble was compacted into subsoil and topped with lime-sand mix.

Underlying the bearing structures and the corners the foundation contains granite slabs. Underneath the porticoes layers of quarry stone masonry courses alternated with those of granite slabs, and throughout the rest of the building with those of limestone. Masonry walls elevated by 2.0 m above the ground level forming a massive 7.5 m thick raft within which galleries were furnished. Expert opinion has it that the maximum pressure on subsoil therein totals 0,32 MPa. Immediately under the slab pilecap there are saturated silty sands and loams with piles having their toes embedded in flowing loamy strata. Currently the

overall settlement of the building by various assessments has reached 0.8...1.0 m with the highest settlement values registered in the heaviest dome section of the cathedral.

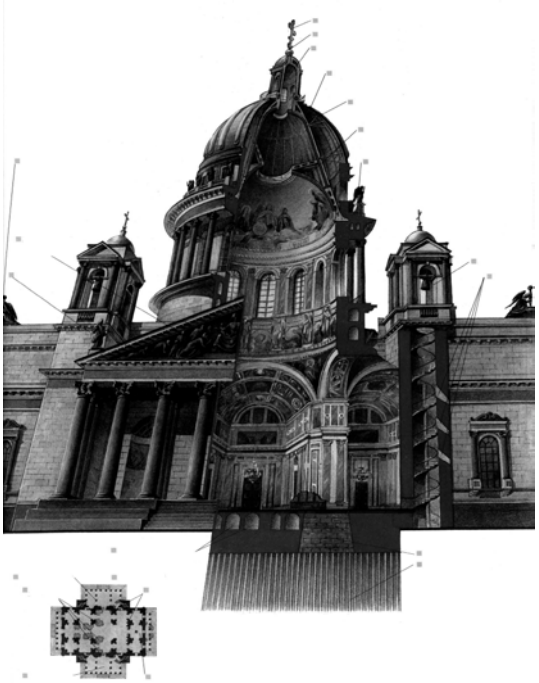

Figure 1. St. Isaac's Cathedral.

In this case the relatively short piles serve as an additional reinforcement of the subsoil. Considering massive (up to 8 m) pile raft and relatively short piles, according to modern assumptions this structure is built on pile-raft foundation. Undoubtedly, uneven loading locally generates excessive strain in the ground. State-of-the-art diagnostic methods and numerical modeling techniques applied to such a complicated structure highlight most critical locations suitable for subsequent strengthening.

Examples of using piles during reconstruction of two important historical monuments in St. Petersburg are given below.

1 USE OF PILES DURING RECONSTRUCTION OF KONSTANTINOVSKY PALACE IN STRELNA

1.1 *Historical background*

Strelna Palace, more widely known as Konstantinovsky Palace, is a large palace located in the nearest suburb of St. Petersburg on the shore of the Gulf of Finland (Fig. 2). Peter the Great was fond of that location where he resolved to construct masonry chambers. Imperial residences in the suburbs of St. Petersburg would commonly begin as modest buildings and at a later date be expanded and reconstructed, graduating to more luxurious and pretentious edifices. Strelna Palace, however, had from its inception been conceived as a stately and imposing structure. It involved leading European and Russian architects of the time, such as Jean Batiste Leblon, Nicolo Micetti, and Francesco-Bartolomeo Rastrelli.

Figure 2. A photograph of Constantinovsky Palace taken in 1910.

This palace was situated on the top of the 8-m high slope of the historical Baltic coast. The slope was reinforced with a retaining structure fashioned into a series of loggias (half-sphere niches with the open space towards the park).

Subsequently, the great Russian reformer lost interest in Strelna and shifted his attention to the town of Peterhof as the place for establishing the official suburban residence town. Therefore the palace, having been constructed up to the roof level, remained uncompleted. It was only following the accession of Empress Catherine that Rastrelli was commissioned to complete its construction. However, the court never moved into the new residence. The luxurious palace was again forgotten for 50 years and, as the case usually is with abandoned buildings, it was decaying quickly due to lack of maintenance and heating.

In 1802, the new owner, Emperor Paul presented the palace to his son Constantine, whereupon it became known as Konstantinovsky Palace. Refinishing of the palace was completed in 1 year. It was designed and supervised by A. Voronikhin. The sumptuous abode of the Grand Duke stood open to welcome its new owner. Fate, however, had no remorse as an enormous fire broke out on December 28, 1803, destroying the entire artistic decorum of the hapless building. Everything was to be renovated by architect L. Ruska. Architect A. Voronikhin designed a series of grottoes. The roof of the grottoes served as a spacious terraced square facing the palace. The structure of the terrace at the same time functioned as a retainer for the palace, conditioning stability of the entire palatial complex.

1.2 *Palace condition survey and site investigation*

Strelna Palace is a 3-story building on a high basement floor (socle floor). It was constructed on linear rubblework foundations on the crest of a natural slope which descends into Lower Park by three tiers. The natural slope in front of the palace was fashioned into a horizontal area 23 m wide in the middle and 17.3 m wide on the edges. The absolute level of the terrace surface is at 12.7 m Baltic Datum (BD) (Fig. 3, 4). The vertical terrace ramp (8.0 m high) is retained by a complex system of masonry structures forming grottoes and lateral loggias on the front elevation (Fig. 3), as well as the suite of wine cellars between the grottoes and the palace. The grotto is divided throughout its length into 9 equal bays, each approximately 4.75 m in length.

Symmetrically on each part of the central grotto there are 3 loggias. The gable wall for both the grottoes and the loggias is the actual retaining wall. The loggias retaining wall contains half-sphere niches forming the volume of every loggia. In these locations the retaining wall is especially thin (around 1.5 m), but gradually increases up to 3.2 m elsewhere.

The retaining structure of Konstantinovsky Palace serves not only as a podium for the palace on the Lower Park side, forming a spacious terrace in front of its north elevation, but also as a structure ensuring the building's stability on the brink of an 8-m slope at the historical coast of the Baltic Sea. Stability of the entire palace depends on the technical condition of its retaining structures.

Figure 3. A photograph of Constantinovsky Palace taken in 2000 before reconstruction.

The authors were commissioned by Governmental Monument Preservation Committee to provide a pertinent condition survey of this monument or, more precisely, of the structure's areas of critical dilapidation (Fig. 3, 4). The surveyors saw an abandoned palace gracing a high slope, strengthened by a retaining structure fashioned into a series of grottoes and loggias. The principal bearing wall, withholding the ground on the slope and the palace on top of it, was considerably damaged in a number of locations. Water had found its way inside, penetrating through fall-outs over piles of brick rubble. Later, as cold weather set in, the water was transformed into ice. Ice stalactites hung on the precipitation.

The structural layout and condition of all foundations, were studied and described. To accomplish this, 28 trial pits were excavated, 35 boreholes were drilled through foundation masonry courses, 2 large trenches were excavated on-site, the rigidity characteristics of brickwork were established, moisture conditions of the walls were studied, and the length of timber piles underneath rubblework foundations were defined.

Figure 4. Dilapidated grottoes of the palace.

As attested by site investigation in the park, underneath 1 m of fill there is a 3-m layer of soft varved clay loam, underlain by medium stiff moraine clay loam (Fig. 5). At the level of around 14.0 m (absolute – 1.3 m), there are medium stiff and stiff deep Cambrian clays.

The slope incorporating the terrace is compounded by lacustrine-glacial clayey sands followed by silty lacustrine-glacial loams. Straight upon the terrace there is a stratum of man-made ground of sand with admixtures of lime cement, above which there is 2 m of brickwork (in the section between the palace and the cellars) serving as a base for the terrace. Above the clayey sand there is a layer of man-made ground about 3 m thick.

Hydro-geological conditions are characterized by the presence of groundwater associated with man-made strata and silty sand inclusions in lacustrine-glacial clay loams which together with clayey sands act as a confining bed. Groundwater is discharged into the Lower Park canal. The groundwater table generally follows surface geometry.

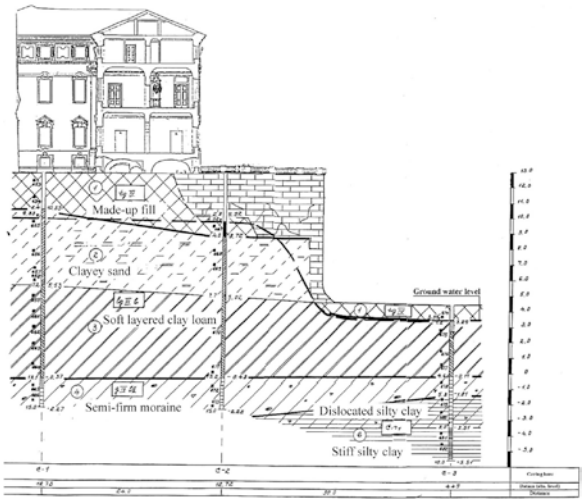

Figure 5. Cross-section of the palace and subsoil profile: 1. Made-up fill, 2. Clayey sand, 3. Soft varved clay loam, 4. Medium-stiff moraine clay loam, 5. Dislocated stiff Cambrian silty clay, 6. Stiff silty Cambrian clay.

1.3 *Condition survey results*

The condition survey results were as follows (see Fig.4-7):

1. Foundations of the dilapidated retaining walls were constructed of bricks. The foundations were no longer capable of being classified as a structure. There was imminent danger of crushed brickwork movement with formation of local bulges.

2. The entire brickwork structure was soaked in water, causing dilapidation through cycles of freezing and thawing.

3. There were no foundations of the transverse walls of the cellars. Footing was level with the cellar's floor. Decomposed timber pile heads supported the transverse walls.

4. Dilapidated terrace gutters had caused weakening of some retaining wall sections adjacent to niches of the loggias and grottoes.

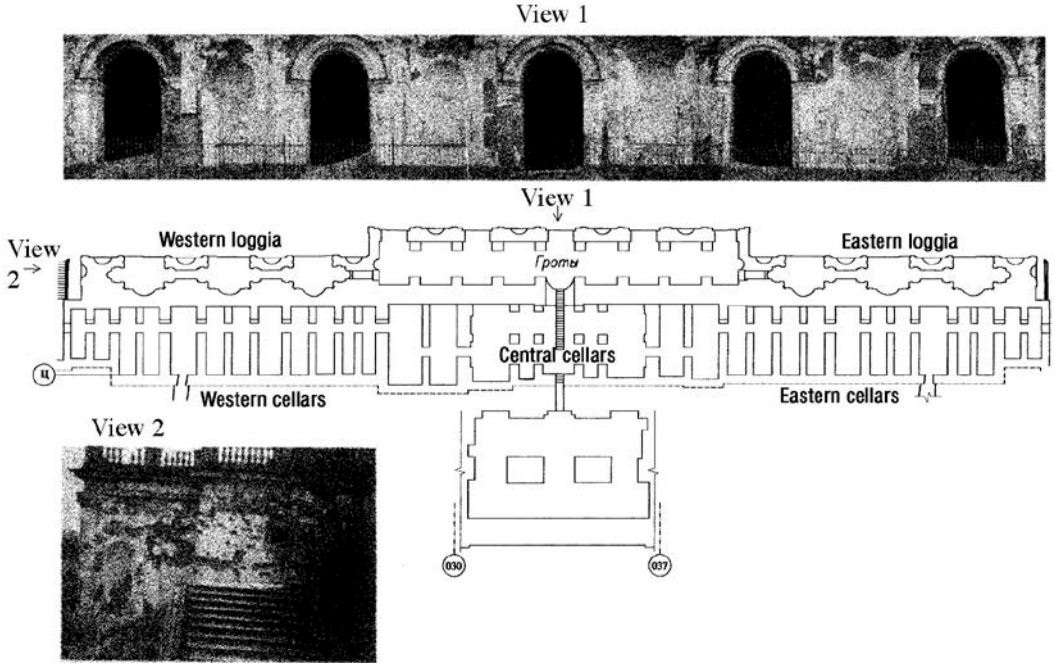

Figure 6. Dilapidated cellars, grottoes, and loggias of Konstantinovsky Palace.

5. The precipitation sewer consisted of three straight courses underneath the retaining structures, designed to divert precipitation and ground water from the

palace. There was water flow through the ground underneath the cellar walls, and through dilapidated retaining wall sections.

6. Most structural damage (fallouts) was associated with the destroyed drainage sections underlying the retaining structures.

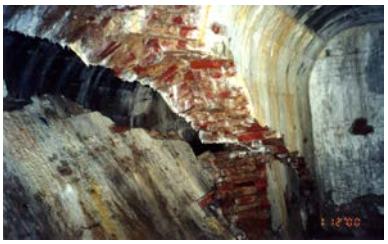

Figure 7. Collapsing cellar wall behind east loggias.

1.4 *Design project of palace reconstruction*

The Palace condition demanded immediate rendering of complex strengthening works.

The design project envisaged pressure grouting and strengthening of brickwork, with underpinning of all retaining structures with piles embedded into stiff stratum (Fig. 8, 9).

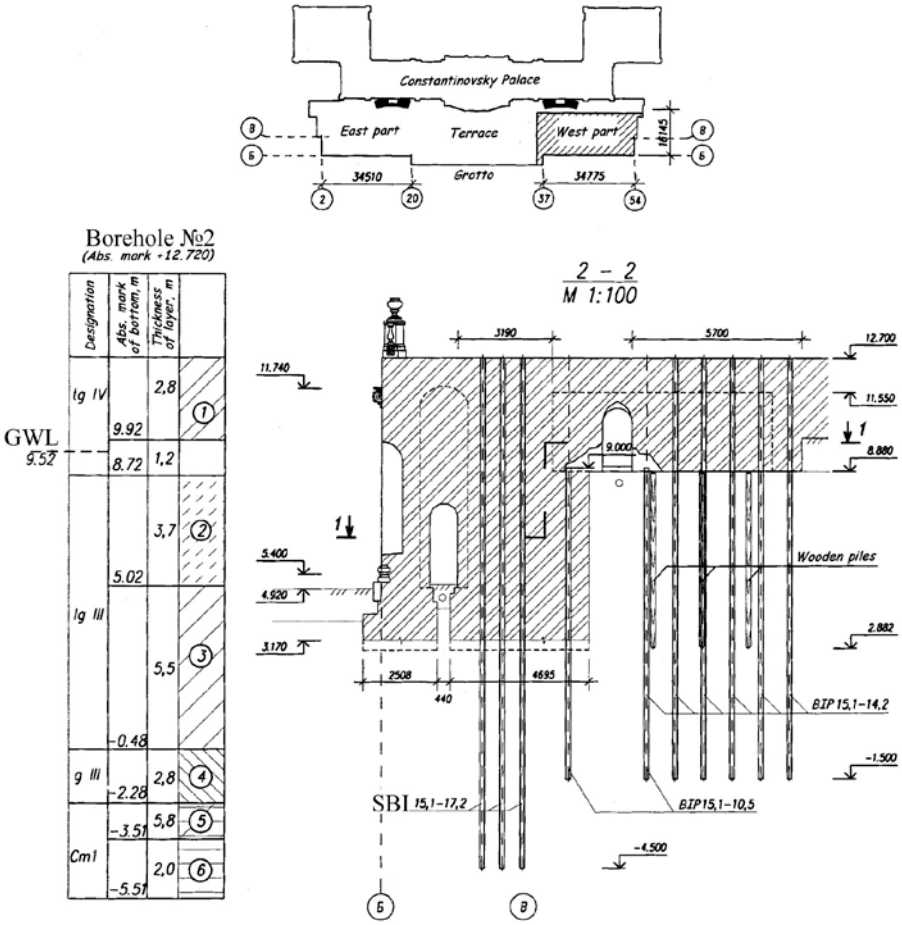

Figure 8. Underpinning of the retaining structure.
See Fig. 5 for soil stratification.

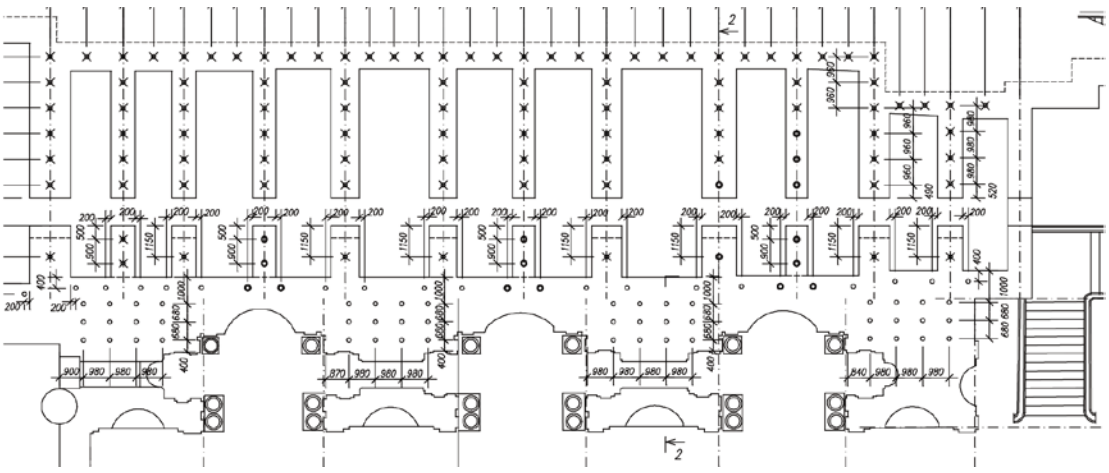

Figure 9. Location of underpinning piles in plan.

Grouting of the brickwork was necessary in order to restore its strength and stiffness. Strengthening was required to properly allow the transfer of loads from the entire structure. Finally, underpinning piles had to be constructed in order to transfer the structure loads onto the incompressible subsoil stratum. It needs to be noted that conventional underpinning piles installed at an angle from the level of the lower terrace (around 4.0 m Baltic Datum) would prove ineffective as the dilapidated foundation brickwork was incapable of accommodating the heads of the underpinning piles, and the retaining wall itself being practically unavailable for underpinning.

Based on the above, the foundations underpinning of the retaining structures was carried out in the following sequence.

Stage One

1. Strengthening of the critically dilapidated structures (3 left and 3 right loggias).

2. Provision of temporary propping scaffolding in cellar chambers installed on wedges in the cellar floors. Wedging of the scaffolding was regularly inspected. The unsupported spans in locations of the brickwork fallouts were propped.

3. Drilling of 42 mm vertical bores above the partitions of the retaining wall from the terrace in front of the palace down to the brick-wall footing level. Subsequently, the brickwork was grouted by intervals with packing lime mortar until completely permeated.

4. Redrilling of the bores by 151-mm core bores down to the top of the firm Cambrian stratum following 70% setting of the mortar. Drilling below foundation footing was either carried out using thixotropic grout or was casing protected. Cement grout with added plasticizing and shrink-proofing agents was pumped into the subsoil and brickwork at 0.2 and 0.1 MPa respectively, followed by a stain-proof reinforcement casing tube being oscillated into the grout mix. The resulting pile was embedded into the Cambrian stratum reinforcing and underpinning the retaining brickwork section. The tube was required to ensure both longer pile life and subsequent possible of deepening of the cellars.

5. Drilling of 42 mm vertical bores paced at approximately 1.0 m from the terrace in front of the palace along each transverse wall down to the brick-wall footing level (absolute level 8.9 m Baltic Datum) in order to reinforce the transverse walls and rear longitudinal wall of the cellars. This was followed by interval grouting and subsequent redrilling of the bores by 151-mm augers, used in the bored piles construction, down to absolute level of 1.5 m Baltic Datum. Those piles were reinforced through their entire length.

6. Construction of pile heads in the dilapidated areas of the transverse walls at the level of the brickwork footing (absolute level 8.8 m Baltic Datum), with subsequent construction of the pile caps and masonry courses within the original scope.

Stage Two

1. Completion of the retaining structure strengthening works.

2. Provision of works described in Stage 1 above for unreinforced sections of the walls.

3. Removal of terrace surface material and construction of a reinforced concrete wall connecting pile heads above the brick vaults.

Stage Three

Provision of the terrace surfacing incorporating drainage and snow melting systems, finished by tiling.

The provided strengthening should serve to ensure the reliability and long life of the retaining structures, preserving their appearance and historic materials almost completely unscathed by any patchwork or replacement of brickwork. Such approach proved most appropriate in relation to the significant architectural monument.

The constructed strengthening option was successful even when faced with an unexpected challenge. The architects suddenly decided to provide front access to the palace from the Lower Park and furnish a vestibule underneath the terrace. To do this, all cellars had to be deepened by 1.0-1.5 m and the transverse brick walls were temporarily suspended on the thin underpinning piles (Fig. 10, 11). Quality of the strengthening was attested by the fact that not one section of the brickwork was in any way displaced. It was therefore ascertained that the strengthening was successful.

Figure 10. Deepening of the basements by 1.0-1.5 m.

Figure 11. Bored pile with tube reinforcement viewed from underneath foundation.

It took about 1.5 years to completely reconstruct Konstantinovsky Palace in Strelna). The palace officially opened as the Congress Palace in 2003 during the tercentenary celebrations of Saint Petersburg (Fig. 12-13).

Figure 12. Cellars of Konstantinovsky Palace, 2004 (at the location of reconstructed retaining cellar wall, see Fig. 10).

Figure 13. Konstantinovsky Palace, south façade. View after a final reconstruction stage (July 2003).

2 USE OF PILES DURING RECONSTRUCTION OF KAMENNOOSTROVSKY THEATRE

2.1 *Historical background*

Kamennoostrovsky (Stone Island) Timber Theatre was constructed in 1828, designed by architect S. Shustov to provide a temporary floor for the Imperial Opera and Ballet Troupe whilst reconstruction of the Large Masonry Theatre was ongoing. The critics noted rare elegance of the structure and it was due to that elegance that following a decade and a half a decision was taken to preserve it by means of adding rubblework foundations (prior to that the lowest courses of the building rested directly on timber piles). The architect Alberto Cavos believed he had managed to prolong the building's life by about 50 years. However the building was able to withstand the passage of time for as long as 180 years. Until the 1930s the Stone Island Theatre was used as a warehouse, when it was renovated and converted into a television theatre and later to a dance studio. The Stone Island Theatre being a world heritage site protected by the UNESCO (Fig. 14).

Figure 14. Kamennoostrovsky Theatre during reconstruction.

2.2 *Development of plan to renovate the theatre*

The Stone Island Theatre was revived in 2006 when the Russian President decreed for it to serve as Second House of Tovstonogov Academic Drama Theatre to commemorate the 80th anniversary of a famous Russian actor Cyril Lavrov.

Over the two centuries, however, thespian field has developed more sophisticated requirements regarding comforts of the audience. Indeed, these days there are codes and standards envisaging roomy foyers and cafes, convenient wardrobes and lavatories. A contemporary theatre is like an iceberg, and its bigger part is not visible to the audience. That invisible space houses stagecraft facilities – upper and lower stage mechanics (e.g. stage terracing, orchestra pit, lighting arrangements, backdrop hoists, etc).

The General Designer was given a highly complicated task featuring what at the time seemed as two mutually exclusive requirements – to convert an old timber building into a contemporary theatre with all the necessary technical sophistication without altering the original historic appearance in any way. The only way to make it happen was to locate all new addenda and enhancements required by a modern state-of-the-art theatre underground, immediately underneath the historic superstructure.

The geotechnical challenge at the Stone Island Theatre was serious due to a high ground water level. The absolute levels at Stone Island are rather low and the area is subject to flooding. Additionally, the subsoil is compounded largely by soft clay. To make matters worse there is a listed building in the vicinity – the Summer Mansion of Baron Kleinmichel.

The area of the theatre's location was levelled with made up ground, the absolute levels being in the order of 1.93…2.27 m BS (Baltic Datum). Made up ground is 0.8…4.5 m thick. Underlain by lacustrine and marine deposits, it is compounded by silty sand, medium grained sand, light silty loams, and silty sand clay. The underside of this stratum is at 5.5…11.0 m. Underneath down to 10.8…17.0 m the site is compounded by lacustrine and glacial deposits of the Baltic Glacial Lake – silty loams with consistency ranging from liquid to liquid-plastic. Directly underneath there are glacial deposits of the Luga Moraine, compounded by silty sand-clay and loams with gravel and pebbles, as well as boulders which are encountered down to the level of 21.0…26.5 m. Underlying the latter lacustrine and glacial deposits are identified – varved silty loams, stiff-plastic and liquid-plastic in consistency. Quaternary deposits extend down to 24.2…30.3 m, corresponding to absolute levels of -22.27… -28.27 m BS, and are underlain by Wendian stratum, being light firm silty clay.

The area has an aquifer located around the boundary of quaternary deposits. Site investigation in October and November 2007 identified ground water at 1.3…1.8 m from the surface, corresponding to the absolute levels of 0.75…0.30 m BS.

Reconstruction implies provision of underground facilities under the entire footprint of the building and extending beyond its perimeter by 6.8 to 25 m (the size of the underground space is 80×40 m). The relative level of the underground structure is at minus 6 m. In order to construct the underground area, excavation was necessary down to relative level –6.7 m. Therefore, an excavation

down to 5.6 m from the surface was necessary to accommodate the underground structure.

3 STAGES OF THE THEATHRE RECONSTRUCTION

The sequence of works adopted for the project is shown in Figures 15-20. The works can be subdivided into 5 stages:

1 Drilling holes in existing walls to accommodate transverse beams of the unit responsible for temporary walls-to-piles loads redistribution.

2 Construction of bored piles, introduction of the transverse steel beams, preparation of rebar cages and concreting for reinforced concrete waling beams to facilitate load transfer. (Fig. 15). Simultaneous construction of the sheet pile cofferdam. Bored piles were of 2-step construction “Titan” type: initiated with oscillation of the casing down to the level of the underground structure subsequently followed with pile construction as such. The casing was necessary to improve bending strength of the top half of the pile, which was needed during excavation for the underground structure.

3 Application of jacking devices on the transverse beams, tightening retaining nuts on bars of the underpinning bored piles thereby engaging the piles to assume loads. Following this the lower sections of the building’s rubblework foundations could be removed (Fig. 16). Following removal of the lower parts of the rubblework foundations a slab is to be cast directly underneath, forming a rigid disc at the level of the foundations (Fig. 17). Stiffness strips are cast under the existing foundations to redistribute loads onto the slab. Bored piles also are embedded into the rigid disk slab. Following this step, the units described in 2 above are no longer required as the loads from the walls of the building are now transferred directly onto piles through the medium of the rigid disk.

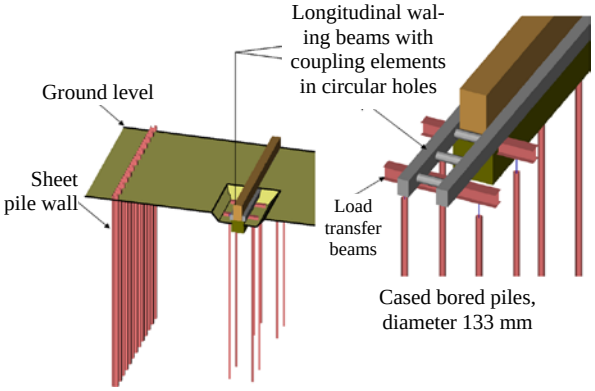

Figure 15. Construction of sheet piles, bored piles, and the unit transferring the load from the walls to the piles.

Figure 16. All loads have been redistributed. Old foundations removed.

4 Excavation of the pit for the underground structure down to the designed level. To provide for stability of the sheet pile cofferdam a waling beam and a shoring system are provided; those are to be supported by the rigid disk and mounted on special

embedded elements in the slab (Fig. 18). Following excavation of the perimeter strips light-duty machinery is introduced into the pit and excavation begins directly underneath the theatre building. As the soil is excavated the piles are propped by struts to form through-section columns and enhance stability.

Figure 17. Construction of the top slab.

5 Construction of bottom slab for the underground structure. Forming embedment slots for the bored piles in the bottom slab. Concreting for the exterior walls, interior walls and columns of the underground structure (Fig. 19). After concreting for the exterior wall of the underground structure and construction of the intermediate slabs at the perimeter sections the spaces between the sheet piles and the underground structure are backfilled. Following completion of the underground structure and backfilling the struts are taken down (Fig. 20). As soon as supports are introduced under the rigid disk slab, temporary through-section columns of bored piles are dismantled at which point the loads come to be transferred through the bottom slab.

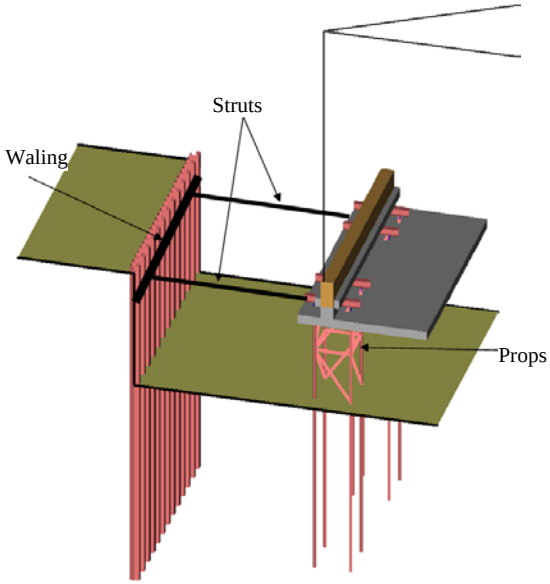

Figure 18. Excavation down to design level with struts.

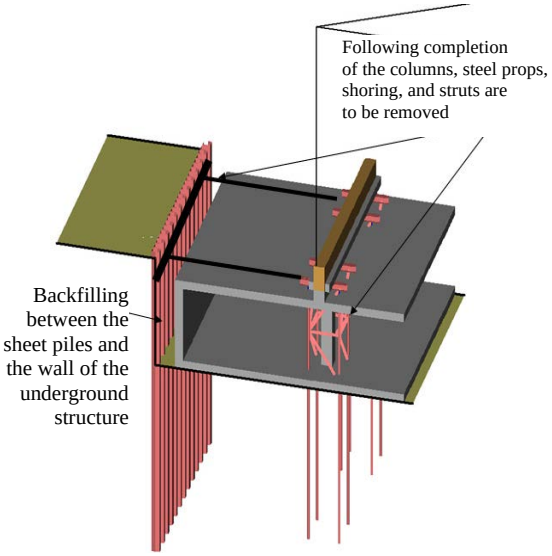

Figure 19. Concreting for the walls and columns of the underground structure.

Figure 20. Constructing the underground structure.

4 MONITORING OF THE THEATRE

Monitoring in situ allowed to assess workability of the suggested design methodology as well as efficiency of the entire concept of geotechnical supervision.

It is worthy of notice that owing to geotechnical monitoring which was ongoing throughout the entire period of construction works the project team managed to rule out any influence of exceeding the permissible level of vibration acceleration (0.15 m/s^2). Cofferdam had been constructed with a very high quality and made it possible to keep the ground water at its natural level. Maximum settlement of the theatre building reached 24 mm, whereat no dangerous differential was ever registered (Fig. 21). Following redistribution of loads from the building onto the piles settlements became fully manageable as it had been made possible to adjust the entire building by means of retaining nuts on bars of the underpinning bored piles. Owing to a high culture of works implementation and a reliable design this was never implemented.

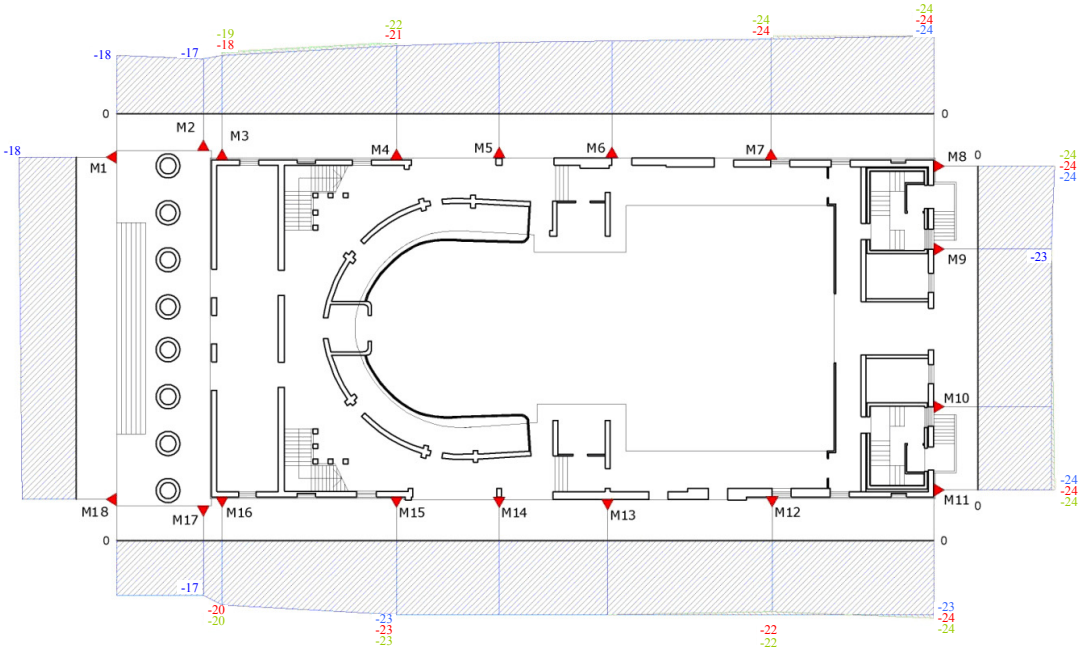

Figure 21. Settlements of Stone Island Theatre (mm).

Horizontal displacement of the sheet piles reached 25…30 mm, and settlement of Kleinmichel's Summer Mansion were never in excess of 9 mm (Fig. 22). It is interesting to point out that the biggest danger to the Dacha was not the nearby excavation for the theatre project but seasonal fluctuations of the foundations related to frost heave in winter followed by spring thaw.

Therefore design, of the underground structure based on two groups of limit states for the existing buildings ensured not only safety of historic structures, but also safety of their interiors, whereas geotechnical monitoring ensured safety of soil in terms of remoulding during all types of construction works.

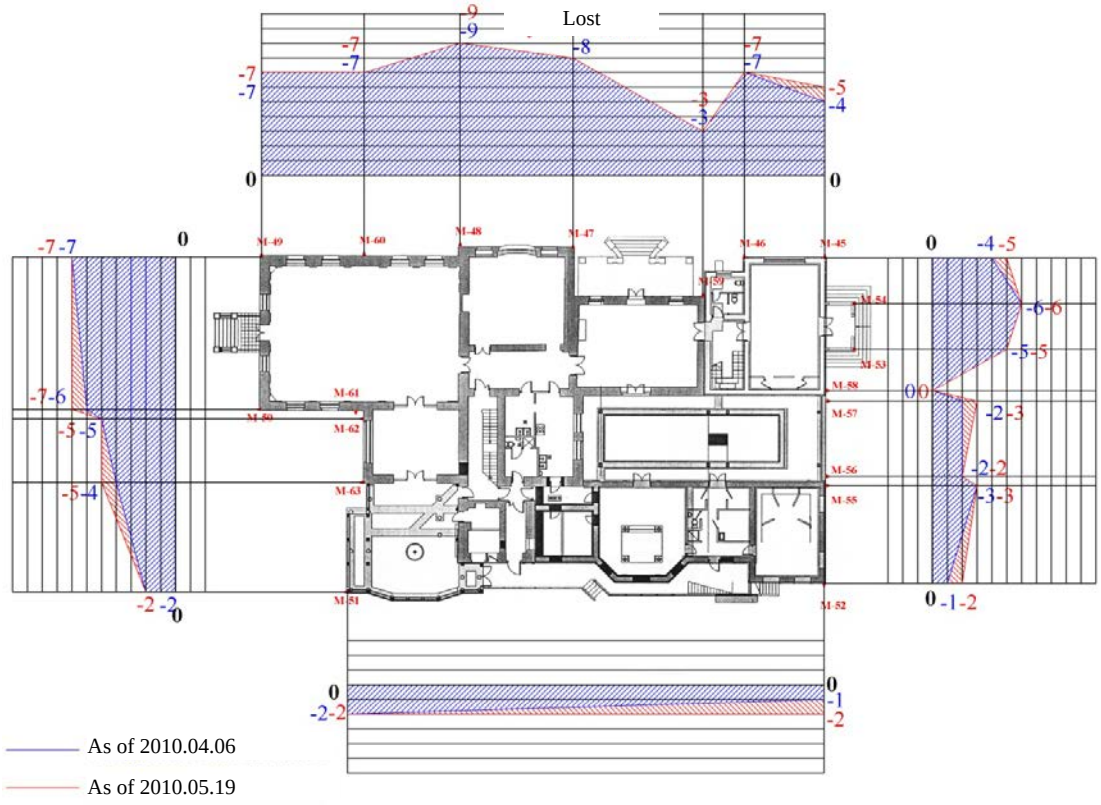

Figure 22. Settlement of Kleinmichel's Summer Mansion (mm).

REFERENCES

Dashko R.E., Alexandrova O.Y. 2003. Causes for deformations of St. Isaac's Cathedral: technical, geological and environmental analyses. // *Recontruction of cities and geotechnical engineering*. ASV Publishers, Saint Petersburg. Volume 5. pp. 57-65.

Ulitsky, V.M, Shashkin, A.G., Shashkin, K.G. 2010. Main regularities of soft clays soil behavior during deep excavations. *Proc. of International Geotechnical Conference 'Geotechnical Challenges in Megacities'*. Moscow, Volume 1, 2010 (in Russian).

Shashkin, A.G., Shashkin, K.G. 2005. Elasto-viscoplastic model of structurally unstable soils. 2005. *Reconstruction of Cities and Geotechnical Engineering*. Saint Petersburg, Volume 9, pp. 221–228 (in Russian).

Evolved earth pressure during excavation against a combined sheet pile wall enhanced by H sections: Centrifuge test

Shi Zheng[1,2], Fang Liu[1,2], Mingjing Jiang[1,2], Haoyu Sun[1,2], Yutai Liu[2]
[1]State Key Laboratory of Disaster Reduction in Civil Engineering, Tongji University, Shanghai, China
[2] Department of Geotechnical Engineering, Tongji University, Shanghai, China

Hiroaki Nakayama[3], Shinji Taenaka[3] & Atsushi Kato[3]
[3] Nippon Steel & Sumitomo Metal Corporation, Japan

Abstract: This paper presents a centrifuge test of a combined wall composed of Hat-type piles and enhancing elements of H sections. The earth pressure against different parts of the wall during excavation was quantitatively revealed under controlled conditions. The results demonstrate remarkable variation of the earth pressure against different parts of the wall at the same elevation due to varied bending stiffness of the wall along the length of the wall. The primary piles act as the primary retaining elements. The fraction of earth pressure retained by the secondary piles decreases with the decreasing depth, and increasing distance from the primary piles.
Keywords: Combined sheet pile wall, earth pressure, centrifuge test

1. INTRODUCTION

Combined sheet pile walls provide economic solution for fast construction and reduction of steel amount, and therefore have been widely used in coastal areas as temporary or permanent retaining systems. They are often constructed by interlocking a series of sheet piles, some of which are enhanced by H sections or by steel tubular piles to achieve high bending stiffness. Figure 1 illustrates a configuration of a combined wall evaluated by Nakayama et al. (2013) in a full-scale field test. This wall was formed by alternating a Hat-type sheet pile (i.e., the secondary pile with less bending stiffness) and an enhanced Hat-type sheet pile welded with an H section (i.e., the primary pile with higher bending stiffness). As reported by Nakayama et al. (2013), the combined wall received different earth pressures behind the primary and secondary piles due to corrugated surface of the wall and various bending stiffness along the length of the wall. Although the effect of corrugated surface of a rigid wall on distribution of earth pressures was experimentally (Tong et al., 2014) and numerically studied (Liu et al., 2012; 2013), but the combined effect of corrugated surface and varied stiffness remains unclear.

As suggested in Eurocode 3 (2007), the primary piles in a combined wall act as retaining elements against the earth pressure while the secondary piles only fill the gap between the primary piles and transmit the loads resulting from earth pressures to the primary piles. This indicates that the secondary piles only resist a small portion of earth pressure. However, distribution of earth pressure on different parts of a combined wall remains quantitatively unclear.

This paper presents a centrifuge test of a combined wall, of which the prototype is illustrated in Figure 1. This study is intended to reveal the earth pressure against different parts of a typical combined wall during excavation, and to quantify the contribution of primary and secondary piles of the wall.

2. CENTRIFUGE MODELING

2.1. Testing apparatus

The centrifuge test was carried out at the Department of Geotechnical Engineering of Tongji University. Figure 2(a) shows the TLJ-150 geotechnical centrifuge with an effective radius of 3 m and a maximum capacity of 150 g-ton. The equipment can provide a maximum acceleration of 200 g, and can deal with a maximum load of 2 tons. Figure 2(b) shows the model box used in the test. The interior space of box is 600 mm long, 400 mm wide, and 500 mm deep.

2.2. Model set-up

Figure 3 illustrates the set-up for modeling a combined wall of a total height of 400 mm in the model (i.e., 14.4 m in the prototype with a similarity ratio N=36). The similarity ratio was

chosen in such way to avoid significant boundary effect (Whitman and Lambe, 1986) and to enable sufficient space for installing micro earth pressure cells on the wall.

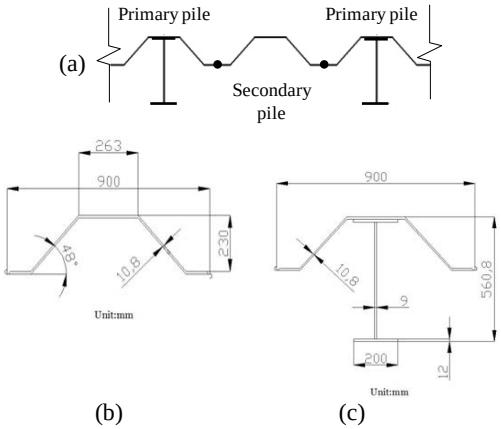

(b) (c)

Figure 1. Illustration of (a) a combined wall used in a full-scale test (Nakayama et al. 2013): (b) a secondary pile and (c) a primary pile

(a) TLJ-150 geotechnical centrifuge

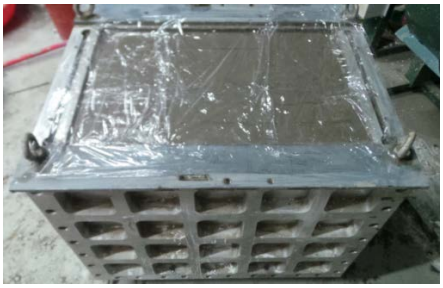

(b) Model box

Figure 2. Apparatus used in the test

As shown in Figure 3(a), a 350 mm wide wall is placed at a distance of 250 mm to the short edge of the box on the excavation side. A 50 mm wide drainage trench is isolated with a vertical porous plate along the long edge in order to accelerate consolidation. The wall is composed of fourteen Hat-type piles in the longitude direction, seven of which are enhanced by seven H sections. Figure 4 illustrates the dimensions of a primary pile and a secondary pile of the model wall, and Figure 5 presents a photo of the wall. For simplicity, interlocking joints between piles were not considered in this study. The wall was manufactured by folding a 0.3 mm thick iron plate into a wave surface of desired dimensions. Then pre-manufactured H sections were glued on the wall with an interval of one Hat-type pile. Initially, the wall was embedded into the soil at a depth of 360 mm, with 40 mm above the soil surface for installing the displacement sensor.

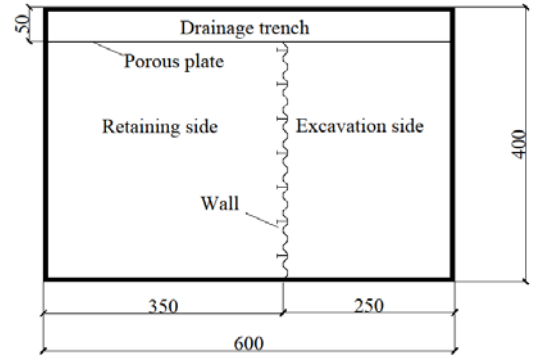

(a) Top view

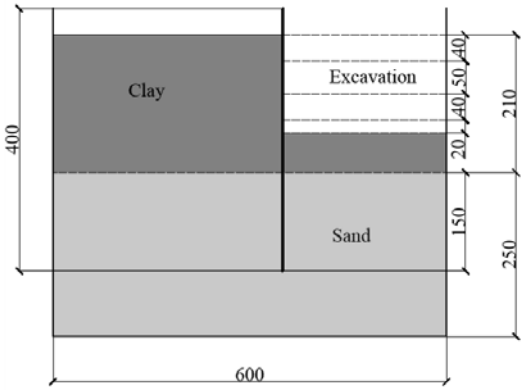

(b) Side view

Figure 3. Illustration of the model (unit: mm)

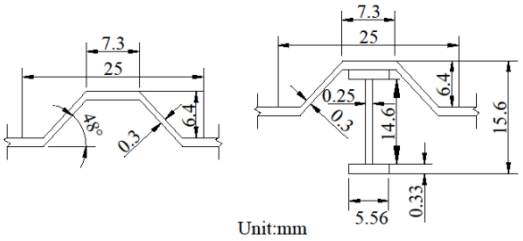

(a) Secondary pile (b) Primary pile

Figure 4. Dimensions of the model wall

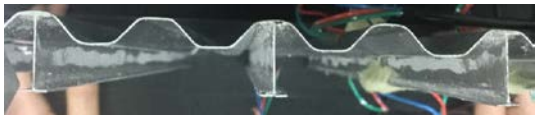

Figure 5. Photo of the model wall

The soil specimen is composed of a sand layer (250 mm thick) underlying a clay layer (210 mm thick). The clay is excavated by four layers up to a total depth of 150 mm. The clay used in the test was a typical clay in Shanghai area (often called No. 4 soil). Before the test, the raw clay was dried, pulverized and screened in order to remove impurities. Table 1 summarizes the basic indexes of the treated clay obtained in laboratory. The sand was collected from Changxing Island, Shanghai, and its gradation curve is given in Figure 6.

Table 1. Basic properties of the clay

Parameter	Value
Bulk density ρ (g/cm^3)	1.78
Liquid limit (%)	38.8
Plastic limit (%)	21.0
Consolidation coefficient C_v (cm^2/min)	0.076
Effective Cohesion c' (kPa)	7.6
Effective internal friction angle ϕ' (°)	29.4
Deformation modulus $E_{s0.1\sim0.2}$ (MPa)	2.7

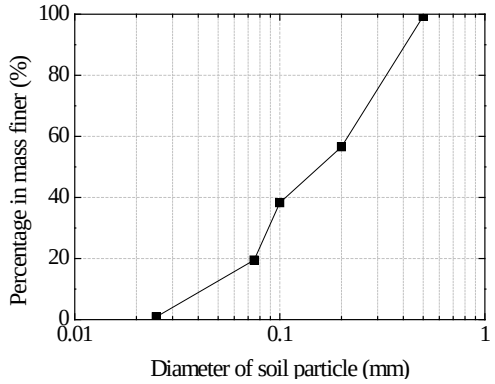

Figure 6. Gradation curve of the sand

Figure 7 illustrates the instrumentation on the wall. On the retaining side of the wall, a total of nine earth pressure cells, four strain gauges and one pore water pressure cell were installed on different parts of the wall at three different depths from the surface of the soil: 85 mm, 160 mm and 243 mm. On the excavation side of the wall, two earth pressure cells were installed at a depth of 243 mm from the surface of the soil. Moreover, a laser displacement sensor was attached to the top of the wall to measure the wall deflection. To monitor the pore water pressure dissipation during consolidation, two pore water pressure cells were embedded on the retaining side of the wall at depths of 85 mm and 243 mm from the surface of the soil.

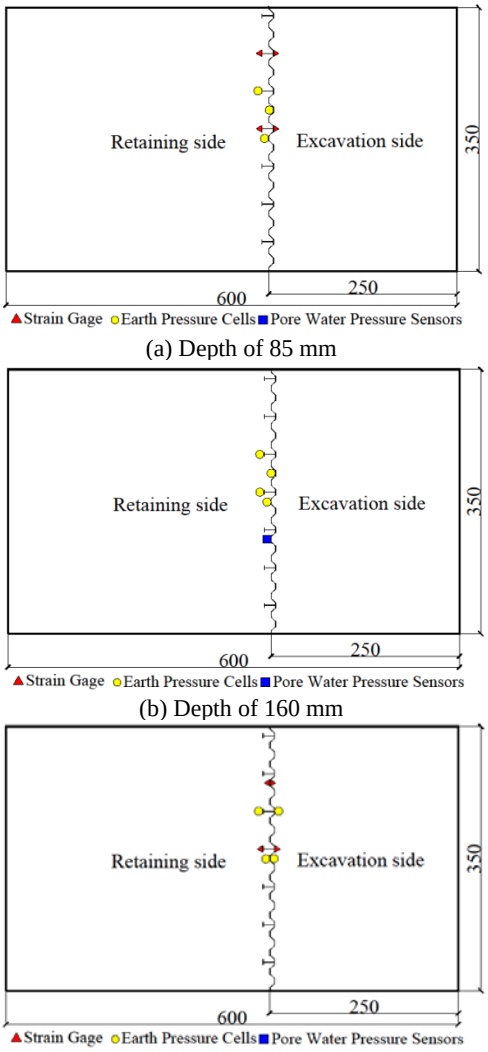

(a) Depth of 85 mm

(b) Depth of 160 mm

(c) Depth of 243 mm

Figure 7. Layout of instrumentation

2.3. Test procedure

The test was conducted through several steps:

(1) *Specimen preparation.* The earth pressure cells and pore water pressure cells were calibrated and attached to the model wall. Before filling the soils, the interior surface of the model box was coated with silicone oil in order to reduce the box-soil friction. The sand layer was prepared by five layers, each of which was 5 cm

thick. For each layer, dried sand was poured into the box and then compacted to reach a target relative density of 47% (i.e., void ratio e = 0.8, density ρ= 1.94 g/cm^3). The wall with sensors was embedded into the sand at the pre-defined depth. Afterward, the clay was saturated in a vacuum mixer, and then filled above the sand layer up to the top of the soil box, higher than the predefined elevation of the ground surface to reserve the room for possible consolidation settlement.

(2) *Consolidation*. According to Wei & Hu (1980), the No. 4 clay in Shanghai is slightly over-consolidated with an over consolidation ratio (OCR) of 1.08 in average. Therefore, the centrifuge acceleration was set as 40 g in the consolidation phase to mimic slightly over-consolidation conditions. The consolidation was terminated once the change of the pore water pressure within an hour is less than 3% of the total reduction.

(3) *T-bar test*. The centrifuge acceleration was adjusted to 36 g. The T-bar test was conducted in flight to evaluate the quality of the soil specimen when the pore water pressures remained relatively stable.

(4) *Excavation*. Excavation was processed by four layers as illustrated in Figure 3(b). For each layer, the centrifuge was terminated from 36 g, and the soil was carefully removed up to the predefined elevation. Then the centrifuge acceleration was increased up to 36 g and sustained until variation of pore water pressures in soils became unremarkable. The centrifuge was stopped for excavating the next layer. During the entire process of excavation, wall deflection and earth pressures were continuously monitored.

(5) *Post-excavation measurement*. The void ratio and water content were measured at different elevations on both sides of walls to characterize the soil right after the centrifuge test. Specimens were also collected at two different depths for the triaxial compression tests of the clay, of which the strength parameters are given in Table 1.

3. RESULTS AND INTERPRETATION

3.1. Pre-excavation measurements

Figure 8 shows dissipation of pore water pressure during consolidation, which took three days. The centrifuge was shut down at night (corresponding to the abrupt drops in the figure) for safety concern and resumed during day time. The accumulated time for the entire process of consolidation is about 20 hours.

Figure 9 presents the profile of penetration resistance obtained from the T-bar test. The records start at about 50 mm, where the T-bar was initially penetrated due to limited space above the model box. The penetration resistance increases sharply at the depth of about 210 mm due to the presence of the sand layer.

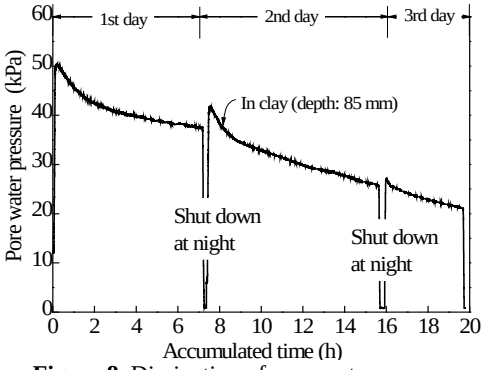

Figure 8. Dissipation of pore water pressure

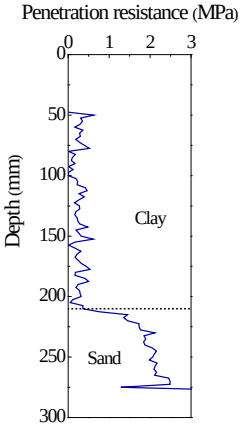

Figure 9. Profile of penetration resistance of T-bar test

3.2. Post-excavation measurements

Table 2 presents post-excavation measurements of void ratio (e) and water content (ω) at different depths. The void ratio of the clay ranges from 1.06 to 1.10, indicating rather homogenous condition in the clay layer. The averaged void ratio of the sand on the retaining side is larger than the initial value (i.e., e = 0.8), because the sand was loosen as a result of wall deflection towards the excavation side.

3.3. Wall deflection

Figure 10 presents horizontal displacement at the top of the wall at different excavation depths. The displacement increases during process of excavation, and exceeds 15 mm (i.e., about 4% of the entire height of the wall) at the excavation depth of 130 mm. The displacement at the final excavation depth was not recorded since displacement sensor was out of range.

Figure 11 presents the measurements obtained from the strain gauges attached on different portions of the wall. A negative value indicates compressive strain, otherwise tensile strain. For the secondary pile, the excavation side is subjected to compressive stresses (i.e., point Be), while the retaining side is subjected to tensile stresses (i.e., point Bb). However, the situation for the primary pile is more complicated. The strain of the primary pile is very small at the depth of 85 mm during the entire process of the excavation, while both excavation and retaining sides of the primary pile are subjected to tensile stresses at the depth of 243 mm.

3.4. Vertical profiles of earth pressure

Figure 12 presents the profile of the earth pressure along depth against the primary pile (i.e., point Ab) and the secondary pile (i.e., point Cb) on the retaining side during excavation. For comparison, the theoretical solutions of the earth pressure at rest and active earth pressure are superimposed in the figure. Note that the internal friction angle of the sand layer was assumed to be 25° according to an available investigation report on a site with a similar material, since no specific test was conducted for the sand used in the study. Before excavation, the measured earth pressure is consistent with the theoretical solution of the earth pressure at rest. The earth pressure decreases during excavation towards the theoretical solution of active earth pressure.

3.5. Transversal distributions of earth pressure

Figure 13 presents the earth pressure against the primary pile (i.e., Ab), the secondary pile (i.e., Cb), and the connector of the two piles (i.e., Bb) on the retaining side at different excavations. The earth pressure generally decreases with the increasing depth of excavation. Regardless the depth, the earth pressure against the primary pile is larger than elsewhere during the entire process of excavation, indicating that the primary piles act as the primary retaining elements of the wall.

Table 2. Measured void ratios and water contents

Depth (mm)	Retaining side		Excavation side	
	e	ω (%)	e	ω (%)
85 (clay)	1.10	41.82	/	/
160 (clay)	1.06	38.52	/	/
243 (sand)	0.88	25.63	0.91	31.53
310 (sand)	0.91	25.02	0.80	24.82
410 (sand)	0.90	25.15	0.80	25.94

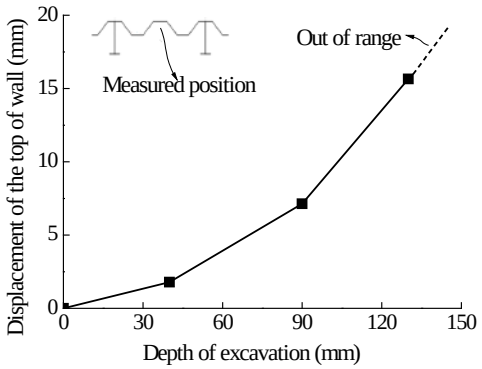

Figure 10. Displacement of the top of wall

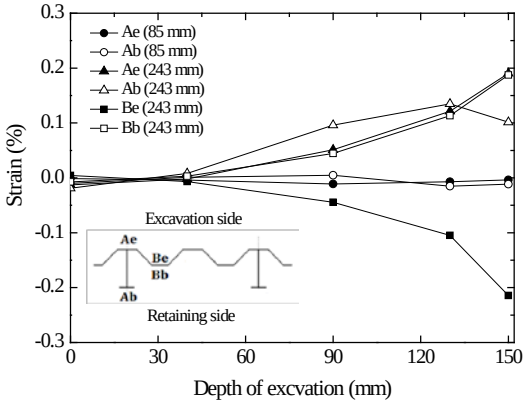

Figure 11. Strain of the combined wall

3.6. Contribution of secondary piles

We define the contribution of the secondary pile using a ratio of earth pressure against the secondary pile to that against the primary pile at the same elevation. Figure 14 presents the pressure ratio at the secondary pile (i.e., point Cb) and at the connector between the primary and secondary pile (i.e., point Bb) at the depth of 160 mm. The ratio is less than 1, indicating that secondary piles of the wall have less contribution than the primary ones to retain pressure. The ratio at point Cb is less than that at point Bb, indicating that the earth pressure decreases with

distance from the primary pile due to decreasing effect of the primary pile.

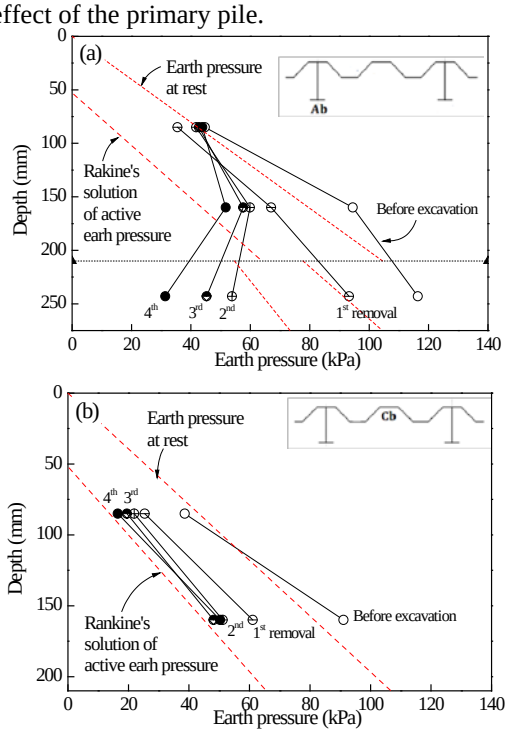

Figure 12. Evolved profiles of earth pressure on the retaining side during excavation against (a) the primary pile and (b) the secondary pile

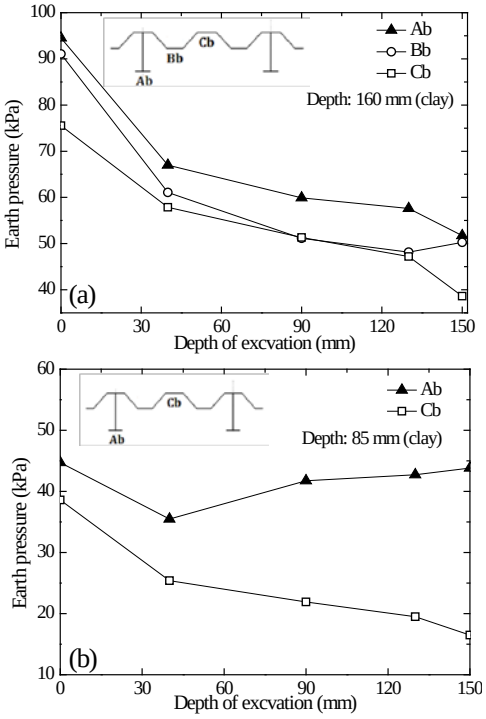

Figure 13. Earth pressure against different parts of the wall at different depths: (a) 160 mm; and (b) 85 mm

Figure 15 presents the ratio of pressure behind the secondary pile (i.e., Point Cb) at two different elevation. The ratio at a larger depth (i.e., 160 mm) ranges from 85% to 90% during excavation, while it decreases rapidly during excavation and reaches about 40% at a lower depth (i.e., 85 mm). This depth-dependency can be explained by varied wall deflection along depth. The earth pressure is transmitted from the secondary pile to the primary pile when the wall deforms. Larger the depth, less wall deflection, and therefore less earth pressure transmitted from the secondary piles to the primary piles.

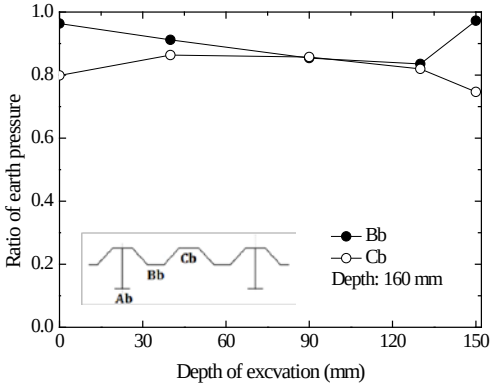

Figure 14. Ratio of earth pressure against different portions of the wall at the same elevation

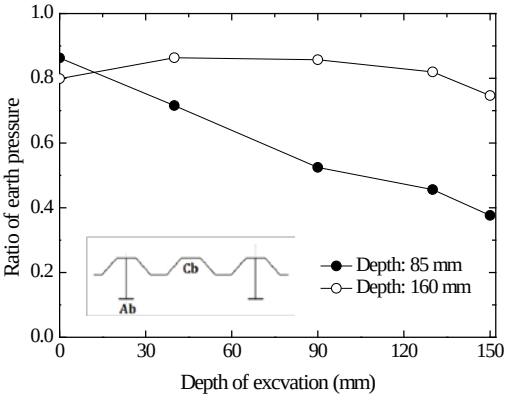

Figure 15. Ratio of earth pressure against the secondary pile at different depths

4. CONCLUSIONS

This paper conducted a centrifuge test of a combined wall composed of Hat-type piles and H sections. The earth pressure against different parts of the wall during excavation were quantitatively revealed under a controlled

condition. The main conclusions drawn from this study are as follows:

(1) The profiles of earth pressure against the wall on the retaining side approach towards the theoretical curve of active earth pressure during excavation.

(2) The primary piles act as the primary retaining elements of the wall. The fraction of earth pressure retained by the secondary piles decreases during excavation with decreasing depth and increasing distance from primary piles.

ACKNOWLEDGEMENT

The study is financially supported by Nippon Steel & Sumitomo Metal Corporation. The second author would also like to acknowledge the support from National Science Foundation of China (No. 41572267) and the Ministry of Science and Technology of China (No. SLDRCE 14-B-11). The centrifuge test received helpful suggestions from Prof. Xianfeng Ma, lab technician Mr. Xiaofeng WU and Mr. Chang'an Sun. Mr. Qi Kang and Mr. Di Wu assisted the test. Their efforts are appreciated.

REFERENCES

European Committee for Standardization. 2007. *Eurocode 3 – Design of steel structures – Part 5: Piling*, 54.

Liu, F., Jiang, M. J., Zhou, W., Nakayama, H. 2013. Differential earth pressure against combined sheet pile walls: full-scale tests and numerical simulations, *Proceedings of TC207 Workshop on Soil-Structure Interaction and Retaining Walls*, Paris, France, pp.282-293.

Liu, F., Zhang, G. Q., Jiang, M. J., Xiong, J. H., Nakayama, H. 2012. Impact of sectional shape of steel sheet pile wall on active earth pressure. *Rock and Soil Mechanics*, Vol. 33, No. S1, pp.315-320. (in Chinese)

Nakayama, H., Toshihiko, S., Noriyoshi, H., Kei, T. & Ryosuke, N. 2013. Full-scale embankment load test on retaining walls combined with hat-type sheet piles and hat-type sheet piles and hat-type +H-shape sheet piles. *Proceedings of the 5th China-Japan Geotechnical Symposium*, Chengdu, China, pp. 411-420.

Tong, Z. X., Zhou, S. P., Zheng, R. H., & Zhang, G. 2014. "Sectional Shape Effects of Steel Sheet Pile Walls on Earth Pressure by Centrifuge Model Tests." *Tunneling and Underground Construction*, ASCE, pp. 601-609

Whitman, R. V., P. C. Lambe. 1986. Effect of boundary conditions upon centrifuge experiments using ground motion simulation. *ASTM Geotechnical Testing Journal*, Vol. 9, No. 2, pp. 61-71.

Wei, D.D., Hu, Z.X. 1980. Experimental study on preconsolidation pressure and compression parameters of shallow soft soil in Shanghai. *Chinese Journal of Geotechnical Engineering*, Vol. 2, No. 4, pp. 13-22. (in Chinese)